

Advances

in Clinical and Experimental Medicine

MONTHLY ISSN 1899-5276 (PRINT) ISSN 2451-2680 (ONLINE)

www.advances.umw.edu.pl

2022, Vol. 31, No. 3 (March)

Impact Factor (IF) – 1.727
Ministry of Science and Higher Education – 70 pts
Index Copernicus (ICV) – 166.39 pts



WROCLAW
MEDICAL UNIVERSITY

Advances
in Clinical and Experimental
Medicine



Advances in Clinical and Experimental Medicine

ISSN 1899-5276 (PRINT)

ISSN 2451-2680 (ONLINE)

www.advances.umw.edu.pl

MONTHLY 2022
Vol. 31, No. 3
(March)

Advances in Clinical and Experimental Medicine (*Adv Clin Exp Med*) publishes high quality original articles, research-in-progress, research letters and systematic reviews and meta-analyses of recognized scientists that deal with all clinical and experimental medicine.

Editorial Office

ul. Marcinkowskiego 2–6
50-368 Wrocław, Poland
Tel.: +48 71 784 11 36
E-mail: redakcja@umw.edu.pl

Publisher

Wrocław Medical University
Wybrzeże L. Pasteura 1
50-367 Wrocław, Poland

© Copyright by Wrocław Medical University,
Wrocław 2022

Online edition is the original version
of the journal

Editor-in-Chief

Prof. Donata Kurpas

Deputy Editor

Prof. Wojciech Kosmala

Managing Editor

Marek Misiak

Scientific Committee

Prof. Sabine Bährer-Kohler
Prof. Antonio Cano
Prof. Breno Diniz
Prof. Erwan Donal
Prof. Chris Fox
Prof. Naomi Hachiya
Prof. Carol Holland
Prof. Markku Kurkinen
Prof. Christos Lionis

Section Editors

Anesthesiology

Prof. Marzena Zielińska

Basic Sciences

Prof. Iwona Bil-Lula
Prof. Bartosz Kempisty
Dr. Anna Lebedeva
Dr. Mateusz Olbromski
Dr. Maciej Sobczyński

Clinical Anatomy, Legal Medicine, Innovative Technologies

Prof. Rafael Boscolo-Berto

Dentistry

Prof. Marzena Dominiak
Prof. Tomasz Gedrange
Prof. Jamil Shibli

Statistical Editors

Wojciech Bombała, MSc
Katarzyna Giniewicz, MSc Eng.
Anna Kopszak, MSc
Dr. Krzysztof Kujawa

Manuscript editing

Marek Misiak, Jolanta Krzyżak

Prof. Raimundo Mateos

Prof. Zbigniew W. Ras
Prof. Jerzy W. Rozenblit
Prof. Silvina Santana
Prof. James Sharman
Prof. Jamil Shibli
Prof. Michal Toborek
Prof. László Vécsei
Prof. Cristiana Vitale

Dermatology

Prof. Jacek Szepietowski

Emergency Medicine, Innovative Technologies

Prof. Jacek Smereka

Gynecology and Obstetrics

Prof. Olimpia Sipak-Szmigiel

Histology and Embryology

Prof. Marzena Podhorska-Okołów

Internal Medicine

Angiology

Dr. Angelika Chachaj

Cardiology

Prof. Wojciech Kosmala
Dr. Daniel Morris

Endocrinology

Prof. Marek Bolanowski

Gastroenterology

Prof. Piotr Eder

Assoc. Prof. Katarzyna Neubauer

Hematology

Prof. Andrzej Deptała

Prof. Dariusz Wołowicz

Nephrology and Transplantology

Assoc. Prof. Dorota Kamińska

Assoc. Prof. Krzysztof Letachowicz

Pulmonology

Prof. Anna Brzecka

Microbiology

Prof. Marzenna Bartoszewicz

Assoc. Prof. Adam Junka

Molecular Biology

Dr. Monika Bielecka

Prof. Jolanta Saczko

Neurology

Assoc. Prof. Magdalena Koszewicz

Assoc. Prof. Anna Pokryszko-Dragan

Dr. Masaru Tanaka

Neuroscience

Dr. Simone Battaglia

Oncology

Prof. Andrzej Deptała

Dr. Marcin Jędryka

Gynecological Oncology

Dr. Marcin Jędryka

Orthopedics

Prof. Paweł Reichert

Otolaryngology

Assoc. Prof. Tomasz Zatoński

Pediatrics

Pediatrics, Metabolic Pediatrics, Clinical Genetics, Neonatology, Rare Disorders

Prof. Robert Śmigiel

Pediatric Nephrology

Prof. Katarzyna Kiliś-Pstrusińska

Pediatric Oncology and Hematology

Assoc. Prof. Marek Ussowicz

Pharmaceutical Sciences

Assoc. Prof. Maria Kepinska

Prof. Adam Matkowski

Pharmacoeconomics, Rheumatology

Dr. Sylwia Szafraniec-Buryło

Psychiatry

Prof. Istvan Boksay

Prof. Jerzy Leszek

Public Health

Prof. Monika Sawhney

Prof. Izabella Uchmanowicz

Qualitative Studies, Quality of Care

Prof. Ludmiła Marcinowicz

Radiology

Prof. Marek Szaśniadek

Rehabilitation

Prof. Jakub Taradaj

Surgery

Assoc. Prof. Mariusz Chabowski

Prof. Renata Taboła

Telemedicine, Geriatrics, Multimorbidity

Assoc. Prof. Maria Magdalena

Bujnowska-Fedak

Editorial Policy

Advances in Clinical and Experimental Medicine (Adv Clin Exp Med) is an independent multidisciplinary forum for exchange of scientific and clinical information, publishing original research and news encompassing all aspects of medicine, including molecular biology, biochemistry, genetics, biotechnology and other areas. During the review process, the Editorial Board conforms to the "Uniform Requirements for Manuscripts Submitted to Biomedical Journals: Writing and Editing for Biomedical Publication" approved by the International Committee of Medical Journal Editors (www.ICMJE.org/). The journal publishes (in English only) original papers and reviews. Short works considered original, novel and significant are given priority. Experimental studies must include a statement that the experimental protocol and informed consent procedure were in compliance with the Helsinki Convention and were approved by an ethics committee.

For all subscription-related queries please contact our Editorial Office:
redakcja@umw.edu.pl

For more information visit the journal's website:
www.advances.umw.edu.pl

Pursuant to the ordinance No. 134/XV R/2017 of the Rector of Wrocław Medical University (as of December 28, 2017) from January 1, 2018 authors are required to pay a fee amounting to 700 euros for each manuscript accepted for publication in the journal Advances in Clinical and Experimental Medicine.

Indexed in: MEDLINE, Science Citation Index Expanded, Journal Citation Reports/Science Edition, Scopus, EMBASE/Excerpta Medica, Ulrich's™ International Periodicals Directory, Index Copernicus

Typographic design: Piotr Gil, Monika Kołęda
DTP: Wydawnictwo UMW
Cover: Monika Kołęda
Printing and binding: Soft Vision Mariusz Rajski

Contents

Editorials

- 217 Simone Battaglia
Neurobiological advances of learned fear in humans

Original papers

- 223 Zheng Li, Chun Li, Ping Li, Yugang Li, Jin Lai, Sanjay Rastogi
Does a single dose of palonosetron have any role in preventing acute chemotherapy-induced nausea and vomiting in pediatric osteosarcoma patients without dexamethasone? A randomized clinical trial
- 231 Erdim Sertoglu, Çiğdem Yücel, Ahmet Omma, Yıldız Hayran, Seda Colak, Sevinc Can Sandıkçı, Ali Hakan Durukan, Taner Özgurtas
Determination of serum vascular endothelial growth factor (VEGF) and VEGF receptor levels with VEGF gene polymorphisms in patients with Behçet's uveitis
- 241 Katarzyna Majka, Marzena Parol, Andrzej Nowicki, Barbara Gambin, Zbigniew Trawiński, Marzena Jaciubek, Andrzej Krupienicz, Robert Olszewski
Comparison of the radial and brachial artery flow-mediated dilation in patients with hypertension
- 249 Jolanta Kiewisz, Anna Pawłowska, Agata Winiarska, Agnieszka Perkowska-Ptasińska, Agnieszka Skowrońska, Janusz Godlewski, Zbigniew Kmieć, Tomasz Stompór
Serum WNT4 protein as an indicator of chronic glomerulonephritis but not a marker of inflammatory cell infiltration and fibrosis: A preliminary study
- 261 Robert Franciszek Łukaszuk, Krzysztof Piotr Nycz, Krzysztof Plens, Anetta Undas
Caprini VTE computerized risk assessment improves the use of thromboprophylaxis in hospitalized patients with pulmonary disorders
- 267 Jolanta Kolasa, Magdalena Frączek-Jucha, Marcin Grabowski, Ewa A. Jankowska, Małgorzata Lelonek, Agnieszka Pawlak, Izabella Uchmanowicz, Jadwiga Nessler
A quasi-experimental study examining a nurse-led educational program to improve disease knowledge and self-care for patients with acute decompensated heart failure with reduced ejection fraction
- 277 Yingcui Wang, Suhua Zhang, Yingying Ma, Aixia Xiang, Hui Sun, Jun Song, Wenjing Yang, Xuanlong Li, Hongxiao Xu
Melatonin protected against myocardial infarction injury in rats through a Sirt6-dependent antioxidant pathway
- 285 Zehra Bedir, Kezban Tuna Ozkaloglu Erdem, Irem Ates, Tulay Ceren Olmez Turk Karakurt, Cebirail Gursul, Didem Onk, Nezahat Kurt, Zeynep Suleyman, Halis Suleyman
Effects of ketamine, thiopental and their combination on the rat liver: A biochemical evaluation
- 293 Radosław Chaber, Artur Gurgul, Jacek Tabarkiewicz, Grażyna Wróbel, Tomasz Szmatoła, Igor Jasielczuk, Olga Haus, Monika Lejman, Blanka Rybka, Renata Ryczan-Krawczyk, Anna Jaśkowiec, Sylwia Paszek, Natalia Potocka, Christopher J. Arthur, Wioletta Bal, Kornelia Łach, Aneta Kowal, Izabela Zawlik, Elżbieta Latos-Grażyńska
MicroRNA gene methylation landscape in pediatric B-cell precursor acute lymphoblastic leukemia
- 307 Qiao Zheng, Si-Min Ruan, Chun-Yang Zhang, Zhong Cao, Ze-Rong Huang, Huan-Ling Guo, Xiao-Yan Xie, Ming-De Lu, Wei Wang, Li-Da Chen
Can monodisperse microbubble-based three-dimensional contrast-enhanced ultrasound reduce quantitative heterogeneity? An in vitro study

Reviews

- 317 Marcin Adamczak, Stanisław Surma, Andrzej Więcek
Acute kidney injury in patients with COVID-19: Epidemiology, pathogenesis and treatment

Research letters

- 327 Juan Mu, Meijing Liu, Jia Wang, Juanxia Meng, Rui Zhang, Yanyu Jiang, Qi Deng
Successful treatment of second-time CAR-T 19 therapy after failure of first-time CAR-T 19 and ibrutinib therapy in relapsed mantle cell lymphoma
- 337 Konrad Stępień, Paweł Skorek, Janusz Włodarczyk, Janusz Wójcik, Tomasz Smęder, Łukasz Trybalski, Lucyna Rudnicka-Sosin, Jarosław Kuźdżał, Piotr Kocoń
Various clinical scenarios of primary melanoma of the esophagus: A retrospective 20-year analysis from two university thoracic surgery centers
- 345 Monika Rosa, Tomasz Jarmoliński, Izabella Miśkiewicz-Migoń, Karolina Liszka, Justyna Miśkiewicz-Bujna, Anna Panasiuk, Jowita Frączkiewicz, Marek Ussowicz
Vedolizumab in highly resistant acute gastrointestinal graft-versus-host disease after allogeneic stem cell transplantation: A single-center pediatric series

Neurobiological advances of learned fear in humans

Simone Battaglia^{A,D–F}

Center for Studies and Research in Cognitive Neuroscience, Department of Psychology, University of Bologna, Italy

A – research concept and design; B – collection and/or assembly of data; C – data analysis and interpretation;
D – writing the article; E – critical revision of the article; F – final approval of the article

Advances in Clinical and Experimental Medicine, ISSN 1899–5276 (print), ISSN 2451–2680 (online)

Adv Clin Exp Med. 2022;31(3):217–221

Address for correspondence

Simone Battaglia
E-mail: simone.battaglia@unibo.it

Funding sources

None declared

Conflict of interest

None declared

Received on January 12, 2022

Accepted on February 16, 2022

Published online on February 23, 2022

Abstract

In the whole animal kingdom, fear learning is an essential process that allows living beings to survive. Therefore, revealing the neurophysiological processes that govern the expression of emotional fear memory and exploring its neurobiological underpinnings are the imperatives of affective neuroscience. Learned fear memories activate defensive behaviors in anticipation of harm, thus minimizing the impact of the threat. However, despite a century of research, the neural circuitry underlying fear learning in humans is still a matter of debate. This editorial will discuss recent evidence of the neural and behavioral correlates of fear learning in humans, with an emphasis on the role of the human prefrontal cortex (PFC).

Key words: prefrontal cortex, amygdala, hippocampus, fear conditioning, fear neural network

Cite as

Battaglia S. Neurobiological advances of learned fear in humans. *Adv Clin Exp Med.* 2022;31(3):217–221.
doi:10.17219/acem/146756

DOI

10.17219/acem/146756

Copyright

© 2022 by Wrocław Medical University
This is an article distributed under the terms of the
Creative Commons Attribution 3.0 Unported (CC BY 3.0)
(<https://creativecommons.org/licenses/by/3.0/>)

The state of art

Learning to recognize and respond to certain stimuli or external contingencies that signal imminent threats is a widely useful and adaptable function for both animals and humans.¹ Fear conditioning is the most frequently adopted experimental design to investigate this circumstance that produces both behaviorally and physiologically conditioned responses.² From an evolutionary perspective, it is highly advantageous to preserve clear memories of the main significant experiences in life. Nonetheless, the so-called indissoluble nature of emotional memory can be extremely damaging and have negative consequences for those individuals who have experienced traumatic events and may endure dreadful memories and severe anxiety. For these reasons, fear conditioning is broadly acknowledged to be a model for translational framework of psychiatric disorders.^{3–6} Thus, to further understand mechanisms of fear learning, many new techniques that allow studying physiological responses of fear conditioning are being developed. These techniques might be applied as measures for dysfunctional and altered fear learning and may help in identifying the individuals who are at risk for developing psychiatric disorders.⁵ In fact, human fear conditioning is generally investigated on different levels: as subjective verbal reports about the experienced fear, as well as behavioral, physiological and neurobiological changes.^{7,8} Among these, physiological changes are the most frequently used measures in the study of human acquired fear memories, as a consequence of their benefit of being unaffected by the participant itself, as well as because of the possibility of a direct comparison with animal research.

Pavlovian fear conditioning is one of the most widely investigated fear-induced behavioral models in the history of cognitive psychology and behavioral neuroscience. It was developed upon the appetitive conditioning paradigm utilized by Pavlov in animals (1903/1928). Its effect occurs as a consequence of repetitive association of an initially innocuous stimulus (i.e., a tone) with an innately aversive stimulus (i.e., a shock pulse). By associating cue to consequence, stimulus presentation usually induces different types of psychophysiological reactions indicating fear. This simple procedure is a fundamental paradigm not only for behavioral and cognitive sciences, but also for medicine, since its application is useful in both psychiatry and neurology. It has taken almost a century of scientific investigation to utilize the classic fear conditioning paradigm in both animals and humans⁹ in order to gain a broad and thorough knowledge of learned fear and its associated processes, such as learning mechanisms, memorization and retrieval. This experimental and clinical paradigm has been extremely effective and valuable in defining the psychological processes governing the genesis and expression of fear and the functioning of emotional and general memory, together with uncovering the neurobiological basis of emotion and learning in healthy subjects and psychiatric populations.^{6,10,11}

The neurobiological model

Currently, the fear conditioning framework has moved beyond the realm of associative learning theory and has become a framework of substantial interest in the neuroscience of learning, memory and emotion.^{12,13} Neural circuits have been mapped, synaptic plasticity in these circuits has been identified, and biochemical and genetic investigations have begun disentangling the mechanisms of fear memories.^{3,14–17} However, despite a century of research, the neural circuitry underlying fear learning in humans is still a matter of debate. Modern neuroimaging technologies have made a significant contribution to the understanding of neuroanatomical brain circuits of human fear conditioning.¹⁸ Specifically, amygdala plays a key role in the acquisition of fear learning, while the prefrontal cortex (PFC) and hippocampus are 2 other crucial neural structures that contribute to this process, representing together the neural network of fear conditioning.^{19–21} It is broadly assumed that connections between these regions govern the acquisition, storage, retrieval, expression, and contextual modulation of fear conditioning (for a review, see the paper by Milad and Quirk²²). In accordance to animal model research, functional neuroimaging, ad hoc lesion studies, and morphology, extinction of previously learned fear is dependent on the integrated functioning of this network, indicating that the brain mechanisms underlying fear acquisition and extinction are phylogenetically maintained throughout species.²³

Over the last century, ad hoc surgical lesions, pharmacological drug administration and physiological data from animal and human studies have established a comprehensive framework of the neural network that supports fear conditioning. Among all, when the amygdala involvement in fear conditioning was recognized, it was acknowledged as the key structure of this network.² Precisely, this brain region is commonly recognized as ‘the locus of fear conditioning’.¹⁵ Furthermore, anatomical studies highlighted the interactions between the central nucleus of the amygdala and downstream structures involved in the expression of fear conditioned responses, namely the hypothalamus, periaqueductal gray, pons, and other brainstem regions.²⁴ Other studies reported the inhibitory mechanisms within the amygdala that have been involved in fear extinction as well, including the lateral division of the central nucleus,²⁵ and inhibitory cells within the lateral and basolateral nuclei.²⁶

Another structure, the hippocampus, is considered essential in contextual fear learning, along with the acquisition and the extinction of context conditioning: lesion studies have provided pivotal insights on the direct projections that the ventral hippocampus (vHPC) has with both infralimbic cortex (IL, in PFC) and the basolateral amygdala,²⁷ suggesting a crucial role of this region in the modulation of contextual fear responses.²⁸ In addition, the hippocampus is supposed to be necessary

in monitoring the context-specific recall of extinction, both directly through connections with the amygdala and indirectly via projections to the ventromedial PFC (vmPFC) (for a review, see the paper by Maren et al.²⁹). Moreover, it has been acknowledged that different hippocampal subregions are involved in different human behavior features – specifically, the dorsal part in spatial-related behaviors and the ventral region in anxiety-related behaviors (for a review, see the paper by Bannerman et al.³⁰). Increasing evidence suggests that the hippocampus and its subregions are involved in several aspects of fear conditioning.¹⁵

Crucially, latest available evidence has identified the PFC as a critical core component in the neural circuit underlying fear conditioning, particularly for the ability of PFC to bidirectionally modulate the expression of previously learned fear. On one hand, the activation in the dorsomedial PFC (dmPFC) occurs for the long-term storage and retrieval of old memories³¹; on the other, the vmPFC forms strong reciprocal connections with the amygdala and other subcortical structures as well as with the lateral cortex. Thus, this subregion seems to be necessary for controlling fear relative to a stimulus that no longer predicts danger,³² representing a relay-station for “bottom-up” information from limbic and subcortical structures signaling emotion detection, as well as for information from lateral PFC (LPFC), conveying response selection and control.³³ Furthermore, Harrison et al.³⁴ have suggested different contributions of anterior and posterior subregions of the vmPFC to the fear learning processes, showing greater anterior vmPFC activity in response to a safety stimulus, as it is likely to compute the value or meaning of safety signals. Nonetheless, recent work suggests that vmPFC may also have a crucial role in fear acquisition, which is processed in its posterior subregion³⁵: crucially, naturally occurring bilateral lesions in the human vmPFC were found to compromise fear conditioning (measured by skin conductance responses), proving that fear conditioning was impaired due to brain injury.³⁶ These findings were supported in a recent meta-analysis²¹ that identified greater activation of the posterior vmPFC (BA11) during late fear conditioning, providing potential causal evidence of a crucial role of the mid-posterior vmPFC in the acquisition of fear.

Converging lines of research have also brought insight on the involvement of PFC in the extinction of fear learning: in concert with the animal studies, neuroimaging studies reported that, besides amygdala activation, vmPFC is particularly important for consolidation of the extinction memory and is especially involved in the recall of extinction in subsequent testing.³⁷ In particular, this subregion may not simply inhibit the expression of amygdala-dependent conditioned threat responses, but signal a change in previously acquired contingencies in order to select the most appropriate response to the current situation.³² The extinction of conditioned fear appears to involve also dorsolateral

PFC (dlPFC). This could be due to its capacity of shifting the attention from the stimulus to the context, but may also be a consequence of its role as a site of explicit short-term memory processes in humans, aimed at maintaining the trace interval.³⁸

Importantly, consistently with signs of PFC functional impairment, it has been observed that patients with post-traumatic stress disorder (PTSD) show normal conditioned fear acquisition and extinction, but appear to be impaired in the recall of extinction memory the following day.³⁹ Specifically, extinction recall was compromised due to the hypoactivation in the vmPFC and hyperactivation in the dorsal anterior cingulate cortex (dACC).⁴⁰ Similar findings were also observed in schizophrenic patients with functionally damaged vmPFC.⁴¹ Taking everything into consideration, this evidence reveals that fear conditioning circuits may be altered in many different psychiatric disorders in humans.⁴²

Conclusions and future perspectives

In conclusion, functional alterations of the neural network underlying fear conditioning or in the emotional regulatory mechanisms might contribute to the etiology of anxiety-related disorders, including panic disorder, specific phobias and PTSD.⁴³ These altered mechanisms are regarded as pivotal factors in the pathogenesis and development of psychiatric disorders characterized by anxiety.^{44–46} Hence, a deep understanding of the psychological and molecular mechanisms underlying such disorders is necessary, and fear conditioning paradigm appears to be the most effective for this purpose. Furthermore, a deeper understanding of fear learning neural networks may also contribute to the advancement of alternative, more precise and individualized treatments for psychiatric disorders.

On this note, some issues and questions come to mind. According to corroborated literature, the human PFC modulates the activity of the amygdala and hippocampus after fear conditioning (i.e., extinction learning) like in animals; however, such assumption is based on limited empirical data. Differently from the classical view,⁴⁷ recent work suggests that the vmPFC may also play a major role in the acquisition of fear,^{21,34–36,48} as processed within its posterior subregion.⁴⁹

Consequently, it is plausible to assume that there are differences between humans and animals in the functional neuroarchitecture of PFC. Thus, it is reasonable and timely relevant now to address this question: what exactly is the role of the prefrontal cortex in human fear conditioning?

ORCID iDs

Simone Battaglia  <https://orcid.org/0000-0003-4133-654X>

References

- Bouton ME. Context, ambiguity, and unlearning: Sources of relapse after behavioral extinction. *Biol Psychiatry*. 2002;52(10):976–986. doi:10.1016/s0006-3223(02)01546-9
- LeDoux JE. Emotion circuits in the brain. *Annu Rev Neurosci*. 2000; 23(1):155–184. doi:10.1146/annurev.neuro.23.1.155
- Milad MR, Quirk GJ. Fear extinction as a model for translational neuroscience: Ten years of progress. *Annu Rev Psychol*. 2012;63:129–151. doi:10.1146/annurev.psych.121208.131631
- Vervliet B, Craske MG, Hermans D. Fear extinction and elapse: State of the art. *Annu Rev Clin Psychol*. 2013;9(1):215–248. doi:10.1146/annurev-clinpsy-050212-185542
- Sevenster D, Hamm A, Beckers T, Kindt M. Heart rate pattern and resting heart rate variability mediate individual differences in contextual anxiety and conditioned responses. *Int J Psychophysiol*. 2015; 98(3):567–576. doi:10.1016/j.ijpsycho.2015.09.004
- Borgomaneri S, Battaglia S, Avenanti A, di Pellegrino G. Don't hurt me no more: State-dependent transcranial magnetic stimulation for the treatment of specific phobia. *J Affect Disord*. 2021;286:78–79. doi:10.1016/j.jad.2021.02.076
- Bradley MM, Lang PJ. Measuring emotion: Behavior, feeling and physiology. In: Lane RD, Nadel L, eds. *Cognitive Neuroscience of Emotion*. New York, USA: Oxford University Press; 2000:242–276.
- Borgomaneri S, Battaglia S, Sciamanna G, Tortora F, Laricchiuta D. Memories are not written in stone: Re-writing fear memories by means of non-invasive brain stimulation and optogenetic manipulations. *Neurosci Biobehav Rev*. 2021;127:334–352. doi:10.1016/j.neubiorev.2021.04.036
- Beckers T, Kryptos AM, Boddez Y, Eftting M, Kindt M. What's wrong with fear conditioning? *Biol Psychol*. 2013;92(1):90–96. doi:10.1016/j.biopsycho.2011.12.015
- Craske MG, Hermans D, Vansteenwegen D, eds. *Fear and Learning: From Basic Processes to Clinical Implications*. Washington, USA: American Psychological Association; 2006. doi:10.1037/11474-000
- Hartley CA, Fischl B, Phelps EA. Brain structure correlates of individual differences in the acquisition and inhibition of conditioned fear. *Cereb Cortex*. 2011;21(9):1954–1962. doi:10.1093/cercor/bhq253
- Dunsmoor JE, Niv Y, Daw N, Phelps EA. Rethinking extinction. *Neuron*. 2015;88(1):47–63. doi:10.1016/j.neuron.2015.09.028
- Dunsmoor JE, Kroes MCW, Moscatelli CM, Evans MD, Davachi L, Phelps EA. Event segmentation protects emotional memories from competing experiences encoded close in time. *Nat Hum Behav*. 2018;2(4):291–299. doi:10.1038/s41562-018-0317-4
- Maren S. Neurobiology of Pavlovian fear conditioning. *Annu Rev Neurosci*. 2001;24(1):897–931. doi:10.1146/annurev.neuro.24.1.897
- Kim JJ, Jung MW. Neural circuits and mechanisms involved in Pavlovian fear conditioning: A critical review. *Neurosci Biobehav Rev*. 2006; 30(2):188–202. doi:10.1016/j.neubiorev.2005.06.005
- Borgomaneri S, Battaglia S, Garofalo S, Tortora F, Avenanti A, di Pellegrino G. State-dependent TMS over prefrontal cortex disrupts fear-memory reconsolidation and prevents the return of fear. *Curr Biol*. 2020;30(18):3672–3679.e4. doi:10.1016/j.cub.2020.06.091
- Battaglia S, Garofalo S, di Pellegrino G. Context-dependent extinction of threat memories: Influences of healthy aging. *Sci Rep*. 2018; 8(12592):1–13. doi:10.1038/s41598-018-31000-9
- Sehlmeyer C, Schöning S, Zwitserlood P, et al. Human fear conditioning and extinction in neuroimaging: A systematic review. *PLoS One*. 2009;4(6):e5865. doi:10.1371/journal.pone.0005865
- Maren S, Quirk GJ. Neuronal signalling of fear memory. *Nat Rev Neurosci*. 2004;5(11):844–852. doi:10.1038/nrn1535
- Lonsdorf TB, Haaker J, Kalisch R. Long-term expression of human contextual fear and extinction memories involves amygdala, hippocampus and ventromedial prefrontal cortex: A reinstatement study in two independent samples. *Soc Cogn Affect Neurosci*. 2014;9(12): 1973–1983. doi:10.1093/scan/nsu018
- Fullana MA, Harrison BJ, Soriano-Mas C, et al. Neural signatures of human fear conditioning: An updated and extended meta-analysis of fMRI studies. *Mol Psychiatry*. 2016;21(4):500–508. doi:10.1038/mp.2015.88
- Milad MR, Quirk GJ. Neurons in medial prefrontal cortex signal memory for fear extinction. *Nature*. 2002;420(6911):70–74. doi:10.1038/nature01138
- Dunsmoor JE, Kroes MCW, Li J, Daw ND, Simpson HB, Phelps EA. Role of human ventromedial prefrontal cortex in learning and recall of enhanced extinction. *J Neurosci*. 2019;39(17):3264–3276. doi:10.1523/JNEUROSCI.2713-18.2019
- LeDoux JE, Iwata J, Cicchetti P, Reis DJ. Different projections of the central amygdaloid nucleus mediate autonomic and behavioral correlates of conditioned fear. *J Neurosci*. 1988;8(7):2517–2529. doi:10.1523/jneurosci.08-07-02517.1988
- Sun N, Cassell MD. Intrinsic GABAergic neurons in the rat central extended amygdala. *J Comp Neurol*. 1993;330(3):381–404. doi:10.1002/cne.903300308
- Mahanty N, Sah P. Calcium-permeable AMPA receptors mediate long-term potentiation in interneurons in the amygdala. *Nature*. 1998;394(6694):683–687. doi:10.1038/246170a0
- Hugues S, Garcia R. Reorganization of learning-associated prefrontal synaptic plasticity between the recall of recent and remote fear extinction memory. *Learn Mem*. 2007;14(8):520–524. doi:10.1101/lm.625407
- Gewirtz JC, McNish KA, Davis M. Is the hippocampus necessary for contextual fear conditioning? *Behav Brain Res*. 2000;110(1–2):83–95. doi:10.1016/S0166-4328(99)00187-4
- Maren S, Phan KL, Liberzon I. The contextual brain: Implications for fear conditioning, extinction and psychopathology. *Nat Rev Neurosci*. 2013;14(6):417–428. doi:10.1038/nrn3492
- Bannerman DM, Rawlins JNP, McHugh SB, et al. Regional dissociations within the hippocampus: Memory and anxiety. *Neurosci Biobehav Rev*. 2004;28(3):273–283. doi:10.1016/j.neubiorev.2004.03.004
- Dixsaut L, Gräff J. The medial prefrontal cortex and fear memory: Dynamics, connectivity and engrams. *Int J Mol Sci*. 2021;22(22):12133. doi:10.3390/ijms222212113
- Phelps EA, Delgado MR, Nearing KI, LeDoux JE. Extinction learning in humans: Role of the amygdala and vmPFC. *Neuron*. 2004;43(6): 897–905. doi:10.1016/j.neuron.2004.08.042
- Myers-Schulz B, Koenigs M. Functional anatomy of ventromedial prefrontal cortex: Implications for mood and anxiety disorders. *Mol Psychiatry*. 2012;17(2):132–141. doi:10.1038/mp.2011.88
- Harrison BJ, Fullana MA, Via E, et al. Human ventromedial prefrontal cortex and the positive affective processing of safety signals. *Neuroimage*. 2017;152:12–18. doi:10.1016/j.neuroimage.2017.02.080
- Battaglia S, Harrison BJ, Fullana MA. Does the human ventromedial prefrontal cortex support fear learning, fear extinction or both? A commentary on subregional contributions [published online ahead of print on October 20, 2021]. *Mol Psychiatry*. 2021. doi:10.1038/s41380-021-01326-4
- Battaglia S, Garofalo S, di Pellegrino G, Starita F. Revaluing the role of vmPFC in the acquisition of Pavlovian threat conditioning in humans. *J Neurosci*. 2020;40(44):8491–8500. doi:10.1523/JNEUROSCI.0304-20.2020
- Milad MR, Wright CI, Orr SP, Pitman RK, Quirk GJ, Rauch SL. Recall of fear extinction in humans activates the ventromedial prefrontal cortex and hippocampus in concert. *Biol Psychiatry*. 2007;62(5): 446–454. doi:10.1016/j.biopsycho.2006.10.011
- Ewald H, Glotzbach-Schoon E, Gerdes ABM, et al. Delay and trace fear conditioning in a complex virtual learning environment-neural substrates of extinction. *Front Hum Neurosci*. 2014;8:1–11. doi:10.3389/fnhum.2014.00323
- Garfinkel SN, Abelson JL, King AP, et al. Impaired contextual modulation of memories in PTSD: An fMRI and psychophysiological study of extinction retention and fear renewal. *J Neurosci*. 2014;34(40): 13435–13443. doi:10.1523/JNEUROSCI.4287-13.2014
- Milad MR, Pitman RK, Ellis CB, et al. Neurobiological basis of failure to recall extinction memory in posttraumatic stress disorder. *Biol Psychiatry*. 2009;66(12):1075–1082. doi:10.1016/j.biopsycho.2009.06.026
- Holt DJ, Lebron-Milad K, Milad MR, et al. Extinction memory is impaired in schizophrenia. *Biol Psychiatry*. 2009;65(6):455–463. doi:10.1016/j.biopsycho.2008.09.017
- Insel T, Cuthbert B, Garvey M, et al. Research Domain Criteria (RDoC): Toward a new classification framework for research on mental disorders. *Am J Psychiatry Online*. 2010;167(7):748–751. doi:10.1176/appi.ajp.2010.09091379
- Rosen JB, Schulkin J. From normal fear to pathological anxiety. *Psychol Rev*. 1998;105(2):325–350. doi:10.1037/0033-295X.105.2.325

44. Duits P, Cath DC, Lissek S, et al. Updated meta-analysis of classical fear conditioning in the anxiety disorders. *Depress Anxiety*. 2015;32(4): 239–253. doi:10.1002/da.22353
45. Lissek S, Baas JMP, Pine DS, et al. Airpuff startle probes: An efficacious and less aversive alternative to white-noise. *Biol Psychol*. 2005; 68(3):283–297. doi:10.1016/j.biopsycho.2004.07.007
46. Lissek S, Powers AS, McClure EB, et al. Classical fear conditioning in the anxiety disorders: A meta-analysis. *Behav Res Ther*. 2005;43(11): 1391–1424. doi:10.1016/j.brat.2004.10.007
47. Schiller D, Delgado MR. Overlapping neural systems mediating extinction, reversal and regulation of fear. *Trends Cogn Sci*. 2010;14(6): 268–276. doi:10.1016/j.tics.2010.04.002
48. Tashjian SM, Zbozinek TD, Mobbs D. A decision architecture for safety computations. *Trends Cogn Sci*. 2021;25(5):342–354. doi:10.1016/j.tics. 2021.01.013
49. Taschereau-Dumouchel V, Kawato M, Lau H. Multivoxel pattern analysis reveals dissociations between subjective fear and its physiological correlates. *Mol Psychiatry*. 2020;25(10):2342–2354. doi:10.1038/ s41380-019-0520-3

Does a single dose of palonosetron have any role in preventing acute chemotherapy-induced nausea and vomiting in pediatric osteosarcoma patients without dexamethasone? A randomized clinical trial

*Zheng Li^{1,A}, *Chun Li^{2,B}, Ping Li^{3,B}, Yugang Li^{4,B,C}, Jin Lai^{5,D–F}, Sanjay Rastogi^{6,D–F}

¹ Department of Orthopaedics, Chengdu Jinniu District People's Hospital, China

² Department of Pathology, China-Japan Friendship Hospital, Beijing, China

³ Department of Orthopaedics, Ya'an People's Hospital, China

⁴ Department of Orthopaedics, The 1st Affiliated Hospital of Chengdu Medical College, China

⁵ Department of Orthopedics, The 72nd Group Army Hospital of People's Liberation Army, Huzhou, China

⁶ Oral and Maxillofacial Surgery, Regional Dental College, Guwahati, India

A – research concept and design; B – collection and/or assembly of data; C – data analysis and interpretation;

D – writing the article; E – critical revision of the article; F – final approval of the article

Advances in Clinical and Experimental Medicine, ISSN 1899–5276 (print), ISSN 2451–2680 (online)

Adv Clin Exp Med. 2022;31(3):223–230

Address for correspondence

Jin Lai

E-mail: laijin14258@gmail.com

Funding sources

None declared

Conflict of interest

None declared

*Zheng Li and Chun Li contributed equally to this manuscript.

Received on June 16, 2021

Reviewed on August 24, 2021

Accepted on September 16, 2021

Published online on March 16, 2022

Cite as

Li Z, Li C, Li P, Li Y, Lai J, Rastogi S. Does a single dose of palonosetron have any role in preventing acute chemotherapy-induced nausea and vomiting in pediatric osteosarcoma patients without dexamethasone? A randomized clinical trial. *Adv Clin Exp Med.* 2022;31(3):223–230. doi:10.17219/acem/142332

DOI

10.17219/acem/142332

Copyright

© 2022 by Wrocław Medical University

This is an article distributed under the terms of the Creative Commons Attribution 3.0 Unported (CC BY 3.0) (<https://creativecommons.org/licenses/by/3.0/>)

Abstract

Background. Chemotherapy-induced nausea and vomiting (CINV) is a troublesome side-effect of chemotherapy in pediatric patients undergoing osteosarcoma treatment. In this context, the role of 5-hydroxytryptamine-3 (5-HT₃) receptor antagonists needs to be explored.

Objectives. To evaluate the superiority of single-dose palonosetron over granisetron in pediatric patients undergoing highly emetogenic chemotherapy (HEC) for osteosarcoma.

Materials and methods. In this double-blind, randomized study, pediatric patients were assessed in terms of acute nausea and vomiting following HEC for osteosarcoma. These children were assigned to group 1 (palonosetron) and group 2 (granisetron) without any other antiemetic prophylaxis. The primary outcome variable was the children's segment with a complete response (CR) during the acute phase of the 1st on-study chemotherapy cycle. The risk factors associated with the emesis were analyzed. The patients were followed up for the first 24 h after chemotherapy.

Results. A total number of 200 children were evaluated in terms of the response, and other factors that might alter the response were assessed in the 2 groups. These 200 children underwent 604 blocks of chemotherapy. Complete responses were documented in 83% and 72% of children receiving palonosetron and granisetron, respectively, during the acute phase. Only dexamethasone, used as a rescue medication, was found to be a significant risk factor that predisposed to the response ($p < 0.05$).

Conclusions. Single-dose palonosetron is an effective alternative to granisetron for preventing CINV in children receiving HEC for osteosarcoma.

Key words: granisetron, chemotherapy, emesis, 5-HT₃ receptor antagonists, palonosetron

Background

Cancer is tormenting and devastating, but with the incessant emergence of medical advances, chemotherapy is launched as one of the reassuring measures. The advent of chemotherapy combined with radiotherapy and surgery re-established hope for survival. However, along with it came a profusion of anguishing side effects. Side effects of chemotherapy are nephrotoxicity, neurotoxicity, ototoxicity, myelosuppression, nausea, and vomiting. Among them, nausea and vomiting are bothersome, especially for children, leading to a compromised quality of life after chemotherapy.^{1,2}

According to the emetogenic classification of Pediatric Oncologic Group of Ontario (POGO) from October 2017, various drugs commonly used for the chemotherapy of osteosarcomas in children are classified as highly emetogenic (cisplatin intravenously (i.v.) ≥ 12 mg/m²/dose; doxorubicin i.v. ≥ 30 mg/m²/dose; and methotrexate i.v. ≥ 12 g/m²/dose) and moderately emetogenic (methotrexate i.v. 5 g/m²/dose; and doxorubicin i.v. 25 mg/m²/dose).³ Moreover, even with the best antiemetic regimes, nausea and vomiting continue to be the most irksome aftermath of chemotherapy in children.³

Cisplatin- or doxorubicin-induced emesis was predominant before the 1980s. In the 1990s, a combination of a corticosteroid and a 5-hydroxytryptamine-3 (5-HT₃) receptor antagonist became customary practice. The use of high-dose metoclopramide and dexamethasone proved to be effective to a certain degree.⁴ However, specific adverse effects, especially extrapyramidal reactions, commonly found in children and adolescents, have curbed the use of high-dose metoclopramide.

5-hydroxytryptamine-3 receptor antagonists are now gold standard for acute chemotherapy-induced nausea and vomiting (CINV) prevention therapy, since emesis is triggered through the activation of 5-HT₃ receptors by serotonin released from enterochromaffin cells in the small intestine, located on vagal afferents.^{5,6} The effectiveness of first-generation 5-HT₃ receptor antagonists in preventing acute CINV ranges from 50% to 70%.³ Although there has been a significant improvement in drug therapy in view of CINV, about 50% of patients present with acute or delayed CINV following moderate emetogenic chemotherapy (MEC) or highly emetogenic chemotherapy (HEC).^{7,8} Consequently, there is an ample scope of research in the field of controlling CINV.

The combination of dexamethasone with first-generation 5-HT₃ receptor antagonists is effective against acute CINV^{9–14}; however, a second-generation 5-HT₃ receptor antagonist, palonosetron, which is dynamic, extremely selective, and has great receptor binding capacity along with prolonged plasma half-life (40 h), is quite potent as a single dose in preventing both acute and delayed CINV related to MEC and HEC.^{9–13} Still, very few studies have been conducted so far to establish

the superiority of single-dose palonosetron over the combination of drugs to control CINV in patients undergoing HEC.^{9,14–16}

No standard pediatric antiemetic treatment has yet been implemented, considering all advances and the inclusion of newer and improved medication regimens in the treatment of CINV. This research was carried out on this unique population prone to nausea and vomiting in order to assess the effectiveness and side effects of antiemetics.

Objectives

The goal of this study was to evaluate the efficacy of palonosetron compared to granisetron in treating CINV in pediatric patients who received HEC for osteosarcoma. The research primarily focused on estimating the prevalence of CINV after applying the 2 drugs.

Materials and methods

Patient recruitment and selection

To fulfil the research objectives, the authors planned a randomized, controlled, double-blind clinical trial, which was conducted at the Department of Pediatrics of Chengdu University, China. The study was approved by the institutional review board and the local ethical committee (protocol CU # RC/IRB/2016/1042). All the procedures performed in the study involving human participants were in accordance with the ethical standards of the institutional research committee of Chengdu Jinniu District People's Hospital and Ya'an People's Hospital in China, and comply with the 1964 Declaration of Helsinki and its later amendments or comparable ethical standards. Written informed consent was obtained from all the participants.

The study enrolled consecutive children with osteosarcoma, aged <18 years, but not below 3 years of age, receiving HEC in the outpatient (daycare) or inpatient settings from August 2016 to August 2019.

All patients without systemic complications who strictly satisfied the inclusion criteria were included.

The exclusion criteria were as follows: children with abnormal liver function test (LFT) or renal function test (RFT) results, or those with organic disorders likely to cause vomiting; children who were on concurrent radiotherapy or received radiotherapy within 1 week prior to the study period; patients who were on antiemetic therapy within the first 24 h of recruitment; patients with known hypersensitivity toward any study drug; and patients with other adverse effects associated with chemotherapy. Furthermore, the anticipatory vomiting could create confusion in the results; the participants were not scheduled for successive chemotherapy.

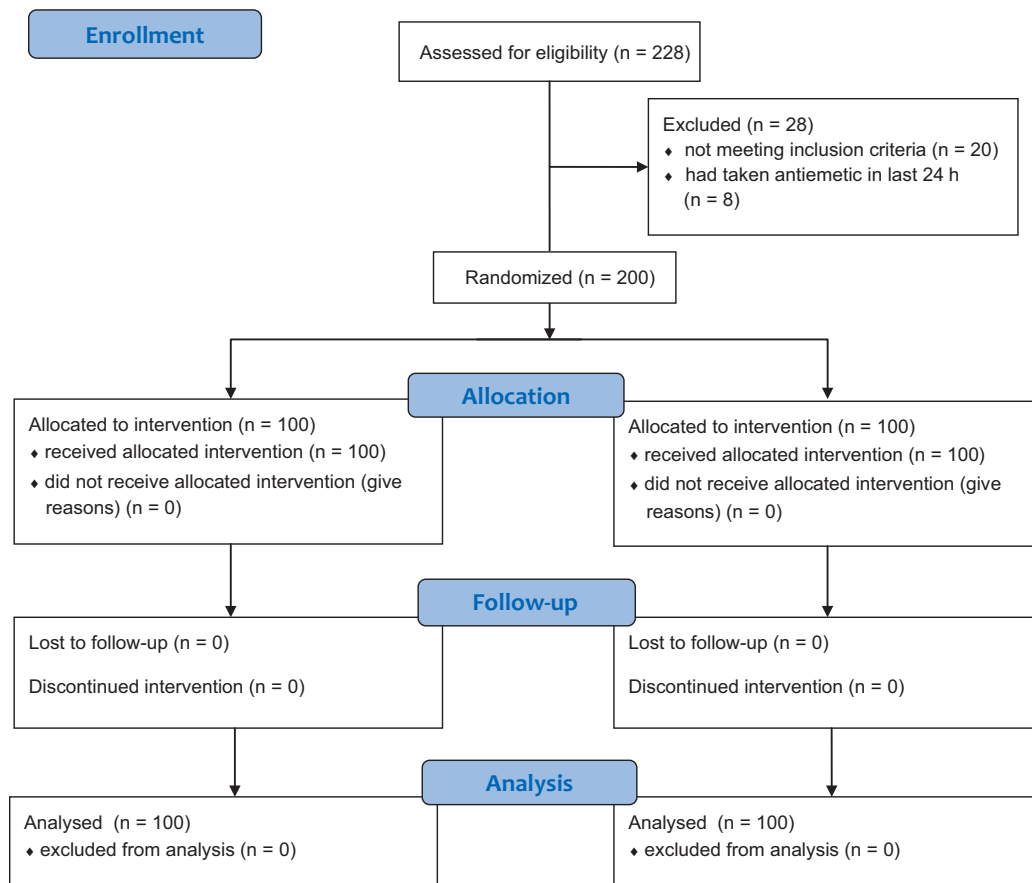


Fig. 1. Patient recruitment and selection (Consolidated Standards of Reporting Trials (CONSORT) flow diagram)

The patient sample size was calculated using the following formula (Equation 1)¹⁷:

$$n = \frac{N}{1 + N(e)^2} \quad (1)$$

where:

- n – sample size;
- N – population size; and
- e – level of precision.

For the present study, the population size was determined based on the number of patients admitted to hospital or referred to treatment due to osteosarcoma (total population size: N = 228 for 1 month, and e is 0.05 at 95% confidence interval (95% CI)). The 2 groups received an equal number of patients. Although, a total of 228 patients were enrolled in the study. Approximately 12% of subjects, i.e., 28 subjects, did not meet the inclusion criteria. Therefore, a total number of 200 patients were evaluated, i.e., 100 patients in each group.

The osteosarcoma therapy regimen according to the EURAMOS-1 guidelines was used¹⁴:

- high-dose methotrexate (12 g/m²) in 1 L of 5% dextrose water solution with 1 mEq/kg of sodium bicarbonate administered as a 4-hour infusion + etoposide (75 mg/m² i.v.) over 1 h in 250–500 mL saline serum and ifosfamide (3 g/m²/day i.v.) over 3 h in 250–500 mL saline serum;
- cisplatin 120 mg/m² (a 4-hour infusion of 60 mg/m² per day), doxorubicin (70 mg/m²) administered as a 6-hour

continuous infusion, and high-dose methotrexate (12 g/m²) in 1 L of 5% dextrose water solution with 1 mEq/kg of sodium bicarbonate, administered as a 4-hour infusion.

The POGO guidelines were followed for classifying the emetogenic potential of each chemotherapy regimen.³ Single- or multiple-day chemotherapy was considered as 1 session.

Standard antiemetic prophylaxis for HEC included a 5-HT₃ receptor antagonists, i.e., palonosetron administered i.v. in a single fixed dose of 20 µg/kg (maximum total dose of 0.75 mg) over 30 s, or granisetron administered i.v. in a single dose of 40 µg/kg over 5 min; it was based on the data available from previous pediatric studies.¹⁵ Both drugs were delivered via the intravenous route 30 min before initiating HEC. Patients with 1–2 episodes of breakthrough vomiting received dexamethasone i.v. (for body surface area (BSA) ≤0.6 m², 2 mg twice a day, and for BSA > 0.6 m², 4 mg twice a day) as a rescue medication.

Patients satisfying the eligibility criteria were randomized, regardless of age and sex, to receive either palonosetron or granisetron, using a computer-generated randomization schedule. The schedule was packed in a sealed envelope, which 2 designated persons opened at the beginning of chemotherapy. All patients were randomly allocated to group 1 (palonosetron; n = 100) or group 2 (granisetron; n = 100).¹⁷

Except for the independent pharmacists dispensing the research drugs at the hospital and the person

responsible for drug allocation, all study staff and participants were blinded to treatment assignment for the study duration. They were also forbidden to reveal any drug allocation data to other persons.

Outcome variables

The evaluation of chemotherapy-induced nausea (CIN) or CINV was based on the following parameters: nausea (presence or absence); and vomiting (frequency, duration and severity).

Following the instructions, the patient or their caregiver kept track of emetic episodes and the degree of nausea in the diaries given. The children used the pediatric nausea assessment tool (PeNAT)¹⁸ to self-report nausea intensity twice a day, in the morning and at bedtime at the very least, as well as any other time the child felt nauseous or their guardian thought the child would feel nauseous. The PeNAT is made up of 3 parts: determining the words or expressions for nausea that are used in each child's family; a script that focuses the child's attention on the subjective symptoms of nausea and explains the PeNAT; and a four-faced nausea severity scale. A co-investigator gave the PeNAT to each kid initially, and then taught the child's caregiver how to use it. The caregiver or a healthcare practitioner might help the patient complete nausea severity evaluation, but they could only record the information supplied by the child. They did not make the proxy evaluation of the child's nausea intensity. While monitoring the acute stages of CINV, the patients or their caregivers were approached in person to encourage adherence to research protocols and collect the completed diaries. The number of times the child vomited was subtracted from the number of vomiting episodes noted in the health record, if the child has not completed the diary in which they mentioned the number of vomiting episodes.

The following definitions were used in the evaluation: 'nausea' – the sensation of being about to vomit; usually, it was a prodromal symptom of vomiting; and 'vomiting' – a retrograde and vigorous removal of the stomach contents.

Acute emesis was identified as any vomiting during the period starting with the first chemotherapy dose and continuing until 24 h after the last chemotherapy dose completed in that block (acute phase). A complete response (CR) was described as the absence of acute vomiting without any rescue medication. If the patient had 1–2 episodes of vomiting without the use of a rescue medication, the response was deemed partial; if the patient had more than 2 episodes of vomiting and/or used a rescue medicine, it was regarded as failure. A rescue medication was given to the children who had more than 2 vomiting episodes.^{9,15}

For children who vomit after receiving dexamethasone, an add-on rescue medicine is allowed – lorazepam at a dose of 0.025 mg/kg for chronic vomiting at the discretion of the treating primary care doctor.

A pre-designed worksheet was prepared for the patient so that all details could be included. To facilitate the documentation of emetic episodes, a notebook was provided to the patient or their caregiver. For a particular session of chemotherapy, the responsibility was given to the child or their parents to inform the researchers on each and every incidence of vomiting for a period of 2, 4, 6, 8, 12, 18, and 24 h from the completion of chemotherapy or the last dose of rescue medicines.

The response was reported as the number and timing of episodes (to distinguish CR/a partial response/failure) and the use of rescue medications. The primary efficacy endpoint was the proportion of CR patients during the acute period in the 1st on-study cycle of chemotherapy. The secondary endpoint was the proportion of patients in the 1st on-study cycle needing rescue antiemetic treatment during the acute period. The response was also analyzed in the group 1 (palonosetron) and group 2 (granisetron) arms of all subsequent chemotherapy sessions during the study period.

To avoid the confounding effect of anticipatory vomiting, the subjects were not included in the subsequent cycles of chemotherapy.

The adverse events related to palonosetron or granisetron were carefully evaluated by taking a relevant history and conducting a physical examination at the time of the initiation of chemotherapy, on discharge and during the next chemotherapy session. Lab investigations were done as per the chemotherapy session scheduled, including complete blood count (CBC), LFT and RFT. All sorts of adverse events were recorded according to Common Terminology Criteria for Adverse Events (CTCAE), v. 4.03, available at the National Cancer Institute website (https://ctep.cancer.gov/protocoldevelopment/electronic_applications/ctc.htm#ctc_40). Adverse events were recorded for up to 10 days from the day of the administration of the drug; the treating physician's opinion on the relationship between adverse events and the study drug was also recorded.

Statistical analyses

The researchers hypothesized that the palonosetron group would be better than the granisetron group in terms of CR following HEC for osteosarcoma. Alternatively, a null hypothesis was given by the researchers, which advocated that there was no statistically significant difference between the 2 groups. The level of significance was adjusted to a p-value equal to 0.05. To test the null hypothesis and compare CR between the 2 groups, the χ^2 test for categorical variables was conducted.

The statistical analysis was carried out using the IBM SPSS Statistics for Windows software, v. 21.0 (IBM Corp., Armonk, USA). The univariate analysis was carried out to evaluate the risk factors associated with emesis, and the frequency distribution was done for the various demographic factors considered and other clinical parameters

in the study. The relative risk (RR) was measured to compare the RR of emesis between the 2 groups. The χ^2 test was used to evaluate the association between the response and antiemetic prophylaxis for the study groups. All data, except for age, were categorical in nature, involving only frequencies with mutually exclusive independent variables and the expected frequency count for each cell of the tables >5 . In the light of these characteristics, the χ^2 test was chosen as the appropriate test for the study.

The statistical analysis was carried out at 95% CI, with the level of significance set at 0.05, i.e., $p < 0.05$ was considered as a statistically significant difference.

Results

The study sample size was 228 patients, randomly allocated to group 1 (palonosetron) and group 2 (granisetron). A total of 28 patients were excluded from the study, and thus 200 were included in the analysis. These 200 patients received 604 blocks of chemotherapy. Figure 1 presents the flow diagram for patient recruitment and selection.

Essentially, the distribution of all variables in the 2 groups was balanced.

Among the 200 subjects equally distributed in the 2 groups, there were 68% males and 32% females in group 1, and 64% males and 36% females in group 2. The mean age in group 1 was 10.2 ± 2.8 years, and in group 2, it was 10.5 ± 1.9 years. There were 37% patients aged ≤ 10 years and 63% aged >10 years in group 1, while group 2 had 31% patients aged ≤ 10 years and 69% aged >10 years (Table 1).

Table 2 shows the response to antiemetic prophylaxis doses in both study groups. A complete response was

observed in 83% of patients in group 1, while in group 2, 72% of patients showed CR. A partial response was evident in 11% of the participants from group 1 and in 23% in group 2. The failure of antiemetic prophylaxis was evident in 6% in group 1, whereas in group 2, the percentage of failure was 5%. The difference in the response to antiemetic prophylaxis between the study groups was statistically significant ($p = 0.002$). The RR value for antiemetic prophylaxis was 0.65 (95% CI: [0.26; 2.81]), i.e., the risk of vomiting was 0.65 times smaller in group 1 than in group 2, with a p-value of 0.040, which was statistically significant (Table 2).

Table 3 presents the RR values in both study groups during the subsequent cycles of chemotherapy. The RR of breakthrough vomiting was lesser in the palonosetron arm across all chemotherapy cycles when compared to the granisetron arm (Table 3).

The univariate analysis results regarding factors that might affect the response to antiemetic prophylaxis in both groups are summarized in Table 4. Gender, age and the type of osteosarcoma did not significantly influence the response in either group ($p > 0.05$). The prophylactic dosage of a rescue medicine, dexamethasone, was the only statistically significant predisposing factor associated with emesis ($p = 0.001$), as shown in Table 4.

Ten patients (2 in group 1 and 8 in group 2) had headaches, and 6 patients (3 in each arm) had constipation requiring laxatives during the 1st on-study chemotherapy cycle. Similarly, 14 patients had abdominal pain (8 in group 1 and 6 in group 2) and 10 patients had diarrhea (4 in group 1 and 6 in group 2). These effects were considered by the treating physician as related to the drug. There were no serious adverse events associated with either drug, and none that required the discontinuation of the therapy.

Table 1. Baseline demographic and disease characteristics in the study groups

Characteristic		Group 1 n = 100	Group 2 n = 100
Gender n (%)	male	68 (68)	64 (64)
	female	32 (32)	36 (36)
Age [years] n (%)	M \pm SD	10.2 \pm 2.8	10.5 \pm 1.9
	≤ 10	37 (37)	31 (31)
	>10	63 (63)	69 (69)
Type of osteosarcoma n (%)	peripheral	33 (33)	39 (39)
	medullary (axial)	67 (67)	61 (61)

Group 1 – palonosetron; Group 2 – granisetron; n – number; M – mean; SD – standard deviation.

Table 2. Response to antiemetic prophylaxis in the study groups (χ^2 test)

Response	Group 1 n = 100	Group 2 n = 100	χ^2	p-value	RR	95% CI	p-value
CR	83 (83)	72 (72)	34.812	0.002*	0.65	[0.26; 2.81]	0.004*
Partial response	11 (11)	23 (23)					
Failure	6 (6)	5 (5)					

Data are presented as n (%). CR – complete response; RR – relative risk; 95% CI – 95% confidence interval; * statistically significant.

Table 3. Relative risk (RR) of vomiting in the palonosetron arm in comparison with the granisetron arm during the subsequent cycles of chemotherapy

Cycle	RR	95% CI
1 st cycle	0.78	[0.48; 1.89]
2 nd cycle	0.61	[0.33; 2.23]
3 rd cycle	0.81	[0.51; 2.95]
4 th cycle	0.88	[0.62; 2.98]
5 th cycle	0.72	[0.47; 3.19]
6 th cycle	0.71	[0.39; 3.69]

95% CI – 95% confidence interval.

Discussion

The prime reason behind this cohort study was to compare single-dose palonosetron with granisetron for CINV after the treatment of osteosarcoma in pediatric patients. The outcomes of this study confirm the hypothesis stating that there would be a significant difference between the groups in terms of CR and RR of breakthrough emesis ($p < 0.05$); group 1 demonstrated a substantial downside incidence of vomiting and a decreased risk of breakthrough vomiting in comparison with group 2.

Based on the end results, the use of palonosetron is warranted in the prevention of CINV in osteosarcoma pediatric patients undergoing HEC, and could be associated with a decreased risk of undesirable side effects, such as breakthrough vomiting in the postoperative period and the resultant inconvenience for patients and their parents.

Due to the multiple adverse effects of chemotherapeutic agents, a combination of antiemetic agents must be tested, such as preventing the stimulation of dopamine D2 receptor in the chemoreceptor trigger zone (CTZ) and binding neurokinin-1 (NK-1) receptor with substance P in the area postrema.^{19,20}

Although the addition of a corticosteroid improves the potency of 5-HT3 receptor antagonists against CINV in different clinical trials, the best standard single-dose

treatment with 5-HT3 receptor antagonists for pediatric emesis has not yet been demonstrated, particularly in the acute chemotherapy phase, i.e., the first 24 h. Few studies have reported the potency of a dopamine D2 receptor antagonist in the prevention of acute emesis⁹; however, the guidelines for the prevention of CINV do not consider those regimens due to faults in the study design.

Although a 5-HT3 receptor antagonist has been administered multiple times to control acute CINV in previous clinical trials, particularly randomized clinical trials (RCTs), the superiority of single-dose pre-chemotherapy administration has not been shown.¹⁰ The contemporary literature indicates that a combination of a 5-HT3 receptor antagonist, a steroid and a NK-1 receptor antagonist¹⁰ is the most common practice for blocking nausea and vomiting initiated by MEC or HEC.⁹

Palonosetron interacts with the 5-HT3 receptor both competitively and non-competitively, while ondansetron and granisetron exhibit strictly competitive antagonistic properties. The dual activity of palonosetron against 5-HT3 receptor is believed to increase the inhibitory effect on the primary receptor, since allosteric interactions can induce receptor conformation changes.⁹

Palonosetron at fixed doses has been found to be safe and potent enough to prevent CINV, whether acute or delayed, in adults.²⁰ However, there is no consensus on using palonosetron at fixed doses in pediatric patients receiving chemotherapy for various malignancies. Recently, the POGO and Multinational Association of Supportive Care in Cancer/European Society for Medical Oncology (MASCC/ESMO) guidelines have been released on the inclusion of palonosetron for pediatric patients receiving MEC and HEC.^{21,22}

In the present study, at all intervals except zero-two, the palonosetron PeNAT mean adjusted scores were significantly lower ($p < 0.001$) than when compared to granisetron. It means that the children have reported less episodes of vomiting when compared to granisetron group. In a similar study, for the granisetron and metoclopramide+dimenhydrinate groups, the proportion

Table 4. Univariate analysis of factors that might affect the response to antiemetic prophylaxis

Potential risk factor for emesis	CR (both groups) n = 155	Partial response or failure		χ^2	p-value
		group 1 n = 17	group 2 n = 28		
Gender	male	104 (67.1)	12 (70.6)	42.34	0.230
	female	51 (32.9)	5 (29.4)		
Age [years]	≤10	46 (29.7)	12 (70.6)	23.91	0.410
	>10	109 (70.3)	5 (29.4)		
Type of osteosarcoma	peripheral	54 (34.8)	8 (47.1)	18.19	0.310
	medullary (axial)	101 (65.2)	9 (52.9)		
Dexamethasone	yes	92 (59.4)	14 (82.4)	27.81	0.001*
	no	63 (40.6)	3 (17.6)		

CR – complete response. Data presented as n (%). * statistically significant.

of CR patients (not more than 1 episode of vomiting) was 80.0% and 27.5%, respectively ($p < 0.001$).¹⁸

Moreover, the findings of the current study are in accordance with previous research, where the rate of CR due to palonosetron was 60–94%.^{15,22–30} This was attributed to the receptor binding potential of palonosetron. Furthermore, long-lasting effects on receptor–ligand binding and functional responses to serotonin can be associated with this sort of receptor interaction. Palonosetron has proven to be effective and safe.

In certain studies, gender, age, the type of tumor, the emetogenicity of the regimen, and the choice of prophylactic agents have been shown to influence the rate of CR.^{15,19–23} In the present study, factors like gender, age, the treatment regimen, and the number of rescue medications (dexamethasone) were evaluated as potential risk factors that might affect the response during the overall treatment. It was found that the use of dexamethasone was the only statistically significant predisposing risk factor. Other factors, like gender, age, the type of osteosarcoma, and the treatment regimen, were not statistically significantly associated with emesis.

The major strength of this study is that a fixed dose of palonosetron was used for pediatric osteosarcoma patients who underwent HEC, and the dosage was based on the child's BSA and body weight. In contrast, other researchers advocated using a single fixed dose of palonosetron regardless of the child's BSA and body weight.^{14,15} Secondly, the PeNAT scale was specially designed for the pediatric group to evaluate CINV more accurately. Thirdly, this study was performed exclusively on pediatric patients who underwent HEC, according to the POGO guidelines for osteosarcoma.

Limitations

This RCT has several limitations. Firstly, it was a single-center study with a smaller sample size to establish the superiority of palonosetron over granisetron. Large multicenter trials are needed to lead to clinically meaningful conclusions. Secondly, the potency of the palonosetron needs to be investigated in other pediatric patients with other malignancies, undergoing MEC or HEC, so that CINV can be controlled more effectively and the patients' quality of life can be improved. Thirdly, the present study was limited to the acute phase of CINV, i.e., the first 24 h, and it did not explore the rate of CR in the delayed phase of CINV. Moreover, the present study was not enrolled in the clinical trial registry for RCTs.

Conclusions

Palonosetron seems to be safe and potent when used in a fixed dose of 20 µg/kg in pediatric patients with osteosarcoma in preventing CINV. It is quite effective alone


in controlling CINV with a minimal requirement for rescue medications. Furthermore, it could be recommended in developing countries with limited resources.


Availability of data and materials


The datasets used and/or analyzed during the current study are available from the corresponding author on a reasonable request.

ORCID iDs


Zheng Li  <https://orcid.org/0000-0001-9567-6924>

Chun Li  <https://orcid.org/0000-0001-7570-5409>

Ping Li  <https://orcid.org/0000-0001-8490-6640>

Yugang Li  <https://orcid.org/0000-0002-5342-7804>

Jin Lai  <https://orcid.org/0000-0002-8170-2332>

Sanjay Rastogi  <https://orcid.org/0000-0001-8573-3075>

References

1. Holdsworth MT, Raisch DW, Frost J. Acute and delayed nausea and emesis control in pediatric oncology patients. *Cancer*. 2006;106(4):931–940. doi:10.1002/cncr.21631
2. Miller M, Kearney N. Chemotherapy-related nausea and vomiting: Past reflections, present practice and future management. *Eur J Cancer Care (Engl)*. 2004;13(1):71–81. doi:10.1111/j.1365-2354.2004.00446.x
3. Patel P, Robinson PD, Thackray J, et al. Guideline for the prevention of acute chemotherapy-induced nausea and vomiting in pediatric cancer patients: A focused update. *Pediatr Blood Cancer*. 2017;64(10). doi:10.1002/pbc.26542
4. Allen JC, Gralla R, Reilly L, Kellick M, Young C. Metoclopramide: Dose-related toxicity and preliminary antiemetic studies in children receiving cancer chemotherapy. *J Clin Oncol*. 1985;3(8):1136–1141. doi:10.1200/JCO.1985.3.8.1136
5. Balfour JA, Goa KL. Dolasetron: A review of its pharmacology and therapeutic potential in the management of nausea and vomiting induced by chemotherapy, radiotherapy or surgery. *Drugs*. 1997;54(2):273–298. doi:10.2165/00003495-199754020-00008
6. Hasler WL. Serotonin receptor physiology: Relation to emesis. *Dig Dis Sci*. 1999;44(8 Suppl):108S–113S. PMID:10490049.
7. Grunberg SM, Deuson RR, Mavros P, et al. Incidence of chemotherapy-induced nausea and emesis after modern antiemetics. *Cancer*. 2004;100(10):2261–2268. doi:10.1002/cncr.20230
8. Hickok JT, Roscoe JA, Morrow GR, King DK, Atkins JN, Fitch TR. Nausea and emesis remain significant problems of chemotherapy despite prophylaxis with 5-hydroxytryptamine-3 antiemetics: A University of Rochester James P. Wilmot Cancer Center Community Clinical Oncology Program Study of 360 cancer patients treated in the community. *Cancer*. 2003;97(11):2880–2886. doi:10.1002/cncr.11408
9. Saito M, Aogi K, Sekine I, et al. Palonosetron plus dexamethasone versus granisetron plus dexamethasone for prevention of nausea and vomiting during chemotherapy: A double-blind, double-dummy, randomised, comparative phase III trial. *Lancet Oncol*. 2009;10(2):115–124. doi:10.1016/S1470-2045(08)70313-9
10. Aapro MS, Grunberg SM, Manikhas GM, et al. A phase III, double-blind, randomized trial of palonosetron compared with ondansetron in preventing chemotherapy-induced nausea and vomiting following highly emetogenic chemotherapy. *Ann Oncol*. 2006;17(9):1441–1449. doi:10.1093/annonc/mdl137
11. Eisenberg P, Figueroa-Vadillo J, Zamora R, et al. Improved prevention of moderately emetogenic chemotherapy-induced nausea and vomiting with palonosetron, a pharmacologically novel 5-HT₃ receptor antagonist: Results of a phase III, single-dose trial versus dolasetron. *Cancer*. 2003;98(11):2473–2482. doi:10.1002/cncr.11817
12. Eisenberg P, MacKintosh FR, Ritch P, Cornett PA, Macciocchi A. Efficacy, safety and pharmacokinetics of palonosetron in patients receiving highly emetogenic cisplatin-based chemotherapy: A dose-ranging clinical study. *Ann Oncol*. 2004;15(2):330–337. doi:10.1093/annonc/mdh047

13. Gralla R, Lichinitser M, Van Der Vegt S, et al. Palonosetron improves prevention of chemotherapy-induced nausea and vomiting following moderately emetogenic chemotherapy: Results of a double-blind randomized phase III trial comparing single doses of palonosetron with ondansetron. *Ann Oncol*. 2003;14(10):1570–1577. doi:10.1093/annonc/mdg417
14. Marina NM, Smeland S, Bielack SS, et al. Comparison of MAPIE versus MAP in patients with a poor response to preoperative chemotherapy for newly diagnosed high-grade osteosarcoma (EURAMOS-1): An open-label, international, randomised controlled trial. *Lancet Oncol*. 2016;17(10):1396–1408. doi:10.1016/S1470-2045(16)30214-5
15. Jain S, Kapoor G, Koneru S, Vishwakarma G. A randomized, open-label non-inferiority study to compare palonosetron and ondansetron for prevention of acute chemotherapy-induced vomiting in children with cancer receiving moderate or high emetogenic chemotherapy. *Support Care Cancer*. 2018;26(9):3091–3097. doi:10.1007/s00520-018-4158-5
16. Chaudhary NK, John RR, Boddu D, Mahasampath G, Nesadeepam N, Mathew LG. Palonosetron is a better choice compared with ondansetron for the prevention of chemotherapy-induced nausea and vomiting (CINV) in a resource-limited pediatric oncology center: Results from a randomized control trial. *J Pediatr Hematol Oncol*. 2019;41(4):294–297. doi:10.1097/MPH.0000000000001357
17. Adam AM. Sample size determination in survey research. *J Sci Res Rep*. 2020;26(5):90–97. doi:10.9734/jsrr/2020/v26i530263
18. Dupuis LL, Taddio A, Kerr EN, Kelly A, MacKeigan L. Development and validation of the pediatric nausea assessment tool for use in children receiving antineoplastic agents. *Pharmacotherapy*. 2006;26(9):1221–1231. doi:10.1592/phco.26.9.1221
19. McNulty R. Are all 5-HT₃ receptor antagonists the same? *J Natl Compr Canc Netw*. 2007;5(1):35–43. doi:10.6004/jnccn.2007.0005
20. van der Vorst MJDL, Toffoli EC, Beusink M, et al. Metoclopramide, dexamethasone, or palonosetron for prevention of delayed chemotherapy-induced nausea and vomiting after moderately emetogenic chemotherapy (MEDEA): A randomized, phase III, noninferiority trial. *Oncologist*. 2021;26(1):e173–e181. doi:10.1634/theoncologist.2020-0305
21. Dupuis LL, Sung L, Molassiotis A, Orsay AD, Tissing W, van de Wetering M. 2016 updated MASCC/ESMO consensus recommendations: Prevention of acute chemotherapy-induced nausea and vomiting in children. *Support Care Cancer*. 2016;25(1):323–331. doi:10.1007/s00520-016-3384-y
22. Nadaraja S, Mamoudou AD, Thomassen H, Wehner PS, Rosthøj S, Schroeder H. Palonosetron for the prevention of nausea and vomiting in children with acute lymphoblastic leukemia treated with high dose methotrexate. *Pediatr Blood Cancer*. 2017;59(5):870–873. doi:10.1002/pbc.24068
23. Uchida M, Mori Y, Nakamura T, et al. Comparison between antiemetic effects of palonosetron and granisetron on chemotherapy-induced nausea and vomiting in Japanese patients treated with R-CHOP. *Biol Pharm Bull*. 2017;40(9):1499–1505. doi:10.1248/bpb.b17-00318
24. Navari RM. Management of chemotherapy-induced nausea and vomiting in pediatric patients. *Paediatr Drugs*. 2017;19(3):213–222. doi:10.1007/s40272-017-0228-2
25. Patil V, Prasada H, Prasad K, Shenoy UV. Comparison of antiemetic efficacy and safety of palonosetron vs ondansetron in the prevention of chemotherapy-induced nausea and vomiting in children. *J Community Support Oncol*. 2015;13(6):209–213. doi:10.12788/jcso.0139
26. Sherani F, Boston C, Mba N. Latest update on prevention of acute chemotherapy-induced nausea and vomiting in pediatric cancer patients. *Curr Oncol Rep*. 2019;21(10):89. doi:10.1007/s11912-019-0840-0
27. Kovács G, Wachtel AE, Basharova EV, Spinelli T, Nicolas P, Kabickova E. Palonosetron versus ondansetron for prevention of chemotherapy-induced nausea and vomiting in paediatric patients with cancer receiving moderately or highly emetogenic chemotherapy: A randomised, phase 3, double-blind, double-dummy, non-inferiority study. *Lancet Oncol*. 2016;17(3):332–344. doi:10.1016/S1470-2045(15)00520-3
28. Vol H, Flank J, Lavoratore SR, et al. Poor chemotherapy-induced nausea and vomiting control in children receiving intermediate or high dose methotrexate. *Support Care Cancer*. 2016;24(3):1365–1371. doi:10.1007/s00520-015-2924-1
29. Parathoduvil AA, Sisupalan A, Rema PL. Comparison of antiemetic effectiveness of palonosetron versus ondansetron in patients on cancer chemotherapy: A prospective observational study in South Indians. *J Clin Diagn Res*. 2017;11(5):FC10–FC14. doi:10.7860/JCDR/2017/25129.9818
30. Tan J, Wang S, Liang X, et al. Palonosetron is nonsuperior to ondansetron in acute phase but provides superior antiemetic control in delayed phase for pediatric patients administered highly emetogenic chemotherapy. *Pediatr Blood Cancer*. 2018;65(2). doi:10.1002/pbc.26815

Determination of serum vascular endothelial growth factor (VEGF) and VEGF receptor levels with *VEGF* gene polymorphisms in patients with Behçet's uveitis

Erdim Sertoglu^{1,A,C-F}, Çiğdem Yücel^{1,B,D}, Ahmet Omma^{2,A,B}, Yıldız Hayran^{3,B,C}, Seda Colak^{3,B,D}, Sevinc Can Sandıkçı^{2,A,B,D}, Ali Hakan Durukan^{4,D-F}, Taner Ozgurtas^{1,D-F}

¹ Department of Clinical Biochemistry, Gulhane School of Medicine, University of Health Sciences, Ankara, Turkey

² Department of Rheumatology, Ankara Numune Training and Research Hospital, University of Health Sciences, Turkey

³ Department of Dermatology, Ankara Numune Training and Research Hospital, University of Health Sciences, Turkey

⁴ Department of Ophthalmology, Gulhane School of Medicine, University of Health Sciences, Ankara, Turkey

A – research concept and design; B – collection and/or assembly of data; C – data analysis and interpretation;

D – writing the article; E – critical revision of the article; F – final approval of the article

Advances in Clinical and Experimental Medicine, ISSN 1899–5276 (print), ISSN 2451–2680 (online)

Adv Clin Exp Med. 2022;31(3):231–240

Address for correspondence

Erdim Sertoglu

E-mail: erdimsertoglu@gmail.com

Funding sources

The study was supported by the Scientific Research Program of University of Health Sciences (grant No. 2018/079).

Conflict of interest

None declared

Received on August 25, 2021

Reviewed on September 7, 2021

Accepted on November 4, 2021

Published online on December 17, 2021

Cite as

Sertoglu E, Yücel Ç, Omma A, et al. Determination of serum vascular endothelial growth factor (VEGF) and VEGF receptor levels with VEGF gene polymorphisms in patients with Behçet's uveitis. *Adv Clin Exp Med.* 2022;31(3):231–240. doi:10.17219/acem/143586

DOI

10.17219/acem/143586

Copyright

© 2022 by Wrocław Medical University

This is an article distributed under the terms of the Creative Commons Attribution 3.0 Unported (CC BY 3.0) (<https://creativecommons.org/licenses/by/3.0/>)

Abstract

Background. Behçet's disease (BD) is a chronic inflammatory vasculitis affecting multiple organs. Uveitis is frequently seen in patients with BD, especially in Turkish population.

Objectives. To investigate vascular endothelial growth factor (*VEGF*) gene polymorphisms along with the levels of VEGF and VEGF receptors in patients with Behçet's uveitis (BU).

Materials and methods. Fifty-five BD-associated uveitis patients and 30 age- and sex-matched controls were included in this case-control study. The genotypes of the single nucleotide polymorphisms (SNPs): rs2010963 (+405G), rs3025039 (+936T) and rs699947 (–2598A) of the *VEGF-A* gene were determined using real-time polymerase chain reaction (RT-PCR) and serum levels of VEGF and VEGF receptors were measured using enzyme-linked immunosorbent assay (ELISA).

Results. No associations of the *VEGF* gene polymorphisms were observed in BD uveitis patients, but arthritis was present in 53.3% of patients not possessing CT genotype in C3025039→T polymorphism ($p = 0.024$). Although there were no statistically significant differences in serum VEGF-A, VEGF-C and soluble vascular endothelial growth factor receptor-3 (sVEGFR-3) levels ($p < 0.05$), serum vascular endothelial growth factor receptor-1 (VEGFR-1) and sVEGFR-3 levels were significantly higher in the BD group ($p < 0.001$ and $p = 0.001$, respectively). In addition, VEGF-C/soluble vascular endothelial growth factor receptor-2 (sVEGFR-2) ratio was significantly higher ($p < 0.001$), while VEGF-A/VEGFR-1 and VEGF-C/sVEGFR-3 ratios were significantly lower ($p < 0.001$ and $p = 0.033$, respectively) in BD patients compared to controls. Also, VEGF-C/sVEGFR-3 ($p = 0.024$, $r = 0.37$) and VEGF-C/sVEGFR-2 ($p = 0.020$, $r = 0.38$) ratios were positively correlated with disease duration.

Conclusions. The significant changes in sVEGFR-3 levels and VEGF-C/sVEGFR-3 ratio has shown that lymphangiogenesis processes might take place in the pathogenesis of BD uveitis, and these parameters can be important indicators of evaluation of BD patients with uveitis together with disease duration.

Key words: vascular endothelial growth factor, *VEGF* gene polymorphism, Behçet's disease, Behçet's uveitis

Background

Behçet's disease (BD) was described by Turkish dermatologist Dr. Hulusi Behçet as a disease with triple symptoms: oral aphthae, genital ulcers and uveitis with hypopyon.¹ Behçet's disease is a systemic immuno-inflammatory vasculitis occurring in young adults that is characterized by endothelial cell dysfunction. The most prominent feature of BD is systemic, dermal and ocular vasculitis with lymphocytic infiltration of vessels with different diameters. Ocular involvement can be the first finding in most BD patients from 2 to 4 years after disease onset, and it is one of the most important causes of morbidity as it may result in blindness.^{2,3} It is also more frequent and more severe in Turkish and Japanese BD patients. In a study conducted in Turkey, eye involvement in form of uveitis/retinal vasculitis was reported in 29.1% of patients, while early age of onset and male gender were poor prognostic factors for ocular findings.^{4,5}

Although many studies have been published since BD was first described, its etiopathogenesis is not fully defined yet. The disease tendency appears to be related to *HLA-B* gene polymorphisms.^{6–10} Human major histocompatibility complex class I chain-related gene A was also shown to be related to the disease pathogenesis.^{8,11} However, the exact mechanisms about the genes related to the disease pathogenesis are still obscure.

Angiogenesis is a multistage process controlled by several pro-angiogenic and anti-angiogenic factors. Vascular endothelial growth factor (VEGF) is a potent endothelium-specific cytokine which modulates vasculogenesis and angiogenesis by acting as a major mitogen for endothelial cells. The VEGF plays an important role in the regulation of angiogenesis, wound healing, inflammation, and tumor progression.¹² Neutrophils, macrophages and vascular endothelial cells, which are involved in BD pathogenesis, primarily produce VEGF. The main stimulant in VEGF production in systemic and retinal endothelial cells is inflammation induced by pro-inflammatory cytokines. Since VEGF is a potent mitogen for dermal and ocular microvascular endothelial cells, VEGF expression in vascular beds of BD patients may be important in the clinical course of the disease. In our previous study, we indicated that elevated serum VEGF and sVEGFR-1, and – more importantly – VEGF/sVEGFR-1 ratio could play an important role in the development of thrombosis in BD.¹³ Thus, it has been suggested that plasma VEGF levels in BD may be affected by the course of the disease and may vary depending on the eye involvement or disease activity. There are also studies showing that VEGF is elevated especially in the active stage of BD and high VEGF levels can be associated with loss of vision as an additional risk factor.^{14,15}

The *VEGF* gene is highly polymorphic and more than 30 different single nucleotide polymorphisms (SNPs) have been previously reported. These polymorphisms are

important due to their effects on VEGF production and their relationship with BD. Studies have shown that both +405G/C (rs2010963) and +936C/T (rs3025039) SNPs reduce VEGF production.^{14–18} However, Salvarani et al. reported that VEGF (rs2010963) and VEGF-2549 18bp insertion/deletion (I/D) polymorphisms were associated with BD susceptibility.¹⁹ In addition, Nam et al. found that in the Korean population, the VEGF (rs2010963) polymorphism was associated with the development of ocular inflammation in BD.²⁰

Objectives

In this study, we aimed to evaluate: (1) the serum levels of VEGF-A, VEGF-C, vascular endothelial growth factor receptor-1 (VEGFR-1), soluble vascular endothelial growth factor receptor-2 (sVEGFR-2) and soluble vascular endothelial growth factor receptor-3 (sVEGFR-3), and correlation of their levels with the severity of BD; (2) the influence of the presence of polymorphisms (rs2010963, rs3025039 and rs699947) on the regulatory region of the VEGF gene, and to emphasize the importance of the detected polymorphisms in terms of disease development and severity in BD patients with ocular involvement in the Turkish population.

Materials and methods

The study protocol was approved by the Institutional Local Ethics Committee of Ankara Numune Training and Research Hospital, Ankara, Turkey (approval No. E-17-1612). The research protocol complies with the Declaration of Helsinki and written informed consent was obtained from all participants.

The present study is a cross-sectional study carried out in 55 Behçet's uveitis (BU) patients and 30 age/sex-matched controls admitted to Rheumatology and Eye Clinics of Gulhane and Numune Training and Research Hospital, Ankara, Turkey.

Criteria from the International Study Group for BD were used to evaluate BD patients.²¹ The disease activity was assessed with the Turkish version of BD Current Activity Form (BDCAF).²² The BDCAF score was calculated by adding up the scores on each item, and ranged from 0 to 12. Behçet's uveitis patients were defined as the ones with edema, non-perfusion, neovascularization, and atrophy of the retina and/or optic disc.²³

Overnight fasting blood samples were obtained from the antecubital vein and collected in blood tubes containing clot activator for serum separation. Sera were obtained by centrifugation at 3000 g × 10 min. For single nucleotide polymorphism (SNP) analysis, whole blood samples were collected into ethylenediamine tetraacetic acid (EDTA)-containing tubes.

Detection of serum levels of the study parameters

Serum VEGF-A(E-EL-H0111), VEGF-C(YLA0798HU), VEGFR-1(E-EL-H1087), sVEGFR-2(YLA1212HU), and sVEGFR-3(YLA1379HU) levels were measured using quantitative enzyme-linked immunosorbent assay (ELISA) kits (Elabscience, Wuhan, China for VEGF-A and VEGFR-1; Shanghai BiotechCo., Shanghai, China for VEGF-C, sVEGFR-2 and sVEGFR-3). The measurements were carried out using ELISA plate reader Bio-Tek Synergy HT (Biotek Instruments Inc., Winooski, USA). Intra- and inter-assay coefficients of variation (CVs) were 4.69% and 4.2%, respectively, with a sensitivity of 18.75 pg/mL for VEGF-A, <8%, <10% and 10.58 pg/mL, respectively, for VEGF-C, 5%, 4% and 75 pg/mL, respectively, for VEGFR-1, <8%, <10% and 22 pg/mL, respectively, for sVEGFR-2, and <8%, <10% and 114 pg/mL, respectively, for sVEGFR-3.

Selection of gene regions and SNP analysis

The reference sequences of the *VEGF* gene to be examined were downloaded from the National Biotechnology Information Center database of the National Library of Medicine within the American National Institutes of Health (NIH; Bethesda, USA). The primer pairs were specifically designed for the respective region of the *VEGF-A* gene for each SNP from the gene promoter region as rs2010963, rs3025039 and rs699947. The DNA concentration and purity were measured using a Nano-Drop 2000 spectrophotometer (Thermo Fisher Scientific, Munich, Germany). Genotyping of the relevant SNPs were performed using Taqman probes (Sigma-Aldrich, St. Louis, USA). The polymerase chain reaction (PCR) was performed for each sample as follows: 10 ng of genomic DNA, mixture of 10 μ L of Probe Master Kit (04707494001; Sigma-Aldrich), 1 μ L Reagent mix (TIB MolBiol, Berlin, Germany) and 4 μ L diH₂O were mixed to carry out polymerase chain reaction described below.

The amplification of DNA regions was carried out with LightCycler 480 (Roche Diagnostics, Basel, Switzerland) real-time PCR (RT-PCR) device. An initial denaturation of 1 min at 95°C was followed by 45 amplification cycles with 5 s at 95°C, 15 s at 60°C and 15 s at 65°C.

Statistical analyses

Statistical analyses were performed using IBM SPSS Statistics for Windows v. 21.0 (IBM Corp., Armonk, USA).

Categorical variables were presented as numbers or percentages and compared using the χ^2 or Fisher's exact test, as appropriate. Numerical variables were tested for normality using histogram and Kolmogorov–Smirnov test. Normally distributed variables were presented as mean (standard deviation (SD)) and variables which were not

normally distributed were presented as median (interquartile range (IQR)). To compare numerical variables, the Mann–Whitney U test was used when the variables were not normally distributed, and Student's t-test was used for normally distributed variables. The correlations between VEGF-A, VEGF-C, VEGFR-1, sVEGFR-2, sVEGFR-3, VEGF-A/VEGFR-1, VEGF-A/sVEGFR-2, VEGF-C/sVEGFR-2, VEGF-C/sVEGFR-3, and patient features such as age, age at diagnosis, and disease duration were analyzed using the Spearman's correlation test. An increase in one parameter as the other parameter decreased was considered as negative correlation, and an increase in one parameter as the other parameter increased was considered as positive correlation. Genotype distribution and allele frequencies of patients with the BD group and control group were analyzed using the χ^2 test. Odds ratios with 95% confidence intervals (95% CIs) were used to describe the risk of uveitis. The level of statistical significance was set at $p < 0.05$.

Results

There was no statistically significant difference between the 2 groups with respect to age and gender. Seventy-three percent (40) of BD patients and 70% (21) of controls were male. The mean age of the BD patients was 37.8 ± 9.1 years while that of controls was 39.2 ± 11 years.

Clinical features and disease manifestations presented by BD patients are summarized in Table 1. Serum levels of VEGF-A, VEGF-C, VEGFR-1, sVEGFR-2 and sVEGFR-3,

Table 1. Clinical features of BD patients

Parameter	Value
Age, mean (SD) [years]	37.8 \pm 9.1
Age at diagnosis, mean (SD) [years]	30.5 \pm 7.6
Disease duration, median (IQR) [months]	60 (36–117)
Female/male, n (%)	15 (27)/40 (73)
Active disease, n (%)	32 (58)
Behçet's Disease Current Activity Form	2.0 (0.0–3.0)
Disease manifestations ever presented by BD patients, n (%)	
Oral ulcers	55 (100)
Genital ulcers	36 (66)
Positive pathology test	9 (16)
Arthritis	25 (45)
Uveitis	55 (100)
Vascular involvement	20 (40)
Gastrointestinal system involvement	1 (2)
Pulmonary aneurism	1 (2)
Patients with family history of BD	6 (11)

Data are expressed as the mean (\pm SD), median (IQR) or number of cases (%) as appropriate. BD – Behçet's disease; SD – standard deviation; IQR – interquartile range.

Table 2. Differences in serum vascular endothelial growth factor (VEGF)-A, VEGF-C, VEGFR-1, sVEGFR-2 and sVEGFR-3 levels according to ocular involvement

Parameter	Patients with uveitis (n = 55)	Controls (n = 30)	p-value
VEGF-A [pg/mL]	163.5 (77.5–260.7)	31.8 (29.5–231.1)	0.188
VEGF-C [ng/mL]	482.8 (398.3–725.9)	522.8 (465.3–726.3)	0.251
VEGFR-1 [pg/mL]	57.9 (12.7–222.2)	1.69 (1.46–9.32)	<0.001
sVEGFR-2 [ng/mL]	3.31 (2.95–4.40)	3.05 (1.88–4.15)	0.076
sVEGFR-3 [ng/mL]	4.54 (3.64–6.15)	3.01 (1.90–4.16)	0.001
VEGF-A/VEGFR-1	1.78 (0.87–17.7)	20.3 (18.0–21.1)	<0.001
VEGF-A/sVEGFR-2	50.6 (24.6–63.2)	15.9 (9.45–102.5)	0.423
VEGF-C/sVEGFR-2	141 (123.9–176.5)	183.7 (155.2–283.4)	<0.001
VEGF-C/sVEGFR-3	96.3 (78.9–118.8)	183.8 (155.2–283.4)	0.033

All values are expressed as median, interquartile range (IQR; 25–75%). The p-values were calculated using Mann–Whitney U test. Values in bold are statistically significant, $p < 0.05$.

VEGF-A – vascular endothelial growth factor A; VEGF-C – vascular endothelial growth factor C; VEGFR-1 – vascular endothelial growth factor receptor-1; sVEGFR-2 – soluble vascular endothelial growth factor receptor-2; sVEGFR-3 – soluble vascular endothelial growth factor receptor-3.

and parameters calculated using factor receptor ratio among patients and control groups are presented in Table 2. According to these data, there were no statistically significant differences in mean serum VEGF-A and VEGF-C levels between the 2 groups. On the other hand, serum VEGFR-1 and sVEGFR-3 levels were statistically significantly higher in BD patients compared to controls, while there was no such difference in sVEGFR-2 levels. In addition, VEGF-C/sVEGFR-2 ratio was significantly higher ($p < 0.001$), while VEGF-A/VEGFR-1 and VEGF-C/sVEGFR-3 ratios were significantly lower ($p < 0.001$ and $p = 0.033$, respectively) in BD patients compared to controls.

When groups of patients with certain clinical manifestations were compared, VEGF-C/sVEGFR-2 ratios were significantly lower while VEGF-A/sVEGFR-2 ratios were above but close to the borderline statistical significance in patients with pathergy when compared to patients without this symptom (125 compared to 151, $p = 0.048$; 20.5 compared to 53.2, $p = 0.053$, respectively). The VEGF-A levels and VEGF-A/VEGFR-2 ratios were also lower

in patients with arthritis; however, no statistically significant difference was obtained ($p = 0.080$ and $p = 0.086$, respectively). Also, considering the relationship between polymorphisms and clinical findings of BD, no arthritis was observed in patients with CT genotype, while arthritis was only present in 53.3% of patients without CT genotype in $C^{3025039} \rightarrow T$ polymorphism ($p = 0.024$).

There was a moderately negative correlation between serum sVEGFR-2 and sVEGFR-3 levels and age ($p = 0.032$, $r = -0.35$ and $p = 0.003$, $r = -0.47$, respectively) and disease duration ($p = 0.048$, $r = -0.33$ and $p = 0.006$, $r = -0.44$, respectively). In addition, VEGF-C/sVEGFR-3 ($p = 0.024$, $r = 0.37$) and VEGF-C/sVEGFR-2 ($p = 0.020$, $r = 0.38$) were positively correlated with disease duration (Table 3 and Fig. 1).

Genotype and allele frequencies of patient and control groups were calculated for detected SNPs. The genotype and allele frequencies of the 3 selected polymorphisms, reported to regulate the production of VEGF, were not significantly different between BD and controls. The presence

Table 3. The correlations between parameters and age, age at diagnosis and disease duration

Parameters	Age		Age at diagnosis		Disease duration	
	p-value	r	p-value	r	p-value	r
VEGF-A [pg/mL]	0.904	0.02	0.777	0.05	0.809	0.04
VEGF-C [ng/mL]	0.406	-0.14	0.664	-0.07	0.878	-0.03
VEGFR-1 [pg/mL]	0.114	0.26	0.404	0.14	0.292	0.18
sVEGFR-2 [ng/mL]	0.032	-0.35	0.478	-0.12	0.048	-0.33
sVEGFR-3 [ng/mL]	0.003	-0.47	0.523	-0.11	0.006	-0.44
VEGF-A/VEGFR-1	0.251	-0.19	0.778	-0.05	0.333	-0.16
VEGF-A/sVEGFR-2	0.302	0.17	0.706	0.06	0.312	0.17
VEGF-C/sVEGFR-2	0.718	0.06	0.997	-0.01	0.020	0.38
VEGF-C/sVEGFR-3	0.052	0.32	0.593	0.09	<0.001	0.55

The p-values and correlation coefficients (r-values) were calculated using Spearman's test. Values in bold are statistically significant, due to $p < 0.05$.

VEGF-A – vascular endothelial growth factor A; VEGF-C – vascular endothelial growth factor C; VEGFR-1 – vascular endothelial growth factor receptor-1; sVEGFR-2 – soluble vascular endothelial growth factor receptor-2; sVEGFR-3 – soluble vascular endothelial growth factor receptor-3.

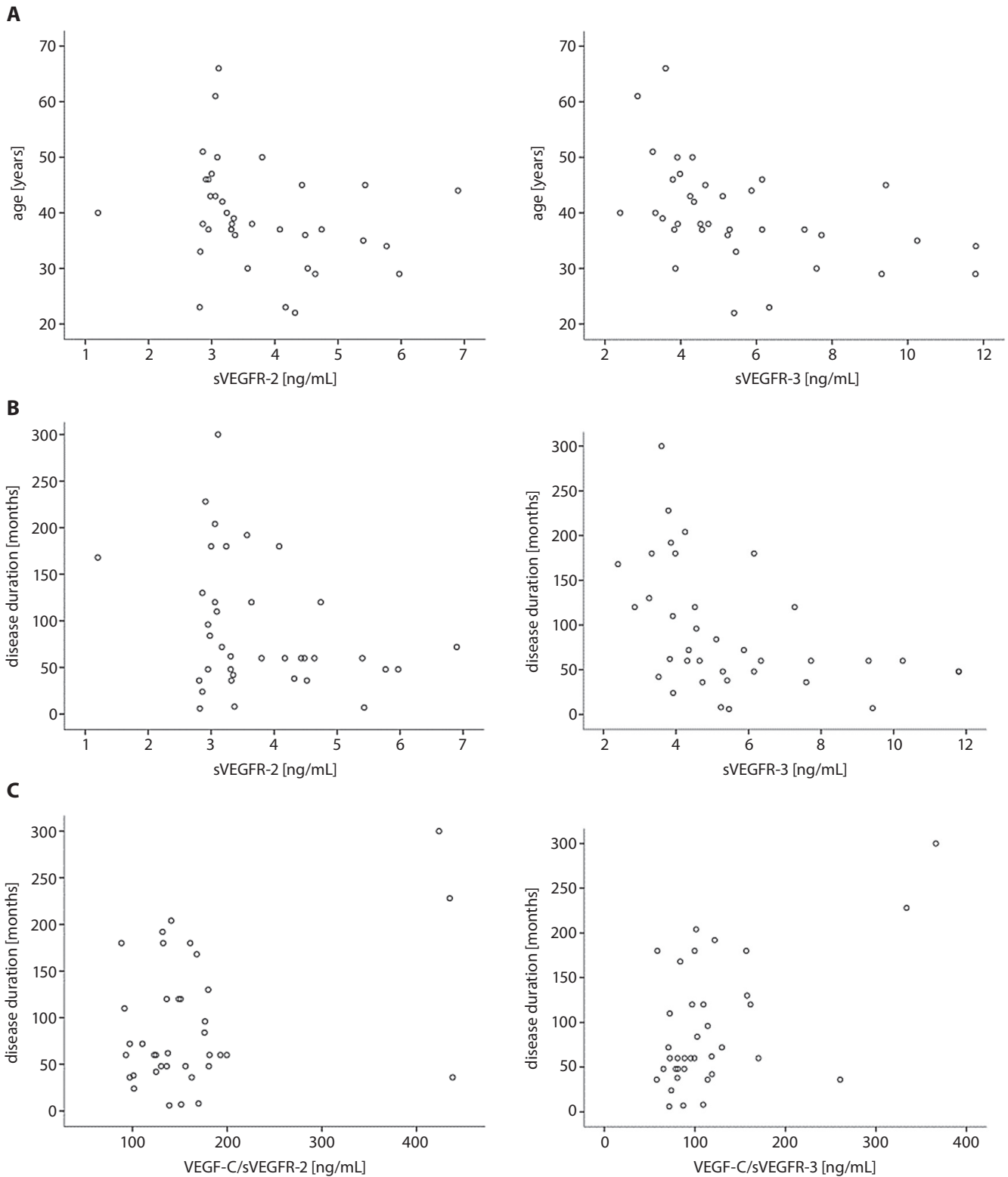


Fig. 1. Correlation analysis of parameters with age and disease duration. A. Correlation of sVEGFR-2 and sVEGFR-3 levels with age of BD patients. Spearman’s test showed that age negatively correlated with sVEGFR-2 ($p = 0.032$, $r = -0.35$) and sVEGFR-3 levels ($p = 0.003$, $r = -0.47$); B. Correlation of sVEGFR-2 and sVEGFR-3 levels with disease duration of BD patients. Spearman’s test showed a negative correlation between disease duration and sVEGFR-2 levels ($p = 0.048$, $r = -0.33$) and sVEGFR-3 levels ($p = 0.006$, $r = -0.44$); C. Correlation of VEGF-C/sVEGFR-2 and VEGF-C/sVEGFR-3 ratios with disease duration of BD patients. Spearman’s test showed that VEGF-C/sVEGFR-3 ($p = 0.024$, $r = 0.37$) and VEGF-C/sVEGFR-2 ($p = 0.020$, $r = 0.38$) were positively correlated with disease duration

sVEGF-R – soluble vascular endothelial growth factor receptor; BD – Behçet’s disease.

Table 4. Genotype and allele frequencies of VEGF-A gene polymorphisms in patients with BD and the association of these polymorphisms with disease pathogenesis

Parameters	BD patients (n = 55)	Controls (n = 30)	OR (95% CI)	p-value
C⁶⁹⁹⁹⁴⁷→A polymorphism				
Genotype (%)				
C/C	37.7	33.3	1.21 (0.48–3.03)	0.683
C/A	44.3	53.3	0.69 (0.29–1.67)	0.415
A/A	18.0	13.4	1.43 (0.41–4.94)	0.570
Allele (%)				
C allele	60	59.8	0.69 (0.20–2.41)	0.570
A allele	40	40.2	0.83 (0.33–2.07)	0.683
C²⁰¹⁰⁹⁶³→G polymorphism				
Genotype (%)				
C/C	36.1	30	1.13 (0.32–4)	0.856
C/G	49.1	56.7	0.74 (0.31–1.78)	0.502
G/G	14.8	13.3	1.32 (0.51–3.37)	0.566
Allele (%)				
C allele	41.7	39.3	0.76 (0.29–1.94)	0.856
G allele	58.3	60.7	1.13 (0.32–4)	0.566
C³⁰²⁵⁰³⁹→T polymorphism				
Genotype (%)				
C/C	76.7	80.3	1.24 (0.43–3.57)	0.686
C/T	23.3	19.7	0.81 (0.28–2.31)	0.686
T/T	0	0	–	–
Allele (%)				
C allele	88.3	90.2	–	–
T allele	11.7	9.8	0.81 (0.28–2.31)	0.686

Allele frequencies of patients and control group were compared using χ^2 test. VEGF-A – vascular endothelial growth factor A; BD – Behçet's disease; OR – odds ratio; 95% CI – 95% confidence interval.

of any genotype or allele did not show any increased disease risk (Table 4).

In the evaluation of treatment patterns of patients, it was observed that only 25 patients were receiving colchicine alone, while the rest of them were receiving combined therapy including any combination of 2 medication from the following: cortisone, colchicine and azathioprine. Twelve patients out of the rest were receiving colchium + cortisone treatment, while 18 were receiving colchium + azathioprine treatment.

Discussion

The most prominent feature of BD is systemic vasculitis and endothelial dysfunction, while the most prominent feature of uveitis is the occurring ophthalmologic complication.²⁴ A considerable evidence suggests that VEGF is also upregulated by pro-inflammatory cytokines, which participate in the pathogenesis of chronic ocular inflammation in BD.²⁵ It is also known that the VEGF gene is highly polymorphic.^{26,27} Although there are many studies

evaluating the relationship between different complications and clinical presentations of BD patients and VEGF levels, the studies investigating the polymorphisms playing a role in the pathogenesis of BD are rare.^{19,20} Considering vasculitis as the pathological lesion underlying most of the clinical findings and incidence of uveitis in Turkish BD patients, we performed the first study in Turkish BD population, aiming to investigate the levels of different VEGFs and VEGFRs, as well as the presence of any genotype or allele related to VEGF.

This is also the first study investigating serum angiogenesis, lymphangiogenesis mediators (VEGF-A, VEGF-C) and corresponding receptor levels (VEGFR-1, sVEGFR-2, sVEGFR-3) simultaneously. Considering uveitis and retinal vasculitis as ocular manifestations in patients with BD, the increased synthesis of VEGF in the retinal cells is crucial in the development of ocular neovascularization.²⁸ From this point of view, several studies revealing increased levels of VEGF in patients with BD in active stage of ocular disease have been performed.^{13–16,29} In these studies, there was a critical difference but no significant correlation between VEGF serum levels of BU patients and

normal control.^{30,31} On the other hand, in a recent study aiming to investigate VEGF levels in the aqueous humor of patients with BU and Fuchs' uveitis syndrome, Simsek et al. observed a significant difference only between Fuchs' uveitis syndrome and control subjects.³² Unlike the findings of Yalçındağ et al. and Ozdamar et al., but compatible with Simsek et al., mean serum VEGF-A levels were not statistically different in our study. Also, VEGF-C levels were not significantly different in BD patients compared to controls in our study.^{30–32} This might be due to the relatively small number of patients in the study group. In addition, considering the fact that the vascular disorder is not the main pathology in most patients with uveitis, and since endothelial dysfunction is a complex, multistep mechanism, VEGF levels may not change directly in the BD group like ours, where only BU comes to the fore. Also, uveitis is rarely known to be progressed together with neovascularization. Considering the overproduction of VEGF, even in the absence of neovascularization, it has been suggested that VEGF plays a pro-inflammatory role rather than an angiogenic role in the pathogenesis of uveitis. Moreover, the increase in VEGF levels may also be due to pro-inflammatory cytokines released from the area of inflammation.^{32,33}

In current literature, there is lack of studies evaluating VEGF-C levels in both uveitis caused by BD and/or other diseases/pathologies. This situation is mainly due to the unique lymphatic circulation of the eye. Although there is no known lymphatic outflow from the eye, recent studies have shown that corneal limbus, ciliary body, lacrimal gland, orbital meninges and extraocular muscles possibly contain lymphatic vessels, and that the choroid might have a lymphatic-like system after the novel lymphatic endothelial markers (e.g., LYVE-1, podoplanin) and lymphangiogenic factors (e.g., VEGF-C) have been proposed to be found in the choroid.³⁴ The presence of lymphatic-like features may be related to clinical implications in inflammatory eye diseases like uveitis.³⁵ Based on this, we evaluated the levels of VEGF-C and its soluble receptors, sVEGFR-2 and sVEGFR-3, in BU patients.³⁵ In our study, we found a significant difference in VEGF-C and sVEGFR-2 levels, while there was only a significant but slight difference in sVEGFR-3 levels between patients and control subjects. Contrary to our findings, Nakao et al. found a significant increase in VEGF-C but not in VEGFR-2 or VEGFR-3 in a study evaluating choroidal neovascularization from uveitis.^{34,36} Another report demonstrates both VEGF-C and sVEGFR-3 levels as below the detection limit in vitreous samples in a study group including uveitis patients.³⁷ On the other hand, various studies aimed to assess the relationship between other inflammatory pathologies of the eye and lymphangiogenesis. However, the complete agreement between the results of these studies and the detailed role of the VEGF-C/VEGFR-3 or VEGF-C/VEGFR-2 pathway has not been shown yet.³⁸ In our study, we found a significant difference in VEGF-C and sVEGFR-2 levels, while there was only a significant but slight difference in sVEGFR-3 levels

between BD patients and control subjects. As a result, there was only a barely significant difference in the VEGF-C/sVEGFR-3 ratio between the BD group and control group. What is more, there was no change in VEGF-C levels in the BD group, while sVEGFR-3 levels increased significantly. Thus, it is of critical importance to evaluate VEGF-C values together with VEGF-C/sVEGFR-3 ratio, as sVEGFR-3 is known to function purely in lymphangiogenesis to counterbalance the VEGF-C increase. Since sVEGFR-3 levels were significantly higher in the BD group in our study, lower VEGF-C/sVEGFR-3 ratios were thought to be individual indicators of the limitation of lymphangiogenesis. On the other hand, sVEGFR-2 plays a key role in both angiogenesis and lymphangiogenesis. That is why we evaluated the changes in both VEGF-A/sVEGFR-2 and VEGF-C/sVEGFR-2 ratio, and had the opportunity to co-evaluate angiogenesis and lymphangiogenesis in the BD group. The obtained data have shown that, considering the receptors, sVEGFR-2 was the only parameter that did not show any significant change. Although there was no change in any of VEGF-A, VEGF-C and sVEGFR-2 levels, there was a significant decrease in VEGF-C/sVEGFR-2 levels. This shows that even though factor levels do not increase in BD patients, the angiogenesis process was only regulated by VEGF-A/sVEGFR-1 ratio, while lymphangiogenesis have been regulated by decrease in both VEGF-C/sVEGFR-2 and VEGF-C/sVEGFR-3 ratios. Besides the slightly significant decrease in VEGF-C/sVEGFR-2 ratio, the limited increase in sVEGFR-3 and borderline significant decrease in VEGF-C/sVEGFR-3 ratio in the BD group can be accepted as a trigger of limited lymphangiogenesis. Apart from this, the significant increase in VEGFR-1 levels and significant decrease in VEGF-A/VEGFR-1 ratio in favor of angiogenesis suppression in the BD group. It also shows the importance of evaluation of sVEGFR-2 levels in conjunction with VEGFR-1 and sVEGFR-3 levels in assessing angiogenesis and lymphangiogenesis. Our data have also shown that the relevant receptors do not always change their levels in the same direction. In clinical situations that do not emphasize significant changes in VEGF levels like our BD group, the evaluation of the growth factors together with their relevant receptors will provide a better understanding of clinical presentation and development of complications. Furthermore, the changes in opposite directions in levels of different receptors reacting with the same factor show that these receptors can be affected by different determinants. Although this study mainly aims to evaluate the process of angiogenesis and lymphangiogenesis in patients with BU by evaluating VEGFs and their receptor levels, the results have also revealed the importance of determinative factors in altering the level of VEGF receptors in disease progression. Inflammation is one of these major determinants. When the importance of inflammation in progression of vascular pathologies is considered, our study has proven that the inflammation can be a key factor in the alteration of receptor

levels. In this manner, the present study can influence and guide the future studies. Furthermore, we suggest that anti-VEGF therapies, which are used quite widely in our era, should not focus solely on the changes in VEGF levels, but also on the receptor levels and related factor/receptor ratios in order to estimate the counterbalancing rate of the relevant factor by its receptors.

In the study by Kamoun et al., serum VEGF levels did not correlate with the age of BD patients or with the disease duration. Although our findings are compatible with the mentioned study in terms of receptor levels and ratios, we observed a negative correlation between serum sVEGFR-2 and sVEGFR-3 levels and age and disease duration, as well as a positive correlation between VEGF-C/sVEGFR-3 and VEGF-C/sVEGFR-2 ratios with disease duration.¹⁶ The fact that sVEGFR-2 and sVEGFR-3 levels show negative correlation with the age and disease duration may suggest that this relationship is related not only to the disease process. However, the positive correlation between VEGF-C/sVEGFR-3 and VEGF-C/sVEGFR-2 ratios only with disease duration is a particularly important and novel finding. Considering the significant decreases in VEGF-C/sVEGFR-2 ratio and VEGF-C/sVEGFR-3 ratio in the patient group may cause a dilemma. Significant correlation of both ratios in the same direction is sufficient to associate these parameters directly with the disease duration. In addition, as a parameter most significantly correlated with disease duration, VEGF-C/sVEGFR-3 ratio demonstrates that the evaluation of the lymphangiogenesis process is important, especially in the follow-up of the disease period in patients with BU.

Since vasculitis is the generally accepted pathology in BD and the change in VEGF levels is revealed in several studies, it is assumed that BD may occur more frequently in the carriers of the VEGF gene polymorphism. There is a limited number of studies evaluating different SNPs of the VEGF which have only been reported in Italian, Korean and Tunisian BD patients.^{16,19,20} Based on these studies, we found it appropriate to evaluate 3 different SNPs that we considered to be common and important (rs2010963 (+405 G), rs3025039 (+936 T) and rs699947 (-2598 A)). In Italian BD patients, -634 C/G, +936 C/T polymorphisms and an 18 bp I/D genotype at -2549 allele of the VEGF promoter region were selected by Salvarani et al., and they showed that the carriers of the -634 C and -2549 I alleles were susceptible to develop BD.¹⁹ In another study performed by Kamoun et al., although there was no association between VEGF polymorphisms and the susceptibility to BD, a positive association between VEGF 18bp I/D polymorphism and ocular involvement was found, and lower frequency of the 18 bp I/I genotype was observed in patients with ocular inflammation among patients with severe BD.¹⁶ Moreover, the distribution of VEGF serum level among the genotypes showed that VEGF level was significantly higher in severe BD patients for VEGF -634 GG and 18 bp D/D genotypes. On the other

hand, Nam et al. reported that there was no association between VEGF gene polymorphisms and BD (-2578 C/A, -1154 G/A, -634 C/G, and -936 C/T alleles were evaluated); however, -634 C/C genotype polymorphism, which had been associated with a lower production of VEGF, showed a slight tendency to be protective against the ocular inflammation in BD.²⁰ Our data were in accordance with those obtained in the Korean population; however, they contradict the reports in the Italian and Tunisian BD populations. The differences between these reports may be explained by the heterogeneity of the genetic background of different populations studied and the disequilibrium between polymorphisms within regions. In the present study, there was no association between the 3 VEGF gene polymorphisms and BU in Turkish patients. Moreover, when VEGF levels were considered in our study, it was not surprising that we obtained similar clinical presentations with the relevant SNPs.

Different treatment strategies were applied to the patients included in the study. Drugs of choice were cortisone, colchicine and azathioprine. Only 25 patients were receiving colchicine alone, while the rest of them were receiving combined therapy including any two of these drugs. Colchicine is known to inhibit the chemotactic activity of neutrophils and its activity in vasculitis is likely associated with the downregulation of cell surface adhesion molecules and decreased neutrophil adhesion and migration. Corticosteroids have an inhibitory effect on VEGF gene expression and circulating VEGF levels in a dose-dependent manner.^{39,40} To our knowledge, there are no studies showing the direct effect of azathioprine treatment on VEGF. When the antiangiogenic effects of colchicine and cortisone are considered, VEGF levels are expected to be lowered in patients receiving the treatment. On the other hand, it was noticed that the statistically significant difference between patients with uveitis and controls was observed in VEGFR-1 levels rather than VEGF-A levels. Considering all the information, it is hardly likely for the treatment patterns to create a significant difference directly on VEGF levels.



Limitations

The present study has some limitations. First, our study had a relatively small sample size. Second, half-lives of circulating factors or receptors were not evaluated in the study since only immediate levels of these parameters were assessed. Third, since this was a cross-sectional study, some of our patients were already taking different types of mostly anti-inflammatory medications for the treatment of BD symptoms; therefore, we could not totally neglect the effects of these medications on VEGF levels or inflammatory markers. Fourth, although so many SNPs associated with VEGF have been reported to date, we were only able to evaluate 3 of them that were supposedly more related to our patient population.

Conclusions

In conclusion, in contrast to the results of the Italian and Tunisian population, no associations with the VEGF gene polymorphisms were observed in Turkish BU patients. The differences in genetic background of different populations and composition of clinical presentation, as well as complications of patient groups in which SNP analysis is performed seem to be especially prominent. This study highlights the need for a further investigation of the role of VEGF polymorphisms and VEGF serum levels in BD susceptibility and its clinical manifestations. Thus, because lymphatic system contributes to the pathogenesis of immune diseases, lymphatic-targeted drug design may provide new agents for the treatment of uveitis.

ORCID iDs

Erdim Sertoglu  <https://orcid.org/0000-0002-4414-9224>
 Çiğdem Yücel  <https://orcid.org/0000-0003-2647-440X>
 Ahmet Omma  <https://orcid.org/0000-0003-2582-7445>
 Yıldız Hayran  <https://orcid.org/0000-0003-1942-7285>
 Seda Colak  <https://orcid.org/0000-0002-5703-6739>
 Sevinc Can Sandıkcı  <https://orcid.org/0000-0001-5921-8029>
 Ali Hakan Durukan  <https://orcid.org/0000-0001-6571-6155>
 Taner Ozgurtas  <https://orcid.org/0000-0003-1110-6671>

References

1. Yazici H. Behçet's syndrome in the 2000s: "Where is the wisdom we have lost in knowledge?". *Clin Exp Rheumatol*. 2016;34(6 Suppl 102): 23–25. PMID:27791957.
2. Al-Mutawa SA, Hegab SM. Behçet's disease. *Clin Exp Med*. 2004;4(3): 103–131. doi:10.1007/s10238-004-0045-0
3. Evereklioglu C. Current concepts in the etiology and treatment of Behçet disease. *Surv Ophthalmol*. 2005;50(4):297–350. doi:10.1016/j.survophthal.2005.04.009
4. Tursen U, Gurler A, Boyvat A. Evaluation of clinical findings according to sex in 2313 Turkish patients with Behçet's disease. *Int J Dermatol*. 2003;42(5):346–351. doi:10.1046/j.1365-4362.2003.01741.x
5. Michelson JB, Friedlaender MH. Behçet's disease. *Int Ophthalmol Clin*. 1990;30(4):271–278. doi:10.1097/00004397-199030040-00010
6. Koné-Paut I, Geisler I, Wechsler B, et al. Familial aggregation in Behçet's disease: High frequency in siblings and parents of pediatric probands. *J Pediatr*. 1999;135(1):89–93. doi:10.1016/s0022-3476(99)70333-1
7. Shenavandeh S, Jahanshahi KA, Aflaki E, Tavassoli A. Frequency of HLA-B5, HLA-B51 and HLA-B27 in patients with idiopathic uveitis and Behçet's disease: A case-control study. *Reumatologia*. 2018;56(2): 67–72. doi:10.5114/reum.2018.75516
8. Zouboulis CC, May T. Pathogenesis of Adamantiades–Behçet's disease. *Med Microbiol Immunol*. 2003;192(3):149–155. doi:10.1007/s00430-002-0167-5
9. Mizuki N, Meguro A, Tohna I, Gül A, Ohno S, Mizuki N. Association of major histocompatibility complex class I chain-related gene A and HLA-B alleles with Behçet's disease in Turkey. *Jpn J Ophthalmol*. 2007;51(6):431–436. doi:10.1007/s10384-007-0473-y
10. Kaya TI, Dur H, Tursen U, Gurler A. Association of class I HLA antigens with the clinical manifestations of Turkish patients with Behçet's disease. *Clin Exp Dermatol*. 2002;27(6):498–501. doi:10.1046/j.1365-2230.2002.01060.x
11. Hirohata S, Kikuchi H. Behçet's disease. *Arthritis Res Ther*. 2003;5(3): 139–146. doi:10.1186/ar757
12. Koch S, Tugues S, Li X, Gualandi L, Claesson-Welsh L. Signal transduction by vascular endothelial growth factor receptors. *Biochem J*. 2011;437(2):169–183. doi:10.1042/BJ20110301
13. Sertoglu E, Omma A, Yucel C, Colak S, Sandıkcı SC, Ozgurtas T. The relationship of serum VEGF and sVEGFR-1 levels with vascular involvement in patients with Behçet's disease. *Scand J Clin Lab Invest*. 2018;78(6):443–449. doi:10.1080/00365513.2018.1488179
14. Yalçındağ A, Gedik-Oğuz Y, Yalçındağ FN. The relationship between serum levels of angiogenin, bFGF, VEGF, and ocular involvement in patients with Behçet's disease. *Graefes Arch Clin Exp Ophthalmol*. 2013;251(7):1807–1812. doi:10.1007/s00417-013-2322-7
15. Cekmen M, Evereklioglu C, Er H, et al. Vascular endothelial growth factor levels are increased and associated with disease activity in patients with Behçet's syndrome. *Int J Dermatol*. 2003;42(11):870–875. doi:10.1046/j.1365-4362.2003.01688.x
16. Kamoun M, Houman MH, Hamzaoui A, Hamzaoui K. Vascular endothelial growth factor gene polymorphisms and serum levels in Behçet's disease. *Tissue Antigens*. 2008;72(6):581–587. doi:10.1111/j.1399-0039.2008.01145.x
17. Watson CJ, Webb NJ, Bottomley MJ, Brenchley PE. Identification of polymorphisms within the vascular endothelial growth factor (VEGF) gene: Correlation with variation in VEGF protein production. *Cytokine*. 2000;12(8):1232–1235. doi:10.1006/cyto.2000.0692
18. Renner W, Kotschan S, Hoffmann C, Obermayer-Pietsch B, Pilger E. A common 936 C/T mutation in the gene for vascular endothelial growth factor is associated with vascular endothelial growth factor plasma levels. *J Vasc Res*. 2000;37(6):443–448. doi:10.1159/000054076
19. Salvarani C, Boiardi L, Casali B, et al. Vascular endothelial growth factor gene polymorphisms in Behçet's disease. *J Rheumatol*. 2004; 31(9):1785–1789. PMID:15338501.
20. Nam EJ, Han SW, Kim SU, et al. Association of vascular endothelial growth factor gene polymorphisms with Behçet disease in a Korean population. *Hum Immunol*. 2005;66(10):1068–1073. doi:10.1016/j.humimm.2005.08.238
21. Criteria for diagnosis of Behçet's disease. International Study Group for Behçet's Disease. *Lancet*. 1990;335(8697):1078–1080. PMID:1970380.
22. Hamuryudan V, Fresko I, Direskeneli H, et al. Evaluation of the Turkish translation of a disease activity form for Behçet's syndrome. *Rheumatology (Oxford)*. 1999;38(8):734–736. doi:10.1093/rheumatology/38.8.734
23. Cingu AK, Onal S, Urgancioglu M, Tugal-Tutkun I. Comparison of presenting features and three-year disease course in Turkish patients with Behçet uveitis who presented in the early 1990s and the early 2000s. *Ocul Immunol Inflamm*. 2012;20(6):423–428. doi:10.3109/09273948.2012.713159
24. Koné-Paut I, Yurdakul S, Bahabri SA, et al. Clinical features of Behçet's disease in children: An international collaborative study of 86 cases. *J Pediatr*. 1998;132(4):721–725. doi:10.1016/s0022-3476(98)70368-3
25. Ferrara N, Davis-Smyth T. The biology of vascular endothelial growth factor. *Endocr Rev*. 1997;18(1):4–25. doi:10.1210/edrv.18.1.0287
26. Hayran Y, Lay I, Mocan MC, Bozduman T, Ersoy-Evans S. Vascular endothelial growth factor gene polymorphisms in patients with rosacea: A case-control study. *J Am Acad Dermatol*. 2019;81(2):348–354. doi:10.1016/j.jaad.2019.03.055
27. Rogers MS, D'Amato RJ. The effect of genetic diversity on angiogenesis. *Exp Cell Res*. 2006;312(5):561–574. doi:10.1016/j.yexcr.2005.10.021
28. Battaglia Parodi M, Iacono P, Verbraak FD, Bandello F. Antivascular endothelial growth factors for inflammatory chorioretinal disorders. *Dev Ophthalmol*. 2010;46:84–95. doi:10.1159/000320011
29. Paroli MP, Teodori C, D'Alessandro M, Mariani P, Iannucci G, Paroli M. Increased vascular endothelial growth factor levels in aqueous humor and serum of patients with quiescent uveitis. *Eur J Ophthalmol*. 2007;17(6):938–942. doi:10.1177/112067210701700611
30. Yalçındağ A, Gedik-Oğuz Y, Yalçındağ FN. The relationship between serum levels of angiogenin, bFGF, VEGF, and ocular involvement in patients with Behçet's disease. *Graefes Arch Clin Exp Ophthalmol*. 2013;251(7):1807–1812. doi:10.1007/s00417-013-2322-7
31. Ozdamar Y, Berker N, Bahar G, et al. Inflammatory mediators and posterior segment involvement in ocular Behçet disease. *Eur J Ophthalmol*. 2009;19(6):998–1003. PMID:19882576.
32. Simsek M, Cakar Ozdal P, Akbiyik F, et al. Aqueous humor IL-8, IL-10, and VEGF levels in Fuchs' uveitis syndrome and Behçet's uveitis. *Int Ophthalmol*. 2019;39(11):2629–2636. doi:10.1007/s10792-019-01112-w
33. Paroli MP, Teodori C, D'Alessandro M, Mariani P, Iannucci G, Paroli M. Increased vascular endothelial growth factor levels in aqueous humor and serum of patients with quiescent uveitis. *Eur J Ophthalmol*. 2007;17(6):938–942. doi:10.1177/112067210701700611
34. Nakao S, Hafezi-Moghadam A, Ishibashi T. Lymphatics and lymphangiogenesis in the eye. *J Ophthalmol*. 2012;2012:783163. doi:10.1155/2012/783163

35. Pavlakovic H, Becker J, Albuquerque R, Wilting J, Ambati J. Soluble VEGFR-2: An antilymphangiogenic variant of VEGF receptors. *Ann N Y Acad Sci.* 2010;1207(Suppl 1):E7–15. doi:10.1111/j.1749-6632.2010.05714.x
36. Nakao S, Zandi S, Kohno R, et al. Lack of lymphatics and lymph node-mediated immunity in choroidal neovascularization. *Invest Ophthalmol Vis Sci.* 2013;54(6):3830–3836. doi:10.1167/iovs.12-10341
37. Takeda A, Yoshikawa H, Fukuhara T, et al. Distinct profiles of soluble cytokine receptors between B-Cell vitreoretinal lymphoma and uveitis. *Invest Ophthalmol Vis Sci.* 2015;56(12):7516–7523. doi:10.1167/iovs.15-17465
38. Decker D, Burr J, Lester K, Zaworski V, Weber S. VEGF, VEGF-C, and VEGF-D increases in aqueous humor samples in a LPS induced model of uveitis in New Zealand white rabbits. ARVO Annual Meeting Abstract. *Invest Ophthalmol Vis Sci.* 2013;54:5010. <https://iovs.arvojournals.org/article.aspx?articleid=2149927>. Accessed November 16, 2021.
39. Leung YY, Yao Hui LL, Kraus VB. Colchine: Update on mechanisms of action and therapeutic uses. *Semin Arthritis Rheum.* 2015;45(3):341–350. doi:10.1016/j.semarthrit.2015.06.013
40. Zeng J, Yang L, Huang F, et al. The metronomic therapy with prednisone, etoposide, and cyclophosphamide reduces the serum levels of VEGF and circulating endothelial cells and improves response rates and progression-free survival in patients with relapsed or refractory non-Hodgkin's lymphoma. *Cancer Chemother Pharmacol.* 2016;78(4):801–808. doi:10.1007/s00280-016-3136-1

Comparison of the radial and brachial artery flow-mediated dilation in patients with hypertension

Katarzyna Majka^{1,2,A,B,D}, Marzena Parol^{3,A,B}, Andrzej Nowicki^{5,C,E,F}, Barbara Gambin^{5,C,E,F}, Zbigniew Trawiński^{5,B,E,F}, Marzena Jaciubek^{1,C,E}, Andrzej Krupienicz^{1,E,F}, Robert Olszewski^{4,5,A,E,F}

¹ Department of Fundamentals of Nursing Faculty of Health Sciences, Warsaw Medical University, Poland

² Military Medical Institute in Warsaw, Poland

³ West Hospital John Paul II, Grodzisk Mazowiecki, Poland

⁴ National Institute of Geriatrics, Rheumatology and Rehabilitation, Warszawa, Poland

⁵ Institute of the Fundamental Technological Research of the Polish Academy of Sciences, Warszawa, Poland

A – research concept and design; B – collection and/or assembly of data; C – data analysis and interpretation; D – writing the article; E – critical revision of the article; F – final approval of the article

Advances in Clinical and Experimental Medicine, ISSN 1899–5276 (print), ISSN 2451–2680 (online)

Adv Clin Exp Med. 2022;31(3):241–248

Address for correspondence

Robert Olszewski
E-mail: robert.olszewski@spartanska.pl

Funding sources

This work was supported by National Science Centre grant No. UMO-2017/25/B/ST7/01601.

Conflict of interest

None declared

Received on September 28, 2021

Accepted on November 17, 2021

Published online on January 18, 2022

Cite as

Majka K, Parol M, Nowicki A, et al. Comparison of the radial and brachial artery flow-mediated dilation in patients with hypertension. *Adv Clin Exp Med.* 2022;31(3):241–248. doi:10.17219/acem/144040

DOI

10.17219/acem/144040

Copyright

© 2022 by Wrocław Medical University
This is an article distributed under the terms of the Creative Commons Attribution 3.0 Unported (CC BY 3.0) (<https://creativecommons.org/licenses/by/3.0/>)

Abstract

Background. Blood flow-mediated dilation (FMD) is a noninvasive assessment of vascular endothelial function in humans. The study of the FMD in hypertensive (HT) patients is an important factor supporting the recognition of the early mechanisms of cardiovascular pathologies, and also of the pathogenesis related to hypertension.

Objectives. To investigate whether FMD measured on the radial artery (FMD-RA) using high-frequency ultrasounds can be used as an alternative to FMD assessed with the lower frequency system on the brachial artery in patients with HT.

Materials and methods. The simultaneous measurements of FMD-RA and FMD measurements in the brachial artery (FMD-BA) were performed on 76 HT patients using 20 MHz and 7–12 MHz linear array probes, and were compared to the FMD measured in healthy groups. All quantitative data are presented as mean \pm standard deviation (SD); the p-values of the normality and tests for variables comparisons are listed. The agreement of the FMD-RA and FMD-BA in HT patients was assessed with the Bland–Altman method, and using the intraclass correlation coefficient (ICC). In some statistical calculations, the FMD-RA values were rescaled by dividing them by a factor of 2.

Results. The mean FMD-RA and FMD-BA in HT patients were $5.16 \pm 2.18\%$ (95% confidence interval (95% CI): [4.50%, 5.82%]) and $2.13 \pm 1.12\%$ (95% CI: [1.76%, 2.49%]), respectively. The FMD-RA and FMD-BA values of HT patients were significantly different than those in respective control groups. The p-values of Mann–Whitney–Wilcoxon tests were less than 0.05. The Bland–Altman coefficient for both measurement methods, FMD-RA and FMD-BA, was 3%, and the ICC was 0.69.

Conclusions. Our findings show that FMD-RA, supplementary to FMD-BA measurements, can be used to assess endothelial dysfunction in the group of HT patients. In addition, the FMD-RA measurements met the criteria of high concordance with the FMD-BA measurements.

Key words: hypertension, brachial artery, radial artery, endothelial function

Background

Hypertension (HT) is one of the most widespread diseases in the world.^{1,2} In combination with other diseases, it causes severe cardiovascular and organ complications. Elevated blood pressure is the largest risk factor for death.³ The World Health Organization (WHO) estimates that 17.7 million people died of cardiovascular disease (CVD) in 2015, and the death of 6.7 million people was due to HT-induced stroke.⁴ In the European Union (EU), the number of deaths caused by CVD is over 2 million per year and constitutes 42% of the total mortality.⁵

Underlying the pathophysiology of HT are many factors and disease processes, such as: genetic factor, vascular resistance, activation of the sympathetic nervous system, renin-angiotensin-aldosterone system, inflammatory factors, stiffness of the arteries, and endothelial dysfunction.² The first changes in various CVDs occur in the endothelium. Early and accurate assessment of endothelial function may help in understanding the etiology of these diseases and in determining the efficacy of vascular disease treatment. Different diagnostics involving invasive and noninvasive methods are used to determine endothelial function and peripheral vascular function.^{6–8} One of the noninvasive methods used for this purpose is brachial artery ultrasound imaging used in order to assess vasodilatation flow-mediated dilation (FMD), depending on endothelial status.⁹

Most of the previously reported FMD measurements were performed in the brachial artery (FMD-BA) with a strictly standardized protocol.⁹ The measurement of the radial artery, FMD-RA, has been rarely studied, but the last 3 decades have led to a huge acceleration in endothelial research.

The literature describes that the radial artery expansion (FMD-RA) was greater compared to FMD-BA, suggesting that FMD-RA may be a useful means of assessing FMD in future clinical trials.^{10,11}

The accuracy of the assessment of arterial diameter and the calculation of the FMD directly depend on the axial resolution of the applied ultrasound (US) scanner. The greater the frequency, the better the accuracy of the vessel diameter measurements.

Pyke and Tschakovsky showed the inverse relationship between peak percentage change in diameter response after cuff release and the baseline diameter – smaller arteries show greater FMD response.¹²

The axial resolution of the standard US scanners working at 7.5–12 MHz, used in the abovementioned papers, is limited to about 0.2–0.3 mm, which is close to the expected dilation of the BA or RA, and thus severely biases the results.

The BA is located at an average depth of more than 1 cm below the skin surface and, due to the attenuation, no higher sounding frequency can be used for imaging.

The RA is located at 2–4 mm below skin surface. Shallow location of the RA allows for an increase of the scanning frequency to 20 MHz with superior axial resolution close to 0.1 mm.⁷

Objectives

The study aimed to investigate the proposed measurement of FMD-RA using high-frequency ultrasounds as an alternative to the standard FMD-BA, in order to distinguish between HT patients and healthy subjects.

Materials and methods

Participants

The study group included 76 patients (aged 71 ± 8.34 years, 34 women and 42 men), with confirmed long-term HT (over 5 years). The baseline clinical characteristics of the subjects are presented in Table 1. The FMD-BA and FMD-RA were compared. Criteria for HT patients: patients with diagnosed HT and taking antihypertensive drugs permanently. The study was conducted from May 1, 2017 to December 18, 2017. Patients with HT, chronically treated, remaining under constant control of a cardiologist, randomly selected, were qualified during a visit to a cardiology clinic for the FMD-BA and FMD-RA examinations.

Table 1. Baseline characteristics of the subjects included in the study

Parameter	Men (42)	Women (34)
Age [years]	71 ± 6.5	72 ± 4.7
BMI [kg/m ²]	29.5 ± 3.6	28.79 ± 3.1
Obesity, n	18	14
Dyslipidemia, n (%)	34 (89)	40 (92)
T2DM, n (%)	11 (35)	8 (32.6)
SBP [mm Hg]	144 ± 13.2	149 ± 12.8
DBP [mm Hg]	82 ± 5.3	78 ± 9.5

BMI – body mass index; T2DM – type 2 diabetes mellitus; SBP – systolic blood pressure; DBP – diastolic blood pressure.

The overall statistics on the clinical data of HT patients are presented in Table 1. We also included FMD data for healthy control group from the previously-measured FMD-RA⁷ and the FMD-BA data published by Pyke and Tschakovsky (cf. Table 2).¹²

This study was carried out in accordance with the Declaration of Helsinki. The consent for the test was approved by the Bioethics Committee (approval No. KBT-4/2/2017) of the National Institute of Geriatrics, Rheumatology and Rehabilitation, Warsaw, Poland. All adult participants gave written informed consent to participate in the study.

Table 2. Descriptive statistics of the data

Variable	Group	Range	Q1	Q3	Median	Mean	SD	CV	N
FMD-BA	HT	0.1–5.0	1.2	3.2	2.1	2.3	1.2	0.46	–
	C*	2.2–19.0	5.8	10.9	7.9	8.6	4.9	0.57	–
FMD-RA	HT	1.0–10.0	3.6	6.4	5.1	5.2	2.1	0.41	+
	C**	6.0	11.0	18.2	15.0	14.7	5.2	0.35	+
RFMD-RA	HT	0.5–5.0	1.8	3.2	2.5	2.6	1.07	0.41	+
Average: ½ (RFMD-RA+FMD-BA)	HT	0.8–4.0	2.0	2.9	2.3	4.2	0.7	0.31	+
Difference: RFMD-RA – FMD-BA	HT	–2.7–4.9	–1.08	1.7	0.1	0.3	1.8	5.4	+

Q1 – 1st quartile; Q3 – 3rd quartile; SD – standard deviation; CV – coefficient of variation; N – result of normality test; FMD-BA – flow-mediated dilation (FMD) measured in the brachial artery; FMD-RA – FMD measured on the radial artery; RFMD-RA – rescaled FMD-RA; HT – hypertension; C* – control group for FMD measurements in the brachial artery adapted from Pyke and Tschakovsky¹²; C** – control group for FMD measurements on the radial artery; + denotes p-value >0.05 in Shapiro–Wilk test; – denotes p-value <0.05 in Shapiro–Wilk test.

FMD measurement procedure in the BA and RA

The experimental setup consisted of 2 independent Sonix Touch units (Analogic, Peabody, USA) with linear array transducers of 7–12 MHz and 20 MHz. The high-frequency, 20-MHz linear array was used to measure FMD-RA, while the linear array transducer 7–12 MHz was used for FMD-BA measurements.

Patients were asked to refrain from smoking, drinking alcohol and caffeine as well as taking any vasoactive drugs and medicines on the day of the study and the day before the examination. Each patient was asked to rest for 10 min before lying down in a quiet room at 25°C to achieve a hemodynamic state. The first step in the measurement procedure was to measure the patient's blood pressure and heart rate. The patient's hand was immobilized using a hand casting made out of silicone rubber (Fig. 1). Each examination started with a preliminary scanning, where the BA and RA with clear anterior and posterior walls and no branching was identified in the upper arm. After obtaining a satisfactory ultrasound image of the RA and BA, the ultrasound transducers were stabilized using



Fig. 1. Experimental setup for simultaneous examining of the flow-mediated dilation in radial and brachial arteries (FMD-RA and FMD-BA) using 20 MHz and 7 MHz linear arrays, respectively

2 NF1030 single knob holders (Noga Engineering & Technology, Shlomi, Israel). The location of the transducer was marked on the skin with an ink marker.

To ensure that the cross-sectional plane was orthogonal to the long axis, the orientation of the transducer was adjusted such that the intima could be seen both in the anterior and posterior walls, and the bright echoes were aligned along the axis of ultrasound propagation. The 2D images of both arteries were then recorded for 5 s to measure their resting base diameters. Then, the flow was stopped by the sphygmomanometer cuff placed on the forearm and inflated for 5 min to the pressure exceeding the systolic blood pressure (SBP) of the examined person by 50 mm Hg. Next, the cuff was released. The RA recording was resumed 10 s before the cuff was released and continued for 3 min. The BA recording was resumed 40 s after the cuff was released and continued for the 60 s. Ultrasound image sequences were recorded in RAW format and then were converted to AVI format. The AVI files have been analyzed offline, using the Brachial Analyzer (BA) software (Vascular Research Tools (VRT) v. 6.7.0 (Medical Imaging Applications LLC, Coralville, USA). The BA software tracks vessel diameter changes in the selected region of the ultrasound artery and calculates the FMD. A detailed description of the measurement method is presented in our previous study.⁷

It should be emphasized that the average calculation time of BA and RA dilations using BA software was about 15–20 min.

The measurements of each vessel diameter and further calculations of FMD for both arteries were done twice by 2 examiners, and recording was verified at least 2 times by the same observer in order to estimate the intra-observer coefficient. The inter-observer coefficient of variation (CV) was 5.8% for BA and 3.5% for RA diameter estimation. For statistical calculation of FMD-BA and FMD-RA, the mean values of the 2 measurements were used. The intra-observer CV was 4.6% for BA and 2.8% for RA diameter estimation.

Graphic recording and measurement of the RA and BA

The diameters of both arteries were measured after selecting, from the recorded artery scans, an area with the best visible internal borders on the anterior and posterior walls. After implementing all settings (i.e., the unification of the scale, increasing the contrast of the background to the artery walls, maximal magnification of the selected artery area), the program registers temporary changes of the vessel diameter (Fig. 2). After determining the diameter of the artery before ischemia (baseline diameter (D_b)), the second recording of the artery scan, after releasing the pressure cuff, was analyzed and the maximum diameter of the artery (D_{max}) was determined. The FMD value was calculated using the following formula (Eq. 1):

$$\text{FMD [\%]} = [(D_{max}/D_b) - 1] \times 100\% \quad (1)$$

where D_{max} is the maximum diameter of the artery after ischemia and D_b is the maximum resting artery diameter before ischemia.

Statistical analyses

Continuous random variables were described by the use of means and standard deviations (SDs). The normality of the variables was studied using the Shapiro–Wilk test. The Mann–Whitney–Wilcoxon and Kolmogorov–Smirnov tests were performed to study the differences between variables. The confidence level of 0.95 was assumed in all statistical calculations throughout the article. The Bland–Altman analysis and intercorrelation coefficient (ICC) were used for the study of the relationships between the 2 methods. The statistical analysis was performed with the use of base packages of free R programming language (R Foundation for Statistical Computing, Vienna, Austria).

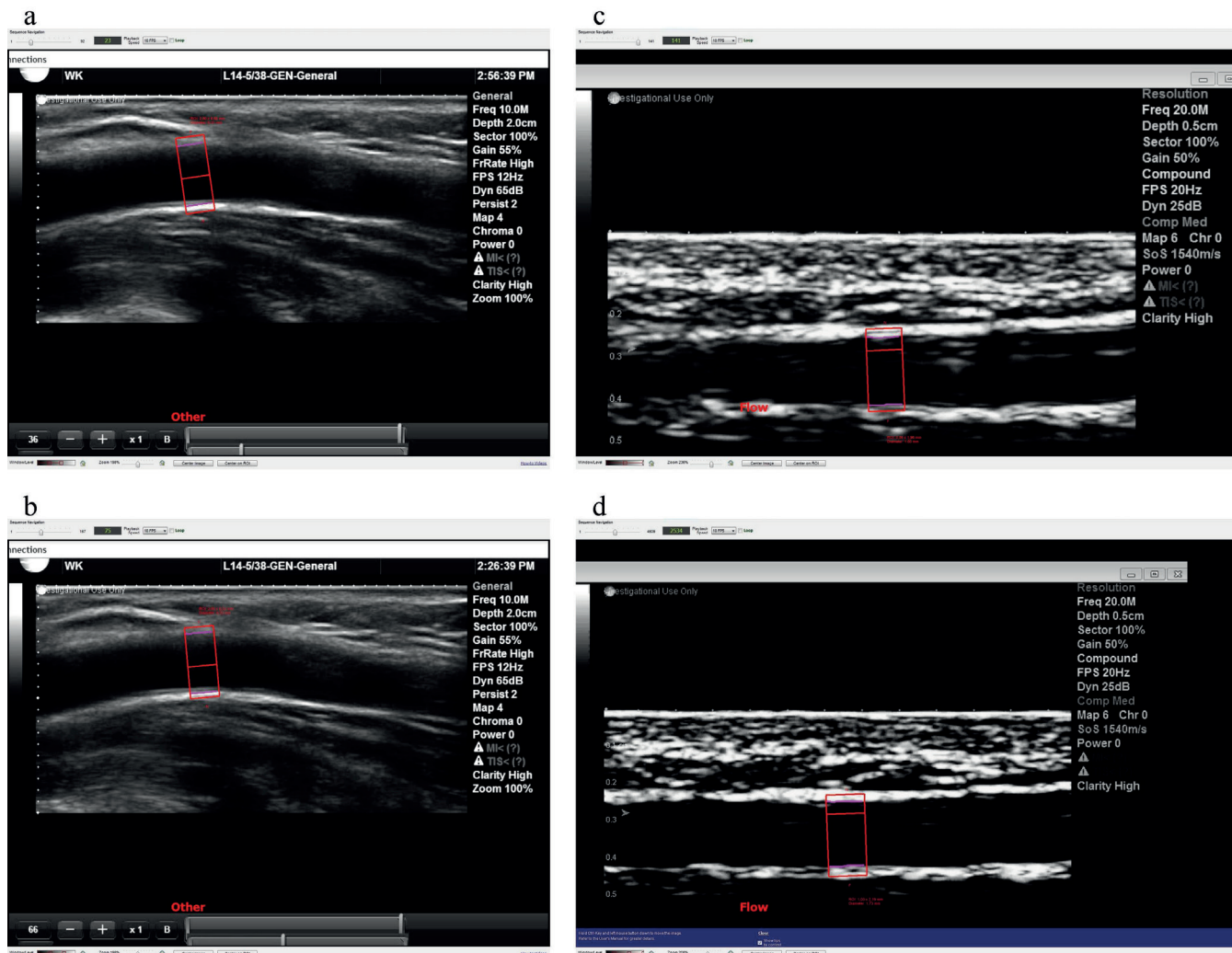


Fig. 2. The analysis of the brachial (A,B) and radial (C,D) arteries diameters change in subsequent phases of the heart cycle in a patient with hypertension (HT): (A and C) before ischemia, (B and D) after five-minute ischemia

Brachial artery: A. Before ischemia, diameter in contraction = 5.31 mm; B. After five-minute ischemia, the artery reaches a maximum diameter of 5.22 mm, blood flow-mediated dilation measured in the brachial artery (FMD-BA) = 1.7%.

Radial artery: C. Before ischemia, diameter in contraction = 1.77 mm; D. After five-minute ischemia, the artery reaches a maximum diameter of 1.83 mm, blood flow-mediated dilation measured on the radial artery (FMD-RA) = 3.3%.

Results

We measured all physical parameters to calculate the FMD in the RA and BA for 76 HT patients, using 2 ultrasonic methods of data acquisition, as described in the Background section. Only the final values of FMD were reported in Table 2, without any additional measured physical parameters.

The median FMD-RA in HT patients was 5.1%, and FMD-BA was more than twice lower at 2.04%. The mean FMD-RA and FMD-BA values for HT patients were $5.16 \pm 2.18\%$ (95% confidence interval (95% CI): [4.50%, 5.82%]) and $2.13 \pm 1.12\%$ (95% CI: [1.76%, 2.49%]), respectively. The lowest FMD-RA value was 0.85% and the highest was 10%, while in the brachial artery the lowest FMD-BA value was 0.10% and the highest was 4.7%. There was no statistical dependency between the FMD-RA and FMD-BA measurements of the same patients, and the p-value of Mann–Whitney–Wilcoxon test was less than 0.05.

Since the comparison of the consistency of the direct results of measurements in the BA and RA is difficult due to the significant difference in the diameter of both arteries, and in addition, this difference is not constant along with the increase of the average value of the measurements, we rescaled the FMD results obtained for the RA by dividing these values by 2. The rescaled FMD-RA (RFMD-RA) is used in the following statistical analyses.

The rescaled FMD-RA was very weakly correlated with FMD-BA, with Spearman’s correlation coefficient of -0.17 . The RFMD-RA was similar to the FMD-BA values. Namely, RFMD-RA was $2.5 \pm 1.7\%$, and its range was 0.5–5%.

The boxplots of FMD-RA, RFMD-RA and FMD-BA were nearly symmetrical about the median (Fig. 3). The interquartile range (IQR) of FMD-RA for HT patients was 2.76%, and the values of the 1st and 3rd quartiles were $Q1 = 3.64\%$ and $Q3 = 6.4\%$. The IQR of FMD-BA for HT patients was 1.78% ($Q1 = 1.22\%$, $Q3 = 3\%$). The same statistical characteristics of the groups of healthy controls were given in Table 2, where additionally, the normality of the variables was studied using the p-value of Shapiro–Wilk test and quite high CV.

The statistically significant differences between FMD-RA and FMD-BA for HT patients, and between 2 FMD measurements in brachial artery for HT patients and respective control groups were confirmed by the p-values less than 0.05, resulting from the performed Mann–Whitney–Wilcoxon tests.

Pyke and Tschakovsky collected data from several research groups of FMD measurements in healthy controls. The range of the reported data was very large, from 2% up to 19.1% ($Q1 = 5.8\%$, $Q3 = 11.0\%$). The mean FMD-BA resulting from these data was equal to 8.6% and the median was slightly lower, being equal to 7.9%.¹²

The span of our FMD-RA data for healthy controls varied from 6% to 25% ($Q1 = 11$, $Q3 = 18.5$), the mean FMD-RA was 14.25% and the median equaled 15%. Both datasets are shown in Table 2.

To depict the relationship between the FMD measured on the RA and BA for the same HT patient, the scatterplot of FMD-RA compared to FMD-BA is shown in Fig. 4. The narrow ranges of FMD values near any fixed value measured in the BA corresponded almost to the entire range of FMD-RA values obtained from the RA, and vice versa. That further confirmed the statistical independence of the 2 measurements in addition to the fact that the regression line was almost horizontal (see Fig. 4), and that Pearson’s and Spearman’s correlation coefficients were both very low and equaled 0.04 and 0.11, respectively.

The mean values of the RFMD-RA and FMD-BA in control groups were 7.37% and 8.63% with the 95% CI of [6.36, 8.39] and [5.11, 12.2], respectively (Fig. 5).

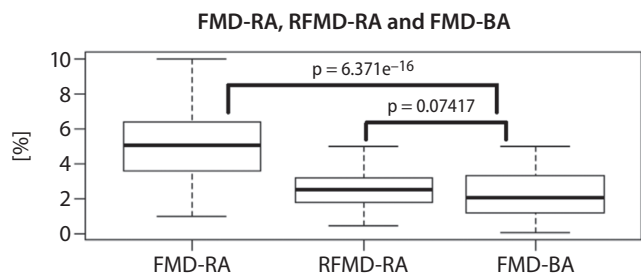


Fig. 3. Tukey’s boxplots of the flow-mediated dilation in hypertensive (HT) patients measured on the radial artery (FMD-RA), rescaled FMD-RA (RFMD-RA), and blood flow-mediated dilation measured in the brachial artery (FMD-BA). Whiskers indicate 1.5 times lower and upper interquartile ranges (IQRs), the box corresponds to the IQR, and the bold transverse line indicates the median value. The p-values of the Mann–Whitney–Wilcoxon test of differences between the 2 indicated groups are overwritten on lines connecting groups

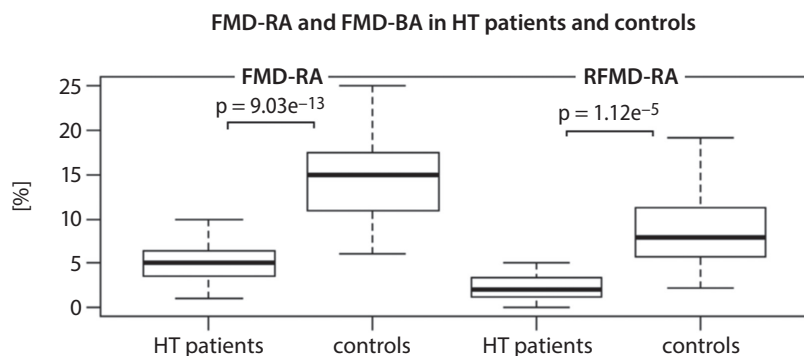


Fig. 4. Tukey’s boxplots of blood flow-mediated dilation (FMD) on the radial artery (FMD-RA) and the brachial artery (FMD-BA) of hypertensive (HT) patients and healthy controls. Whiskers indicate 1.5 times lower and upper interquartile ranges (IQRs), the box corresponds to the IQR, and the bold transverse line indicates the median value. The p-values of the Mann–Whitney–Wilcoxon tests of differences between 2 indicated groups are overwritten on lines connecting groups

RFMD-RA – rescaled FMD-RA.

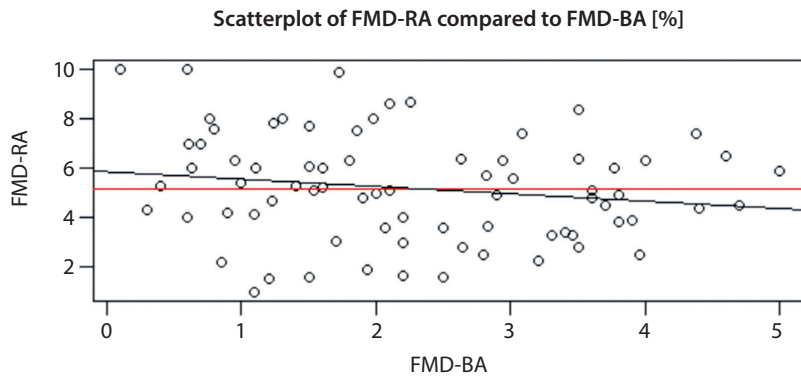


Fig. 5. Scatterplot of blood flow-mediated dilation measured on the radial artery (FMD-RA) compared to blood flow-mediated dilation measured in the brachial artery (FMD-BA). The red line denotes the mean value of FMD-RA, and the black line is the regression line from the linear regression model

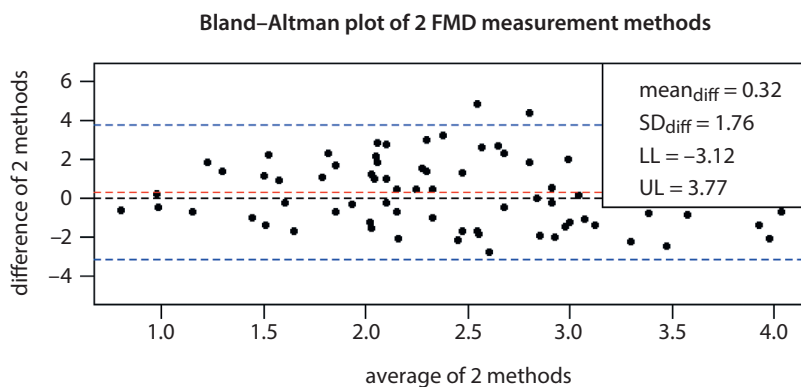


Fig. 6. The Bland-Altman plot of 2 methods of blood flow-mediated dilation (FMD) measurements – in the radial artery (FMD-RA) and the brachial artery (FMD-BA). The black line denotes the difference between the 2 methods equal to zero, the red line equals to mean of differences (Mean_{diff}) and the blue lines (lower limit (LL) – lower line and upper limit (UL) – upper line) are equal to mean ± 1.96 multiplied by the standard deviation (SD) of the differences

The Bland-Altman plot for RFMD-RA and FMD-BA data is shown in Fig. 6. The random distribution of the differences between RFMD-RA and FMD-BA as well as their average values, calculated as $\frac{1}{2}$ (RFMD-RA + FMD-BA), had normal character. The p-values of the Shapiro-Wilk tests were 0.058 and 0.77, respectively, contrary to the difference of the nonscaled FMD-RA and FMD-BA, where the p-value of the Shapiro-Wilk test was 0.021.

Following the Bland-Altman plot, the maximum difference between the 2 methods of FMD measurements for HT patients, RFMD-RA and FMD-BA, was 6.97. The average difference between them was equal to 0.32, with 95% CI of [-3.12, 3.77].

None of the measurements exceeded the value of the Q1 for the control group, which was 5.5% and 5.8% for RFMD-RA and FMD-RA, respectively. The ICC for the RFMD-RA and FMD-BA data was 0.88, so we also had confirmation of a “good agreement” between the 2 measurement methods. The time span (TS) between releasing the cuff and peak dilation for FMD-RA and FMD-BA was in the range of 37–117 s (mean \pm SD equal to 72.19 ± 34.47 s).

Discussion

A main result of our research was the finding of a significant difference in dilation between the 2 arteries in patients with HT. In the process of reactive hyperemia, the smaller RA expands about twice as much as the BA.

The introduction of 20 MHz scanning US improved significantly the precision of measurements of the inner diameter of the RA.⁷ Previous studies by Järvisalo et al. performed in the BA using 7 MHz linear array were not able to precisely measure its actual diameter,¹³ due to the limited axial resolution.⁹ Satisfactory results were obtained only after using an ultrasound linear array transducer with a larger, nearly doubled frequency of 12 MHz. The techniques of FMD-BA measurement analysis rely on the accurate detection of the artery wall edges, and often the image quality is poor, with image artifacts.¹⁴

It has been reported that FMD shows an inverse relationship between peak percentage change in diameter and baseline diameter – the greater the baseline diameter becomes, the smaller is the FMD response.^{12,15} In our study of simultaneous measurements of BA and RA dilation, the mean radial diameter was 2.8 ± 0.8 mm and the BA was 4.1 ± 0.9 mm. Reactive dilatation was almost twice as large in RA when compared to BA, resulting in almost 85% greater FMD. Taking into account better axial and elevation resolution of the high frequency 20 MHz linear array comparing to 7–12 MHz ultrasonography resolution, a better precision of FMD-RA compared to FMD-BA measurements is obtained.¹⁶

Both arteries are rather easily located using linear array scanning, although the position of the RA is anatomically more stable, which facilitates quick positioning of the transducer over it. Setting the head using the tripod fixing over the RA is more robust during the entire measurement cycle.

Calderón-Gerstein et al. studied patients with HT, diabetes, obesity, stroke, or coronary artery disease (CAD), measuring endothelial activity on the BA at high altitudes (3250 m.a.s.l.) by comparing them with the control group.¹⁷ Their results showed that age, height and body mass index (BMI) affected the position of the BA during the study.

The few available reports on FMD-RA concerned the population of patients with HT. According to Westhoff et al., the mean FMD-RA value in HT patients was $6.29 \pm 2.86\%$, but there were differences in the methodology of inducing ischemia, which in their study consisted of inflating the cuff to 300 mm Hg for 3 min, and could affect the measurement result.¹⁸ Bilolikar et al. reported an average increase in the diameter of the RA by $0.48 \pm 0.13\%$ in the peak reactive dilation.¹⁹

Our study showed that the mean RA dilation after short-term ischemia in patients with HT is $5.16 \pm 2.18\%$ and is more than twice that of the BA. The mean value of FMD-BA after ischemia in patients with HT was $2.13 \pm 1.12\%$. Both results show more than 2 times greater mean values of FMD in patients with CAD and HT than in volunteers from control group. Median FMD-RA for patients with HT was 5.01% and the median BA (FMD-BA) for HT patients was 2.04%, for $p < 0.01$.

In the recent report of Nowicki et al., almost a two-fold statistically significant difference in FMD-RA between the group of patients with stable CAD and a group of healthy volunteers was demonstrated.^{7,20} The authors found that the FMD-RA of a healthy patient was $15.26 \pm 4.90\%$, almost 3 times higher than the FMD measured in this study in HT patients ($5.16 \pm 2.18\%$), which also confirms the strength of diagnostic power of HT using FMD-RA measurements.

Palmieri et al., in a study of the brachial FMD in 51 HT patients and 50 normotensive patients, showed that the HT patients had an FMD lower by 35% compared to patients with normal blood pressure ($8.3 \pm 5.4\%$ compared to $12.8 \pm 6.5\%$).²¹

When we applied RFMD-RA in the statistical analysis, only 2 out of 76 results = c/a 3% of differences between the 2 measurement methods were lying outside the upper and lower lines in the Bland–Altman chart. It means that the Bland–Altman coefficient was 3%.

Let us emphasize that rescaling by 2 is justified because of the anatomical nature of the RA, which is on average 2 times narrower than the BA. In particular, this average in the 76 HT studied patients was 2.1.

The entire range of variability of RFMD-RA in patients with HT lies below the Q1 of the range of variability in BA measurements performed in healthy subjects. For the RFMD-RA measurement, the full range up to the Q3 limit is lower than the value of the Q1 of the range of variation of FMD-BA obtained for healthy subjects.

These results prove that RFMD-RA differentiates the group of patients with HT from healthy controls.

So far, FMD studies have been performed by physicians.^{22,23} According to Westhoff et al., the assessment of endothelial function has become a key factor in individual cardiovascular risk: the ultrasound measurement of dilatation through FMD-RA and FMD-BA is the most common technique, but the analysis is time-consuming and requires the work of an experienced researcher.¹⁸ The obtained information may help to introduce the standard of the modern FMD-RA and FMD-BA test method, which will increase the efficiency and speed of the diagnosis in normotensive patients (using screening tests), as well as the treatment of CVDs. Vascular endothelial dysfunction is an independent risk factor for cardiovascular events. It provides important prognostic data in addition to the more traditional cardiovascular risk factors.^{24–26} Despite many studies, the assessment of the endothelium using FMD in the BA has not become a routine examination in patients with arterial HT due to methodological limitations and therefore, with the availability of high frequency linear probes, the assessment of FMD-RA seems very promising. Of course, the next step to complete the clinical implementation of this approach will be to conduct large prospective clinical trials.

We have also used the TS parameter between releasing the cuff and peak dilation. The p-value of the Welch test for TS parameter for both methods was greater than 0.05. It confirmed that the 2 measurements methods, FMD-RA and FMD-BA for HT patients are statistically indistinguishable using the TS parameter values.

Limitations









There were 3 main limitations of our study: inpatient recruiting, data exploration and measurements technical procedures. We recruited HT patients only from 1 outpatient hypertension clinic. We summarized some global statistics of the patients' clinical data in Table 1, yet we did not provide all the information about patients' comorbidities. The extrapolating of our results to relate FMD size with additional diseases of HT patients was beyond the scope of this publication. We plan to conduct such studies soon, using FMD results to classify the absence or existence of additional CVD states affecting the condition of the arteries. The accurate determination of the maximum diameter of the artery after the cuff release is time-consuming. Often, it was close to 20 min, which is a significant limitation.

Conclusions

Our research shows that the dilatation of the endothelium on the radial artery (FMD-RA) in HT patients is on average twice as large as the brachial artery (FMD-BA). The comparison of 2 FMD measuring methods for HT patients, FMD-RA and FMD-BA, showed the high agreement

indicated by 3% Bland–Altman coefficient and by the ICC equal to 6.88. Both FMD measuring methods could be used to distinguish between HT patients and healthy controls, which confirmed their utility as the diagnostic assisting measurements. A proper, stable fixing of the linear array transducer on the RA is technically easier, and the measurement results are also more robust on the accidental slight movement of the arm than over the BA during several minutes of the entire measurement cycle. Hence, the thesis stating that the measurement of FMD-RA performed with the proposed high frequency ultrasound method for patients with HT is not only equally correct but also competitive, regarding the standard measurement on the BA.

ORCID iDs

Katarzyna Majka  <https://orcid.org/0000-0002-2708-8650>
 Marzena Parol  <https://orcid.org/0000-0003-0203-1399>
 Andrzej Nowicki  <https://orcid.org/0000-0002-9260-8237>
 Barbara Gambin  <https://orcid.org/0000-0001-7212-0157>
 Zbigniew Trawinski  <https://orcid.org/0000-0002-6188-7499>
 Marzena Jaciubek  <https://orcid.org/0000-0002-1277-0518>
 Andrzej Krupienicz  <https://orcid.org/0000-0003-4466-3650>
 Robert Olszewski  <https://orcid.org/0000-0002-4210-5279>

References

- Samb B, Desai N, Nishtar S, et al. Prevention and management of chronic disease: A litmus test for health-systems strengthening in low-income and middle-income countries. *Lancet*. 2010;20;376(9754):1785–1797. doi:10.1016/S0140-6736(10)61353-0
- Oparil S, Zaman MA, Calhoun DA. Pathogenesis of hypertension. *Ann Intern Med*. 2003;4;139(9):761–776. doi:10.7326/0003-4819-139-9-200311040-00011
- Piper MA, Evans CV, Burda BU, Margolis KL, O'Connor E, Whitlock EP. Diagnostic and predictive accuracy of blood pressure screening methods with consideration of rescreening intervals: A systematic review for the U.S. Preventive Services Task Force. *Ann Intern Med*. 2015;162(3):192–204. doi:10.7326/M14-1539
- Murray M, King C, Sorensen C, Bunick E, King R. Community awareness of stroke, hypertension and modifiable risk factors for cardiovascular disease in Nkonya-Wurupong, Ghana. *J Public Health Afr*. 2018;9(2):783. doi:10.4081/jphia.2018.783
- Ma Y, Cheng HY, Cheng L, Sit JWH. The effectiveness of electronic health interventions on blood pressure control, self-care behavioural outcomes and psychosocial well-being in patients with hypertension: A systematic review and meta-analysis. *Int J Nurs Stud*. 2019;92:27–46. doi:10.1016/j.ijnurstu.2018.11.007
- Deanfield JE, Halcox JP, Rabelink TJ. Endothelial function and dysfunction: Testing and clinical relevance. *Circulation*. 2007;115:1285–1295. doi:10.1161/CIRCULATIONAHA.106.652859
- Nowicki A, Trawinski Z, Gambin B, et al. 20-MHZ ultrasound for measurements of flow-mediated dilatation and shear rate in the radial artery. *Ultrasound Med Biol*. 2018;44(6):1187–1197. doi:10.1016/j.ultra-smedbio.2018.02.011
- Iadecola C, Yaffe K, Biller J, et al. Impact of hypertension on cognitive function: A scientific statement from the American Heart Association. *Hypertension*. 2016;68(6):e67–e94. doi:10.1161/HYP.0000000000000053
- Charakida M, Masi S, Lüscher TF, Kastelein JJP, Deanfield JE. Assessment of atherosclerosis: The role of flow-mediated dilatation. *Eur Heart J*. 2010;31(23):2854–2861. doi:10.1093/eurheartj/ehq340
- Flammer AJ, Anderson T, Celermajer DS, et al. The assessment of endothelial function: From research into clinical practice. *Circulation*. 2012;126(6):753–767. doi:10.1161/CIRCULATIONAHA.112.093245
- Brandes RP. Endothelial dysfunction and hypertension. *Hypertension*. 2014;6(4):924–928. doi:10.1161/HYPERTENSIONAHA.114.03575
- Pyke KE, Tschakovsky ME. The relationship between shear stress and flow-mediated dilatation: Implication for the assessment of endothelial function. *J Physiol*. 2005;15;568:357–369. doi:10.1113/jphysiol.2005.089755
- Järvisalo MJ, Jartti L, Toikka JO, Hartiala JJ, Rönnemaa T, Raitakari OT. Noninvasive assessment of brachial artery endothelial function with digital ultrasound and 13-MHz scanning frequency: Feasibility of measuring the true inner luminal diameter using the intima-lumen interface. *Ultrasound Med Biol*. 2000;26(8):1257–1260. doi:10.1016/S0301-5629(00)00308-2
- Mitchell AJ, Mills NL, Newby DE, et al. Radial artery vasomotor function following transradial cardiac catheterisation. *Open Heart J*. 2016;3:e000443. <https://openheart.bmj.com/content/3/2/e000443>. Accessed September 4, 2021.
- Harris RA, Nishiyama SK, Wray DW, Richardson RS. Ultrasound assessment of flow-mediated dilation. *Hypertension*. 2010;55(5):1075–1085. doi:10.1161/HYPERTENSIONAHA.110.150821
- Agewall S, Doughty RN, Bagg W, Whalley GA, Braatvedt G, Sharpe N. Comparison of ultrasound assessment of flow-mediated dilatation in the radial and brachial artery with upper and forearm cuff positions. *Clin Physiol*. 2001;21(1):9–14. doi:10.1093/eurheartj/ehi017
- Calderón-Gerstein WS, López-Peña A, Macha-Ramírez R, et al. Endothelial dysfunction assessment by flow-mediated dilatation in a high-altitude population. *Vasc Health Risk Manag*. 2017;21(13):421–426. doi:10.2147/VHRM.S151886
- Westhoff TH, Schmidt S, Vallbracht-Israng K, et al. Small artery elasticity assessed by pulse wave analysis is no measure of endothelial dysfunction. *J Hypertens*. 2007;25(3):571–576. doi:10.1097/HJH.0b013e328014
- Bilolifar AN, Abbas AE, Maldonado YM, Bendick PJ, Dixon S. Prospective radial artery study following induction of reactive hyperemia looping at degree of diameter growth in health subjects. *J Interv Cardiol*. 2013;26(3):310–316. doi:10.1111/joic.12030
- Nowicki A, Trawinski Z, Gambin B, et al. Assessment of high frequency imaging and Doppler system for the measurements of radial artery flow-mediated dilatation. *Archives of Acoustics*. 2019;44(4):637–644. doi:10.24425/aoa.2019.129276
- Palmieri V, Russo C, Pezzullo S, Di Minno MND, Celentano A. Relation of flow-mediated dilation to global arterial load: Impact of hypertension and additional cardiovascular risk factors. *Int J Cardiol*. 2011;20;152(2):225–230. doi:10.1016/j.ijcard.2010.07.020
- Frangi AF, Laclaustra M, Lamata P. A registration-based approach to quantify flow-mediated dilation (FMD) of the brachial artery in ultrasound image sequences. *IEEE Trans Med Imaging*. 2003;22(11):1458–1469. doi:10.1109/TMI.2003.819278
- Giannattasio C, Achilli F, Grappiolo A, et al. Radial artery flow-mediated dilatation in heart failure patients: Effects of pharmacological and nonpharmacological treatment. *Hypertension*. 2001;38(6):1451–1455. doi:10.1161/hy1201.096528
- Gori T, Grotti S, Dragoni S, et al. Assessment of vascular function: Flow-mediated construction complements the information of flow-mediated dilatation. *Heart*. 2010;96(2):141–147. doi:10.1136/hrt.2009.167213
- Wildansky ME, Gokce N, Keaney JF, Vita JA. The clinical implication of endothelial dysfunction. *J Am Coll Cardiol*. 2003;42(7):1149–1160. doi:10.1016/S0735-1097(03)00994-X
- Widmer RJ, Lerman A. Endothelial dysfunction and cardiovascular disease. *Glob Cardiol Sci Pract*. 2014;2014(3):291–308. doi:10.5339/gcsp.2014.43

Serum WNT4 protein as an indicator of chronic glomerulonephritis but not a marker of inflammatory cell infiltration and fibrosis: A preliminary study

Jolanta Kiewisz^{1,A–F}, Anna Pawłowska^{2,B,C,F}, Agata Winiarska^{2,B,C,F}, Agnieszka Perkowska-Ptasińska^{3,B,C,F}, Agnieszka Skowrońska^{4,B,C,F}, Janusz Godlewski^{1,B,C,F}, Zbigniew Kmiec^{2,5,A,E,F}, Tomasz Stompór^{2,A,D–F}

¹ Department of Human Histology and Embryology, School of Medicine, Collegium Medicum, University of Warmia and Mazury, Olsztyn, Poland

² Department of Nephrology, Hypertension and Internal Medicine, School of Medicine, Collegium Medicum, University of Warmia and Mazury, Olsztyn, Poland

³ Nephropathology Lab, Department of Transplantology and Nephrology, Warsaw Medical University, Poland

⁴ Department of Human Physiology, School of Medicine, Collegium Medicum, University of Warmia and Mazury, Olsztyn, Poland

⁵ Department of Histology, Medical University of Gdansk, Poland

A – research concept and design; B – collection and/or assembly of data; C – data analysis and interpretation;

D – writing the article; E – critical revision of the article; F – final approval of the article

Advances in Clinical and Experimental Medicine, ISSN 1899–5276 (print), ISSN 2451–2680 (online)

Adv Clin Exp Med. 2022;31(3):249–259

Address for correspondence

Jolanta Kiewisz

E-mail: jolanta.kiewisz@uwm.edu.pl

Funding sources

None declared

Conflict of interest

None declared

Acknowledgements

The research and publication was financed from statutory grant (No. 61.610.001-300) of the School of Medicine, Collegium Medicum, University of Warmia and Mazury, Olsztyn, Poland.

Received on June 25, 2021

Reviewed on October 14, 2021

Accepted on November 2, 2021

Published online on December 13, 2021

Cite as

Kiewisz J, Pawłowska A, Winiarska A, et al. Serum WNT4 protein as an indicator of chronic glomerulonephritis but not a marker of inflammatory cell infiltration and fibrosis: A preliminary study. *Adv Clin Exp Med.* 2022;31(3):249–259. doi:10.17219/acem/143543

DOI

10.17219/acem/143543

Copyright

© 2022 by Wrocław Medical University

This is an article distributed under the terms of the Creative Commons Attribution 3.0 Unported (CC BY 3.0) (<https://creativecommons.org/licenses/by/3.0/>)

Abstract

Background. The WNT signaling pathway contributes to renal fibrosis, which is a hallmark of chronic kidney disease (CKD). Serum concentration of WNT4 could be used to monitor the kidney disease; however, no data have yet been published on the subject.

Objectives. This study measures WNT4 protein in serum of CKD patients depending on the stage, type of nephropathy, the non-nephrotic (NNP) or nephrotic proteinuria (NP), inflammatory cell infiltration in kidney parenchyma (IHKP), interstitial fibrosis in biopsy and serum creatinine. We also evaluated the usefulness of the serum WNT4 as a marker of fibrosis and IHKP.

Materials and methods. The WNT4 protein level in serum of CKD patients and healthy individuals was measured using enzyme-linked immunoassay (ELISA). Patients' blood biochemical profiles and kidney biopsies were evaluated with common laboratory methods.

Results. The serum level of WNT4 protein was higher in CKD patients (i) regardless of the underlying etiology and at early stages of disease; (ii) with lupus nephritis and Immunoglobulin A (IgA) nephropathy; (iii) without or with a small area of IHKP; and (iv) with a small area covered with fibrosis. No difference was observed between NNP and NP patients. The utility of serum WNT4 as a marker of IHKP and fibrosis was not confirmed. Negative correlations with total and low-density lipoprotein (LDL)-cholesterol were found in CKD and IHKP patients. In patients with serum WNT4 above the median value, serum creatinine was higher. However, no correlation between serum WNT4 and creatinine level was found.

Conclusions. The observed increase in serum WNT4 protein in the early stages of CKD and in patients diagnosed with immune-mediated glomerular disease may suggest that WNT4 may act as a mediator of inflammation. A certain association with the dysregulation of serum lipid metabolism can also be suspected. Serum WNT4 protein may be considered as the indicator of chronic glomerulonephritis, but not a diagnostic marker of IHKP and fibrosis.

Key words: chronic kidney disease, serum, WNT4, kidney fibrosis, inflammatory cells infiltration

Background

Chronic kidney disease (CKD) develops as a consequence of age-related lesions, infections, metabolic disorders, episodes of acute kidney injury, autoimmune glomerulopathies, toxic injury, and many other insults that lead to progressive renal dysfunction. Infiltration of the tubulointerstitial compartment with inflammatory cells followed by interstitial fibrosis and tubular atrophy, as well as progressive glomerular sclerosis, constitute the histopathological appearance of late-stage nephropathies.¹ Chronic kidney disease is defined as abnormalities of kidney structure and/or function that persist for more than 3 months and significantly affect health status.² The CKD is becoming a disease of civilization, affecting up to 15% of the world population.³ Thus, to improve the methods of prevention and detection, and to reduce the costs of treatment of the disease, there is an urgent need to establish molecular markers allowing for its early diagnosis.

The progression of CKD is associated with the acquisition of a mesenchymal phenotype by the epithelial cells of the convoluted tubules in a process called epithelial-mesenchymal transition (EMT). This process of dedifferentiation of highly specialized, polarized and basement membrane-embedded tubular epithelial cells into myofibroblast-like cells which can digest the tubular basement membrane, migrate into the interstitium and start producing matrix proteins, is a well-recognized mechanism of progression in several chronic nephropathies. The expansion of fibrosis is a consequence of chronic and not fully resolved inflammation. Both processes develop upon the activation of cell signal transduction pathways.^{4–8}

The WNT signaling pathways are evolutionary conserved. When the canonical pathway (WNT/ β -catenin signaling) is activated, it promotes regenerative processes. Uncontrolled, sustained WNT/ β -catenin signaling activation induces tubular damage.⁹ The WNT protein acting in a paracrine and an autocrine manner influences WNT/ β -catenin signaling in fibroblasts, macrophages and mesangial cells.^{1,10–13} It has been shown that among WNT family members, WNT4 protein plays a significant role in embryogenic morphogenesis and MET (mesenchymal-to-epithelial transition) occurring during the formation of renal tubules.^{14–16} The activation of cellular signaling pathways through WNT4 protein is suppressed in a healthy adult kidney.¹⁷ The reactivation of the WNT4 expression occurs in pathological states, as demonstrated in the mouse model.¹⁷ The modulated expression of the *Wnt4* mRNA in the convoluted tubules is associated with renal fibrosis.¹⁷ The expression of *Wnt4* gene was found to be reactivated in animal models of unilateral ureteral obstruction.¹⁸ Moreover, WNT4 participates in the tissue regeneration process following experimental acute kidney injury.¹⁹ After angiotensin II treatment, *WNT4* mRNA level increases in human kidney proximal epithelial cells (HK-2 cells) and podocytes.²⁰ The WNT4

activity can be blocked after binding to the Klotho protein, as demonstrated in the in vitro study in human proximal tubular epithelial cells.⁵

It has been shown that an elevated level of WNT1 protein in the blood correlates with an increased risk of myocardial infarction.²¹ However, the serum concentrations of other WNT proteins have not yet been reported in humans. The WNT4 concentration has only been measured in human urine.²²

Objectives

Assuming the contribution of WNT4 protein in kidney fibrosis and progression of CKD, the study aimed to evaluate whether the serum level of WNT4 protein might depend on CKD stage, underlying etiology and degree of proteinuria (nephrotic (NP) and non-nephrotic (NNP)). Moreover, we decided to verify the possible associations between serum WNT4 and creatinine, and the advancement of tubulointerstitial inflammation and fibrosis in kidney biopsy specimens obtained from stable patients with biopsy-confirmed nephropathies.

Materials and methods

All procedures performed in the studies involving human participants were in accordance with the ethical standards of the local Ethics Committee of the Medical Chamber (7/2013/V) and with the 1964 Declaration of Helsinki and its later amendments or comparable ethical standards. The blood was collected following a written informed consent by the participants of the study.

Patients

Stable CKD subjects ($n = 63$; mean age: 46.03 ± 2.11 years, mean \pm standard deviation (SD)) were recruited from patients treated in the Department of Nephrology, Hypertension and Internal Medicine of the Faculty of Medicine at the University of Warmia and Mazury in Olsztyn, Poland, between 2013 and 2016.

The study was performed in patients with clinical suspicion of glomerular disease (primary or secondary) who underwent kidney biopsy, which has been performed based on the standard clinical indications, i.e. nephrotic syndrome, subnephrotic proteinuria, isolated (otherwise unexplained) hematuria, unexplained fall in glomerular filtration rate (GFR), as well as when symptoms of renal injury have occurred in the course of already diagnosed 'systemic' disease (i.e. systemic lupus). None of the patients suffered from diabetes or had a history of cardiovascular events. Well-controlled hypertension (1–3 blood pressure drugs) was observed in 67% of the patients included in the study. Biopsies were not performed intentionally for this study. Patients were excluded if they experienced an 'acute' illness (i.e. infection,

noninfectious inflammation, cardiovascular event) or a disease that had occurred within the last 30 days, and in the case of a known active malignancy, as well as drug or alcohol abuse.

The control group ($n = 42$; mean age 58.31 ± 0.85 years, mean \pm SD) was recruited from volunteers who did not suffer from any kidney disease and were otherwise healthy.

The demographic data were collected at the time of biopsy or blood collection. The diagnosis of nephropathy was established based on a clinical appearance, laboratory and immunological tests, and histopathological assessment.

Material collection and laboratory parameters

Blood samples were collected from overnight fasted patients. After centrifugation for 10 min at 3500 rpm, the serum samples were stored at -80°C . Immediately after the sample collection, serum biochemistry was assayed with a Cobas 6000 multi-analyzer (Roche Diagnostics, Basel, Switzerland) and Uro-dipcheck 400e (ERBA, Mannheim, Germany). The following parameters were analyzed: lipids, glucose, urea, and creatinine; estimated glomerular filtration rate (eGFR) was calculated using the modification of diet in renal disease (MDRD) formula.

Measurement of serum WNT4 concentration

The WNT4 levels in serum samples were determined using a commercially available enzyme-linked immunoassay (ELISA) kit, according to the manufacturer's protocol (CSB-EL026137HU; Cusabio, Wuhan, China). Briefly, reagents, working standards and samples were prepared according to the procedure. Standards and samples were added in a quantity of 100 μL per well. After 2-h incubation at 37°C and liquid removal, wells were filled with biotin antibody and were incubated for 1 h at 37°C . Antibodies were washed out with wash buffer and horseradish peroxidase (HRP)-avidin complexes were added to each well. After 1 h incubation at 37°C , aspiration and washing steps were repeated. The TMB substrate was added and after 30 min at 37°C , the reaction was stopped with the stop solution. All the above reagents were purchased from Cusabio (Wuhan, China). The optical density was established with ChroMate[®] Multichannel Microplate Reader (Awareness Technology, Inc., Wiener Neustadt, Austria). The detection range varied from 23.5 pg/mL to 1500 pg/mL. The sensitivity of the assay was less than 5.8 pg/mL. Each sample was measured in duplicate.

Renal tissue sampling, evaluation and classification

Paraffinized sections (5 μm) were used for routine histopathological assessment. Two pathologists classified and scored the biopsies separately, without knowing the medical history of the patients. The extent of inflammatory infiltration

in the kidney parenchyma (IIKP) and renal fibrosis (Fibrosis) were determined separately, semi-quantitatively, using the following scale: 0 – absence; 1 – small clusters; 2 – mild clusters; 3 – moderately extensive clusters; 4 – wide clusters.

After considering the biochemical analysis and pathological evaluation, the test group was rearranged for research purposes. The data comparison was made between the control and: (i) CKD patients; (ii) CKD group divided into subgroups of patients with the NNP or NP; (iii) CKD group divided according to the Kidney Disease: Improving Global Outcomes (KDIGO) classification based on eGFR values²³; (iv) pathomorphologically diagnosed glomerular kidney disease; (v) semi-quantitatively estimated degree of IIKP; and (vi) semi-quantitatively estimated degree of the kidney fibrosis. The association between the serum WNT4 protein and creatinine levels in the study population was also analyzed.

Statistical analyses

Statistical analyses were conducted using GraphPad Prism v. 7.05 software (GraphPad Software, Inc., San Diego, USA). The Kolmogorov–Smirnov test was used to check whether data were distributed normally (Supplementary Table 1–5). Demographic data and blood biochemistry of control and CKD patients were compared with a Mann–Whitney test. The results of the blood biochemical components were presented as mean \pm SD. The comparison of serum WNT4 protein level in the CKD and control group was determined using the nonparametric equivalent of a Student's *t*-test for independent variables, i.e., Mann–Whitney test. The evaluation of the serum WNT4 protein level between the control group and CKD group divided into subgroups of patients with NNP and NP was conducted with the Kruskal–Wallis test followed by the post hoc corrected Dunn's test (Bonferroni correction). The comparison of serum WNT4 levels with CKD stages involved more than 2 groups of patients. Therefore, the Kruskal–Wallis test was followed by the post hoc corrected Dunn's test (Bonferroni correction). The serum WNT4 levels in patients with distinct types of glomerular disease were compared using the Mann–Whitney test. The association of the serum WNT4 protein with IIKP and fibrosis were estimated with the Kruskal–Wallis test, followed by the post hoc corrected Dunn's test (Bonferroni correction). The possibility of estimation of WNT4 protein in serum was analyzed using linear or multivariate regression depending if 1 (tubulointerstitial lesions) or more than 1 (age, fibrosis) variables were taken into consideration. The receiver operating characteristic (ROC) curves reflecting the sensitivity and specificity of the assay to detect IIKP and fibrosis, and their specific area under the curve (AUC) were calculated. The correlations between WNT4 protein level, blood biochemical parameters and pathomorphological features were calculated using a nonparametric Spearman's test. The analysis of the association of the serum WNT4 protein with serum creatinine was conducted using

the Mann–Whitney test. Potential associations of WNT4 and serum creatinine were analyzed with multivariate regression analysis. A value of 95% was used for the confidence intervals (95% CI). The WNT4 protein amounts are presented as median and interquartile range (IQR). The differences were considered statistically significant when $p < 0.05$.

Results

Clinical-pathological characteristics

Table 1 displays the demographic data and serum biochemistry of the whole studied population (control subjects and CKD patients) enrolled in the analysis. The statistical

Table 1. Demographic data and blood biochemistry of control and chronic kidney disease (CKD) patients enrolled in the analysis

Variable	Control	CKD
N	42	63
Age [years]	58.31 ± 0.85	46.03 ± 2.11****
Gender (M/F)	26/16	33/30
Total cholesterol [mg/dL]	170.7 ± 6.46	220.7 ± 8.91****
HDL [mg/dL]	54.89 ± 3.24	55.18 ± 2.57
LDL [mg/dL]	76.14 ± 7.77	145 ± 8.03****
TG [mg/dL]	61.98 ± 9.38	175.4 ± 9.65****
Glucose [mg/dL]	105.3 ± 4.51	101.2 ± 3.56
Urea [mg/dL]	33.21 ± 1.18	55.15 ± 4.16****
Creatinine [mg/dL]	0.76 ± 0.02	1.87 ± 0.22****
eGFR [mL/min/1.73 m ²]	103.1 ± 2.60	62.92 ± 4.37****

CKD – chronic kidney disease; HDL – high-density lipoprotein; LDL – low-density lipoprotein; TG – triglycerides; eGFR – estimated glomerular filtration rate. The asterisks indicate statistical significance (**** $p < 0.0001$).

analysis showed significant differences between control subjects and CKD patients (Table 1). However, no correlation was observed between the amount of WNT4 protein and age ($p = 0.6550$; $r = -0.0574$).

Associations of serum WNT4 levels with CKD stage and diagnosis of glomerular disease

The statistical comparison of the serum WNT4 levels was performed between the control ($n = 42$) and CKD patient ($n = 63$) groups, as well as between the subgroups of patients with NNP ($n = 23$) and NP ($n = 27$). A significantly higher serum WNT4 concentration was found in the CKD patients (21.71 pg/mL (IQR: 15.47–32.98 pg/mL)) as compared to the control group (16.62 pg/mL (IQR: 12.72–20.78 pg/mL)); $p = 0.0074$; Fig. 1A). No statistically significant differences were found in serum WNT4 levels between control (16.62 pg/mL (IQR: 12.72–20.78 pg/mL)) and NNP (19.19 pg/mL (IQR: 16.18–30.94 pg/mL)) or NP (20.44 pg/mL (IQR: 14.15–32.98 pg/mL)) groups of CKD patients ($p = 0.0904$; Fig. 1B). A statistically significant inverse correlation between WNT4 and serum cholesterol levels was found in the whole CKD group ($p = 0.0084$; Table 2). However, serum WNT4 levels did not correlate with other biochemical parameters or eGFR (Table 2).

Patients with CKD were also grouped according to the KDIGO classification, based on their eGFR values (2013).²³ Patients who had an eGFR value ≥ 60 mL/min/1.73 m² were classified to CKD stage 1–2 ($n = 33$), and those with eGFR < 60 mL/min/1.73 m² – to CKD stage 3–5 ($n = 30$). The Kruskal–Wallis test followed by corrected Dunn’s test showed a higher level of serum WNT4 protein in the blood of patients classified into CKD stage 1–2 (22.78 pg/mL (IQR: 15.32–39.56 pg/mL)) in comparison to control (16.62 pg/mL

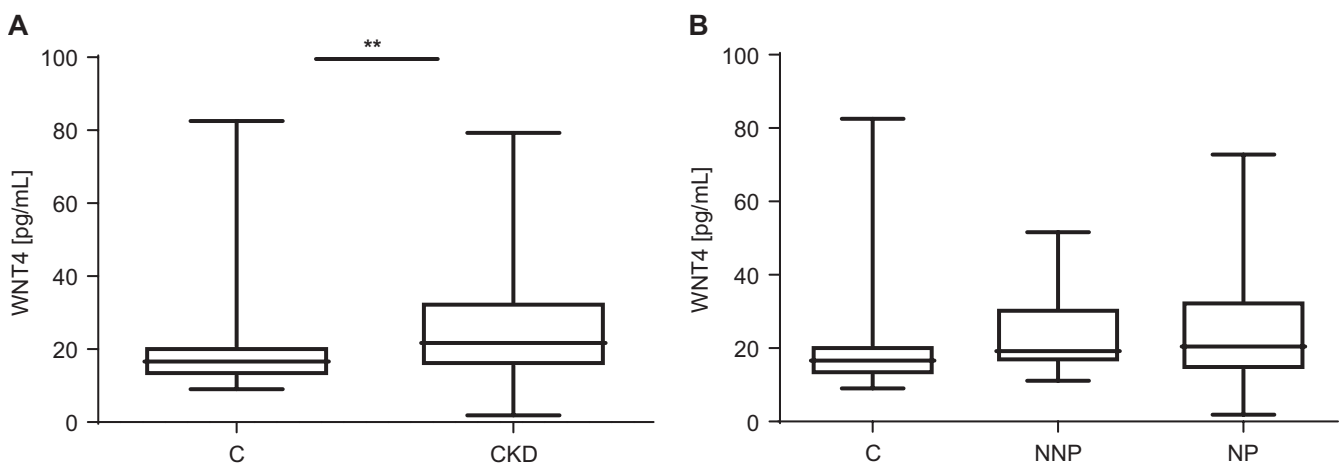


Fig. 1. A. Nonparametric Mann–Whitney test comparison of the concentration of WNT4 protein in the sera of control subjects (C; $n = 42$; 20.39 ± 2.25 pg/mL) and the whole group of chronic kidney disease (CKD; $n = 63$; 26.86 ± 2.03 pg/mL) patients presenting various stages and categories of kidney disease; B. Kruskal–Wallis test evaluation of the serum WNT4 protein level between the control group (C; $n = 42$; 20.39 ± 2.25 pg/mL) and CKD group divided into subgroups of patients with non-nephrotic proteinuria (NNP; $n = 23$; 25.03 ± 2.56 pg/mL) and nephrotic proteinuria (NP; $n = 27$; 25.15 ± 3.11 pg/mL). For each box, the horizontal line inside the box shows the median. The ends of the boxes represent the 1st and 3rd quartiles. The whiskers extend to the highest and lowest values considered outliers (defined as 1.5 times the interquartile range (IQR)). Asterisks indicate statistically significant differences between the groups (** $p = 0.0074$)

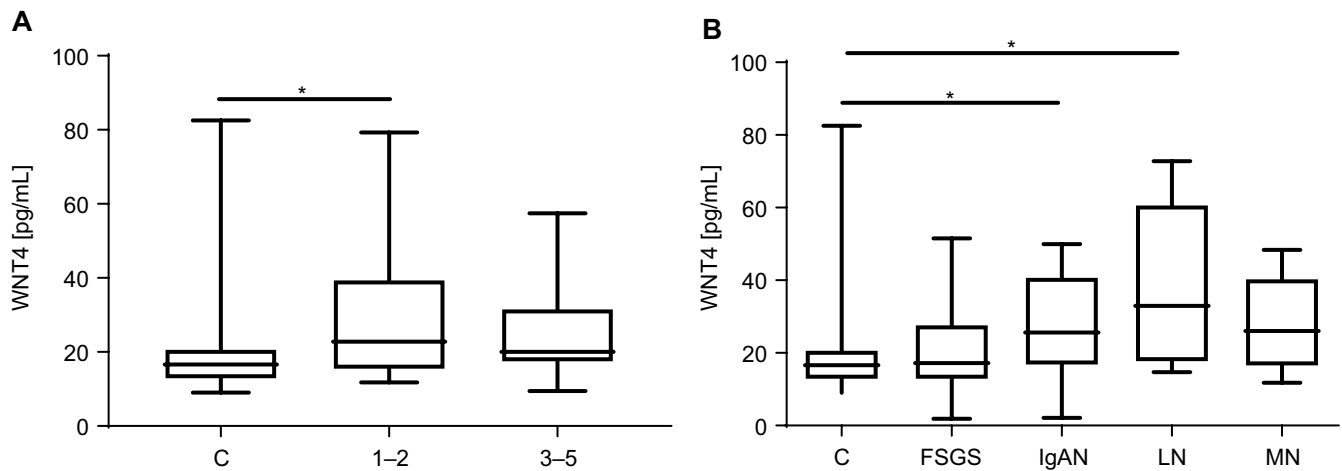


Fig. 2. A. Kruskal–Wallis test comparison of the concentration of WNT4 protein in the serum of control subjects (n = 42) and patients qualified to groups representing different stages of kidney disease depending on Kidney Disease: Improving Global Outcomes (KDIGO) classification (stage 1–2 (n = 33), stage 3–5 (n = 30)); B. Various types of kidney diseases (focal segmental glomerulosclerosis (FSGS) (n = 14), IgA nephropathy (IgAN) (n = 14), lupus nephritis (LN) (n = 5), and membranous nephropathy (MN) (n = 6)). The Kruskal–Wallis analysis showed statistically significant differences between the level of serum WNT4 protein in the control group (n = 42; 20.39 ± 2.25 pg/mL) and patients classified into chronic kidney disease (CKD) stages 1–2 (29.31 ± 3.00 pg/mL; *p = 0.0118) or patients with LN (37.95 ± 10.5 pg/mL; *p = 0.0481) or IgAN (28 ± 5.62 pg/mL; *p = 0.0408) diagnosis. For each box, the horizontal line inside the box shows the median. The ends of the boxes represent the 1st and 3rd quartiles. The whiskers extend to the highest and lowest values considered outliers (defined as 1.5 times the interquartile range (IQR))

Table 2. Correlation coefficients (r) between biochemical parameters of blood and WNT4 protein level in the serum of chronic kidney disease (CKD) patients, patients presenting inflammatory cell infiltration in the kidney parenchyma (IHKP) and patients presenting renal fibrosis (Fibrosis)

Groups	N	Total cholesterol	HDL	LDL	TG	Glucose	Urea	Creatinine	eGFR
Units	–	mg/dL	mg/dL	mg/dL	mg/dL	mg/dL	mg/dL	mg/dL	mL/min/1.73 m ²
CKD	63	-0.33 $\rho = 0.0084$	-0.04	-0.22	-0.15	0.01	-0.07	-0.05	0.08
IHKP	49§	-0.41 $\rho = 0.0036$	-0.17	-0.31 $\rho = 0.0285$	0.08	-0.14	-0.16	-0.1	0.14
Fibrosis	56§	-0.32 $\rho = 0.0159$	-0.10	-0.19	-0.14	-0.03	-0.07	-0.06	0.10

HDL – high-density lipoprotein; LDL – low-density lipoprotein; TG – triglycerides; eGFR – estimated glomerular filtration rate. Statistical significance (p) is presented above the r-value. Paragraph (§) indicates that the group of patients was reduced. Elimination consisted of patients not showing the examined feature. Bold denotes statistical significance.

(IQR: 12.72–20.78 pg/mL); p = 0.0118; Fig. 2A). No statistical significance was observed between the control (16.62 pg/mL (IQR: 12.72–20.78 pg/mL)) and CKD stage 3–5 group (20.07 pg/mL (IQR: 17.28–31.7 pg/mL)), neither between CKD stage 1–2 (22.78 pg/mL (IQR: 15.32–39.56 pg/mL)) and CKD stage 3–5 group (20.07 pg/mL (IQR: 17.28–31.7 pg/mL); p = 0.9999).

Four distinct types of glomerular disease could be diagnosed in the patients: focal segmental glomerulosclerosis (FSGS; n = 14), Immunoglobulin A (IgA) nephropathy (IgAN; n = 14), lupus nephritis (LN; n = 5) and membranous nephropathy (MN; n = 6). However, the nonparametric analysis of independent variables with a Mann–Whitney test showed that patients diagnosed with LN (32.98 pg/mL (IQR: 17.57–60.83 pg/mL); p = 0.0481) or IgAN (25.59 pg/mL (IQR: 16.63–40.89 pg/mL); p = 0.0408) had significantly higher serum WNT4 protein levels as compared to the control group (16.62 pg/mL (IQR: 12.72–20.78 pg/mL); Fig. 2B).

No correlation was found between serum WNT4 protein level and biochemical parameters within the group of patients with CKD or those diagnosed with LN or IgAN (data not shown).

Association of the serum WNT4 protein level with tubulointerstitial lesions in kidney biopsy samples

The evaluation of IHKP of CKD patients revealed 30 subjects in whom the kidney tissue fragments did not show any inflammation or that presented with only small areas of inflammation (group 0–1). The mild, medium and extensive areas of inflammation were observed in biopsies of 33 patients (group 2–4).

In sera of patients with at least small areas of inflammatory cell infiltrates in the biopsy samples (group 0–1), the serum level of WNT4 protein was higher than that of the control group (24.91 pg/mL (IQR: 17.36–34.19 pg/mL)) compared to 16.62 pg/mL (IQR: 12.72–20.78 pg/mL), respectively; p = 0.0142; Fig. 3A), as confirmed with a Kruskal–Wallis test followed by corrected Dunn’s test. No statistical significance was observed between the control group (16.62 pg/mL (IQR: 12.72–20.78 pg/mL)) and group 2–4 (19.19 pg/mL (IQR: 14.8–34.83 pg/mL); p = 0.2594), neither between group 0–1 (24.91 pg/mL (IQR: 17.36–34.19 pg/mL))

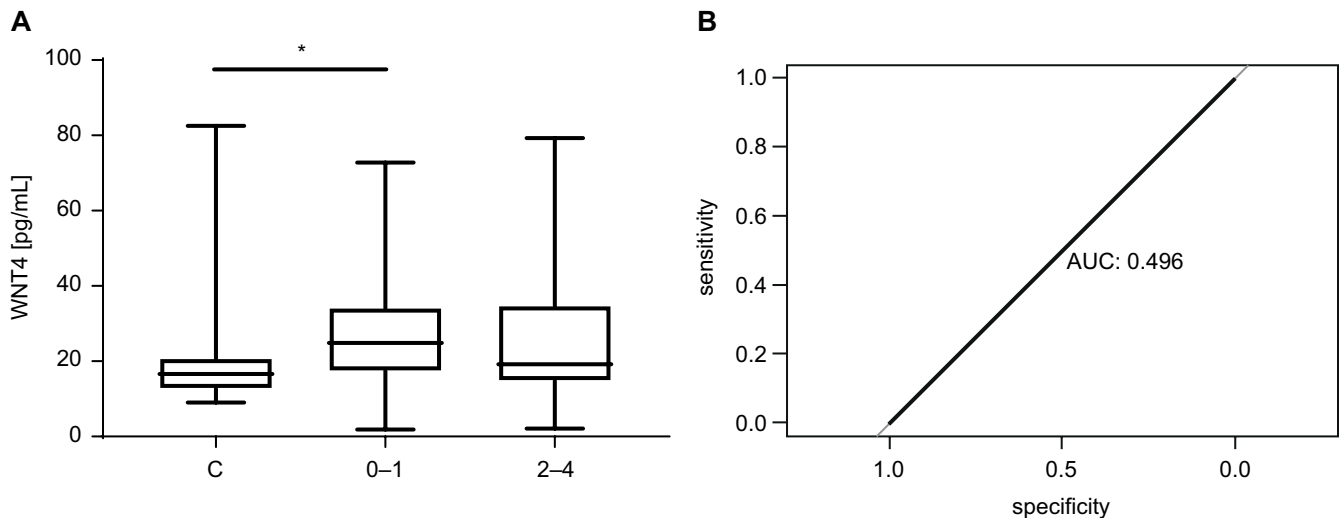


Fig. 3. A. Kruskal–Wallis test comparison presented statistically significant difference between the WNT4 protein level in serum of patients who were classified as chronic kidney disease (CKD) patients without inflammatory cells or with a small area of inflammatory cells infiltration in the biopsied tissue ($n = 30$; 27.83 ± 2.78 pg/mL; group 0–1) in comparison to serum WNT4 level in control subjects (20.39 ± 2.25 pg/mL). Asterisks indicate differences between groups ($*p = 0.0142$; A). The receiver operating characteristic (ROC) curve presenting the area under the curve (AUC) value was estimated to establish sensitivity and specificity of the WNT4 protein in blood measurement for setting the severity of the tubulointerstitial lesions (B). For each box, the horizontal line inside the box shows the median. The ends of the boxes represent the 1st and 3rd quartiles. The whiskers extend to the highest and lowest values considered outliers (defined as 1.5 times the interquartile range (IQR))

and group 2–4 (19.19 pg/mL (IQR: 14.8 – 34.83 pg/mL); $p = 0.8205$; Fig. 3A), in terms of serum WNT4.

Results of linear regression analysis showed that the serum level of WNT4 protein in the blood could not be determined based on the estimation of tubulointerstitial lesions ($p = 0.7507$; $r^2 = 0.0022$). The AUC value for the sensitivity and specificity ROC curve was 0.4960 (Fig. 3B).

The negative correlation was observed between the serum WNT4 protein and the cholesterol level ($p = 0.0036$) as well as the low-density lipoprotein (LDL) level ($p = 0.0285$) in the IIKP group of CKD patients (Table 2).

Association of the serum WNT4 protein level with histological features of kidney fibrosis

No fibrosis or small clusters of fibrosis (group 0–1) were observed in kidney sections of 25 patients. Kidney tissue samples from 38 CKD patients showed mild, moderately increased or large areas of the interstitium, which were occupied by fibrosis (group 2–4).

The comparison of serum WNT4 protein levels between patients with CKD but displaying almost no fibrosis (group 0–1; 27.02 pg/mL (IQR: 17.99 – 35.45 pg/mL)) and control, healthy subjects (16.62 pg/mL (IQR: 12.72 – 20.78 pg/mL)) showed higher values of WNT4 in the CKD 0–1 group ($p = 0.0062$; Fig. 4A). No statistical significance was observed between the healthy group (16.62 pg/mL (IQR: 12.72 – 20.78 pg/mL)) and group 2–4 (19.35 pg/mL (IQR: 14.74 – 33.23 pg/mL)); $p = 0.3034$), neither between group 0–1 (27.02 pg/mL (IQR: 17.99 – 35.45 pg/mL)) and group 2–4 (19.35 pg/mL (IQR: 14.74 – 33.23 pg/mL)); $p = 0.3300$; Fig. 4A).

The estimation of the serum WNT4 protein level could not be determined based on age ($p = 0.3549$; $r^2 = 0.0140$) and fibrosis ($p = 0.3299$; $r^2 = 0.0158$). The AUC value for the sensitivity and specificity ROC curve was 0.5940 (Fig. 4B).

The WNT4 protein serum level was negatively correlated with total cholesterol in CKD patients with renal fibrosis in biopsy specimens ($p = 0.0159$; Table 2).

Association between the serum concentration of WNT4 protein and creatinine

The association between serum WNT4 protein and creatinine was analyzed based on the assumption that WNT4 protein can be considered a novel biomarker for the early detection of kidney disease (which has been suggested by Zhao et al.).²² The method presented earlier by Goliasch et al. was followed to study this assumption.²¹ The entire group (control subjects and CKD patients; $n = 105$) was divided into 2 subgroups, according to serum WNT4 median value (16.62 pg/mL) in the control group, to assess the relationship between the serum levels of WNT4 protein and creatinine in the study sample. Statistical analysis showed that serum creatinine was higher in patients who had WNT4 protein concentration above median as compared to those with the serum WNT4 protein concentration below the median value (1.48 ± 0.18 mg/dL compared to 0.99 ± 0.09 mg/dL, respectively; $p = 0.0354$; Fig. 5A). However, the results of linear regression analysis showed that the serum WNT4 protein level could not be determined based on creatinine level ($p = 0.8429$; $r^2 = 0.0006$).

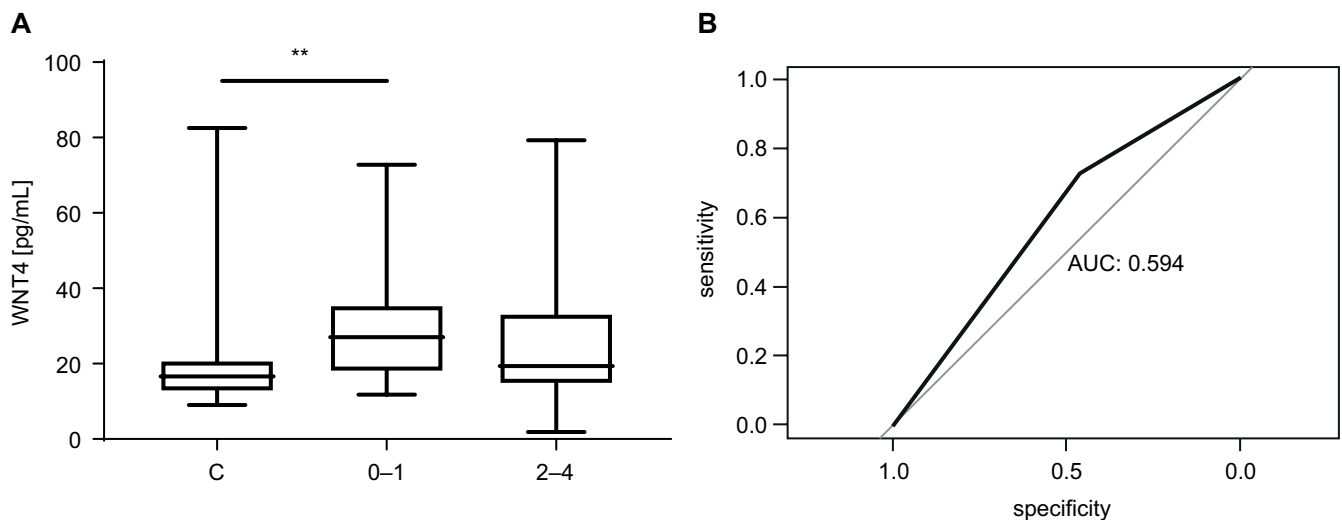


Fig. 4. Serum level of WNT4 protein compared using Kruskal–Wallis test was significantly higher in patients with a small area of fibrosis (group 0–1; 27.83 ± 2.78 pg/mL) than in the group of control subjects (20.39 ± 2.25 pg/mL). Asterisks indicate differences between groups (** $p = 0.0062$; A). The receiver operating characteristic (ROC) curve presenting the area under the curve (AUC) value was estimated to establish sensitivity and specificity of the serum WNT4 protein for setting the advancement of fibrosis (B). For each box, the horizontal line inside the box shows the median. The ends of the boxes represent the 1st and 3rd quartiles. The whiskers extend to the highest and lowest values considered outliers (defined as 1.5 times the interquartile range (IQR))

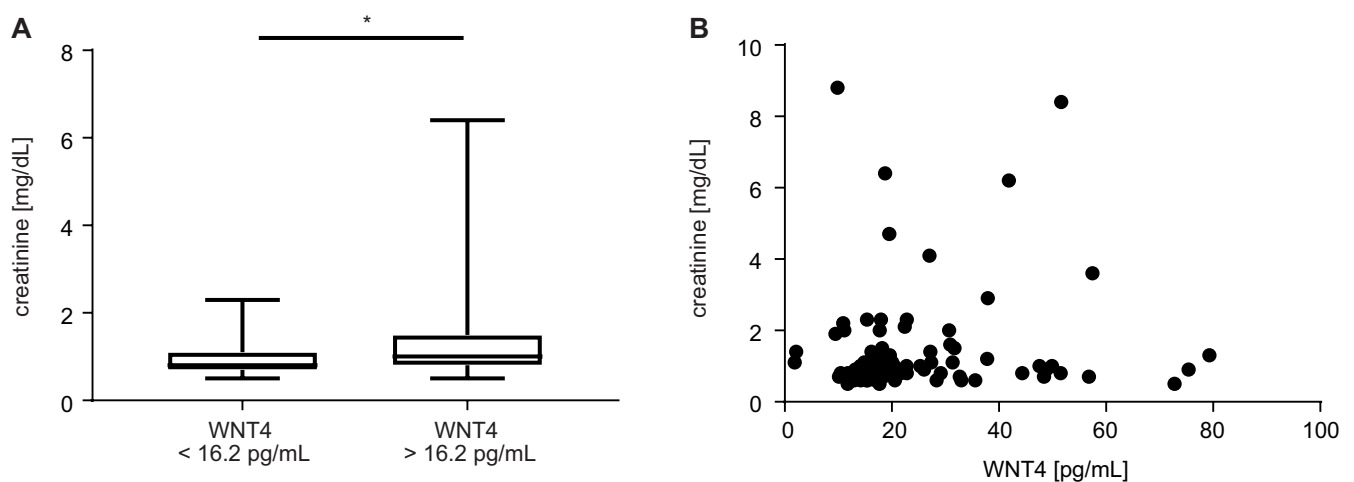


Fig. 5. Serum creatinine concentration in patients divided into 2 groups according to the median WNT4 protein concentration (16.62 pg/mL) in the sera of the total studied population ($n = 105$) which included control subjects and patients with chronic kidney disease (CKD). Mann–Whitney test comparison showed that serum creatinine was higher in patients who had WNT4 protein concentration higher than 16.62 pg/mL (1.48 ± 0.18 pg/mL) in comparison to those with a WNT4 protein concentration lower than 16.62 pg/mL (0.99 ± 0.09 pg/mL). Asterisks indicate the differences between the groups (* $p = 0.0354$; A). Lack of correlation was observed between serum WNT4 protein and creatinine levels ($r = 0.12$; B). For each box, the horizontal line inside the box shows the median. The ends of the boxes represent the 1st and 3rd quartiles. The whiskers extend to the highest and lowest values considered outliers (defined as 1.5 times the interquartile range (IQR))

Discussion

This novel study found that serum WNT4 protein level is higher in patients diagnosed with CKD, classified according to the eGFR value or the type of glomerulopathy, but not according to the presence of NP or NNP. A higher level of serum WNT4 protein in CKD patients as compared to control subjects suggests that mechanisms activating the WNT pathway and influencing WNT4 may become apparent at any stage of the disease and may depend on the underlying pathology, but not on the degree of proteinuria. The potential dependence

on the glomerular filtration rate may be a limitation for WNT4 to be a marker and an indicator of podocyte injury. In our study, the elevated serum WNT4 protein levels in the subgroups of both primary (IgAN) and secondary (LN) glomerular disease might result from the dysregulation of the immune system. Therefore, it seems that the elevated serum WNT4 level, leading to the development of certain glomerular and tubular lesions (as presented in experimental studies)^{17,18,20} reflects also the activation of the immune system.

The increase of serum WNT4 protein level in patients with different kinds of glomerular disease and different

(but not necessary more advanced) stages of CKD may represent a novel and common denominator of not yet identified pathological event in chronic kidney injury. Our findings demonstrate that serum WNT4 protein level is higher in patients with CKD. Moreover, it is also higher in patients without IIKP or those with only minor advancement of IIKP, as well as in those without advanced renal fibrosis. Inspired by the study by Chang et al., we suspect, that WNT4 considered as a marker of podocyte injury can display an identical pattern of expression as inflammatory mediators and act in a comparable way.²⁴ Furthermore, as the WNT4 triggers tissue infiltration with neutrophils²⁵ and facilitates the transformation of stem cells into the fibrogenic fate,²⁶ it cannot be ruled out that the identical mechanism is in action during CKD progression. It would be worth answering this question by conducting studies in a larger group of patients with biopsy-confirmed glomerular disease.

The elevated serum WNT4 protein level may accompany CKD but cannot be considered a marker of IIKP and fibrosis. It is supported by our results showing that serum WNT4 protein correlated with serum total and LDL-cholesterol. Changes in serum lipids such as free fatty acids, triglycerides and glycopospholipids develop in the course of CKD (especially when proteinuria is present), but also significantly impact the course of CKD (although to date lipid-lowering therapies did not show to be nephroprotective).^{27,28} Additionally, the accumulation of lipids can lead the palmitate retention.²⁹ It has been shown that the lipidation of WNT proteins (including coupling of palmitate) is required for their secretion and function. Palmitoylation accounts for the hydrophobicity and poor solubility of WNT proteins, which modulate their ability to activate WNT/ β -catenin signaling.^{30–33} It remains to be addressed whether, in this way, WNT4 can act as the primary ‘switch’ involved in the development of kidney dysfunction and the initiation of fibrosis. It would be of particular interest given that we observed the elevated serum WNT4 protein level mainly in patients in early stages of CKD (stages 1–2), and with early IIKP (stages 0–1) and fibrosis (stages 0–1).

The current study has shown that serum creatinine concentration was higher in a group with serum WNT4 protein concentration above the WNT4 median value (16.62 pg/mL). However, these parameters were not correlated. As far as we know, no other studies measuring the level of WNT4 protein in serum have yet been published. In a single study presenting the WNT4 protein expression as a biomarker for podocyte integrity in the rat model of renal ischemia-reperfusion injury, the serum level of WNT4 protein correlated with serum creatinine.²⁴ Another research showed an increase in WNT4 protein in the urine of patients with minimal change disease and coexisting tubular injury; however, no correlation with serum creatinine level was observed,²² as in our study.

Limitations

We are aware that empirical results presented herein should be considered in light of certain limitations. The observed results are based on a relatively small group of patients (nevertheless, even the ‘large’ trials in the field of glomerular disease usually do not exceed 100 patients). Thus, to not rely solely on the division of CKD depending on the stages (which is an imprecise classification since each class contains patients with the same kidney function, but diverse underlying pathology and clinical presentation), the particular diagnoses of kidney disease were considered, compared with the control group, with CKD group as a whole, but also with the CKD patients divided based on the degree of proteinuria. With this approach, the course of future research has been delineated. On the other hand, primary and immune-mediated secondary glomerular diseases are considered rare and most of the clinical research is performed rather on dozens than hundreds of patients.

Conclusions

The preliminary data presented here suggest that elevated levels of serum WNT4 protein may be associated with the immune system response. Moreover, it accompanies the dysregulation of serum lipids that are associated with CKD. It is observed in the early stages of CKD, IIKP and fibrosis, and may trigger CKD progression. Therefore, it would be interesting to investigate the involvement of WNT4 in the molecular mechanisms responsible for the development of CKD, considering that WNT4 is only an indicator of chronic glomerulonephritis and not a diagnostic marker of IIKP and fibrosis.

ORCID iDs

Jolanta Kiewisz  <https://orcid.org/0000-0002-2738-8952>
 Anna Pawłowska  <https://orcid.org/0000-0002-1455-1730>
 Agata Winiarska  <https://orcid.org/0000-0003-4755-5006>
 Agnieszka Perkowska-Ptasińska  <https://orcid.org/0000-0001-5524-3534>
 Agnieszka Skowrońska  <https://orcid.org/0000-0002-2274-8867>
 Janusz Godlewski  <https://orcid.org/0000-0001-6268-7694>
 Zbigniew Kmieć  <https://orcid.org/0000-0002-9801-8166>
 Tomasz Stompór  <https://orcid.org/0000-0002-3944-0850>

References

1. Maarouf OH, Aravamudhan A, Rangarajan D, et al. Paracrine Wnt1 drives interstitial fibrosis without inflammation by tubulointerstitial cross-talk. *J Am Soc Nephrol*. 2016;27(3):781–790. doi:10.1681/ASN.2014121188
2. National Kidney Foundation. K/DOQI clinical practice guidelines for chronic kidney disease: Evaluation, classification, and stratification. *Am J Kidney Dis*. 2002;39 (2 Suppl 1):S1–S266. PMID:11904577.
3. Coresh J. Update on the burden of CKD. *J Am Soc Nephrol*. 2017;28(4):1020–1022. doi:10.1681/ASN.2016121374
4. Carew R, Wang B, Kantharidis P. The role of EMT in renal fibrosis. *Cell Tissue Res*. 2012;347(1):103–116. doi:10.1007/s00441-011-1227-1
5. Zhou L, Li Y, Zhou D, Tan RJ, Liu Y. Loss of Klotho contributes to kidney injury by derepression of Wnt/ β -catenin signaling. *J Am Soc Nephrol*. 2013;24(5):771–785. doi:10.1681/ASN.2012080865

Supplementary Table 1. Verification of parametric test assumption for control (A) and chronic kidney disease (CKD) (B) group

A.

Control	Age	Total cholesterol	HDL	LDL	TG	Glucose	Urea	Creatinine	eGFR
Minimum	41	105	23	0	0	76	20	0.5	91
25% percentile	55	156	43	0	0	85.5	29	0.7	92
Median	59	166	53.5	53	74	94	32	0.8	99
75% percentile	62	198.5	66.75	95.5	105.5	110	37.75	0.9	109.8
Maximum	70	235	92	156	275	226	46	0.9	144
Lower 95% CI of mean	56.6	157.5	48.25	36.11	43.16	96.23	30.8	0.7143	97.75
Upper 95% CI of mean	60.02	184	61.54	64.72	80.8	114.3	35.63	0.8071	108.4
KS normality test									
KS distance	0.1017	0.1236	0.091	0.2962	0.2819	0.2353	0.1486	0.2001	0.2457
p-value	>0.1000	>0.1000	>0.1000	<0.0001	<0.0001	<0.0001	>0.1000	0.0056	0.0001
Passed normality test ($\alpha = 0.05$)?	yes	yes	yes	no	no	no	yes	no	no

B.

CKD	Age	Total cholesterol	HDL	LDL	TG	Glucose	Urea	Creatinine	eGFR
Minimum	18	62	11	10	53	66	14	0.5	5
25% percentile	30	175	39	103	115	84	32	0.8	32.6
Median	48	210	52	124	169	93	42	1.2	59
75% percentile	59	255	68	187	235	106	64	2	87.7
Maximum	78	470	113	367	408	226	183	8.8	151.9
Lower 95% CI of mean	41.82	202.9	50.06	129	156.1	94.09	46.85	1.429	54.2
Upper 95% CI of mean	50.25	238.5	60.31	161.1	194.6	108.3	63.46	2.309	71.65
KS normality test									
KS distance	0.117	0.1568	0.08205	0.1635	0.07769	51.34	25.63	49.91	3.189
p-value	0.0319	0.0002	>0.1000	<0.0001	>0.1000	<0.0001	<0.0001	<0.0001	0.2030
Passed normality test ($\alpha = 0.05$)?	no	no	yes	no	yes	no	no	no	yes

HDL – high-density lipoprotein; LDL – low-density lipoprotein; TG – triglycerides; eGFR – estimated glomerular filtration rate; 95% CI – 95% confidence interval; KS – Kolmogorov–Smirnov.

Supplementary Table 2. Verification of parametric test assumption for study groups

Study groups	Control	CKD	NP	NNP	1–2	3–5	FSGS	IgAN	LN	MN
Minimum	9.01	1.88	1.88	11.16	11.76	9.46	1.88	2.12	14.7	11.76
25% percentile	12.72	15.47	14.15	16.18	15.32	17.28	12.7	16.63	17.57	16.39
Median	16.62	21.71	20.44	19.19	22.78	20.07	17.18	25.59	32.98	26.04
75% percentile	20.78	32.98	32.98	30.94	39.56	31.7	27.82	40.89	60.83	40.46
Maximum	82.58	79.33	72.79	51.64	79.33	57.48	51.5	49.92	72.79	48.41
Lower 95% CI of mean	15.83	22.8	18.77	19.72	23.19	20.41	13.61	18.19	8.803	13.54
Upper 95% CI of mean	24.94	30.92	31.54	30.33	35.43	30.81	27.53	37.05	67.1	42.46
KS normality test										
KS distance	0.26	0.171	0.1508	0.2046	0.1744	0.1819	0.1623	0.1275	0.1839	0.2098
p-value	<0.0001	<0.0001	>0.1000	0.0136	0.0102	0.0221	>0.1000	>0.1000	>0.1000	>0.1000
Passed normality test ($\alpha = 0.05$)	no	no	yes	no	no	no	yes	yes	yes	yes

95% CI – 95% confidence interval; CKD – chronic kidney disease; NP – nephrotic proteinuria; NNP – non-nephrotic proteinuria; FSGS – focal segmental glomerulosclerosis; IgAN – IgA nephropathy; LN – lupus nephritis; MN – membranous nephropathy; KS – Kolmogorov–Smirnov. 1–2 and 3–5 – CKD group divided according to the Kidney Disease: Improving Global Outcomes (KDIGO) classification based on estimated glomerular filtration rate (eGFR) values.

Supplementary Table 3. Verification of parametric test assumption for groups presenting tubulointerstitial lesions in kidney biopsy samples

IILKP	Control	0–1	2–4
Minimum	9.01	1.88	2.12
25% percentile	12.72	17.36	14.8
Median	16.62	24.91	19.19
75% percentile	20.78	34.19	34.83
Maximum	82.58	72.79	79.33
Lower 95% CI of mean	15.83	22.1	19.95
Upper 95% CI of mean	24.94	33.55	32
KS normality test			
KS distance	0.26	0.1351	0.2107
p-value	<0.0001	>0.1000	0.0007
Passed normality test ($\alpha = 0.05$)?	no	yes	no

95% CI – 95% confidence interval; IILKP – inflammatory cell infiltration in kidney parenchyma; KS – Kolmogorov–Smirnov.

Supplementary Table 4. Verification of parametric test assumption for groups presenting fibrosis in kidney biopsy samples

Fibrosis	Control	0–1	2–4
Minimum	9.01	11.76	1.88
25% percentile	12.72	17.99	14.74
Median	16.62	27.02	19.35
75% percentile	20.78	35.45	33.23
Maximum	82.58	72.79	79.33
Lower 95% CI of mean	15.83	23.01	19.76
Upper 95% CI of mean	24.94	35.66	30.69
KS normality test			
KS distance	0.26	0.1659	0.1923
p-value	<0.0001	0.0740	0.0011
Passed normality test ($\alpha = 0.05$)?	no	yes	no

95% CI – 95% confidence interval; KS – Kolmogorov–Smirnov.

Supplementary Table 5. Verification of parametric test assumption for groups compared to associate the serum WNT4 protein with serum creatinine

Creatinine	WNT4 < 16.2 pg/mL	WNT4 > 16.2 pg/mL
Minimum	0.5	0.5
25% percentile	0.7	0.8
Median	0.8	1
75% percentile	1.1	1.5
Maximum	2.3	6.4
Lower 95% CI of mean	0.8139	1.119
Upper 95% CI of mean	1.173	1.835
KS normality test		
KS distance	0.2531	0.2713
p-value	<0.0001	<0.0001
Passed normality test ($\alpha = 0.05$)?	no	no

95% CI – 95% confidence interval; KS – Kolmogorov–Smirnov.

- Wang XD, Huang XF, Yan QR, Bao CD. Aberrant activation of the WNT/ β -catenin signaling pathway in lupus nephritis. *PLoS One*. 2014;21;9(1):e84852. doi:10.1371/journal.pone.0084852
- Zhou D, Fu H, Zhang L, et al. Tubule-derived Wnts are required for fibroblast activation and kidney fibrosis. *J Am Soc Nephrol*. 2017;28(8):2322–2336. doi:10.1681/ASN.2016080902
- Lu X, Rudemiller NP, Ren J, et al. Opposing actions of renal tubular- and myeloid-derived porcupine in obstruction-induced kidney fibrosis. *Kidney Int*. 2019;96(6):1308–1319. doi:10.1016/j.kint.2019.06.020
- Schunk SJ, Floege J, Fliser D, Speer T. WNT- β -catenin signalling: A versatile player in kidney injury and repair. *Nat Rev Nephrol*. 2021;17(3):172–184. doi:10.1038/s41581-020-00343-w
- Feng Y, Liang Y, Ren J, Dai C. Canonical Wnt signaling promotes macrophage proliferation during kidney fibrosis. *Kidney Dis (Basel)*. 2018;4(2):95–103. doi:10.1159/000488984
- Lin CL, Wang JY, Huang YT, Kuo YH, Surendran K, Wang FS. Wnt/ β -catenin signaling modulates survival of high glucose-stressed mesangial cells. *J Am Soc Nephrol*. 2006;17(10):2812–2820. doi:10.1681/ASN.2005121355
- Zhu D, Yu H, He H, et al. Spironolactone inhibits apoptosis in rat mesangial cells under hyperglycaemic conditions via the Wnt signaling pathway. *Mol Cell Biochem*. 2013;380(1–2):185–193. doi:10.1007/s11010-013-1672-0
- Lan X, Wen H, Aslam R, et al. Nicotine enhances mesangial cell proliferation and fibronectin production in high glucose milieu via activation of Wnt/ β -catenin pathway. *Biosci Rep*. 2018;31;38(3):BSR20180100. doi:10.1042/BSR20180100
- Kispert A, Vainio S, McMahon AP. Wnt-4 is a mesenchymal signal for epithelial transformation of metanephric mesenchyme in the developing kidney. *Development*. 1998;125(21):4225–4234. PMID:9753677.
- Lyons JP, Mueller UW, Ji H, et al. Wnt-4 activates the canonical β -catenin-mediated Wnt pathway and binds Frizzled-6 CRD: Functional implications of Wnt/ β -catenin activity in kidney epithelial cells. *Exp Cell Res*. 2004;15;298(2):369–387. doi:10.1016/j.yexcr.2004.04.036
- DiRocco DP, Kobayashi A, Taketo MM, McMahon AP, Humphreys BD. Wnt4/ β -catenin signaling in medullary kidney myofibroblasts. *J Am Soc Nephrol*. 2013;24(9):1399–1412. doi:10.1681/ASN.2012050512
- Surendran K, McCaul SP, Simon TC. A role for Wnt-4 in renal fibrosis. *Am J Physiol Renal Physiol*. 2002;282(3):F431–F441. doi:10.1152/ajprenal.0009.2001
- Nguyen HT, Thomson AA, Kogan BA, Baskin LS, Cunha GR. Expression of the Wnt gene family during late nephrogenesis and complete ureteral obstruction. *Lab Invest*. 1999;79(6):647–658. PMID:10378507.
- Terada Y, Tanaka H, Okado T, et al. Expression and function of the developmental gene Wnt-4 during experimental acute renal failure in rats. *J Am Soc Nephrol*. 2003;14(5):1223–1233. doi:10.1097/01.asn.0000060577.94532.06
- Chen L, Chen DQ, Wang M, et al. Role of RAS/Wnt/ β -catenin axis activation in the pathogenesis of podocyte injury and tubulo-interstitial nephropathy. *Chem Biol Interact*. 2017;1;273:56–72. doi:10.1016/j.cbi.2017.05.025
- Goliash G, Wiesbauer F, Kastl SP, et al. Premature myocardial infarction is associated with low serum levels of Wnt-1. *Atherosclerosis*. 2012;222(1):251–256. doi:10.1016/j.atherosclerosis.2012.02.017
- Zhao SL, Wei SY, Wang YX, et al. Wnt4 is a novel biomarker for the early detection of kidney tubular injury after ischemia/reperfusion injury. *Sci Rep*. 2016;7;6:32610. doi:10.1038/srep32610
- Kidney Disease. Improving Global Outcomes (KDIGO) CKD Work Group KDIGO 2012 Clinical Practice Guideline for the Evaluation and Management of Chronic Kidney Disease. *Kidney Int*. 2013;Suppl 3:1–150. doi:10.1038/kisup.2012.73
- Chang YC, Hsu SY, Yang CC, et al. Enhanced protection against renal ischemia-reperfusion injury with combined melatonin and exendin-4 in a rodent model. *Exp Biol Med*. 2016;241(14):1588–1602. doi:10.1177/1535370216642528
- Durham AL, McLaren A, Hayes BP, et al. Regulation of Wnt4 in chronic obstructive pulmonary disease. *FASEB J*. 2013;27(6):2367–2381. doi:10.1096/fj.12-217083
- Brack AS, Conboy MJ, Roy S, et al. Increased Wnt signaling during aging alters muscle stem cell fate and increases fibrosis. *Science*. 2007;10;317(5839):807–810. doi:10.1126/science.1144090

27. Chen DQ, Cao G, Chen H, et al. Gene and protein expressions and metabolomics exhibit activated redox signaling and Wnt/ β -catenin pathway are associated with metabolite dysfunction in patients with chronic kidney disease. *Redox Biol.* 2017;12:505–521. doi:10.1016/j.redox.2017.03.017
28. Zhang Y, Ma KL, Ruan XZ, Liu BC. Dysregulation of the low-density lipoprotein receptor pathway is involved in lipid disorder-mediated organ injury. *Int J Biol Sci.* 2016;21;12(5):569–579. doi:10.7150/ijbs.14027
29. Hasegawa S, Jao TM, Inagi R. Dietary metabolites and chronic kidney disease. *Nutrients.* 2017;4;9(4):358. doi:10.3390/nu9040358
30. Komekado H, Yamamoto H, Chiba T, Kikuchi A. Glycosylation and palmitoylation of Wnt-3a are coupled to produce an active form of Wnt-3a. *Genes Cells.* 2007;12(4):521–534. doi:10.1111/j.1365-2443.2007.01068.x
31. Hausmann G, Banziger C, Basler K. Helping wingless take flight: How Wnt proteins are secreted. *Nat Rev Mol Cell Biol.* 2007;8(4):331–336. doi:10.1038/nrm2141
32. Galli LM, Barnes TL, Secret SS, Kadowaki T, Burrus LW. Porcupine-mediated lipid-modification regulates the activity and distribution of Wnt proteins in the chick neural tube. *Development.* 2007;134(18):3339–3348. doi:10.1242/dev.02881
33. Willert K, Brown JD, Danenberg E, et al. Wnt proteins are lipid-modified and can act as stem cell growth factors. *Nature.* 2003;423(6938):448–452. doi:10.1038/nature01611

Caprini VTE computerized risk assessment improves the use of thromboprophylaxis in hospitalized patients with pulmonary disorders

Robert Franciszek Łukaszuk^{1,A–F}, Krzysztof Piotr Nycz^{2,D,E}, Krzysztof Plens^{3,B,C}, Anetta Undas^{4,5,A,D–F}

¹ Department of Lung Diseases, The 5th Clinical Military Hospital, Kraków, Poland

² Department of Lung Diseases, John Paul II Hospital, Kraków, Poland

³ KCRI, Kraków, Poland

⁴ Center for Research and Medical Technology, John Paul II Hospital, Kraków, Poland

⁵ Institute of Cardiology, Jagiellonian University Medical College, Kraków, Poland

A – research concept and design; B – collection and/or assembly of data; C – data analysis and interpretation;

D – writing the article; E – critical revision of the article; F – final approval of the article

Advances in Clinical and Experimental Medicine, ISSN 1899–5276 (print), ISSN 2451–2680 (online)

Adv Clin Exp Med. 2022;31(3):261–266

Address for correspondence

Robert Łukaszuk

E-mail: robertlukaszuk@yahoo.com

Funding sources

None declared

Conflict of interest

None declared

Received on March 4, 2019

Reviewed on September 20, 2019

Accepted on December 5, 2019

Published online on November 4, 2021

Cite as

Łukaszuk RF, Nycz KP, Plens K, Undas A. Caprini VTE computerized risk assessment improves the use of thromboprophylaxis in hospitalized patients with pulmonary disorders. *Adv Clin Exp Med.* 2022;31(3):261–266. doi:10.17219/acem/115080

DOI

10.17219/acem/115080

Copyright

© 2022 by Wrocław Medical University

This is an article distributed under the terms of the Creative Commons Attribution 3.0 Unported (CC BY 3.0) (<https://creativecommons.org/licenses/by/3.0/>)

Abstract

Background. Adequate thromboprophylaxis reduces the risk of venous thromboembolism (VTE) by half in hospitalized patients. A single scoring system is recommended to improve thromboprophylaxis.

Objectives. We investigated the impact of implementing a computerized system to prevent VTE in inpatients with pulmonary diseases and identified predictors of the overuse and underuse of pharmacological thromboprophylaxis.

Materials and methods. We compared the use of thromboprophylaxis with enoxaparin in all patients hospitalized for pulmonary disorders in a tertiary hospital in Kraków, Poland, in 2014 and 2017, before and after introducing a computerized thromboprophylaxis system. Using the Caprini risk assessment, the overuse and underuse of thromboprophylaxis were defined as the use in patients with <5 points and ≥5 points, respectively.

Results. Both cohorts (n = 2007 in 2014 and n = 1570 in 2017) were similar with regard to age and sex. The most frequent causes of hospitalization were intestinal lung disease (39.0%) and lung cancer (20.4%) in 2017, and pneumonia (38.8%) and lung cancer (27.5%) in 2014. Although the use of thromboprophylaxis was comparable in both cohorts, it was used more frequently in high VTE risk patients in 2017 compared with 2014 (96.98% compared to 29.17%, respectively, p < 0.001), with a concomitant reduction in its overuse (2.26% compared to 6.26%, respectively, p < 0.001). In 2017, no predictors of thromboprophylaxis underuse were identified. The overuse was mainly predicted by the diagnosis of airway diseases (odds ratio (OR) = 0.16, 95% confidence interval (95% CI) = 0.02–1.17, p = 0.015).

Conclusions. Our findings indicate the benefits of using a computerized system to manage pharmacological thromboprophylaxis in pulmonary inpatients.

Key words: pulmonary diseases, thromboprophylaxis, Caprini VTE risk assessment

Background

The risk of developing venous thromboembolism (VTE) is associated with a number of clinical situations, including hospitalization that is responsible for 10–20% of the VTE episodes.¹ It has been shown that 42% of hospitalized patients are at intermediate or high risk for VTE^{2,3} and 10% of in-hospital deaths are related to VTE.^{4–6} Adequate thromboprophylaxis reduces the risk of VTE by half,^{7,8} which enhances inpatients' safety, reduces the prevalence of VTE, and decreases the costs of treatment. The American College of Chest Physicians (ACCP) guidelines strongly recommend pharmacological thromboprophylaxis in all patients with high risk for VTE (Grade 1B).^{8,9} Various validated scoring systems are used to identify patients at high risk for developing VTE. It is important to use one of them consistently.¹⁰ Implementation of a computerized model to prevent VTE increases the guideline-appropriate VTE prophylaxis (by 80%) and improves VTE outcomes in inpatients.^{11–13}

The risk of VTE among patients with specific internal diseases is heterogeneous. For example, the reported frequency of VTE among patients with chronic obstructive pulmonary disease (COPD) exacerbation ranges from 5% to 29%,^{14,15} with an up to twenty-fold increase reported among lung cancer patients.¹⁶ A frequent overuse and underuse of thromboprophylaxis was observed in our previous study when the decision to administer prophylaxis was at the discretion of the treating physician.¹⁷ To improve thromboprophylaxis, a computerized system based on the Caprini risk assessment was implemented.

Objectives

We sought to compare the risk of overuse and underuse of pharmacological thromboprophylaxis before and after introducing routine use of a computerized system in a specific group of patients with pulmonary disorders.

Materials and methods

We collected data from the medical records of all patients aged >18 years admitted to the Department of Lung Diseases of the John Paul II Hospital in Kraków, Poland, within 2 time intervals.

The 2017 cohort represents patients hospitalized from April 1, 2017, to December 31, 2017, following the implementation of the use of the Caprini VTE computerized risk assessment tool. After 2014, it became standard practice to routinely use a recommended VTE risk assessment tool for the patients hospitalized in the department.

The 2014 cohort comprises all adult patients hospitalized from April 1, 2014, to December 31, 2014, who were

admitted prior to the implementation of the use of the Caprini tool.¹⁷ All archived records of patients were analyzed and scored using the Caprini VTE risk assessment tool, and the final score was compared with archived records of admitted patients who received thromboprophylaxis.

The computerized Caprini risk assessment model was implemented upon admission to the pulmonary department.¹⁸ Individuals who scored 5 or more points were identified as high-risk for VTE and in need of thromboprophylaxis. Subjects who scored fewer than 5 points (≤ 4 points) were identified as low-risk. Administration of enoxaparin (40 mg once daily, subcutaneous (SQ) injection) on each day of hospitalization was used as thromboprophylaxis for all high-risk patients. Mechanical thromboprophylaxis was not used. Patients who stayed in the hospital for more than 24 h were eligible for inclusion in the study. No additional criteria for including patients in the study were used. The study was carried out in accordance with the local legal and ethical regulations. All patients were classified into one of the 6 groups based on the main cause of hospitalization identified at admission to the hospital and confirmed during discharge (Table 1).

The underuse of thromboprophylaxis was defined as denying thromboprophylaxis in subjects who scored 5 or more points according to the Caprini risk assessment. The overuse of thromboprophylaxis was defined as thromboprophylaxis administration for patients with 4 or fewer points accordingly.

Statistical analysis

Variables were presented as numbers and percentages or median and interquartile ranges (IQRs) as appropriate. Nominal variables in the subgroups were compared with the Pearson's χ^2 test or the Fisher's exact test. Continuous variables were compared using the Mann–Whitney U test. To identify independent predictors of thromboprophylaxis overuse or underuse, a univariate logistic regression analysis was performed. Associations between 2 variables were expressed as odds ratios (OR) along with 95% confidence intervals (95% CI) and analyzed for variables represented in at least 5% of study cohorts. Two-sided p-values below 0.05 were considered statistically significant. All calculations were done with JMP® v. 13.1.0 (SAS Institute Inc., Cary, USA).

Results

The characteristics of the 2 cohorts comprising 2007 individuals in the year 2014 and 1570 in 2017 are presented in Table 1. Both cohorts were similar with regard to age and gender (Table 1). There was no difference in the prevalence of comorbidities between both groups. The median Caprini risk score was 4 in the 2014 cohort and 3 in the 2017

Table 1. Characteristics of the study cohorts in 2014 and 2017 year. Data are shown as the number (percentage)

Variable	All patients			Patients with thromboprophylaxis			Patients without thromboprophylaxis		
	2014 (n = 2007)	2017 (n = 1570)	p-value	2014 (n = 368) (18.4%)	2017 (n = 349) (22.2%)	p-value	2014 (n = 1636) (81.6%)	2017 (n = 1221) (77.8%)	p-value
Demographics									
Age 41–60 years	543 (24.7)	345 (21.9)	0.05	60 (14.4)	42 (12.0)	0.35	483 (27.2)	303 (24.8)	0.15
Age 61–74 years	936 (42.6)	750 (47.7)	0.002	193 (46.4)	171 (49.0)	0.50	741 (41.7)	579 (47.3)	0.002
Age >75 years	444 (20.2)	263 (16.7)	0.007	141 (33.9)	140 (40.1)	0.07	302 (17.0)	123 (10.1)	<0.0001
Men	1253 (57.0)	922 (58.6)	0.33	242 (58.2)	187 (53.6)	0.22	1010 (56.8)	735 (60.1)	0.07
BMI > 25 kg/m ²	1180 (53.7)	1018 (64.7)	<0.0001	268 (64.4)	251 (71.9)	0.03	910 (51.2)	767 (62.7)	<0.0001
Cause of the hospitalization									
Airway diseases*	330 (16.4)	293 (18.7)	0.08	65 (17.7)	32 (9.2)	0.0005	263 (16.1)	261 (21.4)	0.0004
Interstitial lung disease	268 (13.4)	613 (39.0)	<0.0001	11 (3.0)	123 (35.2)	<0.0001	257 (15.7)	490 (40.1)	<0.0001
Lung cancer	551 (27.5)	320 (20.4)	<0.0001	160 (43.5)	97 (27.8)	<0.0001	390 (23.8)	223 (18.3)	0.0003
Pneumonia	778 (38.8)	179 (11.4)	<0.0001	77 (20.9)	37 (10.6)	0.0002	701 (42.9)	142 (11.6)	<0.0001
Respiratory failure	28 (1.4)	148 (9.4)	<0.0001	9 (2.5)	52 (14.9)	<0.0001	19 (1.2)	96 (7.9)	<0.0001
Other	52 (2.6)	17 (1.1)	0.0011	46 (12.5)	8 (2.3)	<0.0001	6 (0.4)	9 (0.7)	0.17
Comorbidities									
Cardiovascular disease	733 (71.9)	773 (49.1)	<0.0001	142 (55.5)	213 (61.0)	0.0001	589 (77.5)	560 (45.8)	<0.0001
Diabetes	81 (8.0)	16 (1.0)	0.003	17 (6.6)	1 (0.3)	0.008	63 (8.3)	15 (1.2)	0.05
Renal disease	2	14 (0.9)	<0.0001	1 [#]	8 (2.3) [#]	0.01 [#]	1 [#]	6 (0.5) [#]	0.005 [#]
Heart failure	14 (0.6)	27 (1.7)	0.002	10 (2.4)	16 (4.6)	0.09	4 (0.2)	11 (0.9)	0.01
Thyroid disorders	33 (3.2)	0.0	<0.0001	3 (1.2) [#]	1 (0.01)	0.26 [#]	30 (4.0)	1 (0.1)	<0.0001
Previous venous thromboembolism	11 (0.5)	33 (3.2)	0.002	8 (1.9)	3 (1.2)	0.46	3 (0.2)	30 (4.0)	1.00
Varicose veins	185 (8.4)	23 (1.5)	<0.0001	78 (18.8)	21 (6.0)	<0.0001	105 (5.9)	2 (0.2)	0.005
Malignancies	545 (24.8)	226 (14.4)	<0.0001	194 (46.6)	120 (34.4)	<0.0001	350 (19.7)	106 (8.7)	<0.0001
Other diseases	44 (4.3)	119 (7.6)	<0.0001	20 (7.8)	94 (26.9)	<0.0001	24 (3.2)	25 (2.0)	0.002
Caprini VTE risk assessment score									
Low risk (1–2 points)	361 (16.4)	476 (30.3)	<0.0001	8 (1.9) [#]	3 (0.9) [#]	0.36 [#]	353 (19.9)	473 (38.6)	<0.0001
Medium risk (3–4 points)	858 (39.1)	766 (48.7)	<0.0001	62 (14.9)	25 (7.2)	0.001	796 (44.8)	741 (60.5)	<0.0001
High risk (≥5 points)	978 (44.5)	331 (21.0)	<0.0001	346 (83.2)	321 (92.0)	0.0003	629 (35.4)	10 (0.8)	<0.0001

BMI – body mass index; * – asthma, chronic obstructive pulmonary disease and bronchiectasis; VTE – venous thromboembolism. For comparisons marked with #, the Fisher’s exact test was used; in all other Pearson’s χ^2 test was used.

cohort ($p < 0.001$, Mann–Whitney U test). Eighty-seven (4.3%) individuals in 2014 and 19 (1.2%) in 2017 were receiving chronic oral anticoagulation treatment. The most common causes of hospitalization in 2014 and 2017 are presented in Table 1. The duration of hospitalization was similar (both groups had a median of 5 days). The proportions of individuals who received thromboprophylaxis with low molecular weight heparin (LMWH) were comparable in both cohorts (Table 1). However, in the 2017 cohort, pharmacological thromboprophylaxis was administered in a markedly larger patient group with high VTE risk compared with the 2014 cohort ($n = 321$, 96.98% compared to $n = 259$, 29.17%, respectively, $p < 0.001$, Pearson’s χ^2 test). The number of inpatients identified as low-risk for VTE was comparable in both cohorts but in the 2017 cohort, the overuse of thromboprophylaxis was significantly lower (Table 2,3).

The main predictors of the underuse of thromboprophylaxis in the 2014 cohort included age (41–60 years) and the presence of interstitial lung disease, pneumonia, and swollen legs (Table 3). Predictors of underuse were not identified in the 2017 cohort. Age (41–60 years) and airway diseases were identified as overuse predictors in the 2017 cohort (Table 2).

Of the total recorded deaths during patients’ hospital stays, 7 in 2014 and 3 in 2017, all of them resulted from end-stage pulmonary diseases. No autopsy was performed. No significant adverse events such as allergic reactions or heparin-induced thrombocytopenia were observed. No major bleeding or symptomatic VTE was recorded. The number of blood recipients who received packed blood cells was similar in both cohorts. Chronic anemia due to lung cancer was the major cause of blood transfusion in 2014 and 2017.

Table 2. Use of thromboprophylaxis according to Caprini VTE risk assessment. Data were shown as the number (percentage)

Variable	Patients with indications for thromboprophylaxis			Patients who did not receive thromboprophylaxis despite indication			Patients without indications for thromboprophylaxis			Patients who received thromboprophylaxis without indication		
	2014	2017	p-value	2014	2017	p-value	2014	2017	p-value	2014	2017	p-value
Number of subjects	888 (100.00)	331 (100.00)	<0.0001	629 (70.83) [#]	10 (3.02) [#]	<0.0001 [#]	1119 (100.00)	1239 (100.00)	<0.0001	70 (6.26)	28 (2.26)	<0.0001
Airway diseases*	138 (15.54)	31 (9.37)	0.0055	88 (9.91) [#]	0 (0.00) [#]	0.37 [#]	192 (17.16)	262 (21.15)	0.0142	17 (1.52)	1 (0.08)	0.0066
Lung cancer	449 (50.56)	98 (29.61)	<0.0001	292 (32.88) [#]	4 (1.21) [#]	0.54 [#]	102 (9.12)	222 (17.92)	<0.0001	4 (0.36) [#]	3 (0.24) [#]	0.68 [#]
Interstitial lung disease	47 (5.29)	109 (32.93)	<0.0001	38 (4.28) [#]	4 (1.21) [#]	0.0035 [#]	221 (19.75)	504 (40.68)	<0.0001	2 (0.18)	18 (1.45)	<0.0001
Respiratory failure	16 (1.80)	50 (15.11)	<0.0001	10 (1.13) [#]	1 (0.30) [#]	0.17 [#]	12 (1.07)	98 (7.91)	<0.0001	3 (0.27) [#]	3 (0.24) [#]	0.38 [#]
Pneumonia	203 (22.86)	38 (11.48)	<0.0001	144 (16.22) [#]	1 (0.30) [#]	0.46 [#]	575 (51.39)	141 (11.38)	<0.0001	18 (1.61)	0 (0.00)	0.001
Other	35 (3.94)	5 (1.51)	0.0341	4 (0.45) [#]	0 (0.00) [#]	1.00 [#]	17 (1.52)	12 (0.97)	0.23	15 (1.34)	3 (0.24)	0.11
Age 41–60 years	105 (11.82)	33 (9.97)	0.69	69 (7.77) [#]	2 (0.60) [#]	0.31 [#]	438 (39.14)	312 (25.18)	<0.0001	24 (2.14)	11 (0.89)	0.64
Age 61–74 years	476 (53.60)	167 (50.45)	0.58	309 (34.80) [#]	5 (1.51) [#]	1.00 [#]	460 (41.11)	583 (47.05)	<0.0001	28 (2.50)	9 (0.73)	0.47
Age >75 years	390 (43.92)	137 (41.39)	0.63	252 (28.38) [#]	3 (0.91) [#]	0.75 [#]	54 (4.83)	126 (10.17)	<0.0001	4 (0.36) [#]	6 (0.48) [#]	0.03 [#]
History of VTE	10 (1.13)	21 (6.34)	<0.0001	2 (0.23)	0 (0.00)	–	1 (0.09) [#]	2 (0.16) [#]	1.00 [#]	0 (0.00)	0 (0.00)	–
Varicose veins	147 (16.55)	120 (36.25)	<0.0001	75 (8.45) [#]	5 (1.51) [#]	0.0041 [#]	38 (3.40)	106 (8.56)	<0.0001	8 (0.71) [#]	5 (0.40) [#]	0.51 [#]
Congestive heart failure	12 (1.35)	17 (5.14)	<0.0001	2 (0.23) [#]	1 (0.30) [#]	0.0463 [#]	2 (0.18)	10 (0.81)	0.0224	0 (0.00)	0 (0.00)	–
Swollen legs	87 (9.80)	86 (25.98)	<0.0001	20 (2.25) [#]	7 (2.11) [#]	<0.0001 [#]	22 (1.97)	26 (2.10)	0.60	9 (0.80) [#]	0 (0.00) [#]	0.06 [#]
Serious lung diseases	716 (80.63)	184 (55.59)	<0.0001	429 (48.31)	5 (1.51)	–	316 (28.24)	216 (17.43)	<0.0001	36 (3.22)	11 (0.89)	0.28
Abnormal pulmonary function	884 (99.55)	191 (57.70)	<0.0001	626 (70.50) [#]	6 (1.81) [#]	0.3041 [#]	1040 (92.94)	239 (19.29)	<0.0001	69 (6.17)	9 (0.73)	<0.0001
Cancer	526 (59.23)	92 (27.79)	<0.0001	333 (37.50) [#]	1 (0.30) [#]	0.0084 [#]	19 (1.70)	27 (2.18)	0.26	2 (0.18) [#]	3 (0.24) [#]	0.14 [#]
Thrombophilia	2 (0.23) [#]	1 (0.30) [#]	1.00 [#]	2 (0.23)	0 (0.00)	–	0 (0.00)	0 (0.00)	–	0 (0.00)	0 (0.00)	–
BMI > 25 kg/m ²	656 (73.87)	243 (73.41)	0.0316	410 (46.17) [#]	9 (2.72) [#]	0.18 [#]	524 (46.83)	775 (62.55)	<0.0001	24 (2.14)	17 (1.37)	0.0166

BMI – body mass index; * – asthma, chronic obstructive pulmonary disease and bronchiectasis; VTE – venous thromboembolism. For comparisons marked with #, the Fisher's exact test was used; in all other, Pearson's χ^2 test was used.

Discussion

The major findings of the current study were:

1. For pulmonary disease inpatients, using the Caprini risk assessment in a computerized system supports the appropriate recommendations of pharmacological thromboprophylaxis, increasing its use in high-risk VTE inpatients while reducing its use in patients with low VTE risk.

2. We have demonstrated that specific pulmonary diseases, like asthma and COPD, have a major impact on the prediction of appropriate thromboprophylaxis

among inpatients. Thus, a better implementation of prophylaxis among inpatients requires evaluation of specific patient groups to identify those at elevated risk of under- or overuse. The current study highlights benefits from a computerized system to support the use of thromboprophylaxis in hospitals and the constant need for optimizing it in specific clinical settings, such as internal medicine wards.

Within 1 year of implementing the Caprini risk assessment in a computerized system to guide thromboprophylaxis among patients admitted to the pulmonary

Table 3. The risk factors of venous thromboembolism (VTE) prophylaxis overuse and underuse

Variable	Overuse in the 2014 cohort		Overuse in the 2017 cohort		Underuse in the 2014 cohort		Underuse in the 2017 cohort	
	OR (95% CI)	p-value	OR (95% CI)	p-value	OR (95% CI)	p-value	OR (95% CI)	p-value
BMI > 25 kg/m ²	0.44 (0.27; 0.72)	0.001	–	NS	1.94 (1.60; 2.35)	<0.001	–	NS
Swollen legs	2.99 (1.44; 6.19)	0.009	–	NS	0.55 (0.33; 0.89)	0.01	32.40 (8.26; 127.11)	<0.001
Varicose veins	–	NS	–	NS	1.83 (1.34; 2.49)	<0.001	6.07 (1.74; 21.15)	0.01
Malignancy	0.09 (0.02; 0.35)	<0.001	–	NS	7.22 (5.83; 8.94)	<0.001	–	NS
Age 41–60 years	–	NS	2.35 (1.09; 5.06)	0.037	0.28 (0.22; 0.37)	<0.001	–	NS
Age 61–74 years	–	NS	–	NS	1.45 (1.21; 1.75)	<0.001	–	NS
Age >75 years	0.23 (0.08; 0.64)	0.001	–	NS	4.81 (3.86; 5.99)	<0.001	–	NS
Abnormal pulmonary function	–	NS	–	NS	7.31 (2.28; 23.49)	<0.001	4.03 (1.13; 14.35)	0.03
Cardiovascular disease	–	NS	–	NS	1.53 (1.27; 1.85)	<0.001	4.17 (0.88; 19.71)	0.04
Diabetes	–	NS	–	NS	1.82 (1.26; 2.62)	0.002	–	NS
Airway diseases	2.11 (1.19; 3.76)	0.016	0.16 (0.02; 1.17)	0.015	–	NS	–	NS
Interstitial lung disease	0.22 (0.05; 0.91)	0.008	2.87 (1.31; 6.25)	0.007	0.37 (0.26; 0.53)	<0.001	–	NS
Lung cancer	0.19 (0.07; 0.52)	<0.001	–	NS	4.66 (3.77; 5.76)	<0.001	–	NS
Pneumonia	–	NS	–	NS	0.42 (0.34; 0.52)	<0.001	–	NS

BMI – body mass index; OR – odds ratio; 95% CI – 95% confidence interval; NS – not significant.

department, there was a significant improvement in the adequate use of prophylaxis, from 38.96% to 96.98%. Furthermore, we detected a rapid decrease of underuse of thromboprophylaxis – from 64.51% to 3.02% – among high-risk patients.

The implementation of health recommendations is an international challenge, illustrated by a 34% median of recommendation adherence, suggesting that patients do not always benefit from medical guidelines.¹⁹ Most data show that the proportion of inpatients at high risk of VTE receiving thromboprophylaxis is between 50% and 68.95%.^{13,19} Bhalla et al.¹¹ showed that the implementation of an obligatory computerized scoring model enforced proper medical practices, which confirms the present study. When the simple computerized system reminder was used, the percentage of inpatients at high risk of VTE receiving thromboprophylaxis increased from 42.8% to 60.0% ($p < 0.001$).¹⁰

The impact of specific diagnoses, such as lung disease, on the use of thromboprophylaxis appears to be underestimated. Our study showed that underuse among pulmonary inpatients is greatest in lung cancer patients, despite evidence showing a high risk of VTE in patients with this type of malignancy.¹⁶ This study highlights the need for education on VTE in cancer patients, who are often perceived as unsuitable candidates for thromboprophylaxis due to a higher bleeding risk.

Respiratory failure and interstitial lung disease comprised larger patient subgroups in 2017 compared with 2014. This is likely a consequence of patients' aging and wider availability of improved diagnostic tools.^{20–23} Age (younger adults) and airway diseases were predictors for

the overuse of thromboprophylaxis. It might be speculated that the first predictor, age, was a consequence of a growing number of relatively young patients with interstitial lung diseases. This growth is the result of the development of tools for detecting connective tissue disease-associated interstitial lung diseases (CTD-ILD).²⁴ The airway diseases predictor was probably connected with physicians awareness that any associated dyspnea could reduce patients' daily activity after admission.^{2,3,12} The main predictors of the underuse of thromboprophylaxis in the 2014 cohort, including age (41–60 years), interstitial lung disease and pneumonia, were absent in the analysis of patients from the 2017 cohort. Current predictors were different from those reported by Spirk et al.,²⁵ indicating that a range of specific diseases diagnosed in patients undergoing prophylaxis can markedly affect predictors of its under- and overuse, and the results of a whole patient population cannot be extrapolated to subgroups.

Limitations

This study has several limitations. The study is retrospective, which causes some problems with data acquisition and their precision (i.e., in some patients, the diagnosis could have been unestablished because some patients suffered simultaneously from different pulmonary diseases). Evaluation of asymptomatic VTE during hospital stay and post-discharge follow-up was beyond the scope of the current study. Cost-effectiveness of thromboprophylaxis and costs of its overuse were not evaluated, although this problem is important in clinical practice.²⁶

Conclusions


We conclude that the use of computerized Caprini VTE risk assessment in all hospitalized patients increases the proportion of patients with pulmonary diseases who can benefit from thromboprophylaxis, and reduces its overuse among patients with low risk of VTE. To optimize thromboprophylaxis, its use should be assessed in departments dealing with patients with specific diseases.

ORCID iDs

Robert Franciszek Łukaszuk  <https://orcid.org/0000-0002-6554-2770>

Krzysztof Piotr Nycz  <https://orcid.org/0000-0001-7546-5222>

Krzysztof Plens  <https://orcid.org/0000-0003-2973-9952>

Anetta Undas  <https://orcid.org/0000-0003-3716-1724>

References

- Anderson FA Jr, Spencer FA. Risk factors for venous thromboembolism. *Circulation*. 2003;107(23 Suppl 1):I9–I16. doi:10.1161/01.CIR.0000078469.07362.E6
- Tapson VF, Decousus H, Pini M, et al; IMPROVE Investigators. Venous thromboembolism prophylaxis in acutely ill hospitalized medical patients: Findings from the International Medical Prevention registry on Venous Thromboembolism. *Chest*. 2007;132(3):936–945. doi:10.1378/chest.06-2993
- Huang W, Anderson FA, Spencer FA, Gallus A, Goldberg RJ. Risk-assessment models for predicting venous thromboembolism among hospitalized non-surgical patients: A systematic review. *J Thromb Thrombolysis*. 2013;35(1):67–80. doi:10.1007/s11239-012-0780-0
- Lindblad B, Sternby NH, Bergqvist D. Incidence of venous thromboembolism verified by necropsy over 30 years. *BMJ*. 1991;302(6778):709–711. doi:10.1136/bmj.302.6778.709
- Kakkar N, Vasishta RK. Pulmonary embolism in medical patients: An autopsy-based study. *Clin Appl Thromb Hemost*. 2008;14(2):159–167. doi:10.1177/1076029607308389
- Heriot GS, Pitman AG, Gonzales M, McKelvie P. The four horsemen: Clinicopathological correlation in 407 hospital autopsies. *Intern Med J*. 2010;40(9):626–632. doi:10.1111/j.1445-5994.2009.01985.x
- Lloyd NS, Douketis JD, Moinuddin I, Lim W, Crowther MA. Anticoagulant prophylaxis to prevent asymptomatic deep vein thrombosis in hospitalized medical patients: A systematic review and meta-analysis. *J Thromb Haemost*. 2008;6(3):405–414. doi:10.1111/j.1538-7836.2007.02847.x
- Kahn SR, Lim W, Dunn AS, et al. Prevention of VTE in nonsurgical patients: Antithrombotic Therapy and Prevention of Thrombosis, 9th ed: American College of Chest Physicians Evidence-Based Clinical Practice Guidelines. *Chest*. 2012;141(2 Suppl):e195S–e226S. doi:10.1378/chest.11-2296
- Gould MK, Garcia DA, Wren SM, et al. Prevention of VTE in nonorthopedic surgical patients: Antithrombotic Therapy and Prevention of Thrombosis, 9th ed: American College of Chest Physicians Evidence-Based Clinical Practice Guidelines. *Chest*. 2012;141(2 Suppl):e227S–e277S. doi:10.1378/chest.11-2297
- Mitchell JD, Collen JF, Petteys S, Holley AB. A simple reminder system improves venous thromboembolism prophylaxis rates and reduces thrombotic events for hospitalized patients. *J Thromb Haemost*. 2012;10(2):236–243. doi:10.1111/j.1538-7836.2011.04599.x
- Bhalla R, Berger MA, Reissman SH, et al. Improving hospital venous thromboembolism prophylaxis with electronic decision support. *J Hosp Med*. 2013;8(3):115–120. doi:10.1002/jhm.1993
- Haut ER, Lau BD, Kraenzlin FS, et al. Improved prophylaxis and decreased rates of preventable harm with the use of a mandatory computerized clinical decision support tool for prophylaxis for venous thromboembolism in trauma. *Arch Surg*. 2012;147(10):901–907. doi:10.1001/archsurg.2012.2024
- Kahn SR, Morrison DR, Cohen JM, et al. Interventions for implementation of thromboprophylaxis in hospitalized medical and surgical patients at risk for venous thromboembolism. *Cochrane Database Syst Rev*. 2013;16(7):CD008201. doi:10.1002/14651858.CD008201.pub2
- Akgun M, Meral M, Onbas O, et al. Comparison of clinical characteristics and outcomes of patients with COPD exacerbation with or without venous thromboembolism. *Respiration*. 2006;73(4):428–433. doi:10.1159/000092952
- Erelel M, Cuhadaroglu C, Ece T, Arseven O. The frequency of deep venous thrombosis and pulmonary embolus in acute exacerbation of chronic obstructive pulmonary disease. *Respir Med*. 2002;96(7):515–518. PMID:12194636
- Blom JW, Osanto S, Rosendaal FR. The risk of a venous thrombotic event in lung cancer patients: Higher risk for adenocarcinoma than squamous cell carcinoma. *J Thromb Haemost*. 2004;2(10):1760–1765. doi:10.1111/j.1538-7836.2004.00928.x
- Łukaszuk RF, Plens K, Undas A. Real-life use of thromboprophylaxis in patients hospitalized for pulmonary disorders: A single-center retrospective study. *Adv Clin Exp Med*. 2018;27(2):237–243. doi:10.17219/acem/68474
- Caprini JA. Risk assessment as a guide for the prevention of the many faces of venous thromboembolism. *Am J Surg*. 2010;199(1 Suppl):S3–S10. doi:10.1016/j.amjsurg.2009.10.006
- Christiansen CF. Prophylaxis of venous thromboembolism in medical patients: Too much or too little? *Clin Epidemiol*. 2012;4:315–318. doi:10.2147/CLEP.S38304
- Heit JA, O'Fallon WM, Petterson TM, et al. Relative impact of risk factors for deep vein thrombosis and pulmonary embolism: A population-based study. *Arch Intern Med*. 2002;162(11):1245–1248. doi:10.1001/archinte.162.11.1245
- Krasiński Z, Krasińska B, Dzieciuchowicz Ł, Urbaneck T, Gabriel M. Heparins in cancer-associated venous thrombosis. *Pol Arch Med Wewn*. 2016;126(6):419–429. doi:10.20452/pamw.3449
- Rosenberg D, Eichorn A, Alarcon M, McCullagh L, McGinn T, Spyropoulos AC. External validation of the risk assessment model of the International Medical Prevention Registry on Venous Thromboembolism (IMPROVE) for medical patients in a tertiary health system. *J Am Heart Assoc*. 2014;3(6):e001152. doi:10.1161/JAHA.114.001152
- Trzeciak P, Desperak P, Ciślak A, Hawranek M, Gaşior R. Clinical characteristics, and in-hospital and long-term outcomes of stable angina treatment in patients below and over 40 years of age (from the PRES-AGE registry). *Kardiol Pol*. 2018;76(1):186–194. doi:10.5603/KP.a2017.0200
- Khanna D, Mittoo S, Aggarwal R, et al. Connective Tissue Disease-associated Interstitial Lung Diseases (CTD-ILD): Report from OMER-ACT CTD-ILD Working Group. *J Rheumatol*. 2015;42(11):2168–2171. doi:10.3899/jrheum.141182
- Spirk D, Nendaz M, Aujesky D, et al. Predictors of thromboprophylaxis in hospitalised medical patients: Explicit Assessment of Thromboembolic Risk and Prophylaxis for Medical Patients in Switzerland (ESTIMATE). *Thromb Haemost*. 2015;113(5):1127–1134. doi:10.1160/TH14-06-0525
- Gussoni G, Foglia E, Frasson S, et al; FADOI Permanent Study Group on Clinical Governance. Real-world economic burden of venous thromboembolism and antithrombotic prophylaxis in medical inpatients. *Thromb Res*. 2013;131(1):17–23. doi:10.1016/j.thromres.2012.10.008

A quasi-experimental study examining a nurse-led educational program to improve disease knowledge and self-care for patients with acute decompensated heart failure with reduced ejection fraction

Jolanta Kolasa^{1,2,A–F}, Magdalena Frączek-Jucha^{3,B,D–F}, Marcin Grabowski^{4,B–F}, Ewa A. Jankowska^{5,6,A,E,F}, Małgorzata Lelonek^{7,A,E,F}, Agnieszka Pawlak^{2,8,A,B,E,F}, Izabella Uchmanowicz^{9,A,B,D–F}, Jadwiga Nessler^{10,A,B,E,F}

¹ Medical Unit Cardiology, Novartis Poland Ltd., Warszawa, Poland

² Mossakowski Medical Research Centre, Polish Academy of Sciences, Department of Applied Physiology, Warszawa, Poland

³ Department of Emergency Medical Care, Jagiellonian University Medical College, John Paul II Hospital, Kraków, Poland

⁴ 1st Department of Cardiology, Medical University of Warsaw, Poland

⁵ Institute of Heart Diseases, Wrocław Medical University, Poland

⁶ Institute of Heart Diseases, University Hospital in Wrocław, Poland

⁷ Department of Noninvasive Cardiology, Medical University of Lodz, Poland

⁸ Department of Invasive Cardiology, Central Clinical Hospital of the Ministry of Interior and Administration, Warszawa, Poland

⁹ Department of Clinical Nursing, Faculty of Health Sciences, Wrocław Medical University, Poland

¹⁰ Department of Coronary Disease and Heart Failure, Jagiellonian University Medical College, John Paul II Hospital, Kraków, Poland

A – research concept and design; B – collection and/or assembly of data; C – data analysis and interpretation;

D – writing the article; E – critical revision of the article; F – final approval of the article

Advances in Clinical and Experimental Medicine, ISSN 1899–5276 (print), ISSN 2451–2680 (online)

Adv Clin Exp Med. 2022;31(3):267–275

Address for correspondence

Jolanta Kolasa

E-mail: jolanta.kolasa@novartis.com

Funding sources

“The Weak Heart” program was funded by Novartis Pharma Poland.

Conflict of interest

J. Kolasa is an employee of Novartis Poland; M. Lelonek, A. Pawlak, J. Nessler, E.A. Jankowska, I. Uchmanowicz and M. Grabowski received honoraria and consulting fees from Novartis and were involved in clinical trials sponsored by Novartis; M. Frączek-Jucha was involved in Novartis clinical trials.

Received on July 8, 2021

Reviewed on October 15, 2021

Accepted on November 16, 2021

Published online on December 2, 2021

Cite as

Kolasa J, Frączek-Jucha M, Grabowski M, et al. A quasi-experimental study examining a nurse-led educational program to improve disease knowledge and self-care for patients with acute decompensated heart failure with reduced ejection fraction. *Adv Clin Exp Med.* 2022;31(3):267–275. doi:10.17219/acem/143989

DOI

10.17219/acem/143989

Copyright

© 2022 by Wrocław Medical University

This is an article distributed under the terms of the Creative Commons Attribution 3.0 Unported (CC BY 3.0) (<https://creativecommons.org/licenses/by/3.0/>)

Abstract

Background. Nurse-led education can improve heart failure (HF) knowledge and self-care behaviors, and consequently lead to better patient outcomes.

Objectives. To assess the effectiveness of “The Weak Heart” educational model in enhancing the level of disease knowledge and self-care behaviors among patients hospitalized with acute decompensated heart failure with reduced ejection fraction (HFREF).

Materials and methods. An evidence-based, standardized educational program was implemented for HF patients in Poland. We compared the initial level of HF knowledge – as rated using a self-developed questionnaire and self-care behaviors, evaluated according to the 9-item European Heart Failure Self-care Behavior Scale (9-EHFScBS) – to the results obtained at the 3-month follow-up period with a sample of patients (n = 231) hospitalized with acute decompensated HF (ADHF).

Results. The results showed a significant increase in total score of HF knowledge test depending on the time of measurement ($\chi^2 = 356.526$, $p < 0.001$) and in all individual questions on HF. The significant change of the 9-EHFScBS self-care questionnaire was also found in total score ($Z = -7.317$, $p < 0.001$), in all domains: autonomous-based adherence ($Z = -5.870$, $p < 0.001$); consulting behavior ($Z = -7.238$, $p < 0.001$); provider-based adherence ($Z = -4.162$; $p < 0.001$) and in relation to all individual statements except statement 7 (“I eat a low salt diet”) and statement 9 (“I exercise regularly”). Within 3 months of hospital discharge, 84% (193 out of 231) of participants visited their primary care physician and 79% (183 out of 231) visited a cardiologist in accordance with their individual treatment plan.

Conclusions. “The Weak Heart” educational model is effective in enhancing the level of HF knowledge and self-care behaviors among patients with decompensation of HFREF.

Key words: heart failure, cardiology, disease management, adherence, disease education

Background

Heart failure (HF) is an important public health problem, with an estimated prevalence of 1–2% among adults and >10% among people aged >70 years in developing countries.¹ In Poland, over 700,000 patients suffer from HF, which can lead to premature death.^{2,3} Heart failure requires multidisciplinary management programs, including self-care education.^{1,4,5} Indeed, self-management interventions often led by nurses are effective at improving knowledge, self-care behaviors, quality of life, and reducing the number of hospitalizations and mortality among patients with HF.^{6–16} Furthermore, the active post-discharge monitoring of patients with HF (e.g. via post-discharge phone calls) should translate into better adherence, a reduction in the number of decompensated HF cases and slower disease progression.^{1,17}

The European Society of Cardiology (ESC), American College of Cardiology Foundation (ACCF) and American Heart Association (AHA) practice guidelines recommend a nurse-led HF education in HF patients.^{1,4,5,18} The correlations between patients' knowledge of HF and self-care skills were found in studies conducted in the USA.^{13,19}

To meet this need, multidisciplinary HF programs, including various types of nurse-led interventions, should be implemented.^{1,18,20–23} Similarly, a disease management system for patients with HF named “KONS” (Comprehensive Care for Patients with Heart Failure) was proposed in Poland.²⁴

Objectives

The purpose of this study was to implement a standardized nurse-led HF education program focused on improving disease knowledge and self-care behaviors in patients hospitalized with acute decompensated heart failure with reduced ejection fraction (HFrEF) and evaluate its effectiveness.

Materials and methods

Study population and design

“The Weak Heart” program was a nurse-led HF educational program conducted in 2019 in 14 cardiology centers in Poland and consisted of 2 hospital educational visits and 3 post-discharge phone calls. Prior to initiating patient education, nurse educators completed HF training and certification in accordance with the HF nurse curriculum developed by experts of Nurses and Medical Technicians and the Heart Failure Section of the Polish Cardiac Society.²⁵ Total number of 259 patients hospitalized due to acute decompensated heart failure (ADHF) were consecutively recruited based on the following inclusion criteria:

diagnosed HF with reduced ejection fraction (ejection fraction (EF) < 40% as evaluated using echocardiography), cognitive function enabling the participation in the program and a declaration of the patient's involvement in the treatment; there were no exclusion criteria to enter the program. To assess the effectiveness of the program in a clinical setting, a prospective, quasi-experimental, pre-test and post-test method was applied.

“The Weak Heart” program was based on HF guidelines of European Society of Cardiology¹ and tailored to the needs of patients with HFrEF. The scope of education included the following topics: basic information about HF, etiology, symptoms, principles of self-care, basics of treatment, and the importance of lifestyle, diet and exercise, based on the content from patient portal (www.slabeserce.pl) displayed on tablet. After completing educational sessions, participants received a heart failure passport²⁶ with an individual treatment plan, a cover letter to primary care physician and a drug dispenser. A detailed description of “The Weak Heart” educational program has already been published.²⁷

Ethical aspects and recommendations

The Bioethical Commission at the University of Warsaw has approved the project (approval No. KB/3/A/2019). The study was performed in accordance with the ethical principles for clinical research based on the Declaration of Helsinki.

Data collection

Trained HF nurses interviewed participants using the questionnaires to assess the level of HF knowledge and self-care behaviors. Measurements were conducted before the implementation of any educational activities (visit 1), before discharge but after finishing all educational activities (visit 2 – only for the assessment of HF knowledge) and at the end of the 3-month follow-up period (visit 5).

Instruments

The research team has developed a 10-item HF knowledge questionnaire to assess the level of disease knowledge. Patient's responses were scored on a scale from 0 to 2 (0 – incorrect response, 1 – partially correct, 2 – correct), based on key words. The maximal score was 20 points – the higher the score, the better the level of HF knowledge. The calculated Cronbach's alpha for the knowledge test was 0.86. The value of the correlation coefficient of individual test items was not less than the minimum acceptable value of 0.20.

The 9-item European Heart Failure Self-care Behavior Scale (9-EHFS CBS) contains 9 statements concerning self-care behaviors among HF patients.^{28,29} The answers to the statements were given on the 5-point Likert scale,

with the result being the aggregation of the points from all statements included in the 9-EHFScBS. The scores vary from 9 to 45 – the higher the score, the lower the self-care capability. The questionnaire also enables the assessment of the level of self-care in terms of individual statements.^{28,29} Additionally, a patient’s self-care can also be measured by computing the scores for each subdimension of self-care: consulting behavior, autonomy-based adherence and provider-based adherence.³⁰ The calculated Cronbach’s alpha for the behavior test was 0.89.

Statistical analysis

Statistical analysis was performed using SAS® software v. 9.4 (SAS Institute, Cary, USA). The Friedman’s test was applied to verify the hypotheses of influence of the intervention program on scores of the knowledge test. Time of measurement was considered the within-group factor: before the commencement of the program (visit 1) compared to directly after finishing all educational activities (visit 2) compared to 3 months after its end (visit 5). The Bonferroni correction was used to adjust the significance value for multiple tests. The adjusted significance level was 0.017.

The Spearman’s rank correlation coefficient was used to verify the correlation between scores on the 1st knowledge test and duration of the disease. The Mann–Whitney U test was conducted to compare the scores of patients participating in any educational activities on HF with those who did not, as well as patients who required several hospitalizations and those hospitalized for the first time.

The verification of assumptions about the impact of the intervention program on self-care behaviors and subjective knowledge was carried out using the Wilcoxon test. Time of measurement was considered the within-group factor: before the commencement of the program (visit 1) compared to 3 months after its end (visit 5). A two-tailed value of $p < 0.05$ was considered significant for all tests.

Results

The final analysis consists of 231 patients who signed written consent and fulfilled all educational visits, while a sample size of 199 patients was required to achieve a statistical significance of $p < 0.05$.²⁷ Out of 259 patients included in the program, all visits were finished regarding 89% of patients (Fig. 1). The baseline characteristics of patients included in the study are presented in Table 1.

The results showed a significant difference in performance in the level-of-knowledge test depending on the time of measurement ($\chi^2 = 356.526, p < 0.001$). The scores from the 1st measurement were significantly lower than those from the 2nd ($Z = -1.227, p_{adj} < 0.001$) and 3rd measurement ($Z = -1.649, p_{adj} < 0.001$). The scores from the 2nd measurement were significantly lower than those from the 3rd measurement ($Z = -0.422, p_{adj} < 0.001$). The results are presented in Table 2. A significant improvement in HF knowledge has been observed for all individual questions (Fig. 2).

The results demonstrated that patients educated on HF prior to the program, patients who underwent several

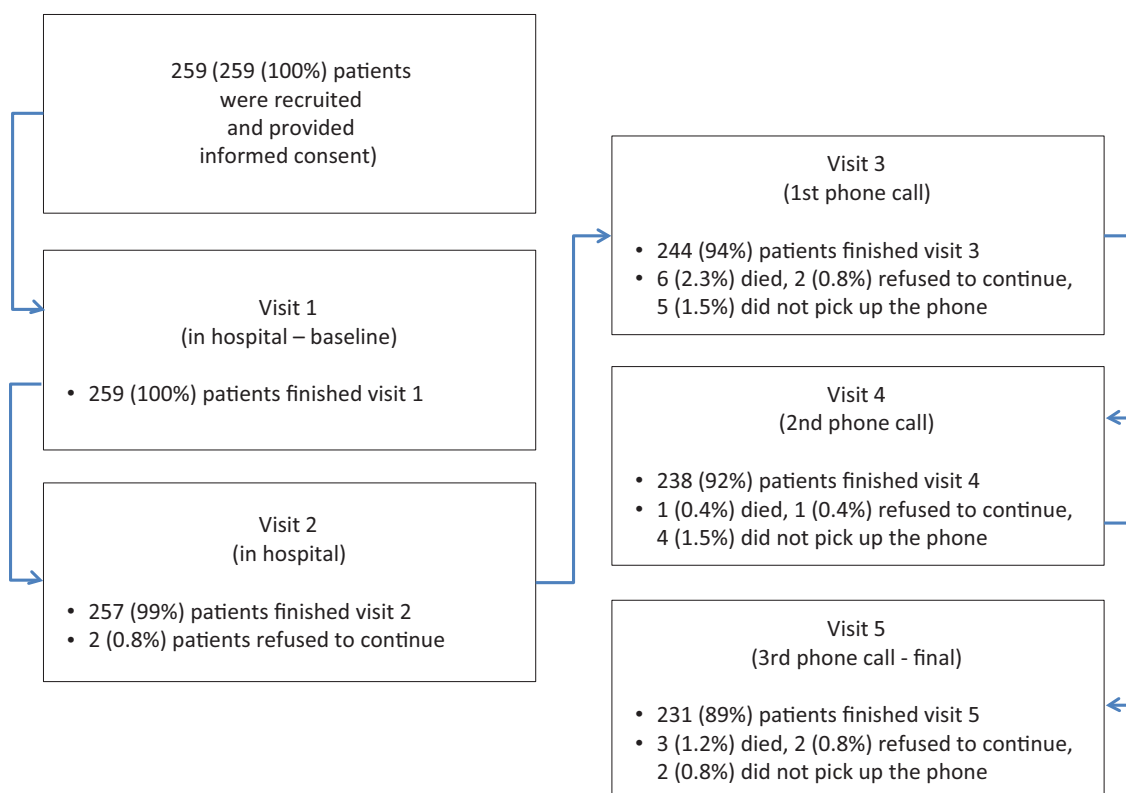
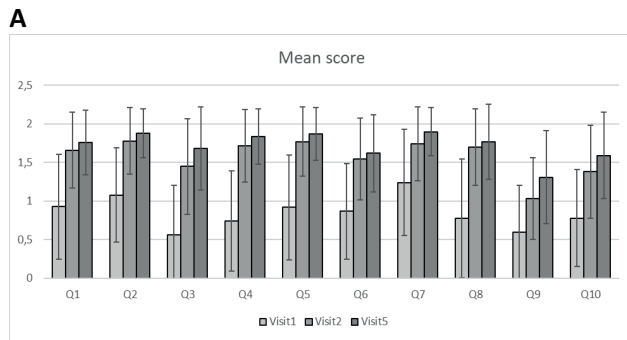
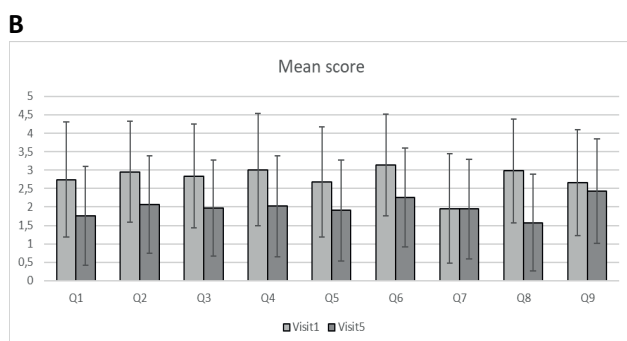


Fig. 1. Patient flowchart



The HF knowledge questionnaire: answers were assessed on 3-point scale (0 – incorrect response, 1 – partially correct response, 2 – correct response). A maximum score for individual question was 2 points with higher score indicating better knowledge.

Individual questions: Q1 – What does HF mean?; Q2 – What are the HF symptoms?; Q3 – What does HF decompensation mean?; Q4 – How HF decompensation can be detected?; Q5 – What diet recommendations do you know?; Q6 – What are the physical activity benefits?; Q7 – What is the role of diuretics in HF treatment?; Q8 – How much time after hospital discharge first ambulatory visit should be scheduled?; Q9 – What drugs are used in HF treatment?; Q10 – What can lead to HF decompensation?



9-EHFScBS questionnaire: answers were assessed on 5-point Likert scale from 1 (completely agree) to 5 (completely disagree). A maximum score for individual question was 5 points with a lower score indicating better self-care.

Individual statements: Q1 – I weigh myself every day; Q2 – If shortness of breath (SOB) increases, I contact my doctor or nurse; Q3 – If legs/feet are more swollen, I contact my doctor or nurse; Q4 – If I gain weight more than 2 kg in 7 days, I contact my doctor or nurse; Q5 – I limit the amount of fluids (not more than 1.5–2 litres a day); Q6 – If I experience fatigue, I contact my doctor or nurse; Q7 – I eat a low-salt diet; Q8 – I take my medication as prescribed; Q9 – I exercise regularly.

Fig. 2. A. Comparison of scores to the individual questions on the heart failure (HF) knowledge; B. Comparison of scores to the 9-item European Heart Failure Self-care Behavior Scale (9-EHFScBS) questionnaire. The comparisons are based on the results of repeated measures analysis of variance (ANOVA) test

hospitalizations and with long-lasting HF scored better on the knowledge test compared to patients not educated previously, hospitalized for the first time and with HF de novo (Table 3).

The results indicate that self-care behaviors improved after the intervention ($Z = -7.317$, $p < 0.001$ (higher score means lower self-care capability)). Enhanced autonomous-based adherence type of self-care behaviors

Table 1. Baseline characteristic of patients with heart failure (HF)

Variable (categorical)	Features	n (%)
Age, years (%)	<40	17 (6.6%)
	40–70	176 (67.9%)
	>70	66 (25.5%)
Gender	female	61 (23.6%)
	male	198 (76.4%)
Education	primary	69 (26.7%)
	secondary	163 (62.9%)
	higher	27 (10.4%)
Residence	city	173 (66.8%)
	rural area	86 (33.2%)
Professional activity	working	60 (23.2%)
	retired	128 (49.4%)
	on pension	71 (27.4%)
Comorbidities*	none	66 (25.5%)
	1	104 (40.1%)
	>1	89 (34.4%)
HF education by HCP	no	194 (74.9%)
	yes	65 (25.1%)
Marital status	single	43 (16.6%)
	married	216 (83.4%)
Mean time from HF diagnosis to the commencement of the program	0	36 (13.9%)
	<1 year	47 (18.1%)
	>1 year	176 (68.0%)
Hospitalizations	none	73 (28.2%)
	once in the last year	99 (38.2%)
	>1 in the last year	87 (33.6%)
Previous HF education	no	194 (74.9%)
	yes, by:	
	cardiologist	51 (19.7%)
	primary care physician	7 (2.7%)
	nurse	7 (2.7%)
Variable (continuous)	Features	Results
Duration of the HF [years]	M (SD)	6.71 (8.85)
	Me	2.98
	Min–Max	0–42
	Q1; Q3	0.27; 9.86

* Comorbidities: diabetes, chronic obstructive pulmonary disease, atrial fibrillation, past stroke. HCP – healthcare personnel; HF – heart failure; M – mean; Me – median; SD – standard deviation; Q1 – 1st quartile; Q3 – 3rd quartile.

($Z = -5.870$, $p < 0.001$) was demonstrated. The level of consulting behavior also significantly increased after 3 months following the intervention ($Z = -7.238$, $p < 0.001$). Likewise, the level of provider-based adherence behaviors was more frequent after 3 months of follow-up than prior to the intervention ($Z = -4.162$; $p < 0.001$). The significant improvement in self-care was seen in all individual questions except statements 7 (“I eat a low salt

Table 2. Comparisons of the scores on heart failure (HF) knowledge test prior to, directly after and 3 months after participation in the program, based on the results of the Friedman’s test

Measurement	Mean rank	Me	χ^2	Dunn–Bonferroni post hoc		
				Z statistic		
				1	2	3
1	1.04	8	$\chi^2 = 356.526,$ $p < 0.001$	–	–	–
2	2.27	16		1.227***	–	–
3	2.69	18		1.649***	0.422***	–

*** $p_{adj} < 0.001$. The Bonferroni correction was used to adjust the p-values for multiple tests; Me – median.

Table 3. Summary of differences in the knowledge test scores based on the results of the Mann–Whitney U-test

Patients	Score on the knowledge test			
	Mean rank	Z-value	Mann–Whitney U test	p-value
Previously educated on HF	165.71	–4.451	3984.00	<0.001
Without prior education on HF	118.04			
>1 hospitalization	144.94	–5.137	4009.50	<0.001
First hospitalization	91.92			

HF – heart failure.

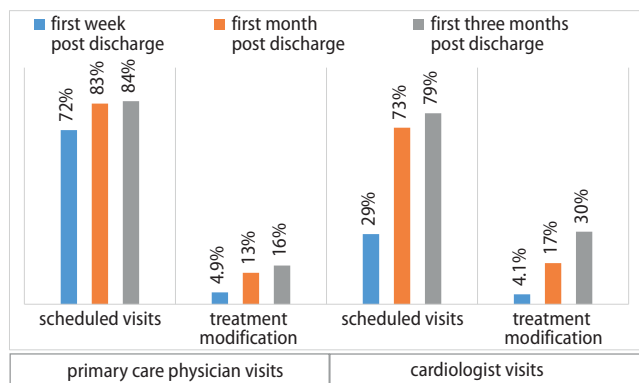


Fig. 3. Fulfillment of ambulatory visits to primary care physicians and cardiologists within the follow-up period in accordance with the individual treatment plan

diet”) and 9 (“I exercise regularly”) of the 9-EHFScBS questionnaire (Fig. 2).

All patients were educated about the importance of post-hospital ambulatory visits and treatment optimization. Most patients fulfilled their individualized post-discharge treatment plan (Fig. 3).

Discussion

Like previous studies, we found disease awareness and self-management skills initially poor among Polish patients with HF.^{31–35} However, “The Weak Heart” model, prepared based on HF guidelines and practical recommendations,^{1,4,7,36} was effective in enhancing HF patients’ knowledge and developing self-management behaviors. In the study, the education program was delivered by a certified nurse educator working in a given cardiology ward. From a practical perspective, it is worth mentioning that

3.5 h in total were allocated to an individual patient’s education. Based on nurses’ feedback, in most cases, the time devoted to education was sufficient from the patient’s point of view, but it caused a considerable burden on staff. Therefore, there is a need to introduce a qualified HF educator working in the cardiology wards responsible for patients’ education, or to consider group education instead – to reduce the staff burden.

This observation is of significance since previous meta-analysis showed that self-management interventions in patients with HF improve the outcomes.^{11,22,35} Therefore, evidence-based educational programs should be considered when designing multidisciplinary programs of coordinated care.²⁴ Unfortunately, any direct comparison of the effectiveness of our program with other educational interventions of this kind is difficult due to the heterogeneity of the design and methodology used in the research (Table 4).

Telephone support may reduce mortality and hospitalizations and improve quality of life among patients with HF.^{20,21,35} Currently, it is the most commonly used monitoring strategy.^{39,41–43} We found post-discharge phone calls performed by nurses had an additional, positive effect on patients’ HF knowledge and self-care behaviors. Yet another important strategy is to deliver educational programs during hospitalization, as patients after an acute episode are at a higher risk of recurrent hospitalizations.⁴³ Moreover, it helps in building a trusting relationship with patients and caregivers.^{38,39} The time of hospitalization can also be used successfully to teach patients perform regular pulse, blood pressure and weight measurements, which was well received by participants of our program.

Early ambulatory visits within 7 days of discharge may lower the risk of hospital readmissions for patients with HF.^{20,21,42,44} According to the study by Chuda et al.,⁴⁵ over 90% of cardiac ward patients were referred to cardiac

Table 4. Summary of recent studies evaluating effectiveness of educational programs for heart failure (HF) patients

Study (author/year/ref)	Study design	Sample size (location)	Population	Key components of intervention/control	Follow-up period	Outcome variables	Main findings
Kolasa et al., 2021	Multicenter, non-randomized, quasi-experimental study; pre-test and post-test methodology (14 centers)	n = 259 (Poland)	HFrEF patients hospitalized with decompensated HF	Intervention: standardized educational program based on the ESC guidelines, multimedia education with the content of www.slabeserce.pl website displayed on tablet, individual treatment plan, HF passport, cover letter to primary care physician. Two individual teaching sessions (60 min) and 3 telephone calls 7, 30 and 90 days post-discharge delivered by a nurse. Control: N/A	3 months	Change in HF knowledge (self-developed questionnaire) and self-care (9-EHFScBS). The percentage of ambulatory visits realized in accordance with the treatment plan.	A significant change in HF knowledge test ($\chi^2 = 356.526$, $p < 0.001$) and in all individual questions. A significant change in self-care in total score ($Z = -7.317$, $p < 0.001$) in all domains: autonomous-based adherence ($Z = -5.870$, $p < 0.001$); consulting behavior ($Z = -7.238$, $p < 0.001$); provider-based adherence ($Z = -4.162$; $p < 0.001$) and in relation to all individual statements except statement 7 ("I eat a low salt diet") and statement 9 ("I exercise regularly"). Within 3 months of hospital discharge, 84% (193 out of 231) of participants visited their primary care physician and 79% (183 out of 231) visited a cardiologist in accordance with their individual treatment plan.
Sahlin et al., 2021 ³⁷	Multicenter, randomized trial (7 centers)	n = 118 (Sweden)	Ambulatory HF patients	Intervention: home-based mobile device in a form of tablet wirelessly connected to a weight scale and incorporated symptom monitoring, interactive education, adjustment of loop diuretics and alerts of HF deterioration. Control: N/A	8 months	Change in self-care behavior (9-EHFScB). The number of in-hospital days due to HF. Event-free survival, defined as the composite endpoint of time to the 1 st occurrence of HF-related emergency room (ER) visit, HF admission, or death and unplanned hospital visits due to HF after 240 days of intervention.	A significant change in self-care (21.5 (13.25; 28) compared to 26 (18; 29.75), $p = 0.014$). Significantly shorter time in the hospital when admitted for HF (2.2 days less, RR: 0.48; 95% CI: [0.32; 0.74]; $p = 0.001$). A significant difference in HF-related event-free survival (HR = 0.50, 95% CI: [0.24; 0.98], $p = 0.046$). Non-significant difference in all-cause hospital admission or death (HR = 0.77, 95% CI: [0.46; 1.28], $p = 0.32$).
Huyh et al., 2019 ³⁸	Multicenter, randomized trial (2 centers)	n = 412 (Tasmania)	Patients hospitalized with HF	Intervention: standard care plus leaflet and video instruction, "transition coach" to provide telephone support, home visits of a cardiac nurse during the 1 st and 2 nd week of discharge, additional telephone calls if needed. Control: standard care including guideline-based care, self-care education during the hospital stays, a standard discharge summary and advice sent to primary care physicians, and treatment plan for comorbidity, and routine preventive care from treating physicians. A follow-up telephone call was conducted within a month after discharge.	3 months	All-cause readmission (defined as at least 24 h unplanned stay in hospital) or death within 30 and 90 days of discharge.	Readmission or death occurred in 74/197 (37%) of usual care patients and 50/215 (23%) of DMP patients within 30 days (RR: 0.62, 95% CI: [0.46; 0.84]), and 113/197 (57%) of usual care patients and 78/215 (36%) of DMP patients within 90 days (RR: 0.63, 95% CI: [0.51; 0.78]).

Study (author/year/ref)	Study design	Sample size (location)	Population	Key components of intervention/control	Follow-up period	Outcome variables	Main findings
Awoke et al., 2019 ⁶	Multicenter non-randomized quasi-experimental study, pre-test and post-test methodology (2 centers)	n = 29 (USA)	Patients hospitalized with HF	Intervention: standardized educational program based on AHA guidelines, standard education based on printed material in a form of visual color-coded guide to monitor symptoms. One teaching session delivered by a nurse reinforced with daily follow-up education sessions and telephone follow-up 7, 30 and 90 days post-discharge. Control: N/A	3 months	All-cause unplanned hospital readmissions 30 days after hospital discharge. Change in HF knowledge (DHFKS) and self-care (SCHFI).	A significant difference in HF knowledge test at day 7 ($p \leq 0.001$) and day 90 ($p \leq 0.032$). A significant difference in self-care maintenance at day 7 ($p \leq 0.000$) and day 30 ($p \leq 0.000$), self-care management at day 7 ($p \leq 0.001$) and day 30 ($p \leq 0.013$), in self-care confidence at day 30 ($p \leq 0.017$), but not at day 7 follow-up call. No significant change in 30-day readmissions ($p \geq 0.05$).
Boyde et al., 2018 ³⁹	Single center, randomized trial	n = 200 (Australia)	Patients diagnosed with HF referred to the hospital	Intervention: multimedia education based on an individual patient's needs (verbal discussions with a HF nurse, written manuals and a DVD to use at home). One teaching session (60–90 min) delivered by a nurse. Control: standard care	12 months	All-cause unplanned hospital readmissions. Change in HF knowledge (DHFKS) and self-care (SCHFI).	No significant change in HF knowledge test at 3 months ($p = 0.132$) and 12 months post-recruitment ($p = 0.612$) between groups. No significant differences in self-care maintenance ($p = 0.241$), management ($p = 0.232$) or confidence ($p = 0.194$) between the intervention and control groups at 3 months and at 12 months, for maintenance ($p = 0.604$), management ($p = 0.903$) or self-confidence ($p = 0.132$). Reduced risk of readmission at 12 months by 30% (RR: 0.703; 95% CI: 0.548; 0.903).
Moon et al., 2018 ⁴⁰	Single-center, quasi-experiment study	n = 38 (South Korea)	Ambulatory patients with HF (EF < 50%)	Intervention: the telephone-based self-management support program. One 30-minute face-to-face education session and 4 telephone follow-up consultations. Control: not described	5 weeks	Change in the self-care behavior (9-EHfScB), NT-proBNP, LVEF, LVEDP and depression score.	A significant change in self-care behavior ($t = 6.65$, $p < 0.001$), decreased N-terminal pro-brain natriuretic peptide level ($U = -2.28$, $p < 0.022$), improved LVEF values ($t = 2.24$, $p < 0.032$), and decreased depression scores ($t = 3.49$, $p < 0.001$).

9-EHfScB – European Heart Failure Self-care Behavior Scale; DHFKS – Dutch Heart Failure Knowledge Scale; SCHFI – Self-Care of Heart Failure Index; ESC – European Society of Cardiology; N/A – not applicable; 95% CI – 95% confidence interval; AHA – American Heart Association; EF – ejection fraction; NT-proBNP – N-terminal pro B-type natriuretic peptide; LVEF – left ventricular ejection fraction; LVEDP – left ventricular end-diastolic pressure; RR – relative risk; HR – hazard ratio; DMP – Disease Management Program; HFREF – heart failure with reduced ejection fraction.

ambulatory care after hospital discharge, compared to only 60% among those discharged from the internal medicine ward. In our program, all patients were educated about the importance of post-discharge ambulatory visits and were given individual treatment plans. This strategy proved to be effective, with 72% of patients fulfilling visits in primary care and 30% visiting a cardiologist within 7 days of discharge.

The results of our study showed that patients undergoing any kind of education before participating in the program and patients hospitalized due to HF many times have higher initial knowledge of HF and obtained higher tests scores than the patients who had not been previously educated or hospitalized due to HF. It suggests that patients build their disease awareness from multiple educational sources and learn through their own experience during hospitalizations.⁴⁶ Although 68% of patients recruited to the study had history of HFrEF for more than 1 year and 72% had been hospitalized for HF decompensation at least once in the previous year, only 25% of participants declared being educated by a healthcare provider prior to the program. According to the participants, the cardiologist (78%), nurses (11%) and primary care physicians (11%) were the healthcare professionals who most frequently delivered disease education. This indicates that currently in Poland, there is no structured approach to health education for HF patients.







Limitations

Some important limitations of the “The Weak Heart” program have to be acknowledged. Firstly, this program had quasi-experimental, non-randomized design, without an appropriate control group, with short observation period and relatively small sample of patients. Secondly, the cohort recruited was relatively young, had a higher education level, lived with family, and the majority lived in the city. However, these factors had a limited impact on the effectiveness of the proposed program. The multivariable analysis, the results of which were presented elsewhere,⁴⁶ has shown that only age may affect self-care behaviors, but not the level of HF knowledge. Lastly, only patients with HFrEF hospitalized with ADHF were included in the study. All these factors suggest that those patients may present a higher level of health literacy and initial disease knowledge and may be significantly different from “an average patient” in routine practice. The other important limitations are the utilization of unstandardized HF knowledge questionnaire and short follow-up period. Finally, limitations resulting from the design of the project including small group size and the lack of longer-term, longitudinal data precludes a comment regarding the impact of investigated intervention on clinical outcomes, only allowing to draw general conclusions about the short-term effect of the tested model on the level of HF knowledge and self-care behaviors in the studied population of HFrEF patients hospitalized due to decompensation.

Conclusions

The HF knowledge and self-care behaviors among patients with HFrEF can be improved by introducing a structured, nurse-led educational programs to clinical practice. “The Weak Heart” educational model created based on HF guidelines recommendations proved to be effective in enhancing the level of HF knowledge and self-care behaviors among patients with HFrEF hospitalized with ADHF. The time spent in hospital should be used to prepare patients for challenges of post-discharge “vulnerable phase” by providing a proper training on self-care skills delivered by certified nurses.

ORCID iDs

Jolanta Kolasa  <https://orcid.org/0000-0003-4160-7821>
 Magdalena Frączek-Jucha  <https://orcid.org/0000-0003-3935-6250>
 Marcin Grabowski  <https://orcid.org/0000-0003-3306-0301>
 Ewa A. Jankowska  <https://orcid.org/0000-0002-9202-432X>
 Małgorzata Lelonek  <https://orcid.org/0000-0003-0756-5541>
 Agnieszka Pawlak  <https://orcid.org/0000-0001-9032-9130>
 Izabella Uchmanowicz  <https://orcid.org/0000-0001-5452-0210>
 Jadwiga Nessler  <https://orcid.org/0000-0002-5076-5816>

References

1. Ponikowski P, Voors A, Anker S, et al. 2016 ESC Guidelines for the diagnosis and treatment of acute and chronic heart failure. *Eur Heart J*. 2016;37(27):2129–2200. doi:10.1093/eurheartj/ehw128
2. Rywik TM, Zieliński T, Piotrowski W, Leszek P, Wilkins A, Korewicki J. Heart failure patients from hospital settings in Poland: Population characteristics and treatment patterns. A multicenter retrospective study. *Cardiol J*. 2008;15(2):169–180. PMID:18651402.
3. Maniecka-Bryła I, Bryła M, Bryła P, Pikala M. The burden of premature mortality in Poland analysed with the use of standard expected years of life lost. *BMC Public Health*. 2015;15:101. doi:10.1186/s12889-015-1487-x
4. Lainscak M, Blue L, Clark AL, et al. Self-care management of heart failure: Practical recommendations from the Patient Care Committee of the Heart Failure Association of the European Society of Cardiology. *Eur J Heart Fail*. 2011;13(2):115–126. doi:10.1093/eurjhf/hfq219
5. Strömberg A. The crucial role of patient education in heart failure. *Eur J Heart Fail*. 2005;7(3):363–369. doi:10.1016/j.ejheart.2005.01.002
6. Riegel B, Dickson VV, Faulkner KM. The situation-specific theory of heart failure self-care: Revised and updated. *J Cardiovasc Nurs*. 2016;31(3):226–235. doi:10.1097/JCN.0000000000000244
7. McDonagh TA, Blue L, Clark AL, et al. European Society of Cardiology Heart Failure Association Standards for delivering heart failure care. *Eur J Heart Fail*. 2011;13(3):235–241. doi:10.1093/eurjhf/hfq221
8. Ditewig JB, Blok H, Havers J, van Veenendaal H. Effectiveness of self-management interventions on mortality, hospital readmissions, chronic heart failure hospitalization rate and quality of life in patients with chronic heart failure: A systematic review. *Patient Educ Couns*. 2010;78(3):297–315. doi:10.1016/j.pec.2010.01.016
9. Jovicic A, Holroyd-Leduc JM, Straus SE. Effects of self-management intervention on health outcomes of patients with heart failure: A systematic review of randomized controlled trials. *BMC Cardiovasc Disord*. 2006;6:43. doi:10.1186/1471-2261-6-43
10. Barnason S, Zimmerman L, Young L. An integrative review of interventions promoting self-care of patients with heart failure. *J Clin Nurs*. 2012;21(3–4):448–475. doi:10.1111/j.1365-2702.2011.03907.x
11. McAlister FA, Stewart S, Ferrua S, McMurray JJ. Multidisciplinary strategies for the management of heart failure patients at high risk for admission: A systematic review of randomized trials. *J Am Coll Cardiol*. 2004;44(4):810–819. doi:10.1016/j.jacc.2004.05.055
12. Kommuri NV, Johnson ML, Koelling TM. Relationship between improvements in heart failure patient disease specific knowledge and clinical events as part of a randomized controlled trial. *Patient Educ Couns*. 2012;86(2):233–238. doi:10.1016/j.pec.2011.05.019

13. Albert NM. Fluid management strategies in heart failure. *Crit Care Nurse*. 2012;32(2):20–33. doi:10.4037/ccn2012877
14. Domingues FB, Clausell N, Aliti GB, Dominguez DR, Rabelo ER. Education and telephone monitoring by nurses of patients with heart failure: Randomized clinical trial. *Arq Bras Cardiol*. 2011;96(3):233–239. doi:10.1590/s0066-782x2011005000014
15. Paul S, Hice A. Role of the acute care nurse in managing patients with heart failure using evidence-based care. *Crit Care Nurs Q*. 2014;37(4):357–376. doi:10.1097/CNQ.0000000000000036
16. Awoke MS, Baptiste DL, Davidson P, Roberts A, Dennison-Himmelfarb C. A quasi-experimental study examining a nurse-led education program to improve knowledge, self-care, and reduce readmission for individuals with heart failure. *Contemp Nurse*. 2019;55(1):15–26. doi:10.1080/10376178.2019.1568198
17. Feltner C, Jones CD, Cene CW, et al. Transitional care interventions to prevent readmissions for persons with heart failure: A systematic review and meta-analysis. *Ann Intern Med*. 2014;160(11):774–784. doi:10.7326/M14-0083
18. Yancy CW, Jessup M, Bozkurt B, et al. 2017 ACC/AHA/HFSA focused update of the 2013 ACCF/AHA guideline for the management of heart failure: A report of the American College of Cardiology/American Heart Association Task Force on Clinical Practice Guidelines and the Heart Failure Society of America. *J Am Coll Cardiol*. 2017;70(6):776–803. doi:10.1016/j.jacc.2017.04.025
19. Riegel B, Moser DK, Anker SD, et al. State of the science: Promoting self-care in persons with heart failure. A scientific statement from the American Heart Association. *Circulation*. 2009;120(12):1141–1163. doi:10.1161/CIRCULATIONAHA.109.192628
20. Ryan J, Kang S, Dolack S, Ingrassia J, Ganeshan R. Change in readmissions and follow-up visits as part of a heart failure readmission quality improvement initiative. *Am J Med*. 2013;126(11):989–994.e1. doi:10.1016/j.amjmed.2013.06.027
21. Van Spall HG, Rahman T, Mytton O, et al. Comparative effectiveness of transitional care services in patients discharged from the hospital with heart failure: A systematic review and network meta-analysis. *Eur J Heart Fail*. 2017;19(11):1427–1443. doi:10.1002/ejhf.765
22. Jonkman NH, Westland H, Groenwold RH, et al. Do self-management interventions work in patients with heart failure? An individual patient data meta-analysis. *Circulation*. 2016;133(12):1189–1198. doi:10.1161/CIRCULATIONAHA.115.018006
23. Cowie MR, Lopatin YM, Saldarriaga C, et al. The Optimize Heart Failure Care Program: Initial lessons from global implementation. *Int J Cardiol*. 2017;236:340–344. doi:10.1016/j.ijcard.2017.02.033
24. Nessler J, Gruchała M, Rozentryt P, et al. Projekt pilotażowy Kompleksowej Opieki nad Osobami z Niewydolnością Serca (KONS) – punkt wyjścia i spodziewane rezultaty. *Kardiologia Pol*. 2019;77(Suppl II):102–109. https://journals.viamedica.pl/kardiologia_polska/article/view/83190/62481. Accessed November 18, 2021.
25. Uchmanowicz I, Lisiak M, Lelonek M, et al. A curriculum for the heart failure nurse: An expert opinion of the Section of Nurses and Medical Technicians and the Heart Failure Section of the Polish Cardiac Society. *Kardiologia Pol*. 2020;78(6):647–652. doi:10.33963/KP.15405
26. Sekcja Niewydolności Serca Polskiego Towarzystwa Kardiologicznego. Heart failure passport [in Polish]. https://slabeserce.pl/files/pdf/paszport_pacjenta.pdf. Accessed September 24, 2021.
27. Kolasa J, Uchmanowicz I, Wleklík M, et al. “The Weak Heart” as an educational model for patients hospitalised due to decompensation of heart failure with reduced ejection fraction. *Folia Cardiol*. 2020;15:99–106. doi:10.5603/FC.a2020.0014
28. Jaarsma T, Arestedt KF, Mårtensson J, Dracup K, Strömberg A. The European Heart Failure Self-care Behaviour scale revised into a nine-item scale (EHFScB-9): A reliable and valid international instrument. *Eur J Heart Fail*. 2009;11(1):99–105. doi:10.1093/eurjhf/hfn007
29. Uchmanowicz I, Wleklík M. Polish adaptation and reliability testing of the nine-item European Heart Failure Self-care Behaviour Scale (9-EHFScBS). *Kardiologia Pol*. 2016;74(7):691–696. doi:10.5603/KP.a2015.0239
30. Vellone E, Jaarsma T, Strömberg A, et al. The European Heart Failure Self-care Behaviour Scale: New insights into factorial structure, reliability, precision and scoring procedure. *Pat Educ Couns*. 2014;94(1):97–102. doi:10.1016/j.pec.2013.09.014
31. Kolasa J, Maciejewski C, Zych A, et al. The role of health education in heart failure patients [in Polish]. *Folia Cardiol*. 2019;14(3):252–257. doi:10.5603/FC.2019.0058
32. Raines E, Dickey SL. An exploration of learning needs: Identifying knowledge deficits among hospitalized adults with heart failure. *AIMS Public Health*. 2019;6(3):248–267. doi:10.3934/publichealth.2019.3.248
33. Nowak K, Stępień K, Furczyńska P, et al. The awareness and knowledge about heart failure in Poland: Lessons from the Heart Failure Awareness Day and internet surveys. *Folia Med Cracov*. 2019;59(2):93–109. PMID:31659353.
34. Płotka A, Prokop E, Migaj J, Straburzyńska-Migaj E, Grajek S. Patients’ knowledge of heart failure and their perception of the disease. *Patient Prefer Adherence*. 2017;11:1459–1467. doi:10.2147/PPA.S126133
35. Lambrinou E, Protopapas A, Kalogirou F. Educational challenges to the health care professional in heart failure care. *Curr Heart Fail Rep*. 2014;11(3):299–306. doi:10.1007/s11897-014-0203-y
36. Seferovic PM, Ponikowski P, Anker SD, et al. Clinical practice update on heart failure 2019: Pharmacotherapy, procedures, devices and patient management. An expert consensus meeting report of the Heart Failure Association of the European Society of Cardiology. *Eur J Heart Fail*. 2019;21(10):1169–1186. doi:10.1002/ejhf.1531
37. Sahlin D, Rezanejad B, Edvinsson ML, Bachus E, Melander O, Gerward S. Selfcare Management Intervention in Heart Failure (SMART-HF): A multicenter randomized controlled trial. *J Card Fail*. 2021;S1071-9164(21)00245-1. doi:10.1016/j.cardfail.2021.06.009
38. Huynh QL, Whitmore K, Negishi K, Marwick TH; ETHELRED Investigators. Influence of risk on reduction of readmission and death by disease management programs in heart failure. *J Card Fail*. 2019;25(5):330–339. doi:10.1016/j.cardfail.2019.01.015
39. Boyde M, Peters R, New N, Hwang R, Ha T, Korczyk D. Self-care educational intervention to reduce hospitalizations in heart failure: A randomised controlled trial. *Eur J Cardiovasc Nurs*. 2018;17(2):178–185. doi:10.1177/1474515117727740
40. Moon MK, Yim JE, Jeon MY. The effect of a telephone-based Self-Management Program led by nurses on self-care behavior, biological index for cardiac function and depression in ambulatory heart failure patients. *Asian Nurs Res (Korean Soc Nurs Sci)*. 2018;12(4):251–257. doi:10.1016/j.anr.2018.10.001
41. Rice H, Say R, Betihavas V. The effect of nurse-led education on hospitalisation, readmission, quality of life and cost in adults with heart failure: A systematic review. *Patient Educ Couns*. 2018;101(3):363–374. doi:10.1016/j.pec.2017.10.002
42. Breathett K, Maffett S, Foraker RE, et al. Pilot randomized controlled trial to reduce readmission for heart failure using novel tablet and nurse practitioner education. *Am J Med*. 2018;131(8):974–978. doi:10.1016/j.amjmed.2018.02.017
43. Son YJ, Choi J, Lee HJ. Effectiveness of nurse-led heart failure self-care education on health outcomes of heart failure patients: A systematic review and meta-analysis. *Int J Environ Res Public Health*. 2020;17(18):6559. doi:10.3390/ijerph17186559
44. Hernandez AF, Greiner MA, Fonarow GC, et al. Relationship between early physician follow-up and 30-day readmission among Medicare beneficiaries hospitalized for heart failure. *JAMA*. 2010;303(17):1716–1722. doi:10.1001/jama.2010.533
45. Chuda A, Berner J, Lelonek M. The journey of the heart failure patient based on data from a single center. *Adv Clin Exp Med*. 2019;28(4):489–498. doi:10.17219/acem/78688
46. Kolasa J, Lisiak M, Grabowski M, et al. Factors associated with heart failure knowledge and adherence to self-care behaviors in hospitalized patients with acute decompensated heart failure based on data from “the Weak Heart” educational program. *Patient Prefer Adherence*. 2021;15:1289–1300. doi:10.2147/PPA.S297665

Melatonin protected against myocardial infarction injury in rats through a *Sirt6*-dependent antioxidant pathway

*Yingcui Wang^{1,B-D,F}, *Suhua Zhang^{2,B,E}, Yingying Ma^{3,C,E}, Aixia Xiang^{4,E}, Hui Sun^{1,E}, Jun Song^{4,C}, Wenjing Yang^{1,E}, Xuanlong Li^{1,E}, Hongxiao Xu^{1,A,D,F}

¹ Department of Cardiology, Qilu Hospital (Qingdao), Cheeloo College of Medicine, Shandong University, China

² Department of Geriatrics, Qilu Hospital (Qingdao), Cheeloo College of Medicine, Shandong University, China

³ Qingdao Jimo District Center for Disease Control and Prevention, China

⁴ Jimo People's Hospital, Qingdao, China

A – research concept and design; B – collection and/or assembly of data; C – data analysis and interpretation;

D – writing the article; E – critical revision of the article; F – final approval of the article

Advances in Clinical and Experimental Medicine, ISSN 1899–5276 (print), ISSN 2451–2680 (online)

Adv Clin Exp Med. 2022;31(3):277–284

Address for correspondence

Hongxiao Xu

E-mail: xuhongxqlh@163.com

Funding sources

This work was supported by Key Fund of Department of Cardiology, Shandong University Qilu Hospital (Qingdao) (QDKY2019ZD04), People's Livelihood Science and Technology Project of Qingdao (application of DEEPVESSEL FFR in coronary artery heart disease complicated with diabetes mellitus), Qingdao Key Health Discipline Development Fund.

* Yingcui Wang and Suhua Zhang contributed equally to the article.

Conflict of interest

None declared

Received on August 8, 2018

Reviewed on February 25, 2019

Accepted on September 1, 2019

Published online on January 25, 2022

Cite as

Wang Y, Zhang S, Ma Y, et al. Melatonin protected against myocardial infarction injury in rats through a *Sirt6*-dependent antioxidant pathway. *Adv Clin Exp Med*. 2022;31(3):277–284. doi:10.17219/acem/112060

DOI

10.17219/acem/112060

Copyright

© 2022 by Wrocław Medical University

This is an article distributed under the terms of the Creative Commons Attribution 3.0 Unported (CC BY 3.0) (<https://creativecommons.org/licenses/by/3.0/>)

Abstract

Background. The *Sirt6*, one of the members of the sirtuin family, has been regarded as a key factor in the pathogenesis of myocardial infarction (MI) through its antioxidant defense mechanisms. A previous study reported that melatonin is an antioxidant drug that can act as an agent for cardioprotection in cardiac ischemia-reperfusion (I/R) injury. However, whether melatonin could protect against cardiac remodeling after myocardial injury via the *Sirt6*-dependent antioxidant pathway remains unknown.

Objectives. To explore the protective effects and the potential mechanisms of melatonin on MI-induced injury in rats.

Materials and methods. A cardiac remodeling model was established through left coronary artery ligation surgery. The dose of melatonin was 10 mg/kg body weight. Four weeks after the treatment for 7 successive days, the infarct size and hemodynamic parameters were evaluated. The relative mRNA level and protein level of *Sirt6* were also determined. Finally, the levels of oxidative stress, including reactive oxygen species (ROS) and superoxide dismutase (SOD), were measured, and the expression of nitric oxide (NO), inducible nitric oxide synthase (iNOS), endothelial nitric oxide synthase (eNOS) and their corresponding phosphorylation were evaluated.

Results. After the treatment with melatonin, infarct size, the left ventricular end-diastolic diameter (LVEDd), and left ventricular end-systolic diameter (LVEDs) and minimum first derivative of developed pressure (min dp/dt) decreased, while left ventricular ejection fraction (LVEF), left ventricular fractional shortening (LVFS) and maximum first derivative of developed pressure (max dp/dt) increased in the melatonin-MI (MM) group compared to the placebo-MI (PM) group. Furthermore, the expressions of *Sirt6*, both in mRNA and protein level, were significantly increased in the MM group treated with melatonin, as compared to the melatonin-control (MC) group treated with melatonin. In addition, melatonin enhanced SOD activity and reduced ROS levels. At the same time, we observed that the eNOS/NO signaling pathways were activated.

Conclusions. Melatonin improved cardiac function through the *Sirt6*-dependent antioxidant pathway in MI rats.

Key words: melatonin, oxidative stress, acute myocardial infarction, sirtuin

Background

Acute myocardial infarction (MI) is generally caused by coronary artery disease (CAD), which remains a leading cause of morbidity and mortality and imposes a tremendous economic burden worldwide.¹ After MI injury, the heart undergoes a series of cardiac wound-healing responses, including cardiomyocyte necrosis and apoptosis, inflammation, and cardiac hypertrophy and fibrosis. As cardiac wound healing progresses, patients suffer from post-MI left ventricular (LV) remodeling, heart failure (HF) or even death.^{2,3}

Oxidative stress plays an important role in the pathophysiology of various cardiovascular disorders, including atherosclerosis, cardiac hypertrophy, cardiomyopathy, HF, ventricular remodeling, and myocardial injury after ischemia followed by reperfusion (I/R). During the development of cardiac remodeling, oxidative stress aggravates heart disease into HF.^{4–6} Elevated oxidative stress may result in peroxidation of proteins, DNA and lipids, triggering mitochondria-induced cell death pathways and contributing to I/R injury.⁷

The *Sirt6* is one of the 7 mammalian sirtuin homologs and it contains a domain with NAD⁺-dependent deacetylase activity.⁸ Among sirtuin family members, both *Sirt1* and *Sirt6* have demonstrated cardioprotective abilities. However, no direct evidence can verify the antioxidative role of *Sirt1* in protecting heart function, while *Sirt6* has been shown to play a vital protective role in cardiomyocytes in I/R through its antioxidative ability.⁹

Melatonin, a hormone synthesized and secreted by the pineal gland, is a well-known antioxidant.^{10,11} Extensive evidence suggests that melatonin has profound cardioprotective effects.^{12,13} For example, Hu et al. demonstrated that melatonin alleviated post-infarction cardiac remodeling and dysfunction by inhibiting Mst1.¹⁴ Zhou et al. demonstrated that melatonin protected against I/R in myocardial infarction by suppressing platelet activation and function.¹⁵ However, whether melatonin could protect against cardiac remodeling after myocardial injury via a *Sirt6*-dependent antioxidant pathway, remains unknown.

Objectives

The aim of the study was to explore the protective effects and the potential mechanisms of melatonin on MI-induced injury in rats.

Materials and methods

The animals

All the experiments were performed with the approval of the Ethics Committee at Shandong University Qilu

Hospital (approval No. KYLL-KS-2021180). Three-month-old male Wistar rats weighing 250–270 g were purchased from Charles River Laboratories (Beijing, China). The rats were randomly divided into 4 groups: placebo-control (PC), melatonin-control (MC), placebo-MI (PM), and melatonin-MI (MM). Each group included 10 rats. In the PM and MM groups, the rat MI model was established through left coronary artery ligation surgery. In addition, the PC group was regarded as a negative control group, and it was designed to show whether the model was established successfully and to eliminate the influence of the operation.

Rat MI model

The rats were placed in an induction chamber and 4% isoflurane was delivered until they reached a deep plane of anesthesia. After the intubation was finished, the chest was opened at the left 4th intercostal space. The pericardial tissue was removed and the left anterior descending artery was visualized under a light microscope (model YAN-6A; Yuyan Instruments Co., Ltd., Shanghai, China) and ligated by a 6-0 silk suture (Yuyan Instruments), 1 mm below the tip of the left atrial appendage. The PC and MC groups underwent surgery without the left anterior descending artery ligation. After ligation, the left artery presented a pale appearance. Echocardiography was used to confirm the successful ligation, which would appear as ST segment and Q wave changes.

Melatonin treatment

For 7 days following the surgical procedures, melatonin (Sigma-Aldrich, St. Louis, USA) dissolved in dimethyl sulfoxide was administered to the MC and MM groups by daily intraperitoneal injection, at a dose of 10 mg/kg body weight. In the placebo groups, an equivalent volume of dimethyl sulfoxide (DMSO) was injected.

Hemodynamic measurement and determination of infarct size

A microtip catheter transducer (Millar Instruments, Houston, USA) was inserted into the right carotid artery and advanced into the left ventricle to measure the following parameters: the left ventricular end-diastolic diameter (LVEDd), left ventricular end-systolic diameter (LVESd), left ventricular ejection fraction (LVEF) and fractional shortening (FS). For the hemodynamic analysis, LV maximum first derivative of developed pressure (max dP/dt), and LV minimum first derivative of developed pressure (min dP/dt) were analyzed. Four weeks after the treatment, the animals were anesthetized again for hemodynamic measurement as described in another study.¹⁶

Infarct size was determined with Masson's trichrome staining as described in an earlier publication.¹⁷ After the animals were sacrificed, the LV myocardium was dissected,

fixed in 4% paraformaldehyde, embedded in paraffin, and then cut into 7- μ m sections. The sections were stained with Accustian Trichrome Stain (Masson) kit (Sigma-Aldrich). Infarct size was determined using the Microsoft Image Composite Editor v. 14.4 (Microsoft Corp., Redmond, USA).

Measurement of *Sirt6* in mRNA and protein levels

The primary rat cardiomyocytes were isolated and cultured from the animals in the 4 groups as described in a previous study.² When the cells were prepared, the expression of *Sirt6* in cardiomyocytes was measured using western blot and quantitative real-time polymerase chain reaction (qRT-PCR). The anti-*Sirt6* (Cell Signaling Technology, Danvers, USA) and tubulin (T5168; Sigma-Aldrich) were used. The following primers were used: *Sirt6*: forward 5'-TCTTCCAGTGTGGT-GTTCCA, reverse 5'-CCTCCATGGTCCAGACTCC; β -*actin*: forward 5'-CCAACCGCGAGAAGATGA, reverse 5'-CCAGAGGCGTACAGGGATAG.

Analysis of oxidative stress (ROS and SOD)

Intracellular reactive oxygen species (ROS) production in cardiomyocytes was evaluated with a fluorometric assay using 2',7'-dichlorofluorescein diacetate (DCFH-DA; Molecular Probes, Eugene, USA), according to the manufacturer's protocols. The cells were incubated with DCFH-DA for 1 h, after which the fluorescence intensity was measured at 488 nm and 525 nm emission wavelengths. Lysate and cardiomyocytes from fresh rat hearts were collected before total superoxide dismutase (SOD) activity was determined, using a commercial SOD Kit (Beyotime Biotech Inc., Jiangsu, China). The 50% inhibition activity of SOD (IC₅₀) values was determined under an optic density (OD) of 560 nm, using a Model 550 Microplate Reader (Bio-Rad Laboratories Inc., Hercules, USA).

Nitric oxide measurement

The level of nitric oxide (NO) in MI cardiac tissue was detected using a diagnostic assay kit (Nanjing Jiancheng Bioengineering Research Institute, Nanjing, China) as described in a previous study.¹⁸

Measurement of iNOS and eNOS with western blot

Total proteins were extracted from LV tissues. Protein concentrations were detected using a Pierce BCA Assay Kit (Thermo Fisher Scientific Inc., Waltham, USA). Then, samples containing 20 μ g protein were resolved with electrophoresis on 10% polyacrylamide gels and transferred to polyvinylidene fluoride (PVDF) membranes. Rabbit

anti-endothelial nitric oxide synthase (eNOS), anti-inducible nitric oxide synthase (iNOS), polyclonal antibodies, rabbit anti-P1177 eNOS, and rabbit anti-GAPDH monoclonal antibody (all from Abcam, Cambridge, USA) were used to detect the levels of iNOS, eNOS and phosphorylated eNOS (p-eNOS) in this assay.

Statistical analyses

Data were shown as median and interquartile range (IQR) due to a small sample size. Statistically significant differences among the groups were analyzed using the Kruskal–Wallis test. Pairwise multiple comparisons post hoc tests were carried out using Dunn's test with a Bonferroni correction. Two-tailed, unpaired Mann–Whitney tests were used to analyze the comparisons between 2 groups. The value of $p < 0.05$ was taken to indicate statistical significance.

Results

Melatonin decreased the myocardial infarct size in the rat MI model

As shown in Fig. 1A, in which the fibrotic scar appears blue and the viable myocardium is red, melatonin did not affect the cardiac structure in the MC group, while in the MM group, melatonin treatment decreased the myocardial infarct size ($U = 0$; $p < 0.0001$). The quantitative analysis confirmed this finding (Fig. 1B).

Melatonin improved hemodynamic parameters

Hemodynamic analyses were performed in all 4 groups. In the MM group, LVEDd, LVESd and min dP/dt decreased, while LVEF, LVFS and max dP/dt increased, but there was no significant difference after Dunn's Bonferroni adjustment (Table 1). No differences in these parameters were observed in the MC group, as shown in Fig. 2.

Melatonin increased *Sirt6* expression both in mRNA and protein levels

After treatment with melatonin, the expressions of *Sirt6* both in mRNA ($p < 0.0001$ after adjustment) and protein levels ($p < 0.0001$ after adjustment) were increased in the MM group compared to the PM group, as shown in Fig. 3 (Table 1).

Melatonin ameliorated MI-induced oxidative stress

Because of the fact that increased oxidative stress deteriorated cardiac remodeling, 2 oxidative stress-related

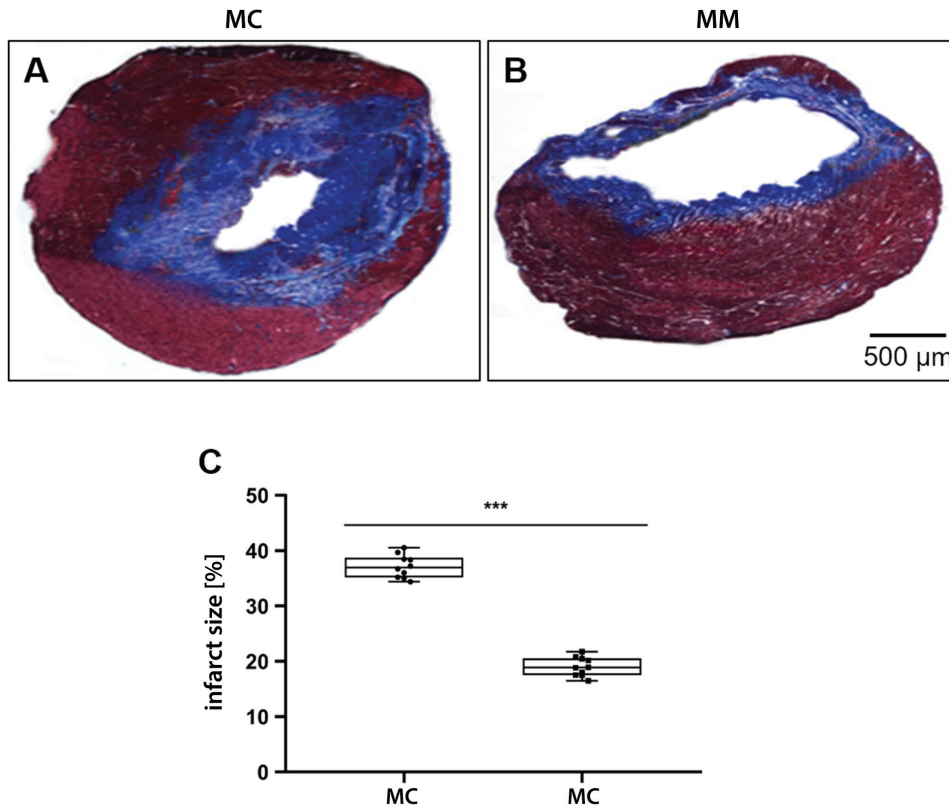


Fig. 1. Melatonin decreased myocardial infarct size in the MM. A,B. Masson's trichrome staining. The fibrotic scar is blue and the viable myocardium is red; C. The statistical analysis of infarct size

MC – the melatonin-treated sham-operated group; MM – the melatonin-treated MI group; *** $p < 0.001$.

Table 1. The comparisons between multiple groups after Kruskal–Wallis test and the comparisons between the melatonin-treated myocardial infarction group (MM) and the placebo-treated myocardial infarction group (PM) after Bonferroni adjustment

Outcomes	Kruskal–Wallis χ^2 test	df	p-value among groups	Comparisons	Bonferroni-adjusted p-value
LVEDd [%]	35.08	3	<0.0001	MM vs. PM	0.3339
LVEF [%]	32.95	3	<0.0001	MM vs. PM	0.3345
Max dP/dt [mm Hg/s]	32.93	3	<0.0001	MM vs. PM	0.3347
LVESd [%]	33.02	3	<0.0001	MM vs. PM	0.3345
LVFS [%]	34.23	3	<0.0001	MM vs. PM	0.3341
Min dP/dt [mm Hg/s]	32.98	3	<0.0001	MM vs. PM	0.3347
<i>Sirt6</i> mRNA expression	32.94	3	<0.0001	MM vs. PM	<0.0001
<i>Sirt6</i> protein expression	30.29	3	<0.0001	MM vs. PM	<0.0001
ROS (fold)	33.01	3	<0.0001	MM vs. PM	0.3343
SOD (fold)	33.01	3	<0.0001	MM vs. PM	0.3336
NO relative level	32.99	3	<0.0001	MM vs. PM	0.3346
eNOS protein/actin	32.97	3	<0.0001	MM vs. PM	<0.0001
p-eNOS protein/actin	33.17	3	<0.0001	MM vs. PM	0.3343
iNOS protein/actin	21.98	3	<0.0001	MM vs. PM	0.0008
p-iNOS protein/actin	24.24	3	<0.0001	MM vs. PM	0.0136

LVEDd – left ventricular end-diastolic diameter; LVEF – left ventricle ejection fraction; max dP/dt – maximum first derivative of developed pressure; LVESd – left ventricular end-systolic diameter; LVFS – left ventricular fractional shortening; Min dP/dt – minimum first derivative of developed pressure; ROS – reactive oxygen species; SOD – superoxide dismutase; NO – nitric oxide; eNOS – endothelial nitric oxide synthase; p-eNOS – phosphorylated eNOS; iNOS – inducible nitric oxide synthase; p-iNOS – phosphorylated iNOS; df – degrees of freedom.

molecules were detected. The results indicated that when treated with melatonin, the ROS level from primary cardiomyocytes was lowered in the MM group compared to the PM group, yet it was nonsignificant after Dunn's Bonferroni adjustment ($p = 0.3343$; Table 1). There was

no significant difference among the PC and MC groups, as shown in Fig. 4A. The SOD activity was enhanced in the MM group compared to the PM group, but it was nonsignificant after Dunn's Bonferroni adjustment ($p = 0.3336$; Table 1), as shown in Fig. 4B.

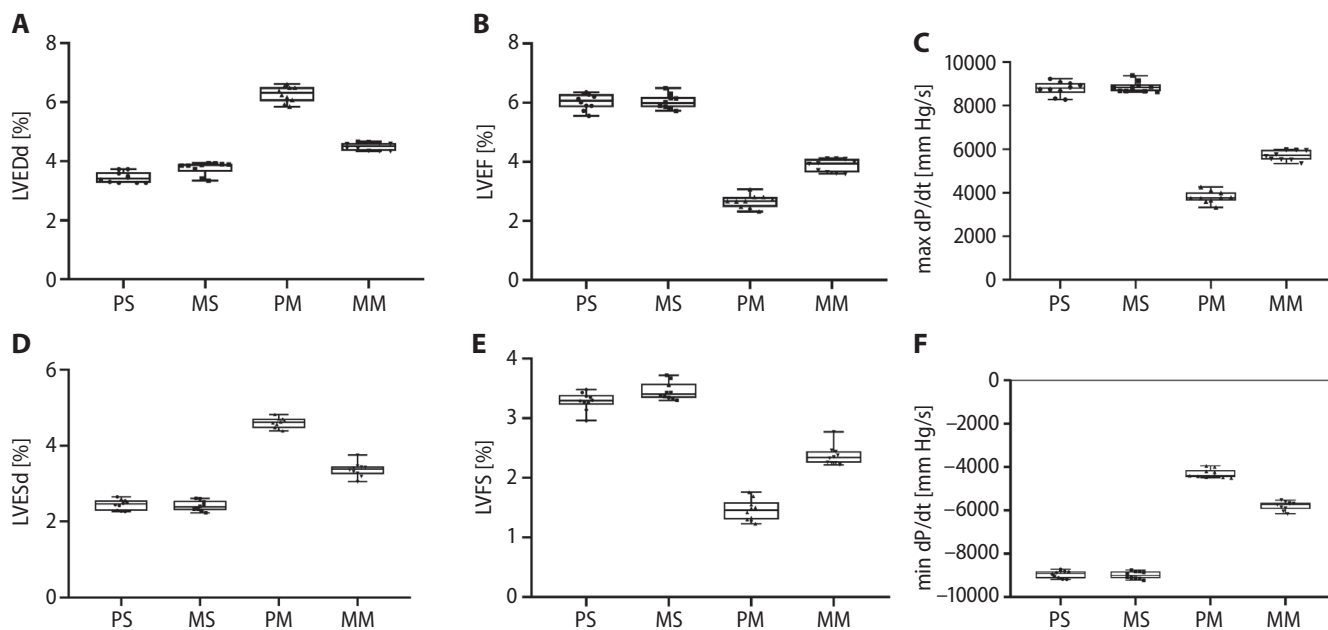


Fig. 2. Melatonin improved hemodynamic parameters. (A) LVEDd, (D) LVESd and (F) min dP/dt decreased significantly, while (B) LVEF, (E) LVFS and (C) max dP/dt increased significantly in myocardial infarction (MI) rats after treatment with melatonin. However, data became nonsignificant after adjustment

LVEDd – the left ventricular end-diastolic diameter; LVESd – left ventricular end-systolic diameter; LVEF – left ventricle ejection fraction; LVFS – left ventricular fractional shortening; PS – placebo-treated sham-operated group; MS – melatonin-treated sham-operated group; PM – placebo-treated myocardial infarction group; MM – melatonin-treated myocardial infarction group.

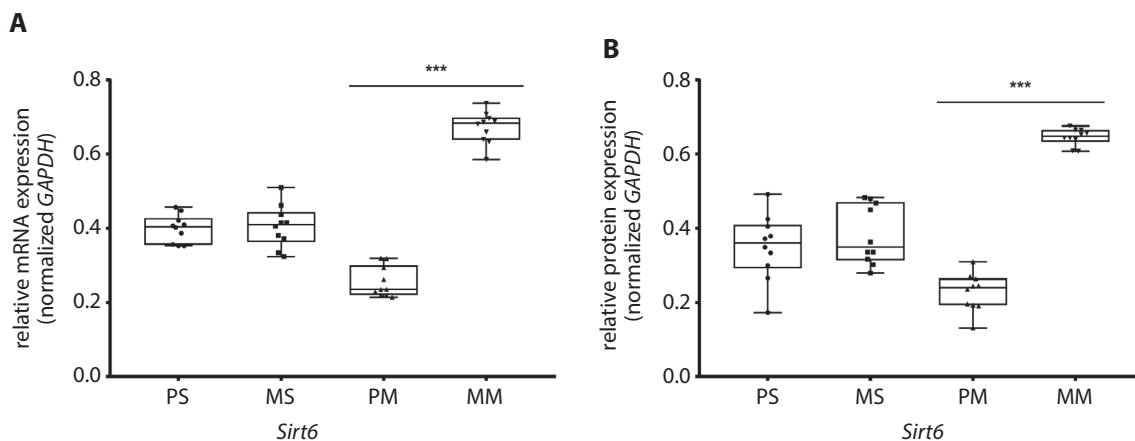


Fig. 3. Melatonin increased *Sirt6* expression both in mRNA and protein level. A. The mRNA level in cardiomyocytes in different groups; B. The protein level in cardiomyocytes in different groups

PS – placebo-treated sham-operated group; MS – melatonin-treated sham-operated group; PM – placebo-treated myocardial infarction group; MM – melatonin-treated myocardial infarction group. PM compared to MM: * $p < 0.05$; ** $p < 0.01$; *** $p < 0.001$.

Melatonin increased eNOS and NO production and inhibited iNOS production

In order to demonstrate whether the important role of melatonin as an antioxidant was involved in NO signaling, we performed assays to measure the production of NO-related molecules. The results showed that the levels of NO ($p = 0.3346$ after adjustment when compared to the PM group), eNOS ($p < 0.0001$ after adjustment) and p-eNOS ($p = 0.3343$ after adjustment when compared to the PM group) were increased in the MM group, but not

in the PC and MC group, as shown in Fig. 5. This indicated that melatonin might promote cardioprotection by activating the eNOS/NO signaling pathway. At the same time, we found that the levels of iNOS ($p = 0.0008$ after adjustment when compared to the PM group) and phosphorylated iNOS (p-iNOS) ($p = 0.0136$ after adjustment when compared to the PM group) were significantly decreased when treated with melatonin in the hearts of the MM rats but not in the PC and MC groups, as shown in Fig. 5C. This indicated that melatonin might promote cardioprotection by inhibiting iNOS (Table 1).

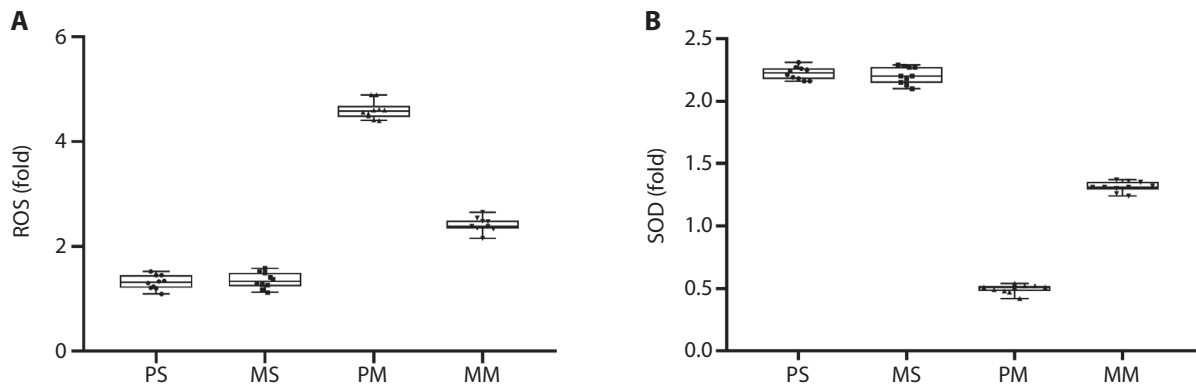


Fig. 4. Melatonin ameliorates myocardial infarction (MI)-induced oxidative stress. A. The determination of reactive oxygen species (ROS) in the 4 groups; B. The determination of superoxide dismutase (SOD) in the 4 groups. Data became non-significant after the adjustment

PS – placebo-treated sham-operated group; MS – melatonin-treated sham-operated group; PM – placebo-treated myocardial infarction (MI) group; MM – melatonin-treated MI group.

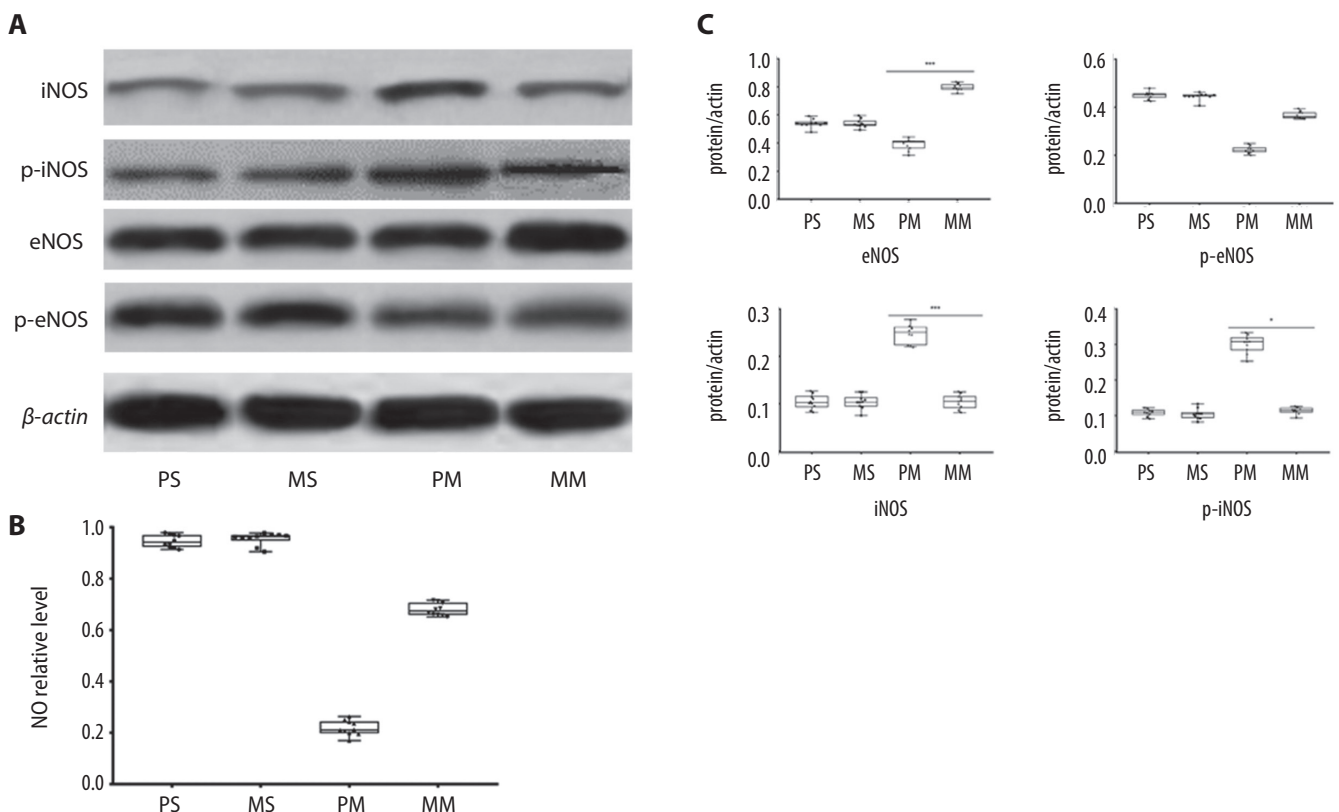


Fig. 5. Melatonin activated the endothelial nitric oxide synthase (eNOS)/nitric oxide (NO) signaling pathway and inhibited the inducible nitric oxide synthase (iNOS) signaling pathway. A. Western blot of iNOS/phosphorylated iNOS (p-iNOS)/eNOS/phosphorylated eNOS (p-eNOS) in the 4 groups; B. Relative NO levels compared in the 4 groups; C. The analysis of the proteins in the 4 groups

PS – placebo-treated sham-operated group; MS – melatonin-treated sham-operated group; PM – placebo-treated myocardial infarction (MI) group; MM – melatonin-treated MI group. PM compared to MM: * $p < 0.05$; ** $p < 0.01$; *** $p < 0.001$.

Discussion

Melatonin can counteract many pathological conditions, such as cardiovascular disorders, carcinogenesis, neurological diseases, and aging.¹⁹ Recently, its cardioprotective function has gained a great deal of attention.^{20–23} More and more evidence suggests that the cardioprotective

functions of melatonin are due to its direct free radical scavenger properties, antioxidant activities and anti-inflammatory effects. In this study, we confirmed the cardioprotective role of melatonin in an animal model of MI, and for the first time we found that melatonin improved cardiac remodeling through a *Sirt6*-dependent antioxidant pathway.

Pharmacological data have clearly demonstrated the powerful antioxidant properties of melatonin.^{24–26} For example, melatonin can protect the brain as a potent antioxidant, anti-inflammatory and antiapoptotic agent.²⁷ Melatonin has been shown to prevent granulosa cells from oxidative damage by targeting JNK-mediated autophagy, which may hold promise for patients with ovulation failure-related disorders.²⁸

In order to investigate the cardioprotective role of melatonin on MI, we established a MI rat model by ligating the left anterior descending coronary artery and verifying ST elevation using electrocardiography (ECG). Four weeks after the treatment with melatonin, infarct size and hemodynamic parameters were measured. Infarct size was reduced significantly after the treatment with melatonin, which indicated that melatonin could protect the infarcted myocardium. Similarly, the results of hemodynamic studies indicated that post-MI cardiac remodeling had improved significantly following the treatment with melatonin.

Accumulated evidence indicates that oxidative stress is responsible for the progression of cardiac remodeling.^{29,30} In order to investigate whether the cardioprotective effect of melatonin functions through its antioxidant role, ROS and SOD levels were measured as the indicators of oxidative stress. Excessive ROS accumulation leads to cellular oxidative stress and elicits an increased pro-inflammatory response, which is associated with cardiac remodeling.^{7,31} Not surprisingly, after the treatment with melatonin, we found that ROS activity reduced significantly and SOD level increased significantly in the MM group. The evidence suggested that melatonin could prevent cardiac remodeling by decreasing oxidative stress.

The NO is a widely known ventricular dilator produced from L-arginine by a family of NOS, including eNOS and iNOS.³² It has been shown that NO plays a role in reducing oxidative stress³³ and in blocking the progression of MI.³⁴ In our study, the expressions of NO, iNOS, eNOS, and their corresponding phosphorylations were determined. The results indicated that the expressions of NO and eNOS were upregulated and the expression of iNOS was lowered in the MM group compared to the PM group. This evidence suggests that melatonin might suppress the processes of oxidative stress by activating the eNOS/NO signaling pathway and inhibiting iNOS signaling pathway.

Interestingly, we found that the expressions of *Sirt6*, both in mRNA and protein levels, were significantly increased in the MM group compared to the PM group. This indicates that *Sirt6* might be the target through which melatonin improves oxidative stress by activating the eNOS/NO signaling pathway in the heart.

In spite of the fact that a dose of 10 mg/kg of melatonin administered via intraperitoneal injection works cardioprotectively in the MM group, there is still no evidence to demonstrate whether this dose works for humans. Actually, it was reported that a total dose of 50 mg has been used during a major vascular surgery.³⁵ Regrettably, those researchers concluded that intracoronary and intravenous

administration of melatonin did not improve the myocardial salvage index in patients with ST-elevation myocardial infarction (STEMI) undergoing primary percutaneous coronary intervention. Hopefully, if the dose of melatonin was increased to 10 mg/kg, it would demonstrate some beneficial effects for the heart, considering its obvious *Sirt6*-dependent antioxidative ability in I/R. However, this speculation still needs to be verified.










Limitations

Firstly, this study proved the effect of melatonin on mouse MI model, but there is still no evidence to demonstrate whether this works for humans. Secondly, the study had no designed not designed dose gradient, so the optimal dose of melatonin for MI could not be obtained. Thirdly, we only analyzed the changes of *Sirt6* expression and did not verify whether the knockout of *Sirt6* would eliminate the cardioprotective effect of melatonin.

Conclusions

The current study demonstrated for the first time that intraperitoneal injection of melatonin could improve the cardiac function via a *Sirt6*-dependent antioxidant pathway in MI rats.

ORCID iDs

Yingcui Wang  <https://orcid.org/0000-0002-1054-5499>
 Suhua Zhang  <https://orcid.org/0000-0002-7982-5587>
 Yingying Ma  <https://orcid.org/0000-0002-6754-5457>
 Aixia Xiang  <https://orcid.org/0000-0001-7790-9982>
 Hui Sun  <https://orcid.org/0000-0003-3941-860X>
 Jun Song  <https://orcid.org/0000-0003-1456-2234>
 Wenjing Yang  <https://orcid.org/0000-0002-6981-5019>
 Xuanlong Li  <https://orcid.org/0000-0001-5763-6702>
 Hongxiao Xu  <https://orcid.org/0000-0002-1119-3050>

References

1. Reed GW, Rossi JE, Cannon CP. Acute myocardial infarction. *Lancet*. 2017;389(10065):197–210. doi:10.1016/S0140-6736(16)30677-8
2. Li F, Zong J, Zhang H, et al. Orientin reduces myocardial infarction size via eNOS/NO signaling and thus mitigates adverse cardiac remodeling. *Front Pharmacol*. 2017;8:926. doi:10.3389/fphar.2017.00926
3. Wang Y, Wang Q, Yu W, Du H. Crocin attenuates oxidative stress and myocardial infarction injury in rats. *Int Heart J*. 2018;59(2):387–393. doi:10.1536/ihj.17-114
4. Sinning C, Westermann D, Clemmensen P. Oxidative stress in ischemia and reperfusion: Current concepts, novel ideas and future perspectives. *Biomark Med*. 2017;11(11):11031–11040. doi:10.2217/bmm-2017-0110
5. Jain AK, Mehra NK, Swarnakar NK. Role of antioxidants for the treatment of cardiovascular diseases: Challenges and opportunities. *Curr Pharm Des*. 2015;21(30):4441–4455. doi:10.2174/1381612821666150803151758
6. Yang J, Sun W, Sun J, et al. Guanxintai exerts protective effects on ischemic cardiomyocytes by mitigating oxidative stress. *Evid Based Complement Alternat Med*. 2017;2017:4534387. doi:10.1155/2017/4534387
7. Zhou T, Prather ER, Garrison DE, Zuo L. Interplay between ROS and antioxidants during ischemia-reperfusion injuries in cardiac and skeletal muscle. *Int J Mol Sci*. 2018;19(2):417. doi:10.3390/ijms19020417

8. Pan H, Guan D, Liu X, et al. SIRT6 safeguards human mesenchymal stem cells from oxidative stress by coactivating NRF2. *Cell Res*. 2016; 26(2):190–205. doi:10.1038/cr.2016.4
9. Wang XX, Wang XL, Tong MM, et al. SIRT6 protects cardiomyocytes against ischemia/reperfusion injury by augmenting FoxO3a-dependent antioxidant defense mechanisms. *Basic Res Cardiol*. 2016; 111(2):13. doi:10.1007/s00395-016-0531-z
10. Yang HL, Zhou WJ, Gu CJ, et al. Pleiotropic roles of melatonin in endometriosis, recurrent spontaneous abortion, and polycystic ovary syndrome. *Am J Reprod Immunol*. 2018;80(1):e12839. doi:10.1111/aji.12839
11. Taniguti EH, Ferreira YS, Stupp IJV, et al. Neuroprotective effect of melatonin against lipopolysaccharide-induced depressive-like behavior in mice. *Physiol Behav*. 2018;188:270–275. doi:10.1016/j.physbeh.2018.02.034
12. Zhou H, Ma Q, Zhu P, Ren J, Reiter RJ, Chen Y. Protective role of melatonin in cardiac ischemia-reperfusion injury: From pathogenesis to targeted therapy. *J Pineal Res*. 2018;64(3). doi:10.1111/jpi.12471
13. Tengattini S, Reiter RJ, Tan DX, Terron MP, Rodella LF, Rezzani R. Cardiovascular diseases: Protective effects of melatonin. *J Pineal Res*. 2008;44(1):16–25. doi:10.1111/j.1600-079X.2007.00518.x
14. Hu J, Zhang L, Yang Y, et al. Melatonin alleviates post-infarction cardiac remodeling and dysfunction by inhibiting Mst1. *J Pineal Res*. 2017;62(1). doi:10.1111/jpi.12368
15. Zhou H, Li D, Zhu P, et al. Melatonin suppresses platelet activation and function against cardiac ischemia/reperfusion injury via PPARgamma/FUNDC1/mitophagy pathways. *J Pineal Res*. 2017;63(4). doi:10.1111/jpi.12438
16. Faria TO, Simoes MR, Vassallo DV, et al. Xanthine oxidase activation modulates the endothelial (vascular) dysfunction related to HgCl2 exposure plus myocardial infarction in rats. *Cardiovasc Toxicol*. 2018; 18(2):161–174. doi:10.1007/s12012-017-9427-x
17. Gao L, Kupfer ME, Jung JP, et al. Myocardial tissue engineering with cells derived from human-induced pluripotent stem cells and a native-like, high-resolution, 3-dimensionally printed scaffold. *Circ Res*. 2017;120(8):1318–1325. doi:10.1161/CIRCRESAHA.116.310277
18. Cao J, Xie H, Sun Y, et al. Sevoflurane post-conditioning reduces rat myocardial ischemia reperfusion injury through an increase in NOS and a decrease in phosphorylated NHE1 levels. *Int J Mol Sci*. 2015; 36(6):1529–1537. doi:10.3892/ijmm.2015.2366
19. Favero G, Franceschetti L, Buffoli B, et al. Melatonin: Protection against age-related cardiac pathology. *Ageing Res Rev*. 2017;35:336–349. doi:10.1016/j.arr.2016.11.007
20. Reiter RJ, Mayo JC, Tan DX, Sainz RM, Alatorre-Jimenez M, Qin L. Melatonin as an antioxidant: Under promises but over delivers. *J Pineal Res*. 2016;61(3):253–278. doi:10.1111/jpi.12360
21. Reiter RJ, Tan DX, Paredes SD, Fuentes-Broto L. Beneficial effects of melatonin in cardiovascular disease. *Ann Med*. 2010;42(4):276–285. doi:10.3109/07853890903485748
22. Ekeloef S, Halladin N, Fonnes S, et al. Effect of intracoronary and intravenous melatonin on myocardial salvage index in patients with ST-elevation myocardial infarction: A randomized placebo controlled trial. *J Cardiovasc Transl Res*. 2017;10(5–6):470–479. doi:10.1007/s12265-017-9768-7
23. Dominguez-Rodriguez A, Abreu-Gonzalez P, Reiter RJ. Melatonin as an agent for cardioprotection in patients with ST-elevation myocardial infarction and short ischaemic time. *Cardiovasc Drugs Ther*. 2017;31(2):227–228. doi:10.1007/s10557-016-6708-8
24. Lin X, Zhao T, Lin CH, et al. Melatonin provides protection against heat stroke-induced myocardial injury in male rats. *J Pharm Pharmacol*. 2018;70(6):760–767. doi:10.1111/jphp.12895
25. Debnath B, Hussain M, Irshad M, et al. Exogenous melatonin mitigates acid rain stress to tomato plants through modulation of leaf ultrastructure, photosynthesis and antioxidant potential. *Molecules*. 2018;23(2):388. doi:10.3390/molecules23020388
26. Kratz EM, Piwowar A. Melatonin, advanced oxidation protein products and total antioxidant capacity as seminal parameters of prooxidant-antioxidant balance and their connection with expression of metalloproteinases in context of male fertility. *J Physiol Pharmacol*. 2017;68(5):659–668. PMID:29375040.
27. Aridas JDS, Yawno T, Sutherland AE, et al. Systemic and transdermal melatonin administration prevents neuropathology in response to perinatal asphyxia in newborn lambs. *J Pineal Res*. 2018;64(4): e12479. doi:10.1111/jpi.12479
28. Cao Y, Shen M, Jiang Y, Sun SC, Liu H. Melatonin reduces oxidative damage in mouse granulosa cells via restraining JNK-dependent autophagy. *Reproduction*. 2018;155(3):307–319. doi:10.1530/REP-18-0002
29. Ayoub KF, Pothineni NVK, Rutland J, Ding Z, Mehta JL. Immunity, inflammation, and oxidative stress in heart failure: Emerging molecular targets. *Cardiovasc Drugs Ther*. 2017;31(5–6):593–608. doi:10.1007/s10557-017-6752-z
30. Wu QQ, Xiao Y, Yuan Y, et al. Mechanisms contributing to cardiac remodelling. *Clin Sci (Lond)*. 2017;131(18):2319–2345. doi:10.1042/CS20171167
31. Dlodla PV, Joubert E, Muller CJF, Louw J, Johnson R. Hyperglycemia-induced oxidative stress and heart disease-cardioprotective effects of rooibos flavonoids and phenylpyruvic acid-2-O-beta-D-glucoside. *Nutr Metab (Lond)*. 2017;14:45. doi:10.1186/s12986-017-0200-8
32. Jin S, Teng X, Xiao L, et al. Hydrogen sulfide ameliorated L-NAME-induced hypertensive heart disease by the Akt/eNOS/NO pathway. *Exp Biol Med (Maywood)*. 2017;242(18):1831–1841. doi:10.1177/1535370217732325
33. Zhang YH, Casadei B. Sub-cellular targeting of constitutive NOS in health and disease. *J Mol Cell Cardiol*. 2012;52(2):341–350. doi:10.1016/j.yjmcc.2011.09.006
34. Hu J, Zhang YX, Wang L, et al. Protective effects of Xinji'er kang on myocardial infarction induced cardiac injury in mice. *BMC Complement Altern Med*. 2017;17(1):338. doi:10.1186/s12906-017-1846-5
35. Ekeloef S, Halladin N, Fonnes S, et al. Effect of intracoronary and intravenous melatonin on myocardial salvage index in patients with ST-elevation myocardial infarction: A randomized placebo controlled trial. *J Cardiovasc Transl Res*. 2017;10(5–6):470–479. doi:10.1007/s12265-017-9768-7

Effects of ketamine, thiopental and their combination on the rat liver: A biochemical evaluation

Zehra Bedir^{1,A,D}, Kezban Tuna Ozkaloglu Erdem^{2,A,B}, Irem Ates^{3,B}, Tulay Ceren Olmezturk Karakurt^{4,B,C}, Cebrail Gursul^{5,C}, Didem Onk^{6,D}, Nezahat Kurt^{7,C}, Zeynep Suleyman^{8,9,D-F}, Halis Suleyman^{8,D-F}

¹ Department of Anesthesiology and Reanimation, Regional Training Research Hospital, University of Health Sciences, Erzurum, Turkey

² Anesthesiology and Reanimation Clinic, Antalya Training and Research Hospital, Turkey

³ Department of Anesthesiology and Reanimation, Faculty of Medicine, Ataturk University, Erzurum, Turkey

⁴ Department of Anesthesiology and Reanimation, Mengucek Gazi Training and Research Hospital, Erzincan Binali Yildirim University, Turkey

⁵ Department of Physiology, Faculty of Medicine, Erzincan Binali Yildirim University, Turkey

⁶ Department of Anesthesiology and Reanimation, Faculty of Medicine, Erzincan Binali Yildirim University, Turkey

⁷ Department of Biochemistry, Faculty of Medicine, Erzincan Binali Yildirim University, Turkey

⁸ Department of Pharmacology, Faculty of Medicine, Erzincan Binali Yildirim University, Turkey

⁹ Department of Nursing, Faculty of Health Sciences, Erzincan Binali Yildirim University, Turkey

A – research concept and design; B – collection and/or assembly of data; C – data analysis and interpretation;

D – writing the article; E – critical revision of the article; F – final approval of the article

Advances in Clinical and Experimental Medicine, ISSN 1899–5276 (print), ISSN 2451–2680 (online)

Adv Clin Exp Med. 2022;31(3):285–292

Address for correspondence

Halis Suleyman

E-mail: halis.suleyman@gmail.com

Funding sources

None declared

Conflict of interest

None declared

Received on August 26, 2021

Reviewed on October 18, 2021

Accepted on November 3, 2021

Published online on December 17, 2021

Cite as

Bedir Z, Ozkaloglu Erdem KT, Ates I, et al. Effects of ketamine, thiopental, and their combination on the rat liver:

A biochemical evaluation. *Adv Clin Exp Med.* 2022;31(3):285–292. doi:10.17219/acem/143573

DOI

10.17219/acem/143573

Copyright

© 2022 by Wroclaw Medical University

This is an article distributed under the terms of the Creative Commons Attribution 3.0 Unported (CC BY 3.0) (<https://creativecommons.org/licenses/by/3.0/>)

Abstract

Background. In the literature, it has been suggested that ketamine-related oxidative organ damage results from increased blood adrenaline level, and thiopental-related oxidative damage is caused by decreased adrenaline level, suggesting that ketamine-thiopental combination (KT) may be beneficial in reducing the hepatotoxic effect of ketamine.

Objectives. To biochemically investigate the effects of ketamine, thiopental and KT on the liver in rats.

Materials and methods. Male albino Wistar type rats received intraperitoneally (ip.) 30 mg/kg ketamine in the ketamine alone (KG) group (n = 6), 15 mg/kg thiopental in the thiopental alone (TG) group (n = 6), and 30 mg/kg ketamine + 15 mg/kg thiopental in the ketamine+thiopental (KTG) group (n = 6). The same volume of distilled water as solvent was given to the healthy (HG) animal group. This procedure was repeated once daily for 30 days. At the end of this period, the animals were killed by decapitation and their livers were removed. In liver tissue, malondialdehyde (MDA), total glutathione (tGSH), total oxidant status (TOS), total antioxidant status (TAS), tumor necrosis factor alpha (TNF- α), interleukin 1 beta (IL-1 β), and interleukin-6 (IL-6) levels were measured. The IL-1 β , IL-6, TNF- α , adrenalin (ADR), noradrenalin (NDR), alanine aminotransferase (ALT), and aspartate aminotransferase (AST) levels were determined in blood samples taken from the tail veins.

Results. In the group treated with ketamine and thiopental alone, MDA, TOS, IL-1 β , IL-6, TNF- α , ADR, NDR, ALT, and AST levels were found to be high, and those of tGSH and TAS to be low. However, there was no significant change in the levels of these parameters in the KTG.

Conclusions. These results indicate that oxidative stress and inflammation developed in the liver tissue of the group that used ketamine and thiopental alone, suggesting that the KT form may be safer in terms of toxicity in the clinical usage.

Key words: hepatotoxicity, ketamine, thiopental, rat

Background

Ketamine is a dissociative anesthetic agent that has strong analgesic and mild hypnotic properties, and causes a rapid effect.¹ The efficacy of various routes of administration such as intravenous, intramuscular, oral, intranasal, rectal, and transdermal has been proven.² The high-dose intravenous form of ketamine is used clinically in short-term surgical procedures, and the low dose is used to create an analgesic effect.^{3,4} It has been shown that ketamine at sub-anesthetic doses has rapid, strong antidepressant effects in patients with resistant depression.⁵ Although there is not enough information on the long-term use of ketamine, its use in the treatment of chronic diseases is increasing.⁶ In fact, it is known that ketamine infusions are used in the treatment of chronic pain.⁷ In the literature, it has been reported that hepatotoxicity seen in patients treated with ketamine infusion causes the termination of ketamine treatment.⁶ Additionally, repeated doses of ketamine over a long or short period increase the risk of developing liver damage.⁸ Hepatotoxicity has been reported in the majority of people using ketamine for a recreational purpose.⁹ The mechanism of liver damage caused by ketamine has not yet been fully elucidated. However, it has been suggested that one of the ketamine damage mechanisms is the blockade of N-methyl-D-aspartate (NMDA) receptors.¹⁰ However, the formation of reactive oxygen species (ROS) and increased lipid peroxidation (LPO) have been implicated in the pathogenesis of ketamine hepatotoxicity.⁹ Previous studies have also reported that pro-inflammatory cytokines such as ROS, interleukin 1 beta (IL-1 β), interleukin-6 (IL-6), and tumor necrosis factor alpha (TNF- α) play a role in the pathogenesis of ketamine-related cell damage.¹¹ In the study by Aksoy et al., it has been reported that ketamine increased the production of catecholamines such as endogenous adrenaline (ADR), noradrenaline (NDR) and dopamine in animals.¹² Another study established that oxidative damage has developed in the brain, heart and bronchial tissues of ketamine group rats with high blood adrenaline levels.¹³

Thiopental is a barbiturate-derivative anesthetic drug.¹⁴ In a study in rats, oxidative damage occurred in the brain, heart and bronchial tissues of the thiopental group, whose blood adrenaline level was low.¹³ It has been reported that thiopental, unlike ketamine, suppresses TNF- α production through inhibition of nuclear factor kappa-B (NF- κ B).¹⁵ This information indicates that keeping blood catecholamine levels within physiological limits may be beneficial in reducing oxidative stress. It also suggests that ketamine+thiopental combination (KT) will not have a toxic effect on the liver.

Objectives

The aim of the study was to biochemically investigate the effect of ketamine, thiopental and KT on rat livers.

Materials and methods

Animals

In total, 24 male albino Wistar rats weighing 255–268 g were used in the experiment. The animals were housed and fed under appropriate conditions in a suitable laboratory environment at normal room temperature (22°C). The study was approved by the Local Animal Experimentation Ethics Committee (date: 21.05.2021, meeting No. E-77040475-641.04-2100132117).

Chemicals

Ketamine used in the experiment was obtained from Pfizer Ltd. Sti. (Istanbul, Turkey), and thiopental sodium from I.E Ulagay (Istanbul, Turkey).

Animal groups

The animals used in the experiment were divided into 4 groups: ketamine alone group (KG), thiopental alone group (TG), ketamine+thiopental group (KTG), and healthy control (HG) group.

Experimental procedure

In this study, 30 mg/kg ketamine was administered intraperitoneally (ip.) to the KG (n = 6), 10 mg/kg thiopental to the TG (n = 6) and 30 mg/kg ketamine + 15 mg/kg thiopental to the KTG (n = 6). The same volume of distilled water as solvent was given to the HG. This procedure was repeated once daily for 30 days. On the 31st day, blood samples were taken from the tail veins of the animals, and immediately afterwards all of the rats were euthanized using an overdose of a general anesthetic (thiopental sodium, 50 mg/kg), their livers were removed. The IL-1 β , IL-6, TNF- α , adrenaline (ADR), noradrenaline (NDR), alanine aminotransferase (ALT), and aspartate aminotransferase (AST) levels were measured in the samples. Malondialdehyde (MDA), total glutathione (tGSH), total oxidant status (TOS), total antioxidant status (TAS), tumor necrosis factor alpha (TNF- α), IL-1 β , and IL-6 levels were measured in a part of the liver tissue.

Biochemical analysis

Protein analysis in tissue

Protein measurement in tissue was performed according to the Bradford method.¹⁶ The principle of this method is based on measuring the absorbance at 595 nm of the colored complex, formed as a result of the interaction of the Coomassie Brilliant Blue G-250 dye (C.I. 42655, Sigma-Aldrich, St. Louis, USA) with the acidic and basic

groups of the proteins. All measurements made in tissue were standardized by dividing to protein.

MDA and tGSH analyses in tissues

The MDA measurements were based on the method used by Ohkawa et al., which includes the spectrophotometric measurement of the absorbance of the pink-colored complex formed by thiobarbituric acid (TBA) and malondialdehyde (MDA; $\mu\text{mol/g}$ protein).¹⁷ Total glutathione (tGSH; nmol/g protein) measurement was made according to the method described by Sedlak and Lindsay.¹⁸

Measurements of TOS and TAS

The total oxidant status (TOS; $\mu\text{mol H}_2\text{O}_2$ equivalent/mg protein) and total antioxidant status (TAS; mmol Trolox equivalent/mg protein) levels of tissue homogenates were determined using a novel automated measurement method and commercially available kits (Rel Assay Diagnostics, Gaziantep, Turkey), both developed by Erel.^{19,20}

TNF- α , IL-1 β and IL-6 analyses in serum and tissues

Samples kept at -80°C on the working day were removed from the deep freezer and thawed at 4°C . Then, 0.1 g of each tissue was taken and 2 mL of phosphate buffer was added, and homogenate was obtained with the help of homogenizer. Next, the samples were centrifuged 20 min at $10,000 \times g$ and the supernatants were carefully collected. The levels of TNF- α (ng/mg protein), IL-1 β (ng/mg protein) and IL-6 (ng/mg protein) were measured using an enzyme-linked immunosorbent assay (ELISA) kit supplied by Eastbiopharm Co. Ltd. (Hangzhou, China).

Analysis of serum ALT and AST

Venous blood samples were collected into tubes without an anticoagulant. After clotting, the serum was separated with centrifugation and stored at -80°C until assay. Using a Cobas 8000 autoanalyzer (Roche Diagnostics GmbH, Mannheim, Germany) with commercially available kits (Roche Diagnostics), serum AST [U/L] and ALT [U/L] activities were measured spectrophotometrically for the liver function tests.

Measurement of ADR and NDR levels

Blood samples were collected from the hearts of rats in 2 mL of ethylenediamine tetraacetic acid (EDTA) vacuum tubes to determine the adrenaline and noradrenaline levels. Within 15 min of venesection, the EDTA samples for the adrenaline and noradrenaline measurements were placed on ice and centrifuged at $3500 \times g$ for 5 min. After centrifugation, the plasma adrenaline and noradrenaline concentrations were measured with an isocratic system

using a high-performance liquid chromatography (HPLC) pump (Hewlett Packard Agilent 1100; Hewlett Packard Enterprise, Spring, USA; flow rate: 1 mL/min; injection volume: 40 μL ; analytical run time: 20 min) and an electrochemical detector. We used a reagent kit for HPLC analysis of the catecholamines in the plasma serum (Chromsystems, Munich, Germany).

Statistical analyses

For statistical analyses, IBM SPSS v. 22 (IBM Corp., Armonk, USA) was used. Biochemical findings were presented with boxplot and p-values for all comparisons were reported in the Table 1. Normality assumption of biochemical variables was checked using Shapiro–Wilk test, and homogeneity of variances assumption was evaluated with Levene's test. The differences between groups were obtained using one-way analysis of variance (ANOVA) for normally distributed variables. The Tukey's honestly significant difference (HSD) test or Games–Howell test was used as post hoc test, according to homogeneity of variances assumption being met or not. Kruskal–Wallis test was used to determine the differences for TAS, OSI, TNF- α , and IL-1 β . Post hoc Dunn's test was applied after Kruskal–Wallis test. The value of $p < 0.05$ was considered statistically significant.

Results

Biochemical findings

Tissue MDA and tGSH analysis

As shown in Fig. 1, the amount of MDA in the liver tissue of animals treated with ketamine and thiopental alone was higher than in the HG and KTG ($p < 0.001$). The amount of MDA in the liver tissue of the KTG animals was close to that in the HG ($p > 0.05$). In addition, ketamine and thiopental caused a decrease in tGSH in the liver tissue of the animals. While the amount of tGSH in the KG and TG was lower than the healthy and KTG ($p < 0.001$), the amount of tGSH in the HG and KTG was almost the same ($p > 0.05$). All p-values for post hoc comparisons are reported in Table 1.

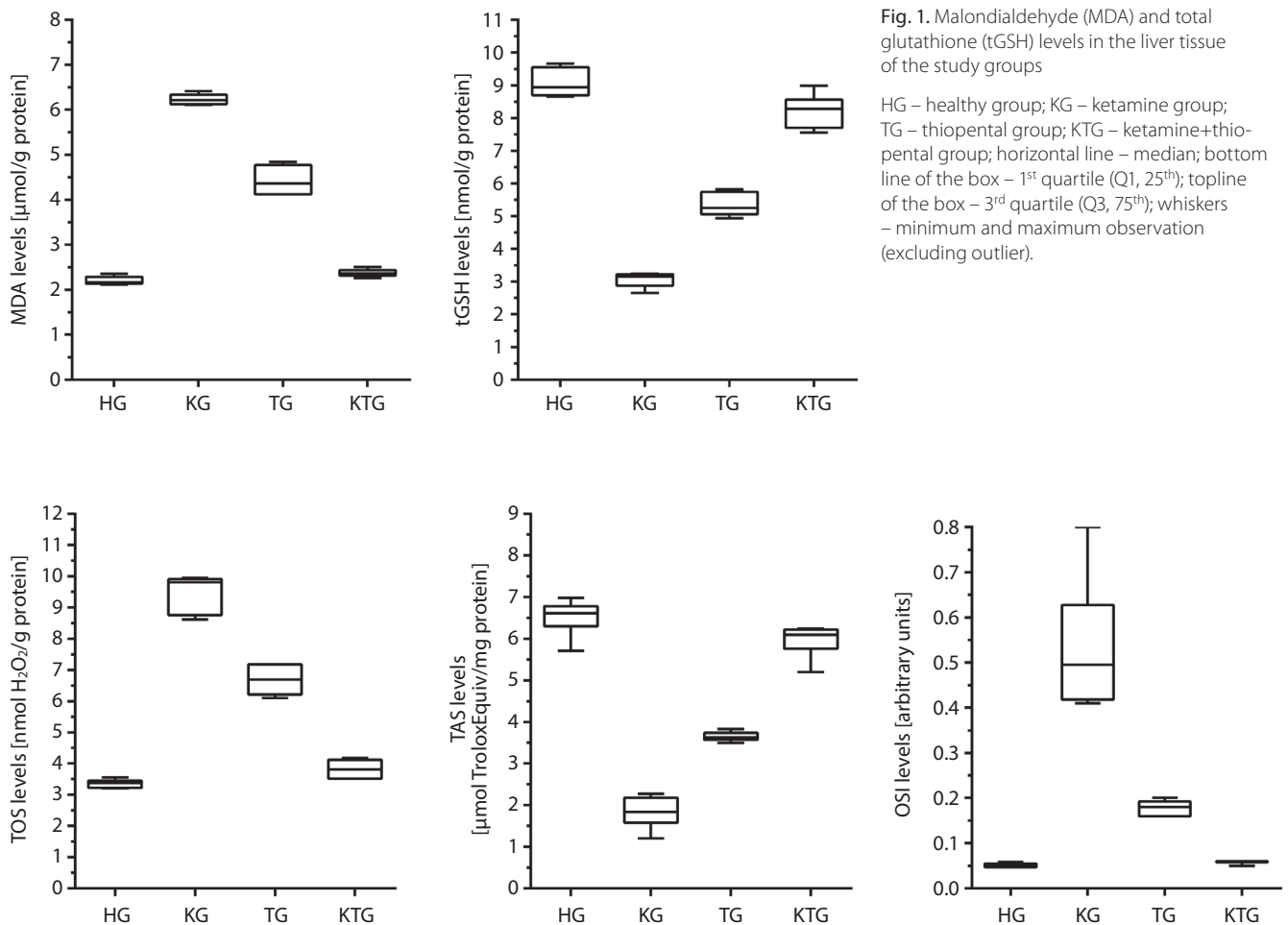
Tissue TOS, TAS and OSI analysis

As presented in Fig. 2, while TOS level was higher in liver tissue of animals from the KTG compared to HG and KTG ($p < 0.001$), TAS level was lower ($p < 0.001$). Statistical analysis showed that the difference between TOS and TAS levels in the liver tissue of the HG and KTG was insignificant ($p > 0.05$). In addition, the Oxidative Stress Index (OSI) value in the KG and TG was higher than that of the HG and KTG ($p < 0.001$). The OSI values between the HG and KTG were close to each other and

Table 1. Analysis of variance (ANOVA) test results and post hoc p-values for group comparisons

Biochemical parameters	ANOVA or KW results		Post hoc test p-values					
	(3;20) or -W	p-value	HG vs KG	HG vs TG	HG vs KTG	KG vs TG	KG vs KTG	TG vs KTG
MDA*	89.1	0.0001	0.0001	0.0001	0.0296	0.0001	0.0001	0.0001
tGSH**	62.2	0.0001	0.0001	0.0001	0.0639	0.0001	0.0001	0.0001
TOS*	97.4	0.0001	0.0001	0.0001	0.0516	0.0001	0.0001	0.0001
TAS ⁺	0.576	0.0001	0.0001	0.0059	0.2880	0.1416	0.0019	0.0936
OSI ⁺	1.360	0.0001	0.0001	0.0039	0.1890	0.1401	0.0021	0.0190
TNF- α ⁺	9.980	0.0001	0.0001	0.0099	0.4620	0.1420	0.0009	0.0459
IL-1 β ⁺	9.867	0.0001	0.0001	0.0110	0.5141	0.1422	0.0011	0.0403
IL-6 ⁺	0.400	0.0001	0.0001	0.0072	0.3270	0.1421	0.0099	0.0461
ALT**	43.6	0.0001	0.0001	0.0001	0.2104	0.1643	0.0001	0.0001
AST**	87.4	0.0001	0.0001	0.0001	0.2165	0.0040	0.0001	0.0001
ADR**	7379.6	0.0001	0.0001	0.0001	0.0001	0.0001	0.0001	0.0001
NDR**	7893.9	0.0001	0.0001	0.0001	0.0001	0.0001	0.0001	0.0001

MDA – malondialdehyde; tGSH – total glutathione; TOS – total oxidant status; TAS – total antioxidant status; TNF- α – tumor necrosis factor alpha; IL-1 β – interleukin 1 beta; ALT – alanine aminotransferase; AST – aspartate aminotransferase; ADR – adrenaline; NDR – noradrenaline; KW – Kruskal–Wallis test; OSI – oxidative stress index; HG – healthy group; KG – ketamine group; TG – thiopental group; KTG – ketamine+thiopental group. *Games–Howell test was performed as the post hoc test after ANOVA (F(3;20)); **Tukey HSD test was performed as the post hoc test after ANOVA (F(3;20)); ⁺ Kruskal–Wallis test was used and Dunn’s test was performed as post hoc test.



were statistically insignificant ($p > 0.05$). All p -values for post hoc comparisons are reported in Table 1.

Serum and tissue TNF- α , IL-1 β and IL-6 analysis

As presented in Fig. 3, TNF- α , IL-1 β and IL-6 levels in the liver tissue of the KG and TG were higher than those of the HG and KTG ($p < 0.001$). There was no significant difference between TNF- α , IL-1 β and IL-6 levels in the HG and KTG ($p > 0.05$). In addition, TNF- α , IL-1 β and IL-6 levels in the blood serum of the KG and TG were higher than in the HG and KTG ($p < 0.001$). The TNF- α , IL-1 β and IL-6 levels in the KTG were found to be similar to those obtained in the HG ($p > 0.05$) (Fig. 5). All p -values for post hoc comparisons are reported in Table 1.

Serum ALT and AST analysis

Serum ALT and AST activities in the KG and TG were higher than those of the HG and KTG ($p < 0.001$). However, the difference between ALT and AST activities in the HG and KTG was found to be insignificant ($p > 0.05$; Fig. 4). All p -values for post hoc comparisons are reported in Table 1.

Blood serum ADR and NDR analysis

As can be seen in Table 2, ADR and NDR levels in the KG were significantly higher compared to the HG and KTG ($p < 0.001$), while they were decreased in TG ($p < 0.001$). In addition, ADR and NDR levels in the KTG were closely related to the HG ($p > 0.05$).

Discussion

In this study, oxidant, antioxidant and pro-inflammatory parameters and ADR and NDR levels were investigated in rats treated with ketamine, thiopental and KT. From our biochemical test results, it can be concluded that oxidative and inflammatory damage in the liver tissue of rats treated with repeated subanesthetic doses of ketamine alone. In addition, the systemic oxidative stress and inflammation was observed. In the literature supporting our biochemical findings, the role of oxidant and pro-inflammatory cytokines such as ROS, IL-1 β , IL-6, and TNF- α in the pathogenesis of ketamine-related cell damage has been shown.¹¹

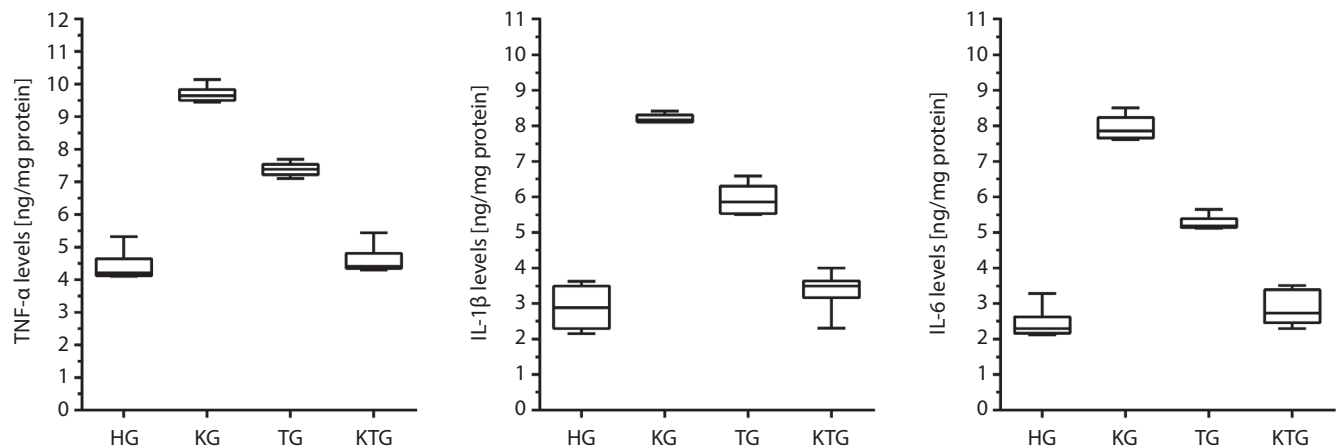


Fig. 3. Tumor necrosis factor alpha (TNF- α), interleukin 1 beta (IL-1 β) and interleukin-6 (IL-6) levels in the liver tissue of the study groups

HG – healthy group; KG – ketamine group; TG – thiopental group; KTG – ketamine+thiopental group; horizontal line – median; bottom line of the box – 1st quartile (Q1, 25th); topline of the box – 3rd quartile (Q3, 75th); whiskers – minimum and maximum observation (excluding outlier).

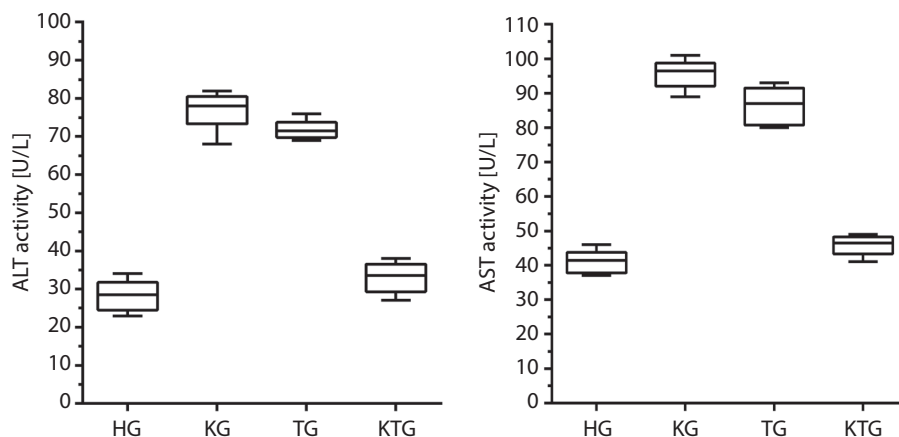


Fig. 4. Alanine aminotransferase (ALT) and aspartate aminotransferase (AST) activity in blood of the study groups

HG – healthy group; KG – ketamine group; TG – thiopental group; KTG – ketamine+thiopental group; horizontal line – median; bottom line of the box – 1st quartile (Q1, 25th); topline of the box – 3rd quartile (Q3, 75th); whiskers – minimum and maximum observation (excluding outlier).

Table 2. The effect of ketamine, thiopental and ketamine+thiopental combination on adrenaline and noradrenaline levels in rats

Groups	ADR	p-value	NDR	p-value
HG	1435.3	0.001	813.8	0.0001
KG	2388.2	0.001	1364	0.0001
TG	779	0.001	291	0.0001
KTG	1513	0.001	710.6	0.0001

HG – healthy group; KG – ketamine group; TG – thiopental group; KTG – ketamine+thiopental group; ADR – adrenaline; NDR – noradrenaline. The analysis of variance (ANOVA) test was used. A value of $p < 0.05$ was considered statistically significant.

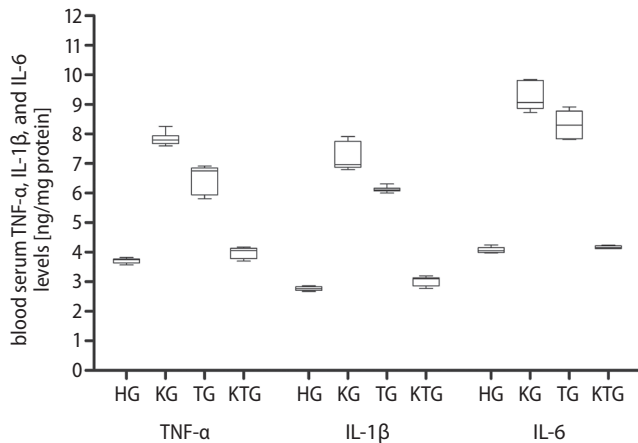


Fig. 5. Tumor necrosis factor alpha (TNF- α), interleukin 1 beta (IL-1 β) and interleukin-6 (IL-6) levels in the blood serum of the study groups

HG – healthy group; KG – ketamine group; TG – thiopental group; KTG – ketamine+thiopental group; horizontal line – median; bottom line of the box – 1st quartile (Q1, 25th); topline of the box – 3rd quartile (Q3, 75th); whiskers – minimum and maximum observation (excluding outlier).

In a previous study, excessive ROS formation and increased lipid peroxidation (LPO) were perceived as the cause of ketamine hepatotoxicity.⁹ In our study, the amount of MDA in the blood serum and liver tissue of animals treated with ketamine alone was found to be higher than in the HG and KTG. These findings indicate that ROS and LPO increased in the ketamine group. MDA is widely used oxidant parameter in oxidative stress-induced LPO. The MDA reacts with nucleic acids and proteins, allowing the damage caused by LPO to continue exacerbated.²² In the studies of Ahiskalioglu et al., it was reported that the subanesthetic dose of ketamine increased the amount of MDA in the brain, heart and bronchi. However, it was emphasized that the amount of MDA in the ketamine+thiopental group was close to that in the control group.¹³

In recent studies, it has been reported that an increase in ROS-related MDA is accompanied by a decrease in GSH stores.²³ Glutathione is an endogenous antioxidant with a low molecular weight, composed of *c*-L-glutamyl-L-cysteinyl-glycine. The sulfhydryl group (–SH) of cysteine is involved in reduction and conjugation reactions, which are generally considered to be the most important functions of GSH.²⁴ Glutathione protects cells from ROS damage by reacting with or detoxifying

hydrogen peroxide (H₂O₂) and organic peroxides.²⁵ It was determined that the amount of tGSH decreased in animal organs given ketamine alone.¹³ In our study, TOS and TAS levels were determined to evaluate oxidative stress in liver tissue in more detail. Total oxidant status and total antioxidant status reflect the total effects of all oxidants and antioxidants in tissues.^{19,20} The fact that MDA and TOS levels are higher in the KG compared to the HG and KTG, and that tGSH and TAS levels are lower compared to KG, indicate that oxidative stress has developed in the liver tissue.

In the previous research, it has been reported that ROS increase pro-inflammatory cytokine production.²⁶ As can be seen from our experimental results, the production of pro-inflammatory cytokines such as TNF- α , IL-1 β and IL-6 increased in the KG with high oxidant parameters and low antioxidants. These cytokines are shown as the response of the immune system in acute and chronic liver damage.²⁷ As is known, if the overproduction of cytokines is not controlled, it can cause serious consequences.²⁸ Previous studies have also reported that pro-inflammatory cytokines such as IL-1 β , IL-6 and TNF- α play a role in the pathogenesis of ketamine-related cell damage.¹¹ In a mouse model of fulminant hepatitis, TNF- α produced by inflammatory cells caused fatal necroinflammatory liver damage.²⁹ There was no information in the literature on the effects of ketamine on hepatic cytokines. However, it has been reported that ketamine increases the expression of IL-1 β and IL-6 in rat spleen.³⁰ In another study, it was emphasized that ketamine induced the production of ROS, IL-1 β , IL-6, and TNF- α in bladder cells.¹¹ In addition, it has been assumed that the toxic effects of ketamine on the central nervous system are related to inflammatory cytokines (such as IL-1 β and IL-6).³¹

Serum ALT and AST activities were found to be high in animals administered with ketamine, whose blood serum and liver tissue oxidant as well as pro-inflammatory cytokine levels were high. These aminotransferases are accepted in literature as sensitive indicators of liver cell damage.³² It has been reported that elevated hepatic oxidant and pro-inflammatory cytokine levels are accompanied by increased blood serum ALT and AST activity.³³ Intravenous ketamine infusion with 16-day intervals in the clinics caused an increase in serum ALT and AST activity in patients.⁸

In our study, MDA, TOS, OSI, IL-1 β , IL-6, TNF- α , ALT, and AST levels were higher in the TG, and their tGSH and TAS levels were lower than those of the HG and KTG. There are studies supporting that thiopental alone increases oxidant levels and decreases antioxidant levels in organ tissues.¹³ It has been reported in the literature that human lymphocytes treated with thiopental exhibit excessive ROS production.³⁴ In another study, it was reported that thiopental did not change MDA and antioxidant levels in the platelets of patients.³⁵ There are data in the literature showing that thiopental suppresses TNF- α production by inhibiting NF- κ B, which does not overlap with our biochemical test results.¹⁵ However, the information stating that ROS increase pro-inflammatory cytokine production supports our biochemical findings.²⁶ In addition, repeated doses of thiopental have been shown to increase the levels of liver enzymes.³⁶

In our study, the use of ketamine and thiopental alone led to an increase in oxidant and pro-inflammatory cytokines in the liver tissue. However, the use of KT did not change the MDA, tGSH, TOS, TAS, IL-6, TNF- α , and IL-1 β levels in the liver tissue. The reason for this can be shown as an increase in catecholamine level of ketamine and a decrease in thiopental. In previous studies, it was observed that oxidative stress increased in the brain, heart and bronchi, in the ketamine group with high blood ADR levels and in the thiopental group with low blood ADR levels. In addition, the damage to these organ tissues of animals administered KT was minimal or nonexistent.¹³ In addition, histopathological damage was observed at a minimum level in the KTG animals whose MDA and tGSH levels were similar to those in the HG. As can be understood from our experimental results, pro-inflammatory cytokine levels in the KTG animals whose oxidant and antioxidant levels were close to the HG were similar to those in the HG. Recently, it has been suggested that thiopental reduces the level of ADR and subsequently induces hyperalgesia in rats. It is assumed that ketamine increases the level of ADR, and that – in the case of suppression of ADR – adrenaline has an important role in controlling the duration of anesthesia. Reducing the amount of endogenous ADR has resulted in prolonged anesthesia time of ketamine.³⁷

Limitations


In further studies, the mechanism of action of ketamine, thiopental and KT on the liver should be clarified – it was not investigated in the present paper. Moreover, effects of long-term use of ketamine in other organs should be elucidated.

Conclusions

The use of ketamine and thiopental alone caused oxidative and pro-inflammatory changes in the liver. However, when these drugs were used as KT, no changes were

observed in oxidative stress and inflammation markers. These results indicate that the KT form may be useful in reducing the risk of toxicity of ketamine and thiopental on the liver in clinical setting. In order to clarify the mechanisms of action of ketamine, thiopental and KT on the liver, it is necessary to measure blood serum catecholamine levels. Further studies on the subject are needed in the future.

ORCID iDs

Zehra Bedir  <https://orcid.org/0000-0001-7347-6649>
 Kezban Tuna Özkaloğlu Erdem  <https://orcid.org/0000-0002-6657-6243>
 İrem Ateş  <https://orcid.org/0000-0001-9867-5011>
 Tülay Ceren Ölmeztürk Karakurt  <https://orcid.org/0000-0001-5013-0127>
 Cebrail Gürsul  <https://orcid.org/0000-0001-6521-6169>
 Didem Onk  <https://orcid.org/0000-0001-8849-0531>
 Nezahat Kurt  <https://orcid.org/0000-0002-1685-5332>
 Zeynep Süleyman  <https://orcid.org/0000-0003-0128-7990>
 Halis Süleyman  <https://orcid.org/0000-0002-9239-4099>

References

1. Saracoglu A. Ketamine: A popular recreational drug. Review. *Turkiye Klinikleri J Med Sci.* 2005;25(3):429–435. <https://www.turkiyeklinikleri.com/article/tr-ketamin-populer-bir-keyif-verici-ilac-36260.html>. Accessed March 12, 2021.
2. Prakash S, Gupta AK, Meena JP, Seth R. A review of the clinical applications of ketamine in pediatric oncology. *Pediatr Blood Cancer.* 2021; 68(1):e28785. doi:10.1002/pbc.28785
3. Launo C, Bassi C, Spagnolo L, et al. Preemptive ketamine during general anesthesia for postoperative analgesia in patients undergoing laparoscopic cholecystectomy. *Minerva Anestesiol.* 2004;70(10): 727–734, 734–738. PMID:15516884.
4. Sin B, Ternas T, Motov SM. The use of subdissociative-dose ketamine for acute pain in the emergency department. *Acad Emerg Med.* 2015;22(3):251–257. doi:10.1111/acem.12604
5. Ng J, Lui LMW, Rosenblat JD, et al. Ketamine-induced urological toxicity: Potential mechanisms and translation for adults with mood disorders receiving ketamine treatment. *Psychopharmacology (Berl).* 2021;238(4):917–926. doi:10.1007/s00213-021-05767-1
6. Bell RF. Ketamine for chronic noncancer pain: Concerns regarding toxicity. *Curr Opin Support Palliat Care.* 2012;6(2):183–187. doi:10.1097/SPC.0b013e328352812c
7. Noppers I, Niesters M, Aarts L, Smith T, Sarton E, Dahan A. Ketamine for the treatment of chronic non-cancer pain. *Expert Opin Pharmacother.* 2010;11(14):2417–2429. doi:10.1517/14656566.2010.515978
8. Noppers IM, Niesters M, Aarts L, et al. Drug-induced liver injury following a repeated course of ketamine treatment for chronic pain in CRPS type 1 patients: A report of 3 cases. *Pain.* 2011;152(9):2173–2178. doi:10.1016/j.pain.2011.03.026
9. Sear JW. Ketamine hepato-toxicity in chronic pain management: Another example of unexpected toxicity or a predicted result from previous clinical and pre-clinical data? *Pain.* 2011;152(9):1946–1947. doi:10.1016/j.pain.2011.04.031
10. Wai MS, Luan P, Jiang Y, et al. Long term ketamine and ketamine plus alcohol toxicity: What can we learn from animal models? *Mini Rev Med Chem.* 2013;13(2):273–279. doi:10.2174/1389557511313020009
11. Cui L, Jiang X, Zhang C, et al. Ketamine induces endoplasmic reticulum stress in rats and SV-HUC-1 human uroepithelial cells by activating NLRP3/TXNIP axis. *Biosci Rep.* 2019;39(10):BSR20190595. doi:10.1042/BSR20190595
12. Aksoy M, Ince I, Ahiskalioglu A, et al. The suppression of endogenous adrenalin in the prolongation of ketamine anesthesia. *Med Hypotheses.* 2014;83(1):103–107. doi:10.1016/j.mehy.2014.03.033
13. Ahiskalioglu EO, Aydin P, Ahiskalioglu A, et al. The effects of ketamine and thiopental used alone or in combination on the brain, heart, and bronchial tissues of rats. *Arch Med Sci.* 2018;14(3):645–654. doi:10.5114/aoms.2016.59508
14. Gaines GY, Rees DI. Anesthetic considerations for electroconvulsive therapy. *South Med J.* 1992;85(5):469–482. doi:10.1097/00007611-199205000-00005

15. Ichiyama T, Nishikawa M, Lipton JM, Matsubara T, Takashi H, Furu-kawa S. Thiopental inhibits NF-kappaB activation in human glioma cells and experimental brain inflammation. *Brain Res.* 2001;911(1): 56–61. doi:10.1016/s0006-8993(01)02672-5
16. Bradford MM. A rapid and sensitive method for the quantitation of microgram quantities of protein utilizing the principle of protein-dye binding. *Anal Biochem.* 1976;72:248–254. doi:10.1006/abio.1976.9999
17. Ohkawa H, Ohishi N, Yagi K. Assay for lipid peroxides in animal tissues by thiobarbituric acid reaction. *Anal Biochem.* 1979;95(2):351–358. doi:10.1016/0003-2697(79)90738-3
18. Sedlak J, Lindsay RH. Estimation of total, protein-bound, and non-protein sulfhydryl groups in tissue with Ellman's reagent. *Anal Biochem.* 1968;25(1):192–205. doi:10.1016/0003-2697(68)90092-4
19. Erel O. A novel automated method to measure total antioxidant response against potent free radical reactions. *Clin Biochem.* 2004; 37(2):112–119. doi:10.1016/j.clinbiochem.2003.10.014
20. Erel O. A new automated colorimetric method for measuring total oxidant status. *Clin Biochem.* 2005;38(12):1103–1011. doi:10.1016/j.clinbiochem.2005.08.008
21. Tsikas D. Assessment of lipid peroxidation by measuring malondialdehyde (MDA) and relatives in biological samples: Analytical and biological challenges. *Anal Biochem.* 2017;524:13–30. doi:10.1016/j.ab.2016.10.021
22. Del Rio D, Stewart AJ, Pellegrini N. A review of recent studies on malondialdehyde as toxic molecule and biological marker of oxidative stress. *Nutr Metab Cardiovasc Dis.* 2005;15(4):316–328. doi:10.1016/j.numecd.2005.05.003
23. Sun LL, Dong HL, Zhang WQ, et al. Lipid peroxidation, GSH depletion, and SLC7A11 inhibition are common causes of EMT and ferroptosis in A549 cells, but different in specific mechanisms. *DNA Cell Biol.* 2021;40(2):172–183. doi:10.1089/dna.2020.5730
24. Forman HJ, Zhang HQ, Rinna A. Glutathione: Overview of its protective roles, measurement, and biosynthesis. *Mol Aspects Med.* 2009; 30(1–2):1–12. doi:10.1016/j.mam.2008.08.006
25. Murray RK, Granner DK, Mayes PA, Rodwell VW. *Harper's Biochemistry.* 25th ed. New York, USA: McGraw–Hill Publishing; 1999.
26. Ha HJ, Yu MR, Choi YJ, Kitamura M, Lee HB. Role of high glucose-induced nuclear factor-kappa B activation in monocyte chemoattractant protein-1 expression by mesangial cells. *J Am Soc Nephrol.* 2002;13(4):894–902. doi:10.1681/ASN.V134894
27. Lacour S, Gautier JC, Pallardy M, Roberts R. Cytokines as potential biomarkers of liver toxicity. *Cancer Biomark.* 2005;1(1):29–39. doi:10.3233/cbm-2005-1105
28. Wu Z, Han M, Chen T, Yan W, Ning Q. Acute liver failure: Mechanisms of immune-mediated liver injury. *Liver Int.* 2010;30(6):782–794. doi:10.1111/j.1478-3231.2010.02262.x
29. Ito H, Ando K, Ishikawa T, et al. Role of TNF-alpha produced by nonantigen-specific cells in a fulminant hepatitis mouse model. *J Immunol.* 2009;182(1):391–397. doi:10.4049/jimmunol.182.1.391
30. Bette M, Schlimme S, Mutters R, Menendez S, Hoffmann S, Schulz S. Influence of different anaesthetics on pro-inflammatory cytokine expression in rat spleen. *Lab Anim.* 2004;38(3):272–279. doi:10.1258/002367704323133655
31. Li Y, Shen R, Wen G, et al. Effects of ketamine on levels of inflammatory cytokines IL-6, IL-1 β , and TNF- α in the hippocampus of mice following acute or chronic administration. *Front Pharmacol.* 2017;8:139. doi:10.3389/fphar.2017.00139
32. Pratt DS, Kaplan MM. Laboratory tests. In: Sorrell MF, Maddrey WC, eds. *Schiff's Diseases of the Liver.* 8th ed. Philadelphia, USA: Lippincott Williams & Wilkins; 1999:205–244.
33. Ajuwon OR, Oguntibeju OO, Marnewick JL. Amelioration of lipopolysaccharide-induced liver injury by aqueous rooibos (*Aspalathus linearis*) extract via inhibition of pro-inflammatory cytokines and oxidative stress. *BMC Complement Altern Med.* 2014;14:392. doi:10.1186/1472-6882-14-392
34. Delogu G, Antonucci A, Moretti S, et al. Oxidative stress and mitochondrial glutathione in human lymphocytes exposed to clinically relevant anesthetic drug concentrations. *J Clin Anesth.* 2004;16(3): 189–194. doi:10.1016/j.jclinane.2003.07.007
35. De La Cruz JP, Zanca A, Carmona JA, de la Cuesta FS. The effect of propofol on oxidative stress in platelets from surgical patients. *Anesth Analg.* 1999;89(4):1050–1055. doi:10.1097/0000539-199910000-00043
36. Fassoulaki A, Andreopoulou K, Williams G, Pateras C. The effect of single and repeated doses of thiopentone and fentanyl on liver function in the rat. *Anaesth Intensive Care.* 1986;14(2):145–147. doi:10.1177/0310057X8601400208
37. Aksoy M, Ahiskalioglu A, Ince I, et al. The relation between the effect of a subhypnotic dose of thiopental on claw pain threshold in rats and adrenalin, noradrenalin and dopamine levels. *Exp Anim.* 2015;64(4): 391–396. doi:10.1538/expanim.15-0028

MicroRNA gene methylation landscape in pediatric B-cell precursor acute lymphoblastic leukemia

Radosław Chaber^{1,2,A–F}, Artur Gurgul^{3,C}, Jacek Tabarkiewicz^{1,4,B,C,E}, Grażyna Wróbel^{5,B,C}, Tomasz Szmatoła^{3,C}, Igor Jasielczuk^{3,B,C}, Olga Haus^{6,C–E}, Monika Lejman^{7,C}, Blanka Rybka^{5,D}, Renata Ryczan-Krawczyk^{5,C,D}, Anna Jaśkowiec^{8,B,C}, Sylwia Paszek^{9,C,D}, Natalia Potocka^{9,C}, Christopher J. Arthur^{10,C–E}, Wioletta Bal^{1,2,D,E}, Kornelia Łach^{1,B–D}, Aneta Kowal^{1,B–D}, *Izabela Zawlik^{1,9,D–F}, *Elżbieta Latos-Grażyńska^{5,C–E}

¹ Institute of Medical Sciences, Medical College of Rzeszów University, Poland

² Clinic of Pediatric Oncology and Hematology, State Hospital 2, Rzeszów, Poland

³ Center for Experimental and Innovative Medicine, University of Agriculture in Krakow, Poland

⁴ Laboratory of Translational Research in Medicine, Centre for Innovative Research in Medical and Natural Sciences, Medical College of Rzeszów University, Poland

⁵ Department of Paediatric Bone Marrow Transplantation, Oncology and Hematology, Wrocław Medical University, Poland

⁶ Department of Clinical Genetics, Faculty of Medicine, Collegium Medicum, Nicolaus Copernicus University, Toruń, Poland

⁷ Laboratory of Genetic Diagnostics, Medical University of Lublin, Poland

⁸ Department of Haematology, Blood Neoplasms and Bone Marrow Transplantation, Wrocław Medical University, Poland

⁹ Laboratory of Molecular Biology, Centre for Innovative Research in Medical and Natural Sciences, Medical College of Rzeszów University, Poland

¹⁰ School of Chemistry, University of Bristol, the United Kingdom

A – research concept and design; B – collection and/or assembly of data; C – data analysis and interpretation; D – writing the article; E – critical revision of the article; F – final approval of the article

Advances in Clinical and Experimental Medicine, ISSN 1899–5276 (print), ISSN 2451–2680 (online)

Adv Clin Exp Med. 2022;31(3):293–305

Address for correspondence

Elżbieta Latos-Grażyńska

E-mail: elzbieta.latos-grazynska@umed.wroc.pl

Funding sources

The study was funded by the Saving Kids with Cancer Foundation (grant No. FNRD.C200.17.003.).

Conflict of interest

None declared

*Izabela Zawlik and Elżbieta Latos-Grażyńska contributed equally to this work.

Received on June 30, 2021

Reviewed on September 6, 2021

Accepted on November 23, 2021

Published online on January 29, 2022

Cite as

Chaber R, Gurgul A, Tabarkiewicz J, et al. MicroRNA gene methylation landscape in pediatric B-cell precursor acute lymphoblastic leukemia. *Adv Clin Exp Med.* 2022;31(3):293–305. doi:10.17219/acem/144170

DOI

10.17219/acem/144170

Copyright

© 2022 by Wrocław Medical University

This is an article distributed under the terms of the Creative Commons Attribution 3.0 Unported (CC BY 3.0) (<https://creativecommons.org/licenses/by/3.0/>)

Abstract

Background. Aberrant DNA methylation is an important mechanism by which the normal patterns of microRNA expression are disrupted in human cancers including B-cell precursor acute lymphoblastic leukemia (BCP ALL), the most common pediatric malignancy.

Objectives. To characterize the methylation profile landscape of microRNA genes in BCP ALL patients.

Materials and methods. We employed Infinium[®] MethylationEPIC BeadChip Arrays to measure the methylation of microRNA genes from bone marrow samples of children with BCP ALL (n = 38) and controls without neoplasms (n = 4).

Results. This analysis revealed differential methylation of the microRNA genes in the pediatric BCP ALL when compared to the control. A subcluster amongst BCP ALL patients with TCF3–PBX1 genetic subtype was also observed. No other differences were observed in association with age, gender or risk group. Several interesting leukemia-related phenotypes are enriched by the genes with hyper- and hypomethylated sites located in promoters as well as gene bodies. The top 3 miRNA genes, promoters of which were the most statistically significantly hypermethylated in BCP ALL were *MIR1273G*, *MIR1304* and *MIR663*, and the top 3 hypomethylated were *MIR4442*, *MIR155* and *MIR3909*.

Conclusions. In this study, a different microRNA genes methylation landscape was shown in pediatric BCP ALL compared to children without neoplasms. A visible subcluster among BCP ALL samples consisted of individuals with TCF3–PBX1 genetic subtype. No other differences were observed in association with age, gender or risk group. Several interesting leukemia-connected phenotypes were found, associated with genes with hyper- and hypomethylated sites located on promoters as well as gene bodies.

Key words: children, microRNA, methylation, BCP ALL

Background

B-cell precursor acute lymphoblastic leukemia (BCP ALL) is the most common malignancy in children.¹ Understanding the molecular and genetic pathways that affect the development and clinical course of BCP ALL is a key to improving the treatment outcomes and is, therefore, an important focus of current research into BCP ALL.

Normal hematopoietic cell development is highly controlled epigenetic regulation of genes via DNA methylation, the chemical modification of histones, and the expression of noncoding RNAs. Each of these epigenetic factors can become dysregulated during leukemic transformation. The DNA methylation is by far the most well-characterized epigenetic modification and is involved in the regulation of gene expression, the maintenance of genome stability, and cellular differentiation.² The methylation of cytosine residues in CpG dinucleotides plays a pivotal role in the establishment of cellular identity by influencing gene expression.³

MicroRNAs (miRNAs) are short, noncoding RNA molecules that regulate gene expression by forming complexes with their mRNA counterparts in order to cause translational repression, either by mRNA degradation or cleavage by deadenylation.^{4,5} Furthermore, miRNAs are key regulators of hematopoiesis and are also involved in leukemogenesis.^{6,7} To date, at least 32 dysregulated miRNAs are known to be associated with ALL prognosis.⁸ Interestingly, aberrant DNA methylation seems to be a major mechanism by which the normal patterns of miRNA expression are disrupted in human cancers,⁹ including ALL.¹⁰ Many tumor suppressor miRNAs appear to be downregulated by DNA hypermethylation, and various oncogenic miRNAs (onco-miRNAs) are known to be upregulated via DNA hypomethylation.⁹

We have previously shown significant differences in genomic methylation profiles in the bone marrow of BCP ALL and healthy control patients.¹¹ Nevertheless, not enough attention was given to the methylation of miRNA genes, which is an important factor affecting oncogenic processes.

Objectives

In this study, we attempted to perform the analysis of methylation profiles of miRNA genes in BCP ALL patients in order to enhance the results of the previous analysis and to shed some light on a potential role of epigenetic regulation of miRNA expression in pediatric leukemia. We have used genome-wide methylation data obtained in our previous work¹¹ and performed an in-depth analysis of the methylation differences in functional elements of miRNA genes in healthy and leukemic bone marrow samples.

Materials and methods

Patients and samples

The approval of the ethics committee for this study was obtained from the Institutional Review Board of the Medical University of Lodz, Poland (approval No. RNN/226/11/KE). Informed consent was obtained from the parents/legal guardians of all participating children. Forty-two samples of bone marrow were obtained in 2015–2016 from 38 patients (male/female 21/17; median age 5.0 years, age range 1.5–17.0 years) with pediatric BCP ALL at the time of diagnosis. The control samples of bone marrow were collected from children in whom other types of cancer and other genetic diseases had been previously excluded. The patients were stratified into prognostic groups according to the ALL IC-BFM 2009 protocol.¹² This stratification is based on the initial clinical features including patient age, white blood cells count at time of diagnosis, presence of specific genetic aberrations, the response to steroids at day 8 of therapy, the cytomorphological response in bone marrow at day 15 and 33, and the minimal residual disease level at day 15. Finally, 5 patients were included into the high-risk group. Various genetic aberrations associated with ALL were detected among most of the patients. Most frequently, hyperdiploidy (>50 chromosomes) (13 patients) and t(12;21) with fusion ETV6-RUNX1 (7 patients) were revealed. Subsequently, t(1;19) with fusion *TCF3-PBX1* (3 patients), hyper/hypotriploidy (3 patients) and IGH rearrangement (3 patients) were detected. Seven patients had other genetic aberrations, which were different than those mentioned above. In 2 cases, the normal karyotype was confirmed.

Samples and DNA methylation profiling

The DNA samples were analyzed with the Infinium® MethylationEPIC BeadChip approach (Illumina, San Diego, USA), according to the manufacturer's protocol. It allowed for the analysis of 850,000 methylation sites per sample. These sites include those within known CpG islands and outside CpG islands, as well as non-CpG methylated sites identified in human stem cells and differentially methylated (DM) sites identified in tumors compared to normal samples and across several tissue types. The assay also includes probes for 7084 CpG sites associated with miRNA genes, out of which 4188 probes were retained for further analysis following quality filtering and extensive annotation analysis. These probes are associated with 1008 different miRNA genes, covering 52.5% of the current version of miRBase (v. 22).¹³

Data quality control and statistical analysis

Our previous study describes the steps taken for data quality control and the identification of DM sites.¹¹ In brief, after initial normalization and removal of batch effects, the ratio of methylated (C) to unmethylated (T) DNA (also called the methylation beta-value (β)) was calculated for each CpG site. A β -value of 0 represents a completely unmethylated CpG site and a β -value of 1 represents a fully methylated CpG site. The differential methylation for individual probes between groups was calculated using the Chip Analysis Methylation Pipeline (ChAMP). The `champ.DMP()` function of ChAMP package pipeline¹⁴ was applied. It uses the `limma` package¹⁵ to calculate the p-value by a linear model. The DMP-determined t-test p-values were corrected for multiple testing using the Benjamini–Hochberg procedure.¹⁶ Adjusted p-values (`adjPs`) <0.05 were considered statistically significant.

The differential methylation analysis was performed with several discrete goals: 1) the identification of general differences between all BCP ALL patients and controls, and 2) the identification of DM sites between standard/intermediate and high-risk group of patients. Additional comparisons have been made within BCP ALL patients group to detect sites associated with confounding factors, such as age (≤ 6 years compared to >6 years) or gender (males compared to females). The differential methylation analysis was also performed between patients with different chromosomal aberrations characteristic of leukemia (ETV6-RUNX1 ($n = 7$), TCF3-PBX1 ($n = 3$), IGH ($n = 3$), hyperdiploidy ($n = 13$), and triploidy ($n = 3$)), using pairwise comparisons between specific cytogenetic subtype and all other leukemia patients with known cytogenetic status ($n = 8$). Cytogenetic diagnosis was performed as previously described.¹¹

Functional gene annotation and target genes prediction

The miRNA genes associated with specific DM sites were analyzed in terms of their disease phenotypes annotated in the available databases. The phenotype enrichment analysis was performed using the WEB-based GENE SeT ANALYSIS (WebGestalt) toolkit (www.webgestalt.org),¹⁷ exploiting information from the Human Phenotype Ontology (www.hpo.jax.org)¹⁸ and PharmGKB (www.pharmgkb.org)¹⁹ databases. The WebGestalt analysis was performed using all annotated human genes (genome option), and it was limited to identifying enriched phenotypes with the Fisher's exact test false discovery rate (FDR)-`adjP` <0.01 and with at least 4 genes within phenotype categories. The prediction of miRNA target genes was done with the use of miRDB tool. Only genes with a prediction score ≥ 95 (implying the highest confidence of gene as a target) were analyzed.²⁰

Results

Differences in miRNA genes methylation profiles between BCP ALL and control samples

General assay performance was evaluated based on control probes. The performance was satisfactory across all studied samples, with all samples passing filtering criteria implemented in the BeadArray Controls Reporter (Illumina) software. After initial filtering, β -values for 800,619 probes were retained and normalized. Subsequently, batch effects were identified and removed by evaluation of components of variation and by the singular value decomposition (SWD) method.²¹ Among all the analyzed probes, 4188 probes associated with 1008 different miRNA genes were identified and analyzed (data available on reasonable request).

Comparison of methylation levels between BCP ALL and control samples resulted in the detection of 578 DM probes. Out of 578 probes, 377 were annotated to promoters of 242 different miRNA genes. Promoter sites were defined as: TSS200 (0–200 nt upstream of transcription start site (TSS)) and TSS1500 (200–1500 nt upstream of TSS). The remaining 201 DM sites were annotated as located within the gene bodies of 74 different miRNAs.

The principal component analysis based on all DM probes reveals visible differences in the miRNA genes methylation profiles between BCP ALL and control samples, with greater variation observed among leukemic samples (Fig. 1). Unsupervised hierarchical clustering (based on Euclidean distance and the DM probes β -values) showed the clear separation of the leukemic and non-leukemic methylation profiles into 2 distinct clusters (Fig. 2). A visible subcluster among BCP ALL samples was created by 3 cases of TCF3-PBX1 genetic subtype (Fig. 2), suggesting that it possesses a distinct miRNA genes methylation profile. No clustering of samples with age, gender or risk

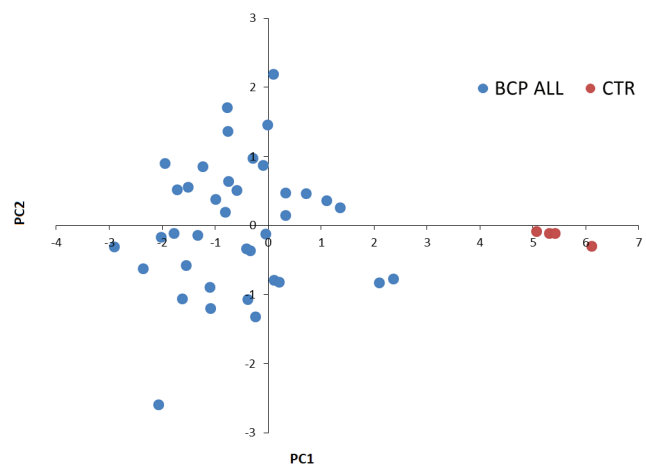


Fig. 1. Principal component analysis using methylation β -values of differentially methylated and miRNA genes-associated probes

BCP ALL – B-cell precursor acute lymphoblastic leukemia; CTR – controls.

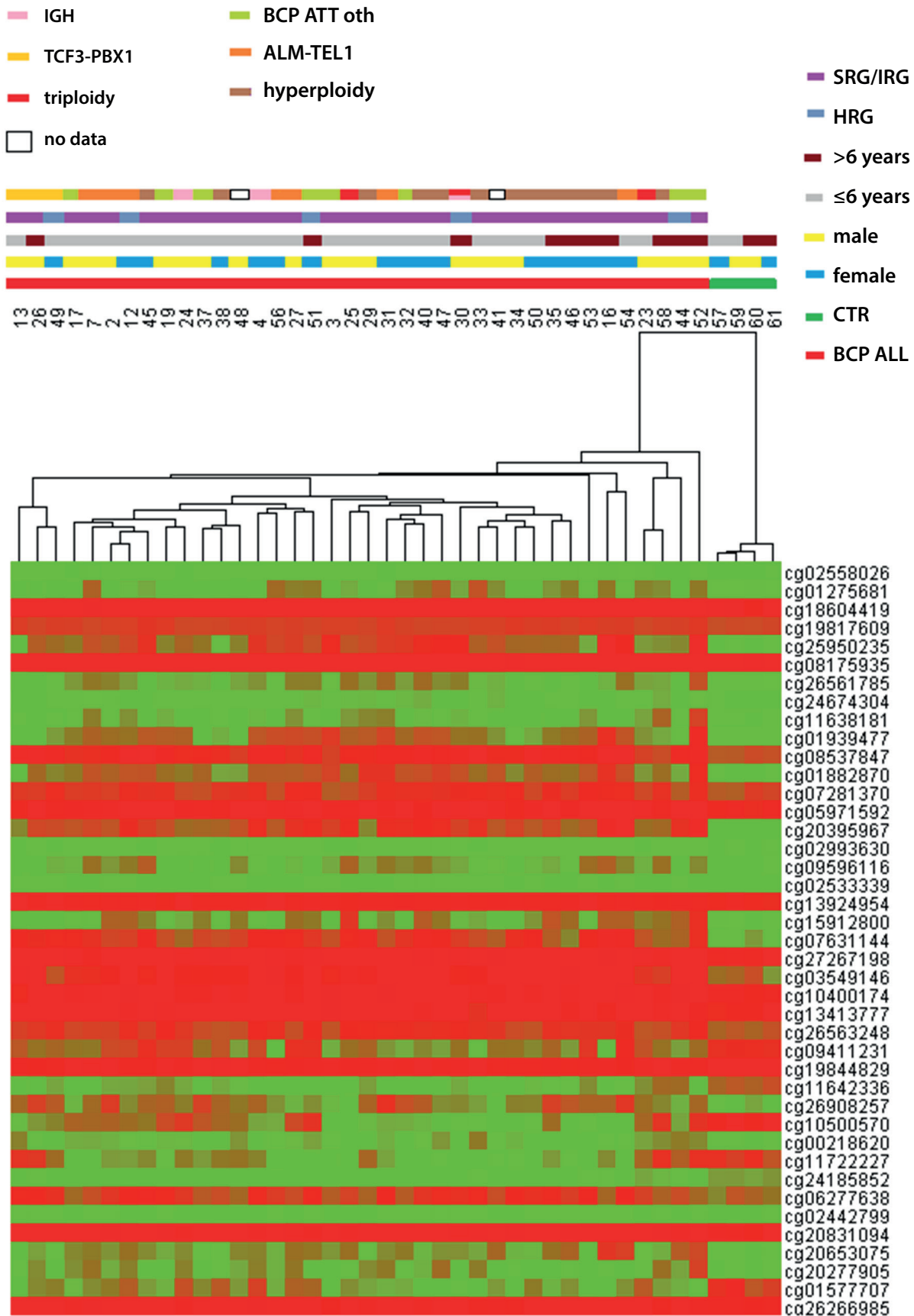


Fig. 2. Hierarchical clustering of the studied B-cell precursor acute lymphoblastic leukemia (BCP ALL) and control samples methylation profiles based on all differentially methylated miRNA genes-associated sites. Only a random subset of probes is shown on the heatmap. The colored bars in upper section classify samples according to disease state, gender, age, risk group, and genetic subtype

CTR – controls.

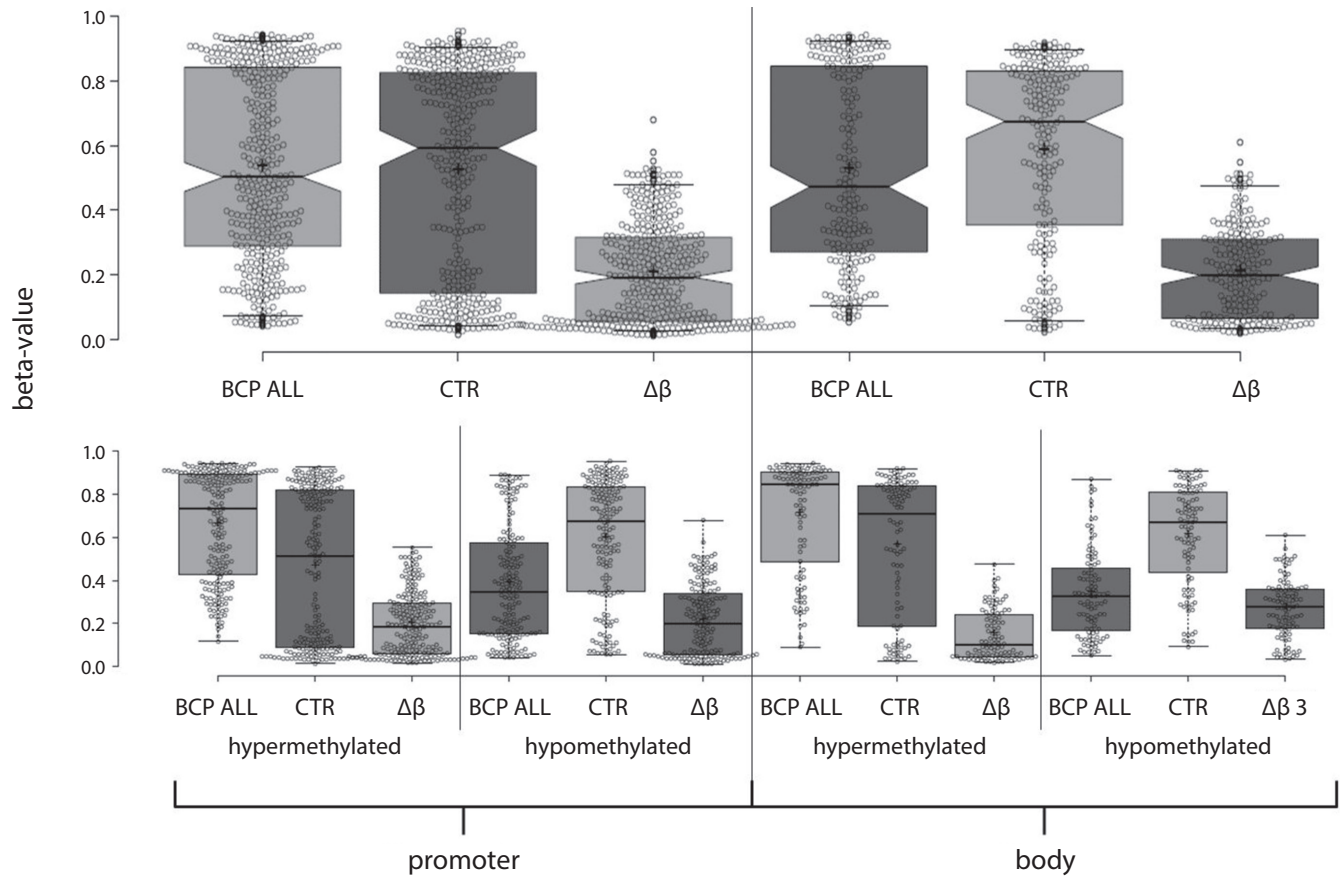


Fig. 3. Boxplot of differentially methylated probes methylation β -values (methylation levels) and delta-beta ($\Delta\beta$) values with respect to study group and probes location in promoter and gene body

BCP ALL – B-cell precursor acute lymphoblastic leukemia; CTR – controls; $\Delta\beta$ – difference in methylation level between groups.

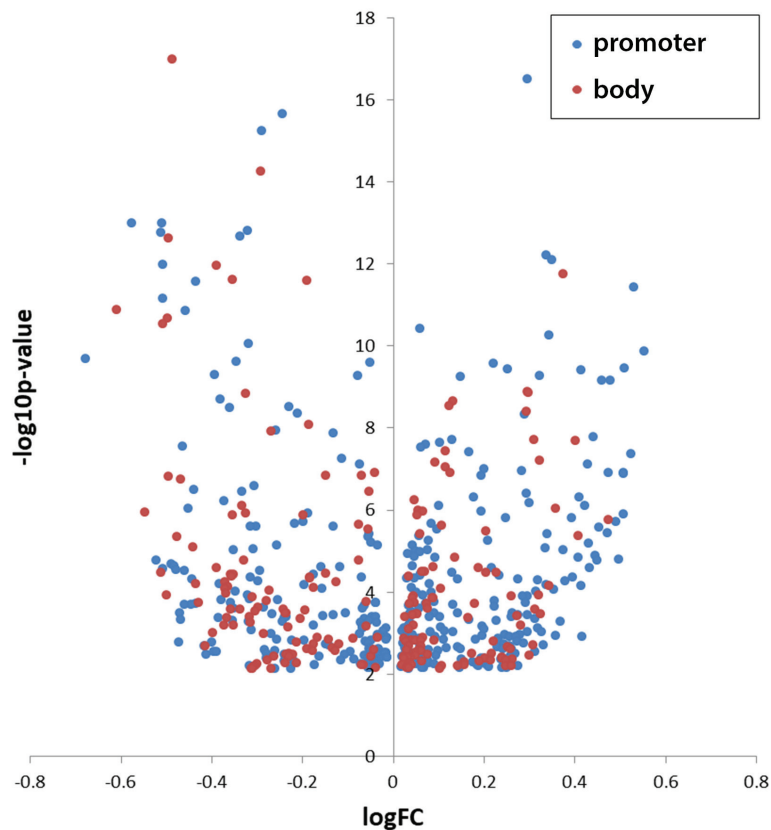


Fig. 4. Volcano plot for sites differentially methylated between B-cell precursor acute lymphoblastic leukemia (BCP ALL) and control samples, with respect to their location in the promoter and gene body of miRNA genes

group was observed, suggesting a lower influence of these factors on global miRNA gene methylation profiles.

The initial analysis of differential methylation of CpG sites between BCP ALL and control samples showed a similar pattern of methylation differences for sites located in promoters and gene bodies of miRNA genes (Fig. 3,4). However, taking into account that the methylation in these regions can have the opposite effect on transcription process, DM CpGs were analyzed separately, depending on their location within the functional element of a given gene.

Differential methylation of miRNA gene promoters in BCP ALL

Changes in methylation profile of miRNA gene promoters in leukemia were studied based on 377 DM (t-test FDR < 0.05) CpG loci between BCP ALL and ccontrols, located within TSS200 and TSS1500 of 242 different miRNA genes (data available on reasonable request). These sites were rarely associated with known CpG islands (17.8% of all) or shores (23.3%), and about half of them (54.9%) were hypermethylated in the BCP ALL group. When comparing the distribution of hyper- and hypomethylated sites across the genome, we found that hypermethylated sites are more commonly situated in CpG islands than hypomethylated (29.5% compared to 3.5%), whereas hypomethylated sites were more common in “open sea” (64.7% compared to 53.8%). The lowest average methylation level was observed for CpGs located within known CpG islands in both the control (17.7%) and BCP ALL samples (43.2%) (Table 1).

A high level of methylation was observed for CpGs located in sites distant from a CpG island (“open sea”; 65.8% in control samples) and was the highest for sites that were hypermethylated in BCP ALL (82.9%) (Table 2).

Table 1. Characteristics of DM miRNA genes promoter-associated sites in B-cell precursor acute lymphoblastic leukemia (BCP ALL), with respect to their location in promoter regions TSS1500 and TSS200

Feature location	TSS1500	TSS200	Promoter
Whole panel			
Number	1934	824	2758
%	70.1	29.9	100.0
All promoter-associated sites			
Number	254	123	377
% of DM	67.4	32.6	100.0
Avg. met. in BCP ALL	0.538	0.520	0.532
Avg. met. in CTR	0.548	0.462	0.520
Hypermethylated in BCP ALL			
Number	134	73	207
% of DM	35.5	19.4	54.9
Avg. met. in BCP ALL	0.673	0.629	0.657
Avg. met. in CTR	0.496	0.393	0.460
Avg. met. difference ($\Delta\beta$)	0.177	0.235	0.197
Hypomethylated in BCP ALL			
Number	120	50	170
% of DM	31.8	13.3	45.1
Avg. met. in BCP ALL	0.387	0.362	0.380
Avg. met. in CTR	0.605	0.563	0.593
Avg. met. difference ($\Delta\beta$)	0.218	0.201	0.213

Sites were classified according to their location in TSS1500, TSS200 and jointly (promoter). The number and percentage of probes in each location is given. Additionally, the average methylation (avg. met.) in both study groups and difference in methylation level between them is provided. DM – differentially methylated; CTR – controls.

The average absolute $\Delta\beta$ (average difference in methylation level) was similar for hyper- (0.197) and hypomethylated (0.213) sites.

The DM sites located in promoters were associated with 242 different miRNA genes. The phenotype enrichment analysis showed that the genes were enriched in several cancer-related disease phenotypes, including hematologic neoplasms, carcinoma, B-cell lymphoma, or leukemia itself (Table 3). Moreover, several interesting leukemia-connected phenotypes were found, when genes associated with hyper- and hypomethylated sites were analyzed separately (data available on reasonable request).

The top 3 miRNA genes whose promoters were the most statistically significantly hypermethylated in BCP ALL were *MIR1273G*, *MIR1304* and *MIR663*, and the top 3 hypomethylated were: *MIR4442*, *MIR155* and *MIR3909*. The analysis of the most probable target genes (top score from miRDB software) for the miRNAs being a product of those genes allowed for the detection of 44 different coding genes, among which we found e.g., pre-B-cell leukemia transcription factor 2 (*PBX2*) and metastasis associated 1 family member 2 (*MTA2*) genes (Table 4).

Differential methylation of miRNA gene bodies in BCP ALL

In total, 201 DM sites located in the gene bodies of 74 different miRNA genes between BCP ALL and control samples were detected (data available on reasonable request). As expected, the DM sites were mainly located outside known CpG islands (80.1%). No sites that were hypomethylated and located within known CpG islands were detected in BCP ALL. Most of the gene body-associated sites were characterized by a high level of methylation in both groups (45–85% on average in control samples). Only sites positioned within CpG islands were characterized by lower methylation level (15.1% in controls (CTR)) (Table 5).

Sites were classified according to their location in open sea, shore, shelf, and island of known CpG islands. The number and percentage of probes in each location is given. Additionally, the average methylation in both study groups and the difference in methylation level between them is provided.

Out of the gene body-associated sites DM between BCP ALL and control groups, 102 (50.7%) were hypermethylated in BCP ALL. The average difference in methylation level (average absolute $\Delta\beta$) between BCP ALL and control samples was higher for hypo- (0.27) than hypermethylated (0.14) sites. The hypermethylated sites were associated with 51 different miRNA genes, out of which 3 most significantly DM were *MIR1273H*, *MIR5096* and *MIR5095*. The sites hypomethylated in BCP ALL were connected with bodies of 45 different miRNA genes. Among the top 3 genes with hypomethylated bodies, we found *MIR548Q*, *MIR3163* and *MIR181A1HG* (the host gene). The analysis of the top 3 hyper- and hypomethylated miRNAs target

Table 2. Characteristics of differentially methylated miRNA genes promoter-associated sites in B-cell precursor acute lymphoblastic leukemia (BCP ALL), with respect to the location in known CpG islands

Feature CGI context	Open sea	Shore	Island	Shelf	All
Whole panel					
Number	1692	483	414	169	2758
%	61.3	17.5	15.0	6.1	100.0
All DM promoter-associated sites					
Number	203	88	67	19	377
% of DM	53.8	23.3	17.8	5.0	100.0
Avg. met. in BCP ALL	0.593	0.482	0.432	0.466	0.532
Avg. met. in CTR	0.658	0.451	0.177	0.568	0.520
Hypermethylated in BCP ALL					
Number	93	48	61	5	207
% of DM	24.7	12.7	16.2	1.3	54.9
Avg. met. in BCP ALL	0.829	0.580	0.448	0.751	0.657
Avg. met. in CTR	0.701	0.336	0.161	0.637	0.460
Avg. met. difference ($\Delta\beta$)	0.128	0.244	0.287	0.114	0.197
Hypomethylated in BPC ALL					
Number	110	40	6	14	170
% of DM	29.2	10.6	1.6	3.7	45.1
Avg. met. in BCP ALL	0.393	0.365	0.269	0.363	0.380
Avg. met. in CTR	0.614	0.589	0.339	0.543	0.593
Avg. met. difference ($\Delta\beta$)	0.221	0.224	0.070	0.180	0.213

Avg. met. – average methylation; DM – differentially methylated; CTR – controls; CGI – Common Gateway Interface.

Table 3. Selected disease phenotypes enriched by miRNA genes with promoter CpGs differentially methylated between B-cell precursor acute lymphoblastic leukemia (BCP ALL) and control samples

Disease	FDR*	miRNA gene
Hematologic neoplasms	7.51E-74	MIR194-2, MIR708, MIR518F, MIR431, MIR574, MIR873, MIR379, MIR485, MIR516B2, MIR589, MIR760, MIR495, MIR516B1, MIR520C, MIR518D, MIR625, MIR367, MIR889, MIR432, MIR548A1, MIR627, MIR548C, MIR885, MIR519D, MIR339, MIR409, MIR517C, MIR579, MIR636, MIR512-2, MIR135A2, MIR520A, MIR654, MIR330, MIR7-3, MIR525, MIR496, MIR876, MIR30B, MIR153-2, MIR124-1, MIR487A, MIR526A2, MIR561, MIR203, MIR186, MIR665, MIR653, MIR101-2, MIR570, MIR34B, MIR154, MIR527, MIR618, MIR518A1, MIR874
Neoplasms	4.34E-23	MIR429, MIR708, MIR146B, MIR25, MIR574, MIR155HG, MIR375, MIR192, MIR625, MIR7-1, MIR199B, MIR143, MIR9-1, MIR27A, MIR125B1, MIRLET7A1, MIR155, MIR215, MIR206, MIR9-3, MIR10A, MIR196B, MIR196A1, MIR200B, MIR145, MIR124-1, MIR138-1, MIR30A, MIR181A1, MIR494, MIR148A, MIR122, MIR203, MIR128-2, MIR137, MIR34B, MIR423
Carcinoma, small cell	3.13E-14	MIR708, MIR146B, MIR25, MIR574, MIR330, MIR124-3, MIR30B, MIR375, MIR196A1, MIR200B, MIR145, MIR124-1, MIR138-1, MIR30A, MIR101-2, MIR124-2, MIR34B, MIR423
Cancer or viral infections	1.05E-11	MIR429, MIRLET7A1, MIR155, MIR146B, MIR206, MIR215, MIR155HG, MIR10A, MIR196B, MIR375, MIR196A1, MIR200B, MIR145, MIR192, MIR124-1, MIR199B, MIR143, MIR30A, MIR148A, MIR122, MIR203, MIR9-1, MIR27A, MIR34B, MIR125B1, MIR423
Lymphoma, large-cell, diffuse	4.02E-07	MIR4505, MIR155, MIR4422, MIR4531, MIR155HG, MIR4485, MIR4439, MIR4442, MIR4517, MIR4462, MIR125B1
Carcinoma	3.85E-05	MIRLET7A1, MIR155, MIR146B, MIR143, MIR138-1, MIR30A, MIR122, MIR203, MIR375, MIR200B, MIR145, MIR124-1
Precursor cell lymphoblastic leukemia-lymphoma	0.0002	MIR1973, MIR196B, MIR1976, MIR128-2, MIR5197, MIR125B1
Leukemia	0.0041	MIR155, MIR181A1, MIR142, MIR10A, MIR196B, MIR128-2, MIR125B1, MIR150
Lymphoma, B-cell	0.0087	MIR196B, MIR155, MIR125B1, MIR155HG, MIR127

* Fisher’s exact test false discovery rate (FDR), as implemented in WebGestalt software.

genes showed 483 potential targets (data available on reasonable request), among which we found few having annotation to leukemia phenotype in PharmGKB database (e.g. *TRIM72*, *SPI1*, *MARVELD3*, *TOPORS*, *SSBP2*, *GAB2*).

Altogether, the miRNA genes with DM sites in gene body significantly enriched 6 disease phenotypes, including hematologic neoplasms, lymphoma, carcinoma, or viral infections (Table 6).

Table 4. Top score target genes for miRNA whose genes are most statistically significantly hyper- and hypomethylated in B-cell precursor acute lymphoblastic leukemia (BCP ALL)

miRNA	Target rank	Target score	Gene symbol	Gene description
Hypermethylated				
MIR1273g	1	97	<i>SLC2A1</i>	solute carrier family 2 (facilitated glucose transporter), member 1
	2	96	<i>CDH8</i>	cadherin 8, type 2
	3	96	<i>NLK</i>	nemo-like kinase
	4	95	<i>TAF5</i>	TAF5 RNA polymerase II, TATA box binding protein (TBP)-associated factor, 100kDa
	5	95	<i>SLC30A5</i>	solute carrier family 30 (zinc transporter), member 5
MIR1304	1	98	<i>FBXO45</i>	F-box protein 45
	2	98	<i>AKR1B1</i>	aldo-keto reductase family 1, member B1 (aldose reductase)
	3	97	<i>PFKFB2</i>	6-phosphofructo-2-kinase/fructose-2,6-biphosphatase 2
	4	97	<i>CAPRN2</i>	caprin family member 2
	5	96	<i>ACBD3</i>	acyl-CoA binding domain containing 3
	6	96	<i>PRR9</i>	proline rich 9
	7	96	<i>USP47</i>	ubiquitin-specific peptidase 47
	8	96	<i>B4GALT6</i>	UDP-Gal:betaGlcNAc beta 1,4-galactosyltransferase, polypeptide 6
	9	95	<i>MKX</i>	mohawk homeobox
	10	95	<i>KIAA1324</i>	KIAA1324
	11	95	<i>FAM122B</i>	family with sequence similarity 122B
MIR663	1	100	<i>ABO</i>	ABO blood group (transferase A, alpha 1-3-N-acetylgalactosaminyltransferase; transferase B, alpha 1-3-galactosyltransferase)
	2	99	<i>ESPN</i>	Espin
	3	98	<i>YIF1B</i>	Yip1 interacting factor homolog B (<i>Saccharomyces cerevisiae</i>)
	4	98	<i>NFIX</i>	nuclear factor I/X (CCAAT-binding transcription factor)
	5	97	<i>DPP9</i>	dipeptidyl-peptidase 9
	6	96	<i>SPTBN4</i>	spectrin, beta, non-erythrocytic 4
	7	95	<i>GRIN2D</i>	glutamate receptor, ionotropic, N-methyl D-aspartate 2D
Hypomethylated				
MIR4442	1	100	<i>MTA2</i>	metastasis associated 1 family, member 2
	2	95	<i>PSME4</i>	proteasome (prosome, macropain) activator subunit 4
MIR155	1	98	<i>WEE1</i>	WEE1 G2 checkpoint kinase
	2	98	<i>IRF2BP2</i>	interferon regulatory factor 2, binding protein 2
	3	98	<i>HIVFP2</i>	human immunodeficiency virus type I enhancer binding protein 2
	4	98	<i>JARID2</i>	jumonji, AT rich interactive domain 2
	5	98	<i>ZNF652</i>	zinc finger protein 652
	6	98	<i>BACH1</i>	BTB and CNC homology 1, basic leucine zipper transcription factor 1
	7	97	<i>TP53INP1</i>	tumor protein p53 inducible nuclear protein 1
	8	97	<i>TM9SF3</i>	transmembrane 9 superfamily member 3
	9	96	<i>FAR1</i>	fatty acyl CoA reductase 1
	10	96	<i>GABRA1</i>	gamma-aminobutyric acid (GABA) A receptor, alpha 1
	11	96	<i>JADE1</i>	jade family PHD finger 1
	12	96	<i>RCN2</i>	reticulocalbin 2, EF-hand calcium-binding domain
	13	95	<i>SOCS5</i>	suppressor of cytokine signaling 5
	14	95	<i>ZIC3</i>	Zic family member 3
MIR3909	1	98	<i>PBX2</i>	pre-B-cell leukemia homeobox 2
	2	97	<i>ARIH1</i>	ariadne RBR E3 ubiquitin protein ligase 1
	3	97	<i>SLITRK4</i>	SLIT and NTRK-like family, member 4
	4	95	<i>SH3D19</i>	SH3 domain containing 19
	5	95	<i>CASKIN2</i>	CASK interacting protein 2

Table 5. Characteristics of differentially methylated miRNA gene bodies-associated sites in B-cell precursor acute lymphoblastic leukemia (BCP ALL) with respect to the location in known CpG islands

Feature CGI location	Open sea	Shore	Island	Shelf	All
Whole panel					
Number	1161	101	106	58	1426
%	81.4	7.1	7.4	4.1	100.0
All DM gene body-associated sites					
Number	161	18	17	5	201
% of DM	80.1	9.0	8.5	2.5	100.0
Avg. met. in BCP ALL	0.542	0.493	0.343	0.654	0.523
Avg. met. in CTR	0.636	0.479	0.151	0.698	0.583
Hypermethylated in BCP ALL					
Number	71	11	17	3	102
% of DM	35.3	5.5	8.5	1.5	50.7
Avg. met. in BCP ALL	0.796	0.664	0.343	0.669	0.703
Avg. met. in CTR	0.670	0.452	0.151	0.595	0.558
Met. difference	0.126	0.212	0.192	0.074	0.145
Hypomethylated in BCP ALL					
Number	90	7	0	2	99
% of DM	44.8	3.5	0.0	1.0	49.3
Avg. met. in BCP ALL	0.341	0.224	–	0.633	0.338
Avg. met. in CTR	0.609	0.522	–	0.854	0.608
Met. difference	0.268	0.298	–	0.221	0.270

Avg. met. – average methylation; DM – differentially methylated; CTR – controls; CGI – Common Gateway Interface.

Table 6. Disease phenotypes enriched by miRNA genes with differentially methylated sites located in gene bodies in B-cell precursor acute lymphoblastic leukemia (BCP ALL)

Disease	FDR*	miRNA gene
Hematologic neoplasms	2.10e-11	MIR301B, MIR487A, MIR548A2, MIR518C, MIR187, MIR425, MIR433, MIR589, MIR34B, MIR124-1
Lymphoma, large-cell, diffuse	1.95e-07	MIR548O2, MIR548AC, MIR548AE2, MIR548H5, MIR548AJ2, MIR155HG, MIR548AI
Neoplasms	3.90e-07	MIR17HG, MIR494, MIR155HG, MIR9-3, MIR137, MIR128-2, MIR375, MIR34B, MIR146A, MIR124-1
Carcinoma, small cell	5.58e-05	MIR124-2MIR375, MIR34B, MIR124-1, MIR124-3
Cancer or viral infections	0.0020	MIR17HGMIR375, MIR34B, MIR155HG, MIR124-1, MIR146A
Neoplasm of unspecified nature of digestive system	0.0031	MIR375MIR34B, MIR124-1, MIR146A

* Fisher’s exact test false discovery rate (FDR), as implemented in WebGestalt software.

miRNA genes differentially methylated in specific leukemia genetic subtypes

To detect miRNA genes potentially associated with separate leukemia genetic subtypes (*ETV6-RUNX1*, *TCF3-PBX1*, *IGH*, hyperdiploidy, triploidy), patients with a specific subtype were compared against all the other patients with known cytogenetic status. This analysis allowed us to detect 21 DM sites in patients with *ETV6-RUNX1*, corresponding to promoters and gene bodies of 12 different miRNA genes (Table 7). Only 7 of these sites were located in promoters and were mainly (71.4%) hypomethylated with an average absolute $\Delta\beta$ of 0.27. Nearly 66.7% of DM sites in *ETV6-RUNX1* cases were located in gene bodies and were predominantly associated with hypomethylation (64.2%

of sites). For *TCF3-PBX1* subtype, we found 56 DM sites associated with 37 miRNA genes (Table 7). Most of the sites were located in promoters (n = 38, 67.8%). Moreover, most of them (89.5% of sites) were hypomethylated in *TCF3-PBX1* cases. The DM sites (between *TCF3-PBX1* cases and other leukemia subtypes) located in gene bodies (n = 18) also showed high $\Delta\beta$ values (around 0.39) and were predominantly (61.1%) hypomethylated. In patients with *IGH* rearrangements, only 3 probes (2 in promoters and 1 in gene body) associated with 3 different miRNA genes were hypomethylated with a low average $\Delta\beta$ of 0.18.

The occurrence of hyperploidy in BCP ALL patients was associated with differential methylation of 34 sites (25 different miRNA genes), the majority of which (61.7%) was located in gene bodies of 14 different genes. The sites located

Table 7. The miRNA genes with differentially methylated sites between specific genetic subtype and all other samples with known cytogenetic status

Promoter		Gene body	
hypo-	hyper-	hypo-	hyper-
eTV6-RUNX1			
MIR320B1	MIR548F3	MIR3163	MIR99AHG
MIR1306	MIR375	MIR548F3	MIR548H2
MIR1205	–	MIR4529	–
MIR320B1	–	MIR548H2	–
MIR219A2	–	MIR548H4	–
–	–	MIR181A1HG	–
TCF3-TBX1			
MIR874	MIR3945	MIR548W	MIR3134
MIR5685	MIR5191	MIR5694	MIR7853
MIR369	MIR497	MIR1268A	MIR5095
MIR1470	MIR1207	MIR548N	MIR1273E
MIR410	–	MIRLET7BHG	MIR5096
MIR140	–	MIR5096	MIR548F3
MIR4287	–	MIR548D1	–
MIR412	–	MIR1273E	–
MIR4720	–	MIR548H4	–
MIR183	–	MIR1237	–
MIR6775	–	–	–
MIR1272	–	–	–
MIR496	–	–	–
MIR5571	–	–	–
MIR6742	–	–	–
MIR135A2	–	–	–
MIR656	–	–	–
MIR4265	–	–	–
MIR3660	–	–	–
IGH			
MIR495	–	MIR548H4	–
MIR6790	–	–	–
Hyperploidy			
MIR650	MIR8089	MIR99AHG	–
MIR7850	MIR6746	MIR1273H	–
MIR548I4	MIR922	MIR5009	–
MIR614	–	MIR663AHG	–
MIR298	–	MIR548AU	–
MIR3666	–	MIR100HG	–
MIR299	–	MIR548AI	–
MIR1297	–	MIR548A2	–
MIR3201	–	MIR548AY	–
–	–	MIR7853	–
–	–	MIR548AE2	–
–	–	MIR548W	–
–	–	MIR548I4	–
–	–	MIR6130	–
Triploidy			
–	–	–	MIR548H4

in promoters showed slightly higher absolute $\Delta\beta$ (0.27) than those located in gene bodies (0.21). Both promoter and gene body-associated sites predominantly showed hypermethylation in patients with hyperploidy, with 71.4% of promoter sites hypomethylated and all sites (100%) located in gene bodies hypomethylated in hyperploidy cases.

Only a single probe, associated with the body of *MIR548H4* gene, was DM (hypermethylated) in samples obtained from patients with triploidy (Table 7).

Discussion

Aberrant expression of some miRNA genes may be a contributing factor in the oncogenesis of many cancers,^{22,23} including acute leukemias.^{24–27} Epigenetic modifications, such as methylation of miRNA genes, regulate the expression of genes.²⁸ Therefore, altered miRNA gene methylation may be regarded as a causal factor for leukemogenesis and it can determine the clinical course of acute leukemia as well.

In this study, 377 sites located in the promoters of 242 different miRNA genes were DM in BCP ALL compared to control samples. Many of these miRNAs participate in cell cycle and differentiation control (Table 4). This research was focused on determining the methylation landscape of miRNA genes only; therefore, the expression level of the examined miRNA remains unknown. Despite the lack of evidence from this study to link the particular miRNA methylation level with its expression, the results obtained by others may indicate such a relationship.^{29–34} Stumpel et al.³⁰ identified 11 miRNAs that were downregulated in t(4;11)-positive infant ALL, as a consequence of CpG hypermethylation. Seven of those miRNAs were reactivated after the exposure to the demethylating agent, zebularine. In our study, 4 out of these 7 genes (*MIR200B*, *MIR429*, *MIR10A* and *MIR432*) were hypermethylated as in the previously mentioned study.³⁰ Their impact on the development and clinical course of leukemia may be significant. For example, the zinc finger E-box binding homeobox 2 (*ZEB2*) gene is the best-known, validated target gene of the miR-200b/a-429 cluster.³¹ Homeobox A3 (*HOXA3*) gene has been described as a potential *MIR10A* targeted gene.³² For *MIR432*, more than 100-fold downregulated expression was observed in t(4;11)-positive infant ALL, as compared with normal bone marrow.³⁰ The *MIR432* is located within the large *MIR127* cluster which is silenced in various malignancies by CpG island hypermethylation and aberrant histone modifications.³³

Schotte et al.³⁴ showed the reduced methylation level at CpG islands in the promoter regions of *MIR196B*, yet it was limited to MLL-rearranged BCP ALL cases. It corresponded to an upregulation of *MIR196B*, suggesting an epigenetic origin for its overexpression. This is in line with the results of our study, where *MIR196B* gene is hypomethylated in all BCP ALL cases.

Table 8. The comparison between the methylation status of selected miRNAs and their expression according to available references

miRNAs	Expression	Reference	β -value BCP ALL	β -value controls	p-value	Methylation
<i>MIR125B</i>	high	Swellam et al. ⁵⁴	0.618	0.109	<0.001	high
<i>MIR203</i>	low	Swellam et al. ⁵⁴	0.335	0.066	0.003	high
<i>MIR181A</i>	low	Nabhan et al. ⁵⁵	0.857	0.777	<0.001	high

The methylation beta-value (β) – the ratio of the methylated (C) to unmethylated (T) signals. The p-value was calculated for the differential methylation between BCP ALL and control individuals. BCP ALL – B-cell precursor acute lymphoblastic leukemia.

The results of other studies²⁷ revealed that the genes of at least 5 miRNAs (*MIR326*, *-200c*, *-125B*, *-203*, and *-181A*) have a significantly different expression in BCP ALL cases compared to healthy controls. According to our study, the gene promoters of 3 out of the abovementioned miRNA (*MIR125B*, *-203* and *-181A*) are DM in BCP ALL patients. The comparison between their methylation status and their expression (according to the available references) was shown in Table 8. The expression of *MIR125B* gene, opposite to *MIR203* and *MIR181A*, was higher in BCP ALL patients, although its promoter was hypermethylated.

Top score target genes for miRNA whose gene promoter sites are most statistically significantly hyper- and hypomethylated in BCP ALL are listed in Table 4. Some of these genes are known to be associated with carcinogenesis. For example, *MIR1273* expression is increased in the pancreas of mouse model of pancreatic cancer.³⁵ The *MIR1304* is a tumor suppressor and HO-1 is its direct target in non-small cell lung cancer.³⁶ The downregulation of *MIR1304* is related to early stage breast cancer.³⁷ The overexpression of *MIR663* significantly suppressed the proliferation and invasion of glioblastoma cells in vitro as well as in vivo.³⁸ The *MIR663* may act as an oncogene in nasopharyngeal carcinoma.³⁹ Interestingly, in our study on childhood BCP ALL, the promoter of *MIR663* was hypermethylated in pediatric acute myeloid leukemia (AML), with significantly lower expression compared to normal bone marrow.⁴⁰

The *MIR4442* was amidst the genes with the top hypomethylated promoters. Although its role in leukemogenesis is unclear, its predicted targets include GTPase activating Rap/RanGAP domain-like 3 and zinc finger protein 765.⁴¹ The next gene with hypomethylated promoter is *MIR155*, which plays a complex role in AML.⁴² The levels of *MIR155* significantly influence the set of genes involved in biologic processes related to antiapoptotic, proliferative, and inflammatory activities.⁴³ The increased expression of *MIR155* causes the downregulation of SPI1 and CEBPB, and consequently may block myeloid differentiation in AML.⁴⁴ Moreover, the expression of HSA21-encoded *MIR155* is altered in B cells of Down syndrome individuals and may play a role in Down syndrome-associated leukemia.⁴⁵ There is also some evidence linking the significantly upregulated *MIR155* expression level to the high levels of minimal residual disease and poor prognosis in ALL patients.⁴⁶ According to the results from other study,⁴⁷ *MIR155* was upregulated in the HCV-4 associated ALL group. Hence,

the increased *MIR155* level may be related to acute leukemia development. Our results, where *MIR155* promoter was hypomethylated, are consistent with this observation.

To sum up, there was a slight predominance of differentially hypermethylated (207/377) over hypomethylated (170/377) promoter-associated sites in miRNA genes in BCP ALL patients. However, the potential impact of miRNAs genes methylation level on their expression has to be established in future studies.

There were also 201 DM gene body associated sites with nearly equal (102:99) distribution between their hyper- and hypomethylated status. They corresponded to 74 different miRNA genes. The function of gene body methylation is not well understood. Typically, DNA promoter methylation is believed to be a marker of transcriptional repression. However, the DNA methylation within the gene body appears to serve a different function than DNA methylation within the promoter region. While there is some evidence that intragenic DNA methylation is related to transcriptional repression,⁴⁸ the bulk of evidence suggests that it is associated with gene activation.⁴⁹ Characteristics of DM in BCP ALL miRNA gene bodies-associated sites are presented in Table 6. Interestingly, a few of the 483 potential target genes of the most hyper- and hypomethylated miRNAs are annotated to leukemia phenotype.

Among different genetic subtypes, only 1 subtype (3 patients) with the translocation t(1;19) generating the *TCF3-PBX1* fusion gene, had a distinct miRNA gene methylation profile. For this subtype there were 56 DM sites found, associated with 37 miRNA genes. Most of the sites were located in promoters and were hypomethylated. According to the previously published data, several miRNAs are downregulated or upregulated in *TCF3/PBX1*-positive ALL.^{50–52}

Herein, we have shown that the miRNA genes of pediatric BCP ALL patients are DM compared to controls. This epigenetic dysregulation seems to play an important role in controlling miRNA expression, therefore affecting the clinical course of BCP ALL. To date, several miRNAs have been observed to have altered expression in patient cohorts compared to healthy individuals, while several studies have identified specific miRNAs that can be used as biomarkers to diagnose ALL, classify it into subgroups and predict the prognosis.^{27,53–55} Moreover, hypermethylated genes can be targeted by hypomethylating agents, such as cytosine analogs, azacitidine or decitabine, which may open up new potential treatment options for this type of leukemia.^{56,57}

Limitations

In this study, we presented a methylation profile of genes for miRNAs in the bone marrow of BCP ALL and healthy subjects; however, due to major constraints, we were not able to determine the expression of DM miRNA genes. Thus, we had to refer to data regarding their expression level from other studies. The second limitation is using only one method for determining DNA methylation level. Additionally, for some of the analyzed miRNAs (i.e., the ones encoded in introns of mRNA genes) we were unable to determine if the observed methylation level of DNA is associated with the regulation of the miRNA or its host mRNA gene expression. However, this does not affect the main goal of this study, which was to select miRNA genes with the most altered methylation as targets for future studies. The last limitation is the small control group. This was due to the limited availability of the bone marrow samples from healthy children. The bone marrow aspiration is an invasive procedure, so performing it without clear medical indications would be highly unethical. Because of that, we were not able to obtain bone marrow samples from completely healthy children. On the other hand, only individuals with any cancer and genetic disease were ruled out, as well as with the normal bone marrow smears, were included in the control group.

Conclusions

In this study, a different were genes methylation landscape was shown in pediatric BCP ALL compared to children without neoplasms. A visible subcluster among BCP ALL samples consisted of individuals with TCF3-PBX1 genetic subtype. No other differences were observed in association with age, gender or risk group. Several interesting leukemia-connected phenotypes were found to be enriched in genes associated with hyper- and hypomethylated sites located on promoters as well as gene bodies.

ORCID iDs

Radosław Chaber  <https://orcid.org/0000-0002-6862-9142>
 Artur Gurgul  <https://orcid.org/0000-0001-5979-144X>
 Jacek Tabarkiewicz  <https://orcid.org/0000-0002-1264-2882>
 Grażyna Wróbel  <https://orcid.org/0000-0003-4374-6083>
 Tomasz Szmatoła  <https://orcid.org/0000-0003-1588-4198>
 Igor Jasielczuk  <https://orcid.org/0000-0001-8583-3850>
 Olga Haus  <https://orcid.org/0000-0002-5206-0553>
 Monika Lejman  <https://orcid.org/0000-0002-8760-0775>
 Blanka Rybka  <https://orcid.org/0000-0002-4216-0673>
 Renata Ryczan-Krawczyk  <https://orcid.org/0000-0002-4936-4951>
 Anna Jaśkowiec  <https://orcid.org/0000-0002-5966-3402>
 Sylwia Paszek  <https://orcid.org/0000-0002-7865-2661>
 Natalia Potocka  <https://orcid.org/0000-0002-5505-3922>
 Christopher J. Arthur  <https://orcid.org/0000-0001-9647-1509>
 Wioletta Bal  <https://orcid.org/0000-0003-4992-5322>
 Kornelia Łach  <https://orcid.org/0000-0001-8339-1374>
 Aneta Kowal  <https://orcid.org/0000-0002-5341-4851>
 Izabela Zawlik  <https://orcid.org/0000-0001-7992-9100>
 Elżbieta Latos-Grażyńska  <https://orcid.org/0000-0002-7154-3702>

References

1. Stiller CA, Kroll ME, Boyle PJ, Feng Z. Population mixing, socioeconomic status and incidence of childhood acute lymphoblastic leukaemia in England and Wales: Analysis by census ward. *Br J Cancer*. 2008;98(5):1006–1011. doi:10.1038/sj.bjc.6604237
2. Nordlund J, Syvänen AC. Epigenetics in pediatric acute lymphoblastic leukemia. *Semin Cancer Biol*. 2018;51:129–138. doi:10.1016/j.semcancer.2017.09.001
3. Deaton AM, Bird A. CpG islands and the regulation of transcription. *Genes Dev*. 2011;25(10):1010–1022. doi:10.1101/gad.2037511
4. Lau NC, Lim LP, Weinstein EG, Bartel DP. An abundant class of tiny RNAs with probable regulatory roles in *Caenorhabditis elegans*. *Science*. 2001;294(5543):858–862. doi:10.1126/science.1065062
5. Fernandes Q. MicroRNA: Defining a new niche in leukemia. *Blood Rev*. 2017;31(3):129–138. doi:10.1016/j.blre.2016.11.003
6. Tapeh BEG, Alivand MR, Solali S. The role of microRNAs in acute lymphoblastic leukaemia: From biology to applications. *Cell Biochem Funct*. 2020;38(4):334–346. doi:10.1002/cbf.3466
7. Ultimo S, Martelli AM, Zauli G, Vitale M, Calin GA, Neri LM. Roles and clinical implications of microRNAs in acute lymphoblastic leukemia. *J Cell Physiol*. 2018;233(8):5642–5654. doi:10.1002/jcp.26290
8. Rashed WM, Hamza MM, Matboli M, Salem SI. MicroRNA as a prognostic biomarker for survival in childhood acute lymphoblastic leukemia: A systematic review. *Cancer Metastasis Rev*. 2019;38(4):771–782. doi:10.1007/s10555-019-09826-0
9. Wang S, Wu W, Claret FX. Mutual regulation of microRNAs and DNA methylation in human cancers. *Epigenetics*. 2017;12(3):187–197. doi:10.1080/15592294.2016.1273308
10. Roman-Gomez J, Agirre X, Jimenez-Velasco A, et al. Epigenetic regulation of microRNAs in acute lymphoblastic leukemia. *J Clin Oncol*. 2009;27(8):1316–1322. doi:10.1200/JCO.2008.19.3441
11. Chaber R, Gurgul A, Wróbel G, et al. Whole-genome DNA methylation characteristics in pediatric precursor B cell acute lymphoblastic leukemia (BCP ALL). *PLoS One*. 2017;12(11):e0187422. doi:10.1371/journal.pone.0187422
12. Ozdemir ZC, Kar YD, Turhan AB, Bor O. Assessment of hematological toxicity in children with acute lymphoblastic leukemia, receiving treatment with ALL IC-BFM 2009 protocol. *OALib Journal*. 2017;4(8):e3807. doi:10.4236/oalib.1103807
13. Kozomara A, Griffiths-Jones S. miRBase: Annotating high confidence microRNAs using deep sequencing data. *Nucleic Acids Res*. 2014;42(D1):D68–D73. doi:10.1093/nar/gkt1181
14. Morris TJ, Butcher LM, Feber A, et al. ChAMP: 450k chip analysis methylation pipeline. *Bioinformatics*. 2014;30(3):428–430. doi:10.1093/bioinformatics/btt684
15. Smyth GK, Limma: Linear models for microarray data. In: Gentleman R, Carey V, Dudoit S, Irizarry R, Huber W, eds. *Bioinformatics and Computational Biology Solutions Using R and Bioconductor*. New York, USA: Springer; 2005:397–420.
16. Benjamini Y, Hochberg Y. Controlling the false discovery rate: A practical and powerful approach to multiple testing journal of the Royal Statistical Society. *J R Stat Soc Series B Stat Methodol*. 1995;57(1):289–300. doi:10.1111/j.2517-6161.1995.tb02031.x
17. Wang J, Duncan D, Shi Z, Zhang B. WEB-based GENE SeT Analysis Toolkit (WebGestalt): Update 2013. *Nucleic Acids Res*. 2013;41(W1):W77–W83. doi:10.1093/nar/gkt439
18. Köhler S, Vasilevsky N, Engelstad M, et al. The Human Phenotype Ontology in 2017. *Nucleic Acids Res*. 2017;45(D1):D865–D876. doi:10.1093/nar/gkw1039
19. Whirl-Carrillo M, McDonagh EM, Hebert JM, et al. Pharmacogenomics knowledge for personalized medicine. *Clin Pharmacol Ther*. 2012;92(4):414–417. doi:10.1038/clpt.2012.96
20. Wong N, Wang X. miRDB: An online resource for microRNA target prediction and functional annotations. *Nucleic Acids Res*. 2015;43(D1):D146–D152. doi:10.1093/nar/gku1104
21. Teschendorff AE, Menon U, Gentry-Maharaj A, et al. An epigenetic signature in peripheral blood predicts active ovarian cancer. *PLoS One*. 2009;4(12):e8274. doi:10.1371/journal.pone.0008274
22. Loginov VI, Rykov SV, Fridman MV, Braga EA. Methylation of miRNA genes and oncogenesis. *Biochemistry (Mosc)*. 2015;80(2):145–162. doi:10.1134/S0006297915020029

23. Weber B, Stresemann C, Brueckner B, Lyko F. Methylation of human MicroRNA genes in normal and neoplastic cells. *Cell Cycle*. 2007;6(9):1001–1005. doi:10.4161/cc.6.9.4209
24. Agirre X, Martínez-Climent JA, Odero MD, Prosper F. Epigenetic regulation of miRNA genes in acute leukemia. *Leukemia*. 2012;26(3):395–403. doi:10.1038/leu.2011.344
25. Hale V, Hale GA, Brown PA, Amankwah EK. A review of DNA methylation and microRNA expression in recurrent pediatric acute leukemia. *Oncology*. 2017;92(2):61–67. doi:10.1159/000452091
26. Memari F, Joneidi Z, Taheri B, Aval SF, Roointan A, Zarghami N. Epigenetics and Epi-miRNAs: Potential markers/therapeutics in leukemia. *Biomed Pharmacother*. 2018;106:1668–1677. doi:10.1016/j.biopha.2018.07.133
27. Grobbelaar C, Ford AM. The role of microRNA in paediatric acute lymphoblastic leukaemia: Challenges for diagnosis and therapy. *J Oncol*. 2019;3:1–14. doi:10.1155/2019/8941471
28. Chhabra R. miRNA and methylation: A multifaceted liaison. *Chem-biochem*. 2015;16(2):195–203. doi:10.1002/cbic.201402449
29. Burke MJ, Bhatla T. Epigenetic modifications in pediatric acute lymphoblastic leukemia. *Front Pediatr*. 2014;2:42. doi:10.3389/fped.2014.00042
30. Stumpel DJPM, Schotte D, Lange-Turenhout EAM, et al. Hypermethylation of specific microRNA genes in MLL-rearranged infant acute lymphoblastic leukemia: Major matters at a micro scale. *Leukemia*. 2011;25(3):429–439. doi:10.1038/leu.2010.282
31. Gregory PA, Bert AG, Paterson EL, et al. The miR-200 family and miR-205 regulate epithelial to mesenchymal transition by targeting ZEB1 and SIP1. *Nat Cell Biol*. 2008;10(5):593–601. doi:10.1038/ncb1722
32. Han L, Witmer PD, Casey E, Valle D, Sukumar S. DNA methylation regulates microRNA expression. *Cancer Biol Ther*. 2007;6(8):1284–1288. doi:10.4161/cbt.6.8.4486
33. Saito Y, Liang G, Egger G, et al. Specific activation of microRNA-127 with downregulation of the proto-oncogene BCL6 by chromatin-modifying drugs in human cancer cells. *Cancer Cell*. 2006;9(6):435–443. doi:10.1016/j.ccr.2006.04.020
34. Schotte D, Lange-Turenhout EAM, Stumpel DJPM, et al. Expression of miR-196b is not exclusively MLL-driven but especially linked to activation of HOXA genes in pediatric acute lymphoblastic leukemia. *Haematologica*. 2010;95(10):1675–1682. doi:10.3324%2Fhaematol.2010.023481
35. Rachagani S, Macha MA, Menning MS, et al. Changes in microRNA (miRNA) expression during pancreatic cancer development and progression in a genetically engineered KrasG12D;Pdx1-Cre mouse (KC) model. *Oncotarget*. 2015;6(37):40295–40309. doi:10.18632/oncotarget.5641
36. Li CG, Pu MF, Li CZ, et al. MicroRNA-1304 suppresses human non-small cell lung cancer cell growth in vitro by targeting heme oxygenase-1. *Acta Pharmacol Sin*. 2017;38(1):110–119. doi:10.1038/aps.2016.92
37. Zhao H, Shen J, Medico L, Wang D, Ambrosone CB, Liu S. A pilot study of circulating miRNAs as potential biomarkers of early stage breast cancer. *PLoS One*. 2010;5(10):e13735. doi:10.1371/journal.pone.0013735
38. Shi Y, Chen C, Zhang X, et al. Primate-specific miR-663 functions as a tumor suppressor by targeting PIK3CD and predicts the prognosis of human glioblastoma. *Clin Cancer Res*. 2014;20(7):1803–1813. doi:10.1158/1078-0432.CCR-13-2284
39. Yi C, Wang Q, Wang L, et al. MiR-663, a microRNA targeting p21(WAF1/CIP1), promotes the proliferation and tumorigenesis of nasopharyngeal carcinoma. *Oncogene*. 2012;31(41):4421–4433. doi:10.1038/onc.2011.629
40. Yan-Fang T, Jian N, Jun L, et al. The promoter of miR-663 is hypermethylated in Chinese pediatric acute myeloid leukemia (AML). *BMC Med Genet*. 2013;14(1):74. doi:10.1186/1471-2350-14-74
41. TargetScanHuman. Human miR-3687/4442. Accessed November 26, 2020.
42. Narayan N, Morenos L, Phipson B, et al. Functionally distinct roles for different miR-155 expression levels through contrasting effects on gene expression, in acute myeloid leukaemia. *Leukemia*. 2017;31(4):808–820. doi:10.1038/leu.2016.279
43. Marcucci G, Maharry KS, Metzeler KH, et al. Clinical role of microRNAs in cytogenetically normal acute myeloid leukemia: miR-155 upregulation independently identifies high-risk patients. *J Clin Oncol*. 2013;31(17):2086–2093. doi:10.1200/jco.2012.45.6228
44. Salemi D, Cammarata G, Agueli C, et al. miR-155 regulative network in FLT3 mutated acute myeloid leukemia. *Leuk Res*. 2015;39(8):883–896. doi:10.1016/j.leukres.2015.04.017
45. Farroni C, Marasco E, Marcellini V, et al. Dysregulated miR-155 and miR-125b are related to impaired B-cell responses in Down syndrome. *Front Immunol*. 2018;9:2683. doi:10.3389/fimmu.2018.02683
46. El-Khazragy N, Noshi MA, Abdel-Malak C, Zahran RF, Swellam M. miRNA-155 and miRNA-181a as prognostic biomarkers for pediatric acute lymphoblastic leukemia. *J Cell Biochem*. 2019;120(4):6315–6321. doi:10.1002/jcb.27918
47. Hassan SS, El-Khazragy N, Elshimy AA, et al. In vitro knock-out of miR-155 suppresses leukemic and HCV virus loads in pediatric HCV-4-associated acute lymphoid leukemia: A promising target therapy. *J Cell Biochem*. 2020;121(4):2811–2817. doi:10.1002/jcb.29512
48. Lorincz MC, Dickerson DR, Schmitt M, Groudine M. Intragenic DNA methylation alters chromatin structure and elongation efficiency in mammalian cells. *Nat Struct Mol Biol*. 2004;11(11):1068–1075. doi:10.1038/nsmb840
49. Bommarito PA, Fry RC. The role of DNA methylation in gene regulation. In: McCullough SD, Dolinoy DC, eds. *Toxicopigenetics*. London, UK: Elsevier; 2019:127–151. doi:10.1016/b978-0-12-812433-8.00005-8
50. Schotte D, De Menezes RX, Akbari Moqadam F, et al. MicroRNA characterize genetic diversity and drug resistance in pediatric acute lymphoblastic leukemia. *Haematologica*. 2011;96(5):703–711. doi:10.3324/haematol.2010.026138
51. Schotte D, Chau JCK, Sylvester G, et al. Identification of new microRNA genes and aberrant microRNA profiles in childhood acute lymphoblastic leukemia. *Leukemia*. 2009;23(2):313–322. doi:10.1038/leu.2008.286
52. Organista-Nava J, Gómez-Gómez Y, Illades-Aguar B, Leyva-Vázquez MA. Regulation of the miRNA expression by TEL/AML1, BCR/ABL, MLL/AF4 and TCF3/PBX1 oncoproteins in acute lymphoblastic leukemia (review). *Oncol Rep*. 2016;36(3):1226–1232. doi:10.3892/or.2016.4948
53. Nemes K, Csóka M, Nagy N, et al. Expression of certain leukemia/lymphoma related microRNAs and its correlation with prognosis in childhood acute lymphoblastic leukemia. *Pathol Oncol Res*. 2015;21(3):597–604. doi:10.1007/s12253-014-9861-z
54. Swellam M, Hashim M, Mahmoud MS, Ramadan A, Hassan NM. Aberrant expression of some circulating miRNAs in childhood acute lymphoblastic leukemia. *Biochem Genet*. 2018;56(4):283–294. doi:10.1007/s10528-018-9844-y
55. Nabhan M, Louka ML, Khairy E, Tash F, Ali-Labib R, El-Habashy S. MicroRNA-181a and its target Smad 7 as potential biomarkers for tracking child acute lymphoblastic leukemia. *Gene*. 2017;628:253–258. doi:10.1016/j.gene.2017.07.052
56. Roelf C, Richter A, Konkolefski C, et al. Decitabine demonstrates anti-leukemic activity in B cell precursor acute lymphoblastic leukemia with MLL rearrangements. *J Hematol Oncol*. 2018;11(1):62. doi:10.1186/s13045-018-0607-3
57. ClinicalTrials. Azacitidine and Combination Chemotherapy in Treating Infants With Acute Lymphoblastic Leukemia and KMT2A Gene Rearrangement. <https://clinicaltrials.gov/ct2/show/record/NCT02828358?view=record>. Accessed January 12, 2021.

Can monodisperse microbubble-based three-dimensional contrast-enhanced ultrasound reduce quantitative heterogeneity? An in vitro study

*Qiao Zheng^{1,A–F}, *Si-Min Ruan^{2,A–F}, Chun-Yang Zhang^{2,B,C}, Zhong Cao^{3,B,C}, Ze-Rong Huang^{2,E}, Huan-Ling Guo^{2,B,C}, Xiao-Yan Xie^{2,E,F}, Ming-De Lu^{2,4,E,F}, **Wei Wang^{2,A,E,F}, **Li-Da Chen^{2,A,E,F}

¹ Department of Medical Ultrasonics, Fetal Medical Center, The First Affiliated Hospital of Sun Yat-sen University, Guangzhou, China

² Department of Medical Ultrasonics, Ultrasonics Artificial Intelligence X-Lab, Institute of Diagnostic and Interventional Ultrasound, The First Affiliated Hospital of Sun Yat-sen University, Guangzhou, China

³ Department of Biomedical Engineering, School of Engineering, Sun Yat-sen University, Guangzhou, China

⁴ Department of Hepatobiliary Surgery, The First Affiliated Hospital of Sun Yat-sen University, Guangzhou, China

A – research concept and design; B – collection and/or assembly of data; C – data analysis and interpretation;

D – writing the article; E – critical revision of the article; F – final approval of the article

Advances in Clinical and Experimental Medicine, ISSN 1899–5276 (print), ISSN 2451–2680 (online)

Adv Clin Exp Med. 2022;31(3):307–315

Address for correspondence

Li-Da Chen

E-mail: chenlda@mail.sysu.edu.cn

Funding sources

Natural Science Foundation of China (Grant No. 81971630); Science and Technology Program of Guangzhou, China (Grant No. 201904010187); Kelin New Star Program for Talents of The First Affiliated Hospital of Sun Yat-sen University, Guangzhou, China (Grant No. Y50168).

Conflict of interest

None declared

* Qiao Zheng and Si-Min Ruan contributed equally to this work.

** Wei Wang and Li-Da Chen were co-corresponding authors to this work.

Received on June 11, 2021

Reviewed on October 28, 2021

Accepted on November 4, 2021

Published online on December 2, 2021

Cite as

Zheng Q, Ruan SM, Zhang CY, et al. Can monodisperse microbubble-based three-dimensional contrast-enhanced ultrasound reduce quantitative heterogeneity?

An in vitro study. *Adv Clin Exp Med.* 2022;31(3):307–315.

doi:10.17219/acem/143585

DOI

10.17219/acem/143585

Copyright

© 2022 by Wrocław Medical University

This is an article distributed under the terms of the Creative Commons Attribution 3.0 Unported (CC BY 3.0) (<https://creativecommons.org/licenses/by/3.0/>)

Abstract

Background. Heterogeneity within the tumor may cause large heterogeneity in quantitative perfusion parameters. Three-dimensional contrast-enhanced ultrasound (3D-CEUS) can show the spatial relationship of vascular structure after post-acquisition reconstruction and monodisperse bubbles can resonate the ultrasound pulse, resulting in the increase in sensitivity of CEUS imaging.

Objectives. To evaluate whether the combination of 3D-CEUS and monodisperse microbubbles could reduce the heterogeneity of quantitative CEUS.

Materials and methods. Three in vitro perfusion models with perfusion volume ratio of 1:2:4 were set up. Both quantitative 2D-CEUS and 3D-CEUS were used to acquire peak intensity (PI) with 2 kinds of ultrasound agents. One was a new kind of monodisperse bubbles produced in this study, named Octafluoropropane-loaded cerasomal microbubbles (OC-MBs), the other was SonoVue®. The coefficient of variation (CV) was calculated to evaluate the cross-sectional variability. Pearson's correlation analysis was used to assess the correlation between weighted PIs (average of PIs of 3 different planes) and perfusion ratios.

Results. The average CVs of quantitative 3D-CEUS was slightly lower than that of 2D-CEUS (0.41 ± 0.17 compared to 0.55 ± 0.26 , $p = 0.3592$). As for quantitative 3D-CEUS, the PI of the OC-MBs has shown better stability than that of SonoVue®, but without a significant difference (average CVs: 0.32 ± 0.19 compared to 0.50 ± 0.10 , $p = 0.0711$). In the 2D-CEUS condition, the average CVs of OC-MBs group and SonoVue® group were 0.68 ± 0.15 and 0.41 ± 0.17 ($p = 0.2747$). As for 3D-CEUS condition, using OC-MBs group and SonoVue®, the r-values of the weighted PI and perfusion ratio were 0.8685 and 0.5643, respectively, while that of 2D-CEUS condition were 0.7760 and 0.3513, respectively.

Conclusions. Our in vitro experiments showed that OC-MBs have the potential in acquiring more stable quantitative CEUS value, as compared to the SonoVue® in 3D-CEUS condition. The combination of 3D-CEUS and OC-MBs can reflect perfusion volume more precisely and may be a potential way to reduce quantitative heterogeneity.

Key words: ultrasonography, three-dimensional imaging, in vitro technique, contrast agent

Introduction

Contrast-enhanced ultrasound (CEUS) is a noninvasive imaging method, using ultrasound contrast agent (UCA) and low mechanical index (MI) ultrasound for dynamic blood perfusion observation in the target tissue. It has been applied in the detection and differential diagnosis of solid tumors, the assessment of nonsurgical treatment and the evaluation of left ventricular function. As is commonly known, one of the inherent limitations of CEUS is its subjectivity. In contrast with traditional CEUS, quantitative CEUS with dedicated software can detect lesions with abnormal perfusion more sensitively.¹ A multitude of quantitative parameters can be used as imaging biomarkers. They can improve the diagnostic efficacy as well as the detection rate of atypical lesions.^{2–4}

However, the quantitative CEUS faces 2 major dilemmas. First, the widely used quantitative two-dimensional CEUS (2D-CEUS) could only obtain a single plane of tumor perfusion.⁵ Due to tumor necrosis, hemorrhage and hypoxia, there is a large heterogeneity within the tumor, which leads to the complexity of blood supply of tumor. Quantitative 2D-CEUS could not fully demonstrate the spatial features of the tumor internal environment,⁶ which would result in greater heterogeneity of quantitative parameters in different planes.⁷ Second, commercially available UCA typically consists of a suspension of phospholipid-coated microbubbles with radius ranging from 1 μm to 10 μm in diameter.⁸ Upon exposure to ultrasound, the microbubbles oscillate and generate harmonic echoes, which make the visualization and quantification of organ perfusion possible. The strength of harmonic signal is proportional to the 6th power of the radius of UCA microbubble,⁹ which means that polydisperse microbubbles can also affect the quantitative results in CEUS. The monodisperse microbubble suspension is narrowband and has acoustically uniform response.¹⁰ Therefore, by using monodisperse bubbles resonating with ultrasound pulse, the sensitivity of CEUS imaging can be increased by 2 to 3 orders of magnitude.¹¹

Herein, we need to reduce the tumor quantitative heterogeneity taking into account 2 aspects. First, the three-dimensional CEUS (3D-CEUS) will be used to reconstruct the entire target lesion stereoscopically combining x, y and z axes through software and improve the accuracy of tumor angiogenesis quantification.¹² One of our previous in vitro studies has found that quantitative 3D-CEUS is more representative of the perfusion volume and with lower heterogeneity when compared with 2D-CEUS.⁷ Second, a new kind of monodisperse microbubbles (Octafluoropropane-loaded cerasomal microbubbles (OC-MBs))¹³ with uniform size and long sonographic duration will be used to resonate with ultrasound pulse.

Objectives

In this study, an in vitro model was designed to observe whether the combination of 3D-CEUS and monodisperse microbubbles can reduce the heterogeneity of quantitative CEUS.

Materials and methods

Materials

Hexadecylamine was obtained from Tokyo Pharmaron Industrial Co. (Tokyo, Japan). Bromohexadecane was obtained from Shanghai Aladdin Co. (Shanghai, China). Poly (sodium 4-styrenesulfonate) (PSS; $\sim 70,000$ MW), poly (allylamine hydrochloride) (PAH; $\sim 15,000$ MW) and methyl thiazolyl tetrazolium (MTT) were synthesized by Sigma–Aldrich (St. Louis, USA). Sodium carbonate (Na_2CO_3), calcium nitrate tetrahydrate ($\text{Ca}(\text{NO}_3)_2 \cdot 4\text{H}_2\text{O}$) and disodium ethylenediaminetetraacetate dihydrate (EDTA) were obtained from Guangzhou Chemical Reagent Factory (Guangzhou, China).

Fetal calf serum, tryptase, Dulbecco's modified Eagle's medium (DMEM) and Penicillin-Streptomycin were purchased from Thermo Fisher Scientific (Waltham, USA). Human umbilical vein endothelial cells (HUVEC) and HepG2 cells were purchased from Sun Yat-sen Animal Experimental Center (Guangzhou, China).

Synthesis of Si-lipid

The method of N-[N-(3-triethoxysilyl) propylsuccinamoyl] dihexadecylamine (Si-lipid) synthesis was reported previously.¹⁴

Preparation of CaCO_3 (PSS-PAH) microspheres

The PSS-doped CaCO_3 microspheres with uniform diameter were synthesized using colloidal aggregation of Na_2CO_3 and $\text{Ca}(\text{NO}_3)_2$.^{15,16} First, 590 mL of $\text{Ca}(\text{NO}_3)_2 \cdot 4\text{H}_2\text{O}$ (0.025 M) and 400 mg of PSS were combined as an aqueous solution, into which 265 mL of Na_2CO_3 (0.025 M) solution was rapidly added under magnetic agitation (600 rpm) for 15 s. Then, the solution was kept for 10 min at 15°C. The PSS-doped CaCO_3 microspheres were acquired and washed by centrifugation with deionized water (4000 rpm, 10 min). The adsorption of PAH onto the PSS-doped CaCO_3 microspheres was conducted in a 0.1 M NaCl solution with 80 mg of PAH. After 15 min, free-PAH was removed and the microbubbles were washed twice with deionized water. Then, CaCO_3 (PSS-PAH) microspheres were obtained.

Preparation of octafluoropropane(OFP)-loaded cerasomal microbubbles (OC-MBs)

The method of synthesis has been previously described.¹⁷ Under water bath sonication, 10 mg of Si-lipid dissolved in 200 μL of ethanol (pH = 3) was injected into 5 mL of CaCO_3 (PSS-PAH) (4 mg/mL) microsphere aqueous solution in a vial. After injection, the vial was kept in water bath sonication for 2 min. Then, the suspensions were incubated at room temperature for 12 h to form a siloxane network on the surface of the microspheres. The free Si-lipid was removed with centrifugation. The EDTA 2Na solution (0.2M) was utilized to remove the CaCO_3 core of the microspheres 3 times. The obtained microbubbles were freeze-dried with mannitol (10% w/w). Finally, the bottle was filled with OFP to acquire OC-MBs.

Characterization of OC-MBs

The morphology of 2 kinds of microbubbles (OC-MBs and SonoVue[®]) was observed using optical microscopy (CKX41; Olympus Corp., Tokyo, Japan). The OC-MBs were also observed with field emission scanning electron microscopy (FE-SEM, Zeiss-Ultra 55; Zeiss Co., Oberkochen, Germany). Twenty microliters of OC-MBs suspension was casted onto copper foil. Then, the specimens were sputtered with gold for 5–10 min and inspected using a FE-SEM with 10 kV accelerating voltage.

Hemolysis assay

The hemolysis assay was conducted according to the previous studies.^{18,19} Human red blood cells were separated from the whole blood through centrifugation for 10 min at 1500 rpm and purified with sterile isotonic phosphate-buffered saline (PBS) via 6 successive washes. The packed red blood cells were suspended in PBS buffer diluting to a concentration of $4.0 \times 10^8/\text{mL}$. Then, 0.5 mL of the diluted human red blood cell suspension was added to 1.5 mL of deionized water (positive control), sterile isotonic PBS (negative control) or PBS buffer containing OC-MBs with concentration of 50 $\mu\text{g}/\text{mL}$, 100 $\mu\text{g}/\text{mL}$, 200 $\mu\text{g}/\text{mL}$, 400 $\mu\text{g}/\text{mL}$, and 800 $\mu\text{g}/\text{mL}$, respectively. After gentle shaking, the samples were allowed to stand at 37°C for 2 h. Finally, after centrifugation for 10 min at 1500 rpm, the supernatants were measured at 541 nm using UV-DU730 absorption spectrophotometer (Beckman Coulter, Inc., Brea, USA) to analyze the release of hemoglobin. The hemolysis percentage of each group was calculated according to the following formula (Eq. 1)^{20,21}:

$$\text{percent hemolysis (\%)} = \frac{A_{\text{sample}} - A_{\text{negative}}}{A_{\text{positive}} - A_{\text{negative}}} \times 100 (\%) \quad (1)$$

where A_{sample} was the absorbance of the supernatant of the sample; A_{positive} was the absorbance of the supernatant of positive group (deionized water); and A_{negative} was the absorbance of the supernatant of negative group (PBS buffer).

Cytotoxicity of OC-MBs

The cytotoxicity of OC-MBs was evaluated using the standard MTT assay.²² The HUVECs and the HepG2 cells were seeded in each of two 96-well plates and cultured in DMEM with 10% fetal calf serum (v/v) overnight. Then, the cells were incubated for 24 h and 48 h in the presence of OC-MBs concentrations of 25 $\mu\text{g}/\text{mL}$, 50 $\mu\text{g}/\text{mL}$, 100 $\mu\text{g}/\text{mL}$, 200 $\mu\text{g}/\text{mL}$, 400 $\mu\text{g}/\text{mL}$, and 800 $\mu\text{g}/\text{mL}$, respectively. Fresh DMEM was added to the negative control group. Then, the culture medium was taken out and the cells were washed with PBS. Fresh medium (100 μL) and 20 μL of MTT assay (5.0 mg/mL) per well were added to all wells and the wells were incubated for 4 h. After removing the medium, the resultant formazan salt crystals were dissolved in 150 μL of dimethyl sulfoxide (DMSO) and analyzed on a microplate reader (Synergy 4; BioTek, Winooski, USA) at 570 nm. A pure DMSO empty group was also analyzed. The percent of cell survival rate was calculated using the following formula (Eq. 2):

$$\text{cell survival rate (\%)} = \frac{A_{\text{sample}} - A_{\text{empty}}}{A_{\text{positive}} - A_{\text{empty}}} \times 100 (\%) \quad (2)$$

where A_{sample} was the absorbance of supernatant of sample; A_{negative} was the absorbance of supernatant of negative group (fresh DMEM) and A_{empty} was the absorbance of supernatant of empty group (pure DMSO).

In vitro experiment of OC-MBs

Establishment of the in vitro model

Three polyvinyl chloride pipes with outer diameter of 2 mm and an inner diameter of 1 mm were divided into 3 parts (inflow part, perfusion model part and outflow part) with tin foil. The perfusion model was located in the middle of the tubes with a length of the pipe of 8 cm, 16 cm and 32 cm, respectively, to simulate the different blood supply levels of the tumor. The perfusion model was divided into annular (8 cm) and spherical (16 cm and 32 cm) model. The pipe could not be folded and the inner diameter was not to be too narrow. The volume ratio of the perfusion model was 1:2:4.

The perfusion model was fixed in a water tank with sound-absorbing sponges on the base of the tank (Fig. 1). The 3D ultrasonic probe was fixed upon the perfusion model below the water surface. The inflow end was connected to the syringe pump (WZ-50C6; Smiths Medical, Minneapolis, USA) to ensure that the contrast medium was perfused at a constant rate (200.0 mL/h). The outflow end was put into a 1000 mL beaker.

Image acquisition and quantitative analysis of CEUS

Contrast-enhanced ultrasound (CEUS) examinations were performed using an Aplio 500 ultrasound scanner (Toshiba Medical Systems, Tokyo, Japan) with a 3D imaging

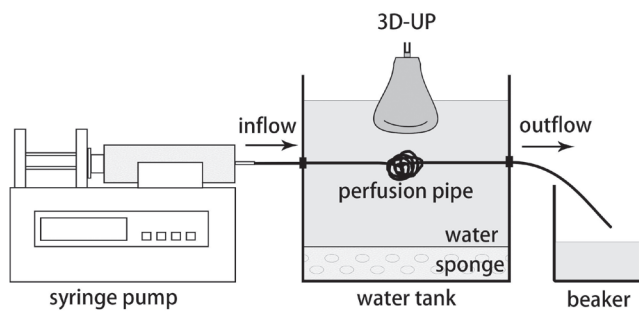


Fig. 1. Device schematic diagram of in vitro experiment

UP – ultrasonic probe.

probe (PVT375MV, frequency: 2–8 MHz; Toshiba Medical Systems). The probe was fixed with a shelf under the water surface and above the perfusion model. The maximum cross section of the perfusion model was regarded as the 0° plane. Then, the probe was rotated to obtain 45° plane and 90° plane images.

Two-dimensional ultrasound (2D-US), real-time 2D-CEUS and 3D-CEUS were performed in each plane. Two kinds of ultrasound contrast agents, including OC-MBs and SonoVue® (Bracco Imaging, Milan, Italy), were dissolved in 0.9% saline with microbubble concentration of $4 \times 10^6/\text{mL}$ and gently shaken until they became a milky white suspension. The UCA was injected through the inner tube at a constant speed of 200 mL/h. The duration of each imaging was 2 min and it was repeated 6 times. During the interval of each measurement, 0.9% saline was used to rinse the tubes in order to remove the microbubbles attaching on the tube wall, which might affect the experimental results. The original image data were stored for quantitative analysis.

The online software analysis package used was Aplio 500 v. 3.7 (CHI-Q) (Toshiba Medical Systems). This study focused on the peak intensity (PI), the maximum average peak intensity of flow perfusion in the region of interest (ROI). It has been reported that PI can accurately reflect

the blood volume of the tissue when the instrument settings and the UCA dose remain unchanged.²³

Statistical analysis

Continuous data following normal distribution were expressed as the mean \pm standard deviation (SD). The paired sample t-test was applied to evaluate the differences of the average of coefficient of variation (CV). Pearson's correlation analysis was used to determine the correlation between weighted PI (the average value of PI at 0°, 45° and 90° planes) and the 2 imaging methods, as well as the correlation between weighted PI and perfusion volume (1:2:4). The level of significance was set at a two-tailed $p < 0.05$. The statistical analysis was performed using IBM SPSS v. 22.0 software (IBM Corp., Armonk, USA).

Results

Homogeneity of OC-MBs

The image of the optical microscopy and the transmission electron microscopy (TEM) of OC-MBs were shown in Fig. 2A and Fig. 2B. The average diameter of OC-MBs was 2.0 μm , with high size uniformity. The image of the optical microscopy of SonoVue® suspension and OC-MBs were compared in Fig. 3A and Fig. 3B. The OC-MBs microbubbles had higher homogeneity.

Hemolysis assay and in vitro cytotoxicity of OC-MBs

The blood biocompatibility of OC-MBs should be considered for using as an UCA. Hemolysis assay was conducted to evaluate the blood compatibility. When hemolysis occurs, the hemoglobin presented in red blood cells will be released into solution, coloring it red. The density

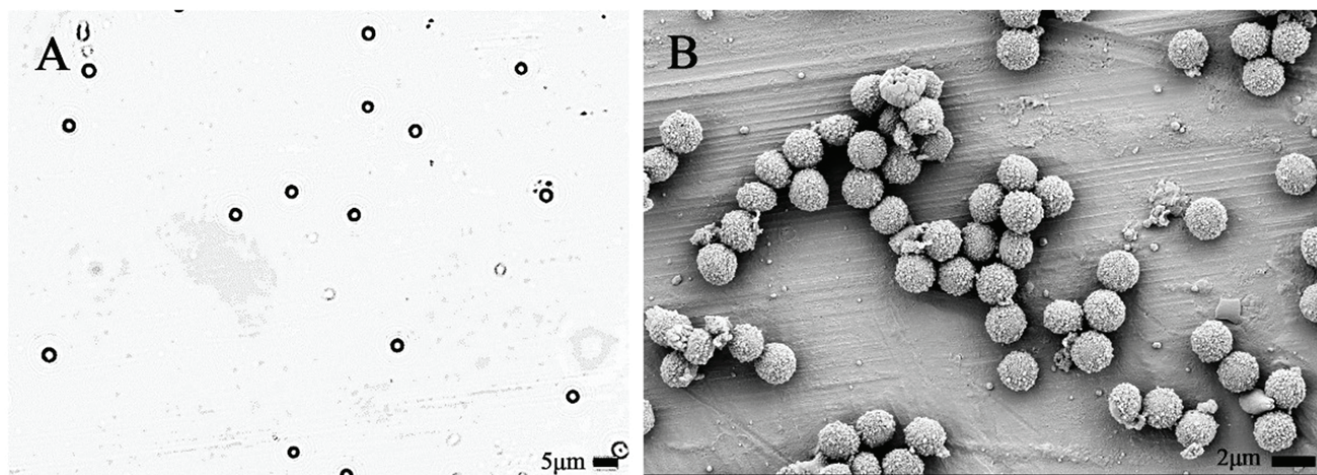


Fig. 2. Optical microscope image ($\times 400$) (A) and scanning electron microscopy image (B) of octafluoropropane-loaded cerasomal microbubbles (OC-MBs) of 2.0 μm

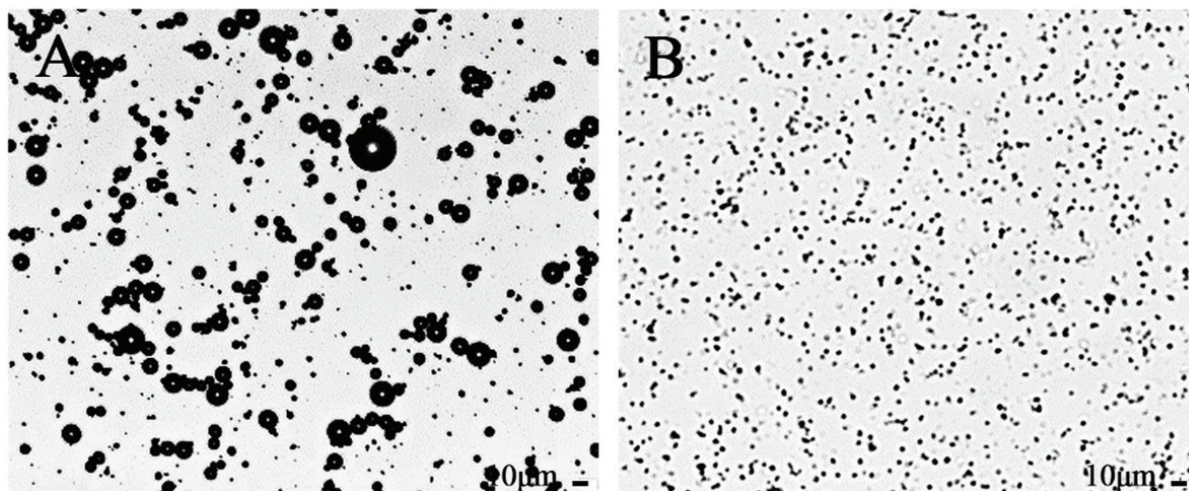


Fig. 3. Optical microscope image (x200) of SonoVue® (A) and octafluoropropane-loaded cerasomal microbubbles (OC-MBs) (B)

of this red color is correlated with hemolytic activity and can be estimated by measuring the ultraviolet (UV) absorbance of a supernatant at 541 nm. The tube with the highest concentration of OC-MBs (800 μg/mL) was light red (Fig. 4). The solution of concentration ranged from 50 μg/mL to 400 μg/mL and was nearly transparent. The OC-MBs only experienced approx. 1.3% hemolysis at the highest experimental concentration of 800 μg/mL (Fig. 4). Consequently, it can be concluded that OC-MBs have negligible hemolytic activity.

The cytotoxicity of an UCA is vital to its biomedical application. In vitro cytotoxicity was tested on HUVEC and HepG2 cell lines. An MTT assay was used to estimate the cytotoxicity of OC-MBs. As shown in Fig. 5, HUVECs retained 88% cell viability after incubation with

OC-MBs for 48 h at a high concentration of 800 μg/mL, while the cell viability of HepG2 cell was higher than 95%. The cell viability presented no significant difference when measurements at 24 h and 48 h were compared.

The OC-MBs present prominent biocompatibility and may have the potential to use them as a new UCAs in vivo.

Ultrasound images of 2 UCAs

The model had an irregular shape on the imaging plane, and the diameter of the tube was uniform in structure. The ultrasound images of 2 UCAs were shown in Fig. 6 (OC-MBs: A and B, SonoVue®: C and D). When 2D-CEUS was used, the signals were similar for both UCAs (Fig. 6A,C). Yet, for 3D-CEUS, OC-MBs group could obtain clearer signals as compared to SonoVue® group, and the boundary of the perfusion pipe was sharper in the OC-MBs group (Fig. 6B,D).

Variability of quantitative CEUS of 2 UCAs in 3 different sections

The PI values of different perfusion models, UCAs and CEUS mode are shown in Table 1 and Table 2. The PI of each model in different cross sections was the average of 6 measurements and was shown as the mean ±SD. Each CV was calculated with the SD and the mean of the PI of 3 different cross sections in the same perfusion model, CEUS mode and UCA. The average CV of 3D-CEUS was slightly lower than that of 2D-CEUS, without significant difference (0.41 ± 0.17 compared to 0.55 ± 0.26 , $p = 0.3592$, $T = -1.009$, degrees of freedom (df) = 5) (Table 3). When we used the 3D-CEUS, the average CVs of OC-MBs group and SonoVue® group were 0.32 ± 0.19 and 0.50 ± 0.10 , respectively. The PI of the OC-MBs has shown better stability than SonoVue®, but without significant difference ($p = 0.0711$, $T = -3.547$, $df = 2$). In the 2D-CEUS conditions, the average CVs of OC-MBs group and SonoVue® group were 0.68 ± 0.15 and 0.41 ± 0.17 ($p = 0.2747$, $T = 1.490$, $df = 2$), respectively.

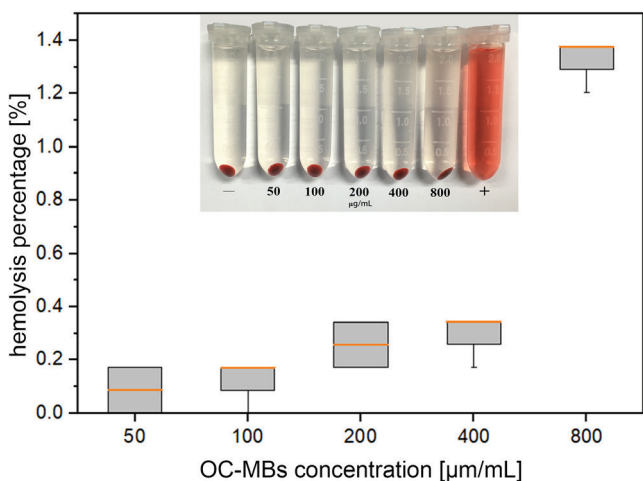


Fig. 4. Hemolysis caused by octafluoropropane-loaded cerasomal microbubbles (OC-MBs) at different concentrations. Deionized water was used as a positive control and phosphate-buffered saline (PBS) was used as a negative control. The data is shown in box and whisker plot format. The median value is displayed inside the “box” with orange line. The upper side and lower side of the “box” refer to the 1st quartile and the 3rd quartile. The maximum and minimum values are displayed with vertical lines connecting the points to the “box”

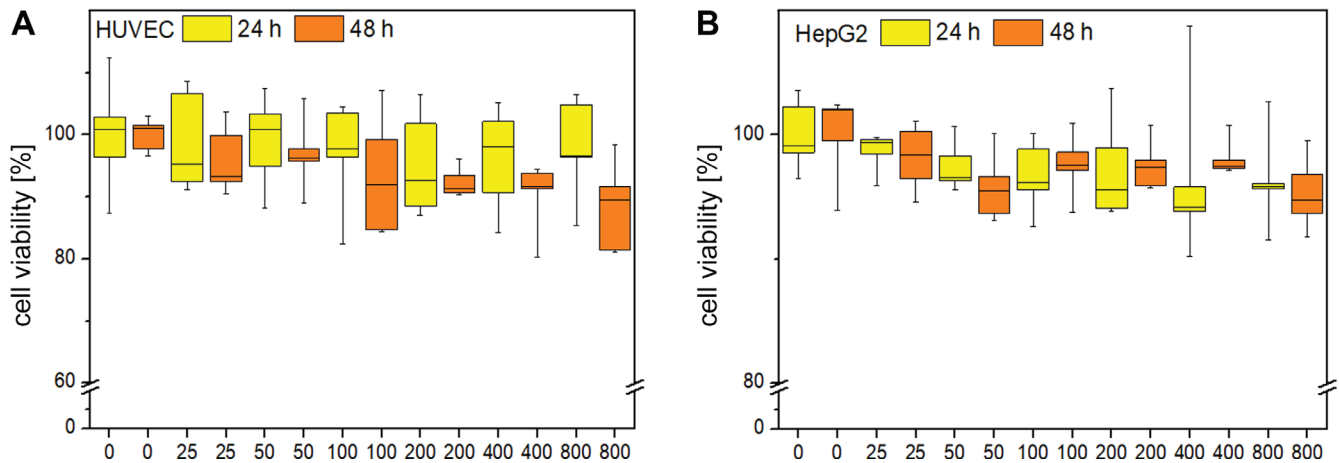


Fig. 5. In vitro cell viability of human umbilical vein endothelial cells (HUVEC) (A) and HepG2 cells (B) incubated with octafluoropropane-loaded cerasomal microbubbles (OC-MBs) at different concentrations for 24 h and 48 h. The data is shown in box and whisker plot format. The median value is displayed inside the “box” with brown line. The upper side and lower side of the “box” refer to the 1st quartile and the 3rd quartile. The maximum and minimum values are displayed with vertical lines connecting the points to the “box”. The yellow “box” refers to the results of 24 h, while the orange “box” refers to the results of 48 h

Table 1. The peak intensity (PI) values and coefficient of variation (CV) of 2 ultrasound contrast agents (UCA) in different perfusion models using 3D-CEUS

Length of perfusion model [cm]	UCA	PI (AU $\times 10^{-6}$)			CV
		0°	45°	90°	
8	OC-MBs	1.35 \pm 0.19	1.05 \pm 0.00	0.73 \pm 0.01	29.72%
	SonoVue®	0.20 \pm 0.13	0.19 \pm 0.00	0.42 \pm 0.00	49.16%
16	OC-MBs	3.36 \pm 0.13	4.51 \pm 0.16	4.08 \pm 0.11	14.58%
	SonoVue®	3.55 \pm 0.09	1.61 \pm 0.05	2.13 \pm 0.07	41.40%
32	OC-MBs	2.66 \pm 0.05	7.48 \pm 0.10	4.16 \pm 0.10	51.77%
	SonoVue®	1.67 \pm 0.12	0.84 \pm 0.01	3.07 \pm 0.00	60.71%

CEUS – contrast-enhanced ultrasound; OC-MBs – octafluoropropane-loaded cerasomal microbubbles.

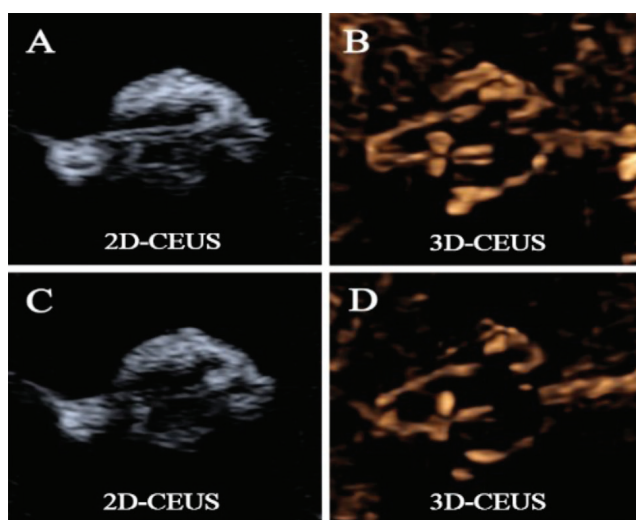


Fig. 6. Two-dimensional contrast-enhanced ultrasound (2D-CEUS) and three-dimensional contrast-enhanced ultrasound (3D-CEUS) images of 32 cm perfusion model: A,B. Octafluoropropane-loaded cerasomal microbubbles (OC-MBs); C,D: SonoVue®

Correlation between the actual perfusion volume and the weighted PI

In our study, the weighted PI was defined as the average PIs of 3 different planes (0°, 45° and 90°) in the same conditions. For 2D-CEUS, the weighted PIs of OC-MBs group of these 3 perfusion models were 0.92, 6.37 and 6.57, respectively, while the corresponding values of SonoVue® group were 0.57, 3.52 and 2.11, respectively. For 3D-CEUS, the weighted PIs of OC-MBs group were 0.96, 3.99 and 4.77, respectively. By contrast, the corresponding values of SonoVue® group were 0.27, 2.43 and 1.86, respectively (Table 4).

As the weighted PIs presented the normal distribution, the correlation between the weighted PI and the perfusion volume (1:2:4) of the in vitro model was evaluated with Pearson’s correlation analysis. As for 3D-CEUS conditions, the r-value of the weighted PI and perfusion ratio using OC-MBs group and SonoVue® were 0.8685 ($p = 0.3302$) and 0.5643 ($p = 0.6183$), respectively, while that of 2D-CEUS conditions were 0.7760 ($p = 0.4345$) and 0.3513 ($p = 0.7715$), respectively (Table 4). The OC-MBs group had higher correlation between the perfusion volume and quantitative CEUS value compared to the SonoVue® group

Table 2. The peak intensity (PI) values and coefficient of variation (CV) of 2 ultrasound contrast agents (UCA) in different perfusion model using 2D-CEUS

Length of perfusion model [cm]	UCA	PI (AU×10 ⁻⁴)			CV
		0°	45°	90°	
8	OC-MBs	1.55 ±0.00	1.00 ±0.01	0.20 ±0.00	73.75%
	SonoVue®	0.42 ±0.00	1.05 ±0.01	0.23 ±0.01	75.60%
16	OC-MBs	9.94 ±0.00	3.45 ±0.00	5.71 ±0.01	51.71%
	SonoVue®	3.12 ±0.00	2.77 ±0.00	4.68 ±0.11	28.94%
32	OC-MBs	2.89 ±0.00	12.66 ±0.00	4.17 ±0.16	80.78%
	SonoVue®	2.57 ±0.00	1.80 ±0.00	1.96 ±0.11	19.24%

CEUS – contrast-enhanced ultrasound; OC-MBs – octafluoropropane-loaded cerasomal microbubbles.

Table 3. Paired sample t-test was used to compare the mean CVs of 3D-CEUS and 2D-CEUS and mean CVs of OC-MBs group and SonoVue® group in the 3D-CEUS group and 2D-CEUS group

Values	CV of 3D-CEUS	CV of 2D-CEUS	3D-CEUS group		2D-CEUS group	
			CV of OC-MBs group	CV of SonoVue® group	CV of OC-MBs group	CV of SonoVue® group
Mean ±SD	0.41 ±0.17	0.55 ±0.26	0.32 ±0.19	0.50 ±0.10	0.68 ±0.15	0.41 ±0.17
T	-1.009		-3.547		1.490	
df	5		2		2	
p-value	0.3592		0.0711		0.2747	

CV – coefficient of variation; 2D-CEUS – two-dimensional contrast-enhanced ultrasound; 3D-CEUS – three-dimensional contrast-enhanced ultrasound; OC-MBs – octafluoropropane-loaded cerasomal microbubbles; SD – standard deviation; df – degrees of freedom.

Table 4. The weighted peak intensity (PI) (the average value of PI at 0°, 45° and 90° planes) values of different ultrasound contrast agents, perfusion models and contrast-enhanced ultrasound mode, and the correlation between weighted PIs and the perfusion volume. Pearson's correlation analysis was used to determine the correlation between weighted PI and perfusion volume (1:2:4)

Perfusion ratio	2D-CEUS (n = 3)		3D-CEUS (n = 3)	
	OC-MBs	SonoVue®	OC-MBs	SonoVue®
	weighted PI (AU×10 ⁻⁴)	weighted PI (AU×10 ⁻⁶)	weighted PI (AU×10 ⁻⁴)	weighted PI (AU×10 ⁻⁶)
1	0.92	0.57	0.96	0.27
2	6.37	3.52	3.99	2.43
4	6.57	2.11	4.77	1.86
r-value*	0.7760	0.3513	0.8685	0.5643
p-value	0.4345	0.7715	0.3302	0.6183

* r-value – correlation coefficient between weighted PI and perfusion volume (1:2:4); 2D-CEUS – two-dimensional contrast-enhanced ultrasound; 3D-CEUS – three-dimensional contrast-enhanced ultrasound; OC-MBs – octafluoropropane-loaded cerasomal microbubbles.

in 2D- and 3D-CEUS. The OC-MBs were technically feasible and they may have the potential to improve the accuracy of tumor perfusion assessment.

Discussion

The spatial distribution of blood vessels is closely related to the nature of the tumor. However, due to the necrosis, bleeding and hypoxia of the tumor, there is a large

heterogeneity within the tumor, which causes large intra-volume heterogeneities in quantitative perfusion parameters.²⁴ Two previous animal studies have shown that a small deviation in transducer position could result in quantitative errors up to 40.3%²⁵ and plane to plane variation of parametric perfusion maps could be up to 22%.²⁶ In order to solve this problem, real-time 3D-CEUS and monodisperse microbubbles were used to explore whether the measurement variation could be reduced and whether it could improve the correlation between quantitative analysis and actual blood flow.

With the help of contrast agent, the traditional 2D-CEUS greatly improves the ability of detecting tumor microvessels. However, 2D-CEUS only shows tumor blood vessels through a single plane and it cannot fully show its vascular characteristics if the blood vessels are rich or poorly positioned. The 3D-CEUS was developed to solve this problem. The 3D technique can show the spatial relationship of vascular structure after post-acquisition reconstruction. Previous study has shown that real-time 3D-CEUS could overcome sampling errors in tumors by imaging the tumor as a whole.^{27,28} However, based on the testing of our setup, the average CV of 3D-CEUS was slightly lower than that of 2D-CEUS (p = 0.3592) without significant difference. The reason might be that the perfusion model was not complex enough to simulate the internal structure of the tumor.

In the OC-MBs group, as well as in the SonoVue® group, the r-values of the weighted PI and perfusion ratio were higher when 3D-CEUS was used as compared to 2D-CEUS.

As 3D-CEUS could carry on with a volumetric imaging system, multiple planes could be captured simultaneously. The continuity and spatial relationships of the blood vessels were more clearly displayed with 3D-CEUS.⁶ As a result, the quantitative measurement from a single 3D plane is more representative than results obtained in 2D.²⁴

Another important component of CEUS is UCA. As a kind of phospholipid membrane microbubbles, SonoVue[®] can generate nonlinear harmonic signals under ultrasound scanning and has good contrast effects, which has been proven through research and has been widely used in 2D-CEUS.²⁹ In our preliminary studies, we found that for quantitative analysis, 3D-CEUS had better stability, accuracy and feasibility than 2D in both, in vitro as well as in vivo models.^{7,30} However, the phospholipid membrane of SonoVue[®] can easily burst under high energy ultrasonic irradiation and uneven particle size will affect the quantitative results. Therefore, in order to optimize the accuracy of quantitative 3D-CEUS, a new kind of monodisperse UCA with better stability is needed.

Si-lipid is a new type of organic-inorganic composite lipid synthesized from organic alkoxy silanes and lipid molecules. The double-layer vesicle structure with silica framework on the surface has higher morphological stability than traditional lipid vesicles. In recent years, there have been studies focused on the application of Si-lipid in UCA production.^{31–33} As for loaded gas, perfluorocarbon gas, such as OFP,³⁴ has extremely low water solubility and good biocompatibility, which can effectively prolong the durability of microbubbles.^{35,36} Therefore, in this study, Si-lipid and OFP were chosen to prepare OC-MBs. The CaCO₃ template method was applied to maintain the uniformity of microbubble size. Our study showed that the OC-MBs microbubbles had higher homogeneity with size distribution of 2.0 μm. As a new kind of ultrasound contrast agent, the cytotoxicity and blood biocompatibility are vital to its biomedical application. The OC-MBs have negligible hemolytic activity, present prominent biocompatibility and may have the potential to be used as new UCAs in vivo.

In the present study, under the condition that the microbubble concentration was controlled at about 4×10⁶/mL, the imaging effects of both SonoVue[®] and OC-MBs group had no significant difference in 2D-CEUS; as for 3D-CEUS, the continuity, integrity and signal strength of the phantom were significantly better in OC-MBs group than those of the SonoVue[®] group (Fig. 6). After quantitative analysis, the PI of the OC-MBs has shown better stability than SonoVue[®] in 3D-CEUS condition (Table 1). It shows that under the protection of silica framework, OC-MBs have better stability and imaging capability than SonoVue[®]. The results of the Pearson's linear correlation test show that there was a linear correlation trend between the quantitative results and the actual perfusion volume, and compared with SonoVue[®], OC-MBs have a trend of optimizing quantitative CEUS.




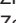
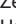




Limitations

We acknowledge several limitations of this study. First, the acoustic properties of the silicone tube used in the in vitro model are still different from the blood vessel. If better materials are to be found in the future, it is expected to reduce the impact of sound attenuation on the results. Second, only 3 in vitro models were used in this study, and more models should be involved to mimic the heterogeneity of in vivo target.

Conclusions

In the present study, we successfully prepared monodisperse OFP-loaded cerasomal microbubbles (OC-MBs) with high stability, size uniformity and biocompatibility. Our in vitro experiments showed that OC-MBs have the potential in acquiring more stable quantitative CEUS value, as compared to the SonoVue[®] in 3D-CEUS condition. The combination of 3D-CEUS and OC-MBs can reflect perfusion volume more precisely and may be a potential way to reduce quantitative heterogeneity.

ORCID iDs

Qiao Zheng  <https://orcid.org/0000-0002-3040-2137>
 Si-Min Ruan  <https://orcid.org/0000-0002-1121-3664>
 Chun-Yang Zhang  <https://orcid.org/0000-0002-4696-0176>
 Zhong Cao  <https://orcid.org/0000-0003-4004-1037>
 Ze-Rong Huang  <https://orcid.org/0000-0003-3388-8571>
 Huan-Ling Guo  <https://orcid.org/0000-0002-5806-5339>
 Xiao-Yan Xie  <https://orcid.org/0000-0002-9761-9525>
 Ming-De Lu  <https://orcid.org/0000-0002-9771-8144>
 Wei Wang  <https://orcid.org/0000-0002-9485-583X>
 Li-Da Chen  <https://orcid.org/0000-0001-9904-2195>

References

- Jung EM, Wiggermann P, Greis C, et al. First results of endocavity evaluation of the microvascularization of malignant prostate tumors using contrast enhanced ultrasound (CEUS) including perfusion analysis: First results. *Clin Hemorheol Microcirc.* 2012;52(2–4): 167–177. doi:10.3233/CH-2012-1594
- Shan QY, Chen LD, Zhou LY, et al. Focal lesions in fatty liver: If quantitative analysis facilitates the differentiation of atypical benign from malignant lesions. *Sci Rep.* 2016;6:18640. doi:10.1038/srep18640
- Kapetas P, Clauser P, Woitek R, et al. Quantitative multiparametric breast ultrasound: Application of contrast-enhanced ultrasound and elastography leads to an improved differentiation of benign and malignant lesions. *Invest Radiol.* 2019;54(5):257–264. doi:10.1097/RLI.0000000000000543
- Maxeiner A, Fischer T, Schwabe J, et al. Contrast-enhanced ultrasound (CEUS) and quantitative perfusion analysis in patients with suspicion for prostate cancer. *Ultraschall Med.* 2019;40(3):340–348. doi:10.1055/a-0594-2093
- Williams R, Hudson JM, Lloyd BA, et al. Dynamic microbubble contrast-enhanced US to measure tumor response to targeted therapy: A proposed clinical protocol with results from renal cell carcinoma patients receiving antiangiogenic therapy. *Radiology.* 2011;260(2): 581–590. doi:10.1148/radiol.11101893
- Dong FJ, Xu JF, Du D, et al. 3D analysis is superior to 2D analysis for contrast-enhanced ultrasound in revealing vascularity in focal liver lesions: A retrospective analysis of 83 cases. *Ultrasonics.* 2016;70: 221–226. doi:10.1016/j.ultras.2016.05.007

7. Ruan SM, Zheng Q, Wang Z, et al. Comparison of real-time two-dimensional and three-dimensional contrast-enhanced ultrasound to quantify flow in an in vitro model: A feasibility study. *Med Sci Monit*. 2019;25:10029–10035. doi:10.12659/msm.919160
8. Stride E, Saffari N. Microbubble ultrasound contrast agents: A review. *Proc Inst Mech Eng H*. 2003;217(6):429–447. doi:10.1243/09544110360729072
9. Kollmann C, Putzer M. Ultrasound contrast agents: Physical basics [in German]. *Radiologe*. 2005;45(6):503–512. doi:10.1007/s00117-005-1188-z
10. Frinking P, Segers T, Luan Y, Tranquart F. Three decades of ultrasound contrast agents: A review of the past, present and future improvements. *Ultrasound Med Biol*. 2020;46(4):892–908. doi:10.1016/j.ultrasmedbio.2019.12.008
11. Segers T, Kruijzinga P, Kok MP, Lajoinie G, de Jong N, Versluis M. Mono-disperse versus polydisperse ultrasound contrast agents: Non-linear response, sensitivity, and deep tissue imaging potential. *Ultrasound Med Biol*. 2018;44(7):1482–1492. doi:10.1016/j.ultrasmedbio.2018.03.019
12. Chen M, Wang WP, Jia WR, et al. Three-dimensional contrast-enhanced sonography in the assessment of breast tumor angiogenesis: Correlation with microvessel density and vascular endothelial growth factor expression. *J Ultrasound Med*. 2014;33(5):835–846. doi:10.7863/ultra.33.5.835
13. Zhang C, Wang Z, Wang C, et al. Highly uniform perfluoropropane-loaded cerasomal microbubbles as a novel ultrasound contrast agent. *ACS Appl Mater Interfaces*. 2016;8(24):15024–15032. doi:10.1021/acsami.5b03668
14. Katagiri K, Hashizume M, Ariga K, Terashima T, Kikuchi J. Preparation and characterization of a novel organic-inorganic nanohybrid “cerasome” formed with a liposomal membrane and silicate surface. *Chemistry*. 2007;13(18):5272–5281. doi:10.1002/chem.200700175
15. Zhang CY, Cao Z, Zhu WJ, Liu J, Jiang Q, Shuai XT. Highly uniform and stable cerasomal microcapsule with good biocompatibility for drug delivery. *Colloids Surf B Biointerfaces*. 2014;116:327–333. doi:10.1016/j.colsurfb.2014.01.013
16. Tong W, Dong W, Gao C, Mohwald H. Charge-controlled permeability of polyelectrolyte microcapsules. *J Phys Chem B*. 2005;109(27):13159–13165. doi:10.1021/jp0511092
17. Zhang C, Wang Z, Wang C, et al. Highly uniform perfluoropropane-loaded cerasomal microbubbles as a novel ultrasound contrast agent. *ACS Appl Mater Interfaces*. 2016;8(24):15024–15032. doi:10.1021/acsami.5b03668
18. Schellinger JG, Pahang JA, Johnson RN, et al. Melittin-grafted HPMA-oligolysine based copolymers for gene delivery. *Biomaterials*. 2013;34(9):2318–2326. doi:10.1016/j.biomaterials.2012.09.072
19. Parnham MJ, Wetzig H. Toxicity screening of liposomes. *Chem Phys Lipids*. 1993;64(1–3):263–274. doi:10.1016/0009-3084(93)90070-j
20. Saxena V, Diaz A, Clearfield A, Batteas JD, Hussain MD. Zirconium phosphate nanoplatelets: A biocompatible nanomaterial for drug delivery to cancer. *Nanoscale*. 2013;5(6):2328–2336. doi:10.1039/c3nr34242e
21. Shen M, Cai H, Wang X, et al. Facile one-pot preparation, surface functionalization, and toxicity assay of APTS-coated iron oxide nanoparticles. *Nanotechnology*. 2012;23(10):105601. doi:10.1088/0957-4484/23/10/105601
22. Fischer D, Li YX, Ahlemeyer B, Krieglstein J, Kissel T. In vitro cytotoxicity testing of polycations: Influence of polymer structure on cell viability and hemolysis. *Biomaterials*. 2003;24(7):1121–1131. doi:10.1016/s0142-9612(02)00445-3
23. Lassau N, Chami L, Benatsou B, Peronneau P, Roche A. Dynamic contrast-enhanced ultrasonography (DCE-US) with quantification of tumor perfusion: A new diagnostic tool to evaluate the early effects of antiangiogenic treatment. *Eur Radiol*. 2007;17(Suppl 6):F89–F98. doi:10.1007/s10406-007-0233-6
24. El Kaffas A, Sigrist RMS, Fisher G, et al. Quantitative three-dimensional dynamic contrast-enhanced ultrasound imaging: First-in-human pilot study in patients with liver metastases. *Theranostics*. 2017;7(15):3745–3758. doi:10.7150/thno.20329
25. Hoyt K, Sorace A, Saini R. Quantitative mapping of tumor vascularity using volumetric contrast-enhanced ultrasound. *Invest Radiol*. 2012;47(3):167–174. doi:10.1097/RLI.0b013e318234e6bc
26. Feingold S, Gessner R, Guracar IM, Dayton PA. Quantitative volumetric perfusion mapping of the microvasculature using contrast ultrasound. *Invest Radiol*. 2010;45(10):669–674. doi:10.1097/RLI.0b013e3181ef0a78
27. Wang HJ, Hristov D, Qin JL, Tian L, Willmann JK. Three-dimensional dynamic contrast-enhanced US imaging for early antiangiogenic treatment assessment in a mouse colon cancer model. *Radiology*. 2015;277(2):424–434. doi:10.1148/radiol.2015142824
28. Wang H, Kaneko OF, Tian L, Hristov D, Willmann JK. Three-dimensional ultrasound molecular imaging of angiogenesis in colon cancer using a clinical matrix array ultrasound transducer. *Invest Radiol*. 2015;50(5):322–329. doi:10.1097/RLI.0000000000000128
29. Leong-Poi H, Song J, Rim SJ, Christiansen J, Kaul S, Lindner JR. Influence of microbubble shell properties on ultrasound signal: Implications for low-power perfusion imaging. *J Am Soc Echocardiogr*. 2002;15(10 Pt 2):1269–1276. doi:10.1067/mje.2002.124516
30. Zheng Q, Zhang JC, Wang Z, et al. Assessment of angiogenesis in rabbit orthotopic liver tumors using three-dimensional dynamic contrast-enhanced ultrasound compared with two-dimensional DCE-US. *Jpn J Radiol*. 2019;37(10):701–709. doi:10.1007/s11604-019-00861-z
31. Katagiri K, Hamasaki R, Ariga K, Kikuchi J. Layered paving of vesicular nanoparticles formed with cerasome as a bioinspired organic-inorganic hybrid. *J Am Chem Soc*. 2002;124(27):7892–7893. doi:10.1021/ja0259281
32. Liang XL, Gao J, Jiang LD, et al. Nanohybrid liposomal cerasomes with good physiological stability and rapid temperature responsiveness for high intensity focused ultrasound triggered local chemotherapy of cancer. *ACS Nano*. 2015;9(2):1280–1293. doi:10.1021/nn507482w
33. Steinberg Y, Schroeder A, Talmon Y, et al. Triggered release of aqueous content from liposome-derived sol-gel nanocapsules. *Langmuir*. 2007;23(24):12024–12031. doi:10.1021/la702311f
34. Koch M, Franck CM. Partial discharges and breakdown in C3F8. *J Phys D Appl Phys*. 2014;47(40):11. doi:10.1088/0022-3727/47/40/405203
35. Kabalnov A, Bradley J, Flaim S, et al. Dissolution of multicomponent microbubbles in the bloodstream: 2. Experiment. *Ultrasound Med Biol*. 1998;24(5):751–760. doi:10.1016/s0301-5629(98)00033-7
36. Kabalnov A, Klein D, Pelura T, Schutt E, Weers J. Dissolution of multicomponent microbubbles in the bloodstream: 1. Theory. *Ultrasound Med Biol*. 1998;24(5):739–749. doi:10.1016/s0301-5629(98)00034-9

Acute kidney injury in patients with COVID-19: Epidemiology, pathogenesis and treatment

Marcin Adamczak^{A-F}, Stanisław Surma^{B-D}, Andrzej Więcek^{E,F}

Department of Nephrology, Transplantation and Internal Medicine, Medical University of Silesia, Katowice, Poland

A – research concept and design; B – collection and/or assembly of data; C – data analysis and interpretation; D – writing the article; E – critical revision of the article; F – final approval of the article

Advances in Clinical and Experimental Medicine, ISSN 1899–5276 (print), ISSN 2451–2680 (online)

Adv Clin Exp Med. 2022;31(3):317–326

Address for correspondence

Marcin Adamczak
E-mail: madamczak1@op.pl

Funding sources

None declared

Conflict of interest

None declared

Received on May 27, 2021

Reviewed on October 22, 2021

Accepted on November 2, 2021

Published online on January 25, 2022

Abstract

Acute kidney injury occurs in about 30% of patients hospitalized with coronavirus disease 2019 (COVID-19) and is one of the most common extrapulmonary complications of this disease. The highest risk of acute kidney injury is found in hospitalized patients who require mechanical ventilation. The pathogenesis of acute kidney injury in COVID-19 is multifactorial and seems to not be fully understood. Both direct and indirect mechanisms of kidney injury caused by severe acute respiratory syndrome coronavirus 2 (SARS-CoV-2) should be considered. The histological picture of kidney specimens obtained from patients with acute kidney injury in the course of COVID-19 is dominated by acute tubular necrosis. Some patients also have acute interstitial nephritis, blood clots in the kidney vessels and focal segmental glomerulosclerosis (the variant with collapsing vascular loops). Acute kidney injury in COVID-19 is primarily caused not by direct viral effect, but by indirect pathophysiological mechanisms. The histopathological findings in these patients does not differ from the majority of the other patients with acute kidney injury. The main pathophysiological mechanisms underlying acute kidney injury in COVID-19 are: hemodynamic abnormalities, hypoxia and cytokine storm. The methods of treating the underlying disease, i.e., COVID-19 in patients with acute kidney injury and those without acute kidney injury are similar. However, it should be stressed that in the treatment of COVID-19 accompanied by acute kidney injury, the contraindication to remdesivir is estimated using glomerular filtration rate (eGFR) <30 mL/min/1.73 m². The general principles of management in patients with both, COVID-19 and acute kidney injury do not differ from the principles of management in patients with acute kidney injury due to the other causes.

Key words: acute kidney injury, COVID-19, SARS-CoV-2

Cite as

Adamczak M, Surma S, Więcek A. Acute kidney injury in patients with COVID-19: Epidemiology, pathogenesis and treatment. *Adv Clin Exp Med.* 2022;31(3):317–326. doi:10.17219/acem/143542

DOI

10.17219/acem/143542

Copyright

© 2022 by Wrocław Medical University

This is an article distributed under the terms of the Creative Commons Attribution 3.0 Unported (CC BY 3.0) (<https://creativecommons.org/licenses/by/3.0/>)

Introduction

Severe acute respiratory syndrome coronavirus 2 (SARS-CoV-2) was first identified in December 2019 in Wuhan, China. This coronavirus belongs to the zoonotic viruses, and its genetic material is single-stranded ribonucleic acid (RNA). The SARS-CoV-2 causes coronavirus disease 2019 (COVID-19), which is an acute infectious disease of the respiratory system. The disease was declared a global pandemic by the World Health Organization (WHO) on 11 March, 2020. Coronavirus disease 2019 is characterized by a mortality of about 3% and an usual transmission rate (the number of newly infected persons per previously infected person) of about 2.5–3.0.¹

Objectives

The purpose of this article was to present data on the effects of COVID-19 on the kidneys based on a review of the current literature. The review specifically considers the effect of COVID-19 on the risk of developing acute kidney injury and the risk of renal replacement therapy.

Pathogenesis and clinical manifestations of COVID-19

From the pathophysiological point of view, it is important to note that SARS-CoV-2 has a lipophilic envelope that determines its way of spreading inside the infected organism and the spike (S) protein, which is involved in the penetration of virus inside the cell.¹ The SARS-CoV-2 mainly infects bronchial epithelial cells and type II pneumocytes, where it binds to the surface receptor, angiotensin-converting enzyme type 2 (ACE2).¹ The SARS-CoV-2 spreads in the human body due to its lipophilic properties, mainly through continuity, but not through blood. This is confirmed by the analyses completed by the Chinese Center for Disease Control and Prevention. The greatest amount of SARS-CoV-2 RNA has been detected in the lavage from the bronchial tree, then in the sputum, nasal discharge, pharyngeal discharge and feces. In this study, using the reverse transcription polymerase chain reaction (RT-PCR), viremia in the blood was detected only in trace amounts and no SARS-CoV-2 RNA was found in the urine (i.e., viruria).² Similar results were obtained by Wu et al. in a study involving 132 patients with COVID-19, where viremia was found only in 4 patients (3%).³ The analysis by Peng et al. of urine and blood samples in 9 patients with COVID-19 and moderately severe symptoms showed that SARS-CoV-2 RNA was present in only 2 blood samples and in only 1 urine sample.⁴ The SARS-CoV-2 RNA was not found in urine samples collected from 10 patients with COVID-19 (almost half of whom required oxygen therapy during hospitalization).⁵

Similarly, in the study by Wölfel et al. involving 9 patients with moderately severe COVID-19, no SARS-CoV-2 RNA was found in the blood or urine during the entire hospitalization period.⁶ Wang et al. analyzed the occurrence of SARS-CoV-2 RNA in 307 blood samples and 72 urine samples taken from 205 patients with COVID-19 (nearly 20% of them were characterized by a severe course of the disease). The SARS-CoV-2 RNA in the blood was found in only 1% of the samples, while it was not found in the urine.⁷ In another study, viremia was found in approx. 15% of patients with severe COVID-19.⁸

The SARS-CoV-2 viremia seems to be a factor that worsens the prognosis in patients with COVID-19. In the study by Tan et al. involving 33 patients with COVID-19, viremia was found in 4 of them. The clinical status of patients with viremia deteriorated rapidly due to septic shock.⁹ In the study by Fajnzylber et al., which included 88 hospitalized patients with COVID-19, in 27% of them SARS-CoV-2 RNA was found in the blood. Patients with viremia were characterized by a greater severity of respiratory disease symptoms, a lower number of lymphocytes in the blood, and a higher concentration of both, C-reactive protein (CRP) and interleukin 6 (IL-6) in the plasma. Moreover, among these patients, the mortality was higher than in patients without viremia (32% compared to 8%, respectively; odds ratio (OR) = 5.5; $p = 0.02$).¹⁰

In the course of COVID-19, there are 3 phases of varying severity of disease, covering the time from the onset of disease to a recovery or death (Fig. 1).¹¹

The 1st phase covers the onset of the disease and is characterized by mild to moderate flu-like symptoms. The dominant symptoms in the 2nd phase are associated with the development of pneumonia (connected to hypoxemia and dyspnea). Patients in the 3rd phase suffer from severe, generalized inflammation and symptoms of sepsis. These patients require hospitalization in the intensive care unit (ICU). High mortality is observed in patients in the 3rd phase of the disease.¹¹ The severity of the course, the type of clinical symptoms, and the mortality in the course of COVID-19 depend on age (greater severity over the age of 65) and comorbidities (mainly diabetes, cardiovascular diseases including hypertension, chronic lung diseases and chronic kidney diseases).¹¹

Epidemiology and clinical characteristics of acute kidney injury in patients with COVID-19

Acute kidney injury is one of the most common beyond pulmonary complications of COVID-19.¹² Patients with acute kidney injury in the course of COVID-19 are characterized by high mortality. According to the epidemiological studies, the incidence of acute kidney injury in COVID-19 varies greatly depending on the population

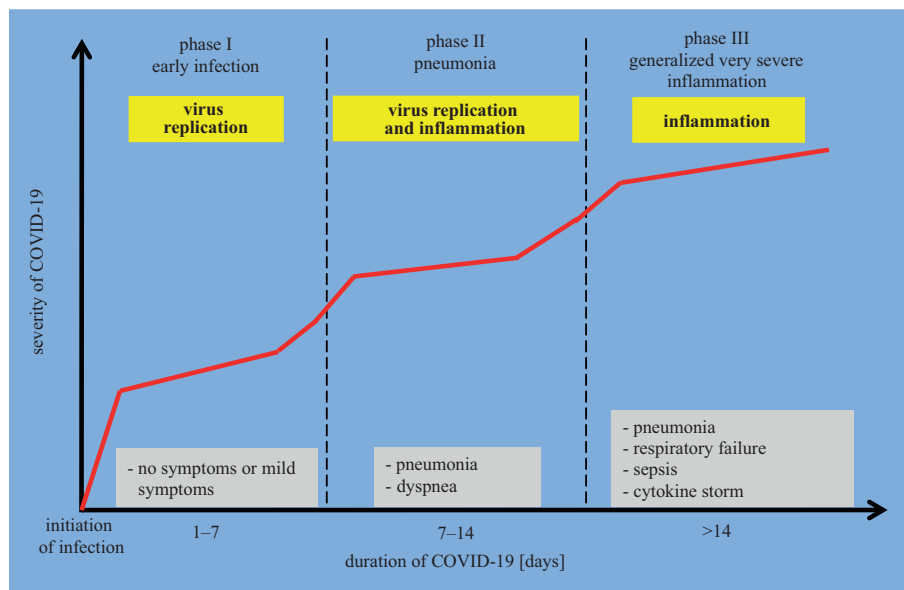


Fig. 1. Course of coronavirus disease 2019 (COVID-19) in severe cases

studied and the region of the world from which the published data is derived (Table 1).

A study by Fisher et al. comparing the incidence of acute kidney injury in hospitalized patients with and without COVID-19 showed a higher incidence of acute kidney injury in patients with COVID-19, when compared to the control group (56.9% compared to 25.1%, respectively).¹⁷ A literature review by Hassanein et al. showed that acute kidney injury occurred in 0.5–56.9% of hospitalized COVID-19 patients.²³ The differences in the incidence of acute kidney injury in COVID-19 depending on the location of the study and the timing of the observation (i.e., early studies from Asia, later studies from Europe and the United States) were shown in a meta-analysis by Fu et al. They found that in China (a meta-analysis of 62 studies), the incidence of acute kidney injury in hospitalized COVID-19 patients was 5.6%. In contrast, a meta-analysis of 20 studies conducted in Europe and the United States showed that the incidence of acute kidney injury in hospitalized COVID-19 patients was 28.6%.²⁴ Similar results

were presented by Lin et al. in a meta-analysis of 79 studies, showing that the incidence of acute kidney injury in patients with COVID-19 was 4.3%, 11.6% and 22.6% in Asia, Europe, and the United States, respectively.²⁵ A meta-analysis of 39 clinical trials (n = 25,566) by Fabrizi et al. showed that the incidence of acute kidney injury in hospitalized patients with COVID-19 was 15.4% (95% confidence interval (95% CI): 10.7–20.1%; p < 0.0001).²⁶ Another meta-analysis of 26 studies (n = 5,497) by Hansrivijit et al. showed that the incidence of acute kidney injury in hospitalized patients with COVID-19 was 8.4% (95% CI: 6.0–11.7%).²⁷

Acute kidney injury in the course of COVID-19 can occur at any stage of the disease, but it is most often found in the 3rd phase (Table 2). Predominantly, it develops in patients at the onset of artificial ventilation.^{16,20} In a study by Hirsch et al. including 5,449 patients with COVID-19 hospitalized in 13 hospitals in New York (USA), it was shown that acute kidney damage occurred in as many as 90% of patients who required artificial ventilation. However, in those who did not require it, this

Table 1. Epidemiology of acute kidney injury in the course of coronavirus disease 2019 (COVID-19) in hospitalized patients^{13–22}

Authors	Number of hospitalized patients with COVID-19	Country of origin	Analyzed period	Prevalence of acute kidney injury in hospitalized patients	Necessity of kidney replacement therapy in hospitalized patients
Shi et al.	416	China	I–II 2020	1.9%	0.4%
Cheng et al.	1392	China	I–II 2020	7.1%	1.1%
Portoles et al.	1603	Spain	II–IV 2020	20.8%	1.1%
Chan et al.	3235	USA	II–IV 2020	43.4%	8.7%
Fisher et al.	3345	USA	III 2020	56.9%	4.9%
Argenziano et al.	1000	USA	III–IV 2020	33.9%	13.8%
Richardson et al.	5700	USA	III–IV 2020	24.0%	3.2%
Hirsch et al.	5449	USA	III–IV 2020	36.6%	5.2%
Zahid et al.	469	USA	III–IV 2020	27.3%	4.7%
Kolhe et al.	1161	UK	III–V 2020	26.2%	7.6%

Table 2. Epidemiology of acute kidney injury in the course of coronavirus disease 2019 (COVID-19) in hospitalized patients in the intensive care unit (ICU)^{16,18,20,28–32}

Authors	Number of patients with COVID-19	Country of origin	Analyzed period	Prevalence of acute kidney injury in hospitalized patients in ICU	Necessity of kidney replacement therapy in hospitalized patients in ICU
Xu et al.	239	China	I–II 2020	49.8%	5.0%
Yu et al.	226	China	II 2020	25.2%	10.6%
Chan et al.	976	USA	II–IV 2020	56.6%	19.2%
Mohamed et al.	173	USA	III 2020	60.7%	44.5%
Suleyman et al.	141	USA	III 2020	69.5%	17.0%
Argenziano et al.	236	USA	III–IV 2020	78.0%	35.2%
Hirsch et al.	1395	USA	III–IV 2020	76.0%	not given
Doher et al.	201	Brazil	III–V 2020	50.2%	17.0%

percentage was 22%.²⁰ A meta-analysis by Fabrizi et al. showed that in patients with severe COVID-19, the incidence of acute kidney injury was 53% (95% CI: 42.7–63.3%).²⁶ Similar results were found in the meta-analysis by Hansrivijit et al., which showed that the incidence of acute kidney injury was higher in critically ill patients, when compared to other COVID-19 hospitalized patients (19.9% compared to 7.3%).²⁷

In another study, Chan et al. found that acute kidney injury occurred in 76% of patients with COVID-19 hospitalized in the ICU.¹⁶ In the recently published meta-analysis by Silver et al., including 54 studies in 30,657 patients suffering from COVID-19, the incidence of acute kidney injury was assessed at 28%, while among patients hospitalized in the ICU it was 46%.³³

Thus, it has been unequivocally shown in all publications that the highest incidence of acute kidney injury in breakthrough COVID-19 occurs in patients hospitalized in ICUs.

The results of the abovementioned epidemiological studies indicate that patients with COVID-19 are at high risk of acute kidney injury. This risk increases with the severity of clinical symptoms of COVID-19. The significant discrepancies in the incidence of acute kidney injury in hospitalized COVID-19 patients between studies conducted in Asia (low frequency) and in Europe and the United States (high frequency) may result primarily from the differences in indications for hospitalization, and thus, the differences in the general status of hospitalized patients.^{24,25}

The risk of acute kidney injury from COVID-19 depends mainly on the severity of the disease. The general clinical status in the course of COVID-19 and the incidence of acute kidney injury are influenced by similar factors, such as: demographic features (age over 60, male gender, and African descent), comorbidities (chronic kidney disease, diabetes mellitus, cardiovascular diseases, arterial hypertension, obesity and chronic obstructive pulmonary disease).³¹ In the previously cited meta-analyses by Fu et al., Lin et al., in a meta-analysis by Tian et al. including 11 studies, and in a study by Chan et al., the influence of various factors in patients with COVID-19 on the risk

of acute kidney injury was assessed. Numerous demographic and clinical features that significantly increased the risk of acute kidney injury in patients with COVID-19 were described (Table 3).^{16,24,25,34} Factors with the most important impact on the risk of acute kidney injury in the course of COVID-19 were those related to the severity of a patient's condition, i.e., the need to use catecholamines infusion (in the course of septic shock), and the need to use artificial ventilation (due to respiratory failure).^{23,24,31}

Pathogenesis of acute kidney injury in COVID-19 patients

The pathogenesis of acute kidney injury in COVID-19 is multifactorial and not yet fully understood. In patients with COVID-19, acute kidney injury may be prerenal or renal. Both direct and indirect mechanisms of kidney injury induced by SARS-CoV-2 should be taken into account (Fig. 2).³⁵

Table 3. Risk factors of acute kidney injury in patients with coronavirus disease 2019 (COVID-19)^{24,25,34}

Coexisting factor	Risk of acute kidney injury	Reference
Age over 60 years	OR = 3.5, 95% CI: [2.9; 4.3]	25
Male sex	OR = 1.4, 95% CI: [1.1; 1.7]	24
Severe COVID-19 course	OR = 6.0, 95% CI: [2.5; 14.6]	25
Artificial ventilation required	OR = 9.4, 95% CI: [5.2; 17.3]	34
Need to use catecholamines	OR = 19.4, 95% CI: [16.8; 22.3]	34
CKD	OR = 1.6, 95% CI: [1.4; 1.9]	24
Diabetes	OR = 1.5, 95% CI: [1.2; 1.8]	24
Cardiovascular disease	OR = 1.5, 95% CI: [1.1; 2.0]	24
Arterial hypertension	OR = 1.5, 95% CI: [1.3; 1.7]	24
Obesity	OR = 1.8, 95% CI: [1.6; 2.0]	34
COPD	OR = 1.7, 95% CI: [1.4; 2.1]	34

CKD – chronic kidney disease; COPD – chronic obstructive pulmonary disease; OR – odds ratio; 95% CI – 95% confidence interval.

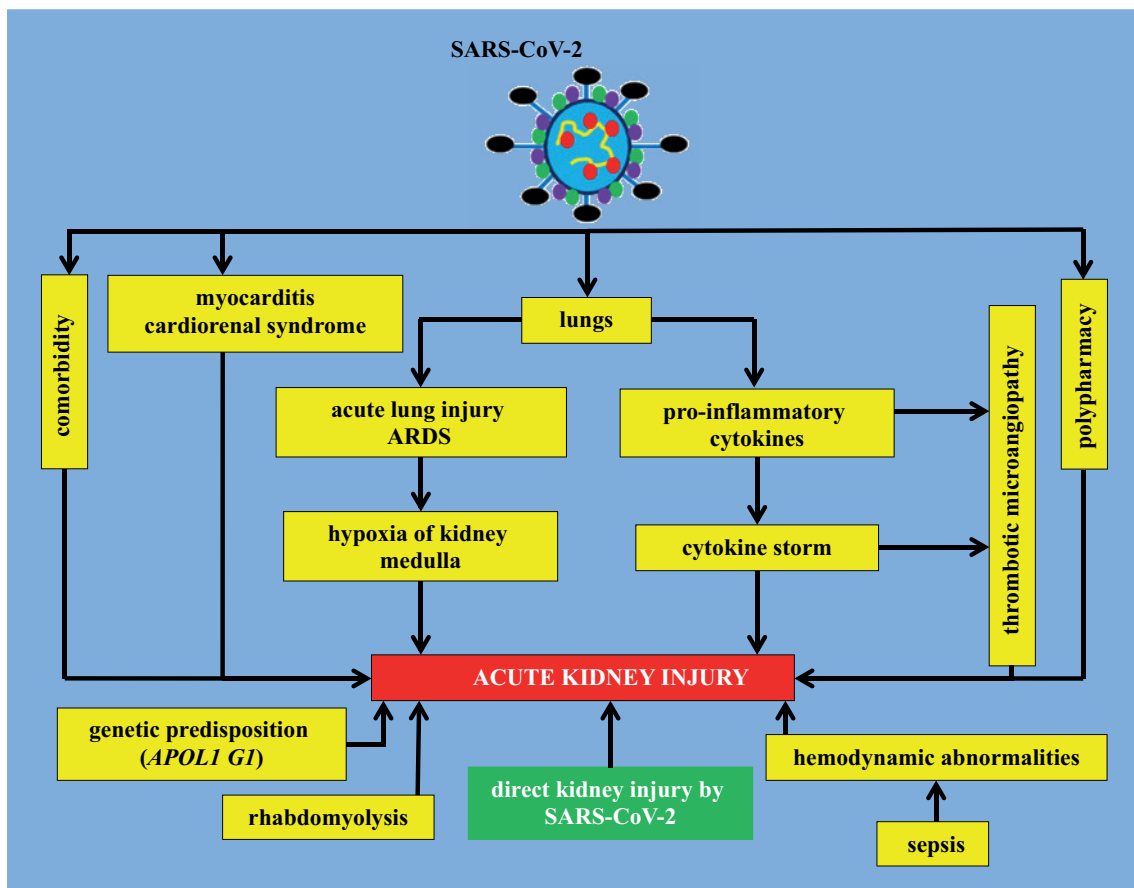


Fig. 2. Mechanisms of acute kidney injury in coronavirus disease 2019 (COVID-19)

ARDS – acute respiratory distress syndrome; SARS-CoV-2 – severe acute respiratory syndrome coronavirus 2; *APOLI G1* – apolipoprotein L1 polymorphisms.

Indirect mechanisms

Dehydration and hypotension (prerenal acute kidney injury)

Important pathophysiological mechanisms of prerenal acute kidney injury in patients with COVID-19 include: dehydration due to fever (temperature >38.5°C), nausea, vomiting or diarrhea, which often accompanies COVID-19 (11% of COVID-19 patients have gastrointestinal symptoms). The cause of dehydration may also be the displacement of fluid into the so-called third space (fluid escapes into the pleural cavities; accumulation of fluid in skeletal muscles occurs in the course of rhabdomyolysis). Moreover, hypotension due to either dehydration, sepsis or heart failure (in the course of myocarditis or cardiomyopathy) also plays a role in the pathogenesis of prerenal acute kidney injury in COVID-19 patients.^{36,37} A study by Hirsch et al. showed that in 66% of patients with COVID-19 and acute kidney injury, urine sodium concentration was below 35 mmol/L, which suggests a prerenal mechanism of acute kidney injury.²⁰ This observation indicates that the factors mentioned above, leading to prerenal acute kidney injury, play a key role in the pathogenesis of acute kidney injury in patients with COVID-19.

Acute tubular necrosis

In the few studies conducted so far in patients with acute kidney injury, in whom histopathological analyses have been completed, acute tubular necrosis was found in a significant proportion of patients (in biopsy studies, in 60% of patients with acute kidney injury).^{19,38} The histological image was dominated by widening of the lumen of the renal tubules and the remaining cell debris within them. In addition, damage to the brush border and vacuolar degeneration in the proximal tubular epithelium cells were observed.³⁹

Several possible mechanisms may be involved in the pathogenesis of acute renal tubular necrosis in COVID-19. Prolonged dehydration and hypotension might lead to acute tubular necrosis. The so-called cytokine storm induced by SARS-CoV-2 infection, causing hemodynamic changes that interfere with renal perfusion (reduction in blood pressure), may also promote acute tubular necrosis.³⁸ Moreover, it has been shown that interleukin 6 (IL-6) and tumor necrosis factor α (TNF-α) are characterized by direct nephrotoxic properties. The expression and release of these cytokines are particularly increased in the cytokine storm accompanying COVID-19. The SARS-CoV-2 has been shown to increase the production of metalloproteinase ADAM17 in cells, which in turn increases the release of TNF-α and IL-6.^{40,41}

Passive renal congestion due to heart failure also promotes acute tubular necrosis. Lung injury caused by COVID-19 may lead to hypoxia of the renal medulla and, consequently, acute tubular necrosis.^{37,42} Other risk factors for acute renal tubular necrosis in patients with COVID-19 are: increased pressure in the chest (e.g., when using ventilation with positive end-expiratory pressure), sepsis, rhabdomyolysis (in 19% of hospitalized COVID-19 patients), and the use of iodinated contrast agents and other nephrotoxic drugs (including nonsteroidal anti-inflammatory drugs).^{23,37} In addition, the deposition of complement components C5b-C9, which form a membrane attack complex (MAC), has been found in tubular cells. The stimulation of the complement system in COVID-19 and the production of MAC may lead to direct destruction of the proximal tubular cells.^{3,39,43-45}

Acute interstitial nephritis

In some patients with acute kidney injury in the course of COVID-19, infiltration of mononuclear cells within the renal interstitium has been found.³⁷ The pathophysiological mechanisms involved in the pathogenesis of acute interstitial nephritis include increased expression of signal transducer and activator of transcription 1 (STAT1) and of interferon regulatory factor 3 (IRF3) by interferon γ (INF- γ) and TNF- α , and increased secretion of pro-inflammatory cytokines by macrophages.⁴⁶⁻⁴⁹ In the pathogenesis of acute interstitial nephritis in COVID-19 patients, allergic reactions to drugs, especially to frequently used antibiotics, may also play a role.⁵⁰

Prothrombotic state in kidneys

In COVID-19, coagulation is increased.^{51,52} Radiological examinations in some COVID-19 patients may show kidney infarctions.⁵³ Moreover, the histopathological examination in these patients may show micro clots in the vessels of the glomeruli.^{52,54} The pathophysiological mechanisms of thrombotic changes include: an increase in serum angiotensin II concentration, the so-called cytokine storm, the increased secretion of von Willebrand factor by damaged vascular endothelium, the occurrence of antibodies similar to cardiolipin, antiphospholipid and anti-2-glycoprotein antibodies, as well as damage to endothelial cells, caused directly by MAC.⁴⁹⁻⁵⁸

Direct mechanisms

There is no clear evidence whether SARS-CoV-2 directly contributes to acute renal tubular damage and glomerulopathy.

As previously mentioned, viremia is rare in patients with COVID-19, which makes a direct damage mechanism unlikely in most of the patients.⁵⁹ Hypothetically, SARS-CoV-2 could pass into the kidneys through continuity by infecting vascular endothelial cells. However, it seems that there is insufficient evidence to support this hypothesis.

The issue of infection of vascular endothelial cells by the SARS-CoV-2 virus has been a subject of *in vitro* studies on organoids and cell cultures. The study by Monteil et al. assessed the possibility of direct infection of human vascular endothelial cells using the capillary organoid formed from induced pluripotent stem cells. The organoid was incubated with SARS-CoV-2 and the occurrence of SARS-CoV-2 RNA inside the vascular endothelial cells was analyzed by RT-PCR after 3 and 6 days. The SARS-CoV-2 RNA was found inside these cells, and SARS-CoV-2 replication was observed in vascular endothelial cells. Moreover, the supernatant taken from the organoid culture on day 6 of the experiment was found to infect Vero E6 cells (renal epithelial cells isolated from primates), indicating that the cells of the capillary organoid were multiplying and releasing new SARS-CoV-2 virions.⁶⁰ However, the results of the studies on organoids were not confirmed by Ahmetaj-Shala et al. in a study with cell culture. In this study, vascular endothelial cells were incubated for 1 h with SARS-CoV-2, and then 24 and 72 h later they were analyzed by indirect immunofluorescence microscopy for the occurrence of virus inside the cells (staining for the occurrence of nucleocapsid (N) protein and S protein). Using this method, SARS-CoV-2 has not been found to occur inside vascular endothelial cells.⁶¹

The endocytosis of SARS-CoV-2 requires the coexistence of the proteins ACE2 and TMPRSS2 on the cell surface. The ACE2 protein is present on the endothelial cells of arteries and veins.⁶² The TMPRSS2, in turn, is present on vascular endothelial cells, but its expression is variable.⁶³

To sum up, the results of the presented *in vitro* studies are inconsistent and do not allow for unequivocal confirmation of the hypothesis that SARS-CoV-2 spreads through continuity by infecting vascular endothelial cells. Moreover, to date, this issue has not been analyzed *in vivo*.

The results of histopathological examinations do not clearly confirm the occurrence of SARS-CoV-2 in kidney cells. In a study by Su et al. using autopsy material from 26 patients with COVID-19 and acute damage to the renal tubules, particles similar to the virus were found in 6 of them by electron microscopy.⁵⁴ However, the results of an electron microscopy examination are not specific. The occurrence of similar structures in the cytoplasm of endothelial cells, which in fact were organelles involved in intracellular transport with clathrin-coated vesicles, was demonstrated in kidney biopsy material obtained before 2020, i.e., before the COVID-19 pandemic.⁶⁴

In the previously mentioned study, the identification of SARS-CoV-2 proteins was carried out using immunofluorescence staining. Nevertheless, this study used antibodies against SARS-CoV and not SARS-CoV-2, reducing the reliability of the obtained results, in which the presence of the SARS-CoV-2 protein was found in 3 out of 26 samples.⁵⁴ In the autopsy study completed by Diao et al., which included material from 6 patients with COVID-19, *in situ* hybridization with the use of rabbit monoclonal antibody

against SARS-CoV-2 RNA demonstrated the occurrence of virus RNA within the kidney tissue in all patients.⁴⁵ However, there are significant doubts related to the specificity of the hybridization technique used in this study.^{65,66} In 32 samples of homogenized kidneys obtained from patients with COVID-19 and acute kidney injury, Braun et al. found the occurrence of SARS-CoV-2 RNA in 23 of them.⁶⁷ A significant limitation of this study seems to be the fact that it is not possible to determine in which kidney structures SARS-CoV-2 RNA was detected. In the study by Puelles et al., which included autopsies of those who died due to COVID-19, the presence of SARS-CoV-2 RNA in the kidneys was demonstrated by RT-PCR. Moreover, in this study using laser microdissection, SARS-CoV-2 was found to occur in the renal medulla, cortex, glomerulus and renal interstitium in 50% (3 out of 6) of samples. The SARS-CoV-2 titer was highest in the glomeruli.⁶⁸

The occurrence of SARS-CoV-2 RNA in kidney autopsy material does not conclusively prove the pathogenicity of the virus. In order to allow the SARS-CoV-2 virus to enter the cell, it is necessary that ACE2 (the virus receptor) and TMPRSS2 (a serine protease that cleaves the S protein) should coexist on its surface. The ACE2 is expressed in the proximal tubular nephron (about 100 times bigger than in the lung), while TMPRSS2 is expressed in the urinary tract epithelium.^{69–71} Thus, SARS-CoV-2 is unable to enter podocytes and proximal tubular cells of the nephron using the ACE2 and TMPRSS2 mechanism.

The protein CD147 is located in the podocytes and cells of the proximal tubules of the nephron, which is also suspected to be involved in the process of SARS-CoV-2 virus penetration into the cell. The effectiveness of this alternative route for virus entry into the cell is unknown. Perhaps, in some patients, the SARS-CoV-2 virus causes the direct damage to the podocytes and proximal tubular cells through this mechanism (i.e., with the participation of the CD147 protein). In such patients, the histopathological changes described in some of the subjects with acute kidney injury in the course of COVID-19 can be found: acute tubular necrosis and focal segmental glomerulosclerosis (the variant with collapsing vascular loops). In kidneys with focal segmental glomerulosclerosis (the variant with collapsing vascular loops), the confluence of the foot processes of podocytes, the detachment of podocytes from the glomerular basement membrane and the formation of pseudo-crescents have been observed.^{72,73} It is worth mentioning that a similar focal segmental glomerulosclerosis (the variant with collapsing vascular loops) is also found in other virus infections, such as human immunodeficiency virus 1 (HIV-1), human T-cell leukemia-lymphoma virus 1 (HTLV1), cytomegalovirus, parvovirus B19, and Epstein–Barr virus.⁷²

The occurrence of the abovementioned podocytopathy in the course of COVID-19 is favored by the APOL1 G1 polymorphism (apolipoprotein L1) and an increase in CD147 expression in damaged podocytes, which may

allow SARS-CoV-2 to penetrate the cells. It seems that patients with coexisting diabetes and/or obesity are particularly at risk of developing focal segmental glomerulosclerosis (the variant with collapsing vascular loops) in the course of COVID-19, as they have an increased expression of CD147 in podocytes.^{73,74} The penetration of SARS-CoV-2 through CD147 into the podocyte may result in disturbances in the structure and function of the cytoskeleton, stimulation of the mitogen-activated protein kinase (MAPK) pathway, and increased production of pro-inflammatory cytokines.³⁷ In patients with focal segmental glomerulosclerosis (the variant with collapsing vascular loops), significant proteinuria is found.³⁸

Thus, the presented data indicate that acute kidney damage in COVID-19 is primarily caused by indirect pathophysiological mechanisms, and does not differ in the histopathological picture, in the vast majority of patients, from acute kidney damage of a different etiology. The main pathophysiological mechanisms underlying acute kidney injury in COVID-19 include hemodynamic disorders, hypoxia, and the so-called cytokine storm.

Prognosis of patients with acute kidney injury in COVID-19

Acute kidney injury in COVID-19 patients is often irreversible. Gupta et al. showed that there was a need for dialysis on the day of discharge from hospital in 34% of patients. On the other hand, 18% of patients needed dialysis on day 60 of observation after the discharge from hospital.⁷⁵

The occurrence of acute kidney injury in a patient with COVID-19 is unfavorable in terms of prognosis. A study by Chan et al. found that in-hospital mortality in patients with COVID-19 was 50% in patients with acute kidney injury, compared to 8% in patients without acute kidney injury (OR = 9.2; 95% CI: 7.5–11.3).¹⁶ The meta-analysis by Fabrizi et al. showed that the OR for the incidence of acute kidney injury in deceased COVID-19 positive patients was greater than among the survivors (OR = 15.4; 95% CI: 11.4–20.99; $p < 0.001$).²⁶ The meta-analysis by Lin et al. showed that the occurrence of acute kidney injury in hospitalized patients with COVID-19 was associated with a significant increase in the risk of death (OR = 11.05; 95% CI: 9.13–13.36).²⁵ Similar results were obtained by Fisher et al. in a study involving 3,345 patients with COVID-19. They found that mortality in patients with COVID-19 and acute kidney injury was significantly higher than in hospitalized patients with COVID-19 but without acute kidney injury (33.7% compared to 9.3%, respectively).¹⁷ A meta-analysis of 142 studies by Fu et al., including 49,048 patients hospitalized with COVID-19, showed a significant increase in the risk of death in patients with coexisting acute kidney injury (relative risk (RR): 4.6; 95% CI: 3.3–6.5).²⁴ In the meta-analysis by Hansrivijit et al., it was shown that the estimated OR for mortality from acute kidney injury was 13.33 (95% CI: 4.05–43.91).²⁷

Treatment of acute kidney injury in COVID-19

The general principles of management in patients with COVID-19 and acute kidney injury, developed by the Acute Disease Quality Initiative (ADQI) Working Group, do not differ from the principles of management in patients with acute kidney injury due to other causes. The methods of therapy in COVID-19 patients are summarized in Table 4.⁵⁰

Methods of therapy of the underlying disease, i.e., COVID-19, in patients with acute kidney injury and in patients without acute kidney injury, are similar. However, it should be stressed that in the treatment of COVID-19 accompanied by acute kidney injury, the contraindication to remdesivir is estimated glomerular filtration rate (eGFR) <30 mL/min/1.73 m².⁵⁰ The abovementioned recommendation for the use of remdesivir is due to the possible accumulation of the solvent substance, i.e., cyclodextrin derivative (sulfobutylether- β -cyclodextrin (SBECD)).⁷⁶ Animal studies have shown that SBECD has nephrotoxic and hepatotoxic properties.⁷⁷ Observational studies in patients with COVID-19 and impaired kidney function treated with remdesivir by Thakare et al. (including 46 patients) and Estiverne et al. (including 18 patients), and case reports of patients with COVID-19 and impaired kidney function, did not confirm significant toxicity of such treatment.^{78–81} Nevertheless, in the study by Estiverne et al., 2 out of 18 observed patients showed a significant increase in the activity of serum transaminases.⁷⁹ It is necessary to conduct clinical trials to answer the question of whether the benefits of remdesivir in patients with acute kidney injury in the course of COVID-19 might outweigh the potential risks caused by the toxicity of such treatment.⁷⁶

In the treatment of acute kidney injury in a patient

Table 4. Principles of management in a patient with coronavirus disease 2019 (COVID-19) and acute kidney injury

Patients at increased risk of acute kidney injury (AKI) and patients with AKI
Applying standard principles of care for prevention and treatment of multiple organ failure
Individualization of fluid therapy
Consideration of vigorous hemodynamic monitoring
Monitoring serum creatinine concentration and urine volume
Maintaining normal blood glucose concentration
If possible, considering using alternative diagnostic methods for testing with iodine-based contrast agents, but without delaying the radiological examination
If possible, avoidance of nephrotoxic drugs
Risk of AKI when choosing a strategy for artificial ventilation
Additionally, patients with stage II/III AKI
Kidney replacement therapy consideration
Avoidance of vascular access for hemodialysis using a subclavian vein puncture

with COVID-19, kidney replacement therapy is often necessary (Table 1,2). A review of the literature by Hasanein et al. showed a large variation in the frequency of the need for kidney replacement therapy in patients with acute kidney injury due to COVID-19, ranging from 0.8% to 31%.²³ The meta-analysis by Fabrizi et al. showed that the frequency of the need for renal replacement therapy in patients with COVID-19 was 4.3% (95% CI: 3.1–5.5%; $p < 0.0001$).²⁶ The meta-analysis by Hansrivijit et al. found that the incidence of renal replacement therapy was 3.6% (95% CI: 1.8–7.1%).²⁷

The method of kidney replacement therapy in patients with COVID-19 is similar to the treatment of patients with acute kidney injury with another etiology. So far, no benefit has been found of an earlier initiation of renal replacement therapy. Continuous techniques should be preferred (nevertheless, the type of treatment depends mainly on a center's experience and the availability of the treatment method). The best location to place a hemodialysis catheter is in the right jugular vein. Heparin should also be used in some patients in between hemodialysis treatments. For continuous techniques, local use of citrate should be preferred. Peritoneal dialysis can also be used.^{50,82,83}

In order to reduce the risk of infection of medical personnel, the video transmission from the dialysis room has been used in some dialysis centers, allowing for remote patient supervision. Moreover, some of the centers have used longer than usual drains for hemodialysis, which allowed for the positioning of the hemodialysis machine outside the room in which the patient was staying.²³

Limitations of the study

The main limitation of this review paper is that we analysed results from the studies published before November 2021, i.e., during the still ongoing COVID-19 pandemic. The studies discussed in paper covered the period before the introduction of vaccination against COVID-19. Therefore we were not able to anticipate the influence of both vaccination and new variants SARS-CoV-2 virus on the acute kidney injury epidemiology and pathogenesis. Mechanisms by which SARS-CoV-2 affects kidney function presented in this review paper are not well understood and undoubtedly require further research.

Conclusions

Acute kidney injury in the course of COVID-19 occurs in approx. 30% of patients requiring hospitalization. In COVID-19, acute kidney injury is most often caused by prerenal causes. In the histological picture of acute kidney injury in the course of COVID-19, acute tubular necrosis was found to be dominating. The principles of prevention and treatment of acute kidney injury in the course of COVID-19 are similar to those of acute kidney injury in the course

of other infections. The contraindication to the use of remdesivir is eGFR < 30 mL/min/1.73 m². It must be emphasized that acute kidney injury in the course of COVID-19 is an unfavorable prognostic factor.

ORCID iDs

Marcin Adamczak  <https://orcid.org/0000-0002-0804-1718>

Stanisław Surma  <https://orcid.org/0000-0001-8073-6664>

Andrzej Więcek  <https://orcid.org/0000-0002-8625-4188>

References

- Dömling A, Gao L. Chemistry and biology of SARS-CoV-2. *Chem*. 2020; 6(6):1283–1295. doi:10.1016/j.chempr.2020.04.023
- Jin X, Li Y, Song Y, et al. Progress in research on the detection of the novel coronavirus in human samples of different groups. *Eur Rev Med Pharmacol Sci*. 2020;24(20):10879–10884. doi:10.26355/eurrev_202010_23452
- Wu J, Liu J, Li S, et al. Detection and analysis of nucleic acid in various biological samples of COVID-19 patients. *Travel Med Infect Dis*. 2020;37:101673. doi:10.1016/j.tmaid.2020.101673
- Peng L, Liu J, Xu W, et al. SARS-CoV-2 can be detected in urine, blood, anal swabs, and oropharyngeal swabs specimens. *J Med Virol*. 2020; 92(9):1676–1680. doi:10.1002/jmv.25936
- Lo I, Lio C, Cheong H, et al. Evaluation of SARS-CoV-2 RNA shedding in clinical specimens and clinical characteristics of 10 patients with COVID-19 in Macau. *Int J Biol Sci*. 2020;16(10):1698–1707. doi:10.7150/ijbs.45357
- Wölfel R, Corman VM, Guggemos W, et al. Virological assessment of hospitalized patients with COVID-2019. *Nature*. 2020;581(7809): 465–469. doi:10.1038/s41586-020-2196-x
- Wang W, Xu Y, Gao R, et al. Detection of SARS-CoV-2 in different types of clinical specimens. *JAMA*. 2020;323(18):1843–1844. doi:10.1001/jama.2020.3786
- Huang C, Wang Y, Li X, et al. Clinical features of patients infected with 2019 novel coronavirus in Wuhan, China. *Lancet*. 2020;395(10223): 497–506. doi:10.1016/S0140-6736(20)30183-5
- Tan C, Li S, Liang Y, Chen M, Liu J. SARS-CoV-2 viremia may predict rapid deterioration of COVID-19 patients. *Braz J Infect Dis*. 2020;24(6): 565–569. doi:10.1016/j.bjid.2020.08.010
- Fajnzylber J, Regan J, Coxen K, et al. SARS-CoV-2 viral load is associated with increased disease severity and mortality. *Nat Commun*. 2020;11(1):5493. doi:10.1038/s41467-020-19057-5
- Dos Santos WG. Natural history of COVID-19 and current knowledge on treatment therapeutic options. *Biomed Pharmacother*. 2020;129: 110493. doi:10.1016/j.biopha.2020.110493
- Yang X, Yu Y, Xu J, et al. Clinical course and outcomes of critically ill patients with SARS-CoV-2 pneumonia in Wuhan, China: A single-centered, retrospective, observational study. *Lancet Respir Med*. 2020; 8(5):475–481. doi:10.1016/S2213-2600(20)30079-5
- Shi S, Qin M, Shen B, et al. Association of cardiac injury with mortality in hospitalized patients with COVID-19 in Wuhan, China. *JAMA Cardiol*. 2020;5(7):802–810. doi:10.1001/jamacardio.2020.0950
- Cheng Y, Luo R, Wang X, et al. The incidence, risk factors, and prognosis of acute kidney injury in adult patients with coronavirus disease 2019. *Clin J Am Soc Nephrol*. 2020;15(10):1394–1402. doi:10.2215/CJN.04650420
- Portolés J, Marques M, Lopez-Sanchez P, et al. Chronic kidney disease and acute kidney injury in the COVID-19 Spanish outbreak. *Nephrol Dial Transplant*. 2020;35(8):1353–1361. doi:10.1093/ndt/gfaa189
- Chan L, Chaudhary K, Saha A, et al. AKI in hospitalized patients with COVID-19. *J Am Soc Nephrol*. 2021;32(1):151–160. doi:10.1681/ASN.2020050615
- Fisher M, Neugarten J, Bellin E, et al. AKI in hospitalized patients with and without COVID-19: A comparison study. *J Am Soc Nephrol*. 2020;31(9):2145–2157. doi:10.1681/ASN.2020040509
- Argenziano MG, Bruce SL, Slater CL, et al. Characterization and clinical course of 1000 patients with coronavirus disease 2019 in New York: Retrospective case series. *BMJ*. 2020;369:m1996. doi:10.1136/bmj.m1996
- Richardson S, Hirsch J, Narasimhan M, et al. Presenting characteristics, comorbidities, and outcomes among patients hospitalized with COVID-19 in the New York City Area. *JAMA*. 2020;323(20):2052–2059. doi:10.1001/jama.2020.6775
- Hirsch JS, Ng JH, Ross DW, et al. Acute kidney injury in patients hospitalized with COVID-19. *Kidney Int*. 2020;98(1):209–218. doi:10.1016/j.kint.2020.05.006
- Zahid U, Ramachandran P, Spitalewitz Z, et al. Acute kidney injury in COVID-19 patients: An inner city hospital experience and policy implications. *Am J Nephrol*. 2020;51:786–796. doi:10.1159/000511160
- Kolhe NV, Fluck RJ, Selby NM, Taal MW. Acute kidney injury associated with COVID-19: A retrospective cohort study. *PLoS Med*. 2020;17(10): e1003406. doi:10.1371/journal.pmed.1003406
- Hassanein M, Radhakrishnan Y, Sedor J, et al. COVID-19 and the kidney. *Clev Clin J Med*. 2020;87(10):619–631. doi:10.3949/ccjm.87a.20072
- Fu E, Janse R, de Jong Y, et al. Acute kidney injury and kidney replacement therapy in COVID-19: A systematic review and meta-analysis. *Clin Kidney J*. 2020;13(4):550–563. doi:10.1093/ckj/sfaa160
- Lin L, Wang X, Ren J, et al. Risk factors and prognosis for COVID-19-induced acute kidney injury: A meta-analysis. *BMJ Open*. 2020;10(11): 042573. doi:10.1136/bmjopen-2020-042573
- Fabrizi F, Alfieri C, Cerutti R, Lunghi G, Messa P. COVID-19 and acute kidney injury: A systematic review and meta-analysis. *Pathogens*. 2020;9(12):1052. doi:10.3390/pathogens9121052
- Hansrivijit P, Qian C, Boonpheng B, et al. Incidence of acute kidney injury and its association with mortality in patients with COVID-19: A meta-analysis. *J Invest Med*. 2020;68(7):1261–1270. doi:10.1136/jim-2020-001407
- Mohamed MM, Lukitsch I, Torres-Ortiz AE, et al. Acute kidney injury associated with coronavirus disease 2019 in urban New Orleans. *Kidney360*. 2020;1(7):614–622. doi:10.34067/KID.0002652020
- Xu J, Yang X, Yang L, et al. Clinical course and predictors of 60-day mortality in 239 critically ill patients with COVID-19: A multicenter retrospective study from Wuhan, China. *Crit Care*. 2020;24(1):394. doi:10.1186/s13054-020-03098-9
- Yu Y, Xu D, Fu S, et al. Patients with COVID-19 in 19 ICUs in Wuhan, China: A cross-sectional study. *Crit Care*. 2020;24(1):219. doi:10.1186/s13054-020-02939-x
- Suleyman G, Fadel RA, Malette KM, et al. Clinical characteristics and morbidity associated with coronavirus disease 2019 in a series of patients in metropolitan Detroit. *JAMA Netw Open*. 2020;3(6): e2012270. doi:10.1001/jamanetworkopen.2020.12270
- Doher M, Torres de Carvalho F, Scherer P, et al. Acute kidney injury and renal replacement therapy in critically ill COVID-19 patients: Risk factors and outcomes: A single-center experience in Brazil. *Blood Purif*. 2021;50(4–5):520–530. doi:10.1159/000513425
- Silver S, Beaubien-Souligny M, Shah P, et al. The prevalence of acute kidney injury in patients hospitalized with COVID-19 infection: A systematic review and meta-analysis. *Kidney Med*. 2020;3(1):83–98. doi:10.1016/j.xkme.2020.11.008
- Tian L, Shao X, Hang Y, Yang W, Mou S, Zhu C. Risk factors for acute kidney injury in patients with coronavirus disease 2019 (COVID-19): A metaanalysis. *Research Square*. 2020. doi:10.21203/rs.3.rs-111264/v1
- Farouk S, Fiaccadori E, Cravedi P, Campbell KN. COVID-19 and the kidney: What we think we know so far and what we don't. *J Nephrol*. 2020;33(6):1213–1218. doi:10.1007/s40620-020-00789-y
- Ronco C, Reis T. Kidney involvement in COVID-19 and rationale for extracorporeal therapies. *Nat Rev Nephrol*. 2020;16(6):308–310. doi:10.1038/s41581-020-0284-7
- Izzedine H, Jhaveri KD. Acute kidney injury in patients with COVID-19: An update on the pathophysiology. *Nephrol Dial Transplant*. 2021; 36(2):224–226. doi:10.1093/ndt/gfaa184
- Chueh T, Zheng C, Hou Y, Lu K. Novel evidence of acute kidney injury in COVID-19. *J Clin Med*. 2020;9(11):3547. doi:10.3390/jcm9113547
- Perico L, Benigni A, Casiraghi F, Ng L, Renia L, Remuzzi G. Immunity, endothelial injury and complement-induced coagulopathy in COVID-19. *Nat Rev Nephrol*. 2021;17(1):46–64. doi:10.1038/s41581-020-00357-4
- Hu B, Huang S, Yin L. The cytokine storm and COVID-19. *J Med Virol*. 2021;93(1):250–256. doi:10.1002/jmv.26232
- Zipeto D, Palmeira J, Argañaraz G, Argañaraz E. ACE2/ADAM17/TMPRSS2 interplay may be the main risk factor for COVID-19. *Front Immunol*. 2020;11:576745. doi:10.3389/fimmu.2020.576745

42. Grasselli G, Zangrillo A, Zanella A, et al. Baseline characteristics and outcomes of 1591 patients infected with SARS-CoV-2 admitted to ICUs of the Lombardy region, Italy. *JAMA*. 2020;323(16):1574–1581. doi:10.1001/jama.2020.5394
43. Wang K, Chen W, Zhang Z, et al. CD147-spike protein is a novel route for SARS-CoV-2 infection to host cells. *Signal Transduct Target Ther*. 2020;5(1):283. doi:10.1038/s41392-020-00426-x
44. Tai W, He L, Zhang X, et al. Characterization of the receptor-binding domain (RBD) of 2019 novel coronavirus: Implication for development of RBD protein as a viral attachment inhibitor and vaccine. *Cell Mol Immunol*. 2020;17(6):613–620. doi:10.1038/s41423-020-0400-4
45. Diao B, Wang C, Wang R, et al. Human kidney is a target for novel severe acute respiratory syndrome coronavirus 2 (SARS-CoV-2). *Nat Commun*. 2021;12(1):2506. doi:10.1101/2020.03.04.20031120
46. Zhu L, Yang P, Zhao Y, et al. Single-cell sequencing of peripheral mononuclear cells reveals distinct immune response landscapes of COVID-19 and influenza patients. *Immunity*. 2020;53(3):685–696. doi:10.1016/j.immuni.2020.07.009
47. Huang F, Wang Q, Guo F, et al. FoxO1-mediated inhibition of STAT1 alleviates tubulointerstitial fibrosis and tubule apoptosis in diabetic kidney disease. *EBioMedicine*. 2019;48:491–504. doi:10.1016/j.ebiom.2019.09.002
48. Nightingale J, Patel S, Suzuki N, et al. Oncostatin M, a cytokine released by activated mononuclear cells, induces epithelial cell-myofibroblast transdifferentiation via Jak/Stat pathway activation. *J Am Soc Nephrol*. 2004;15(1):21–32. doi:10.1097/01.asn.0000102479.92582.43
49. Zhang F, Mears JR, Shakib L, et al. IFN- and TNF- α drive a CXCL10+ CCL2+ macrophage phenotype expanded in severe COVID-19 lungs and inflammatory diseases with tissue inflammation. *Genome Med*. 2021;13(1):64. doi:10.1186/s13073-021-00881-3
50. Nadim MK, Forni LG, Mehta RL, et al. COVID-19-associated acute kidney injury: Consensus report of the 25th Acute Disease Quality Initiative (ADQI) Workgroup. *Nat Rev Nephrol*. 2020;16(12):747–764. doi:10.1038/s41581-020-00356-5
51. Evans P, Rainger E, Mason J, et al. Endothelial dysfunction in COVID-19: A position paper of the ESC Working Group for Atherosclerosis and Vascular Biology, and the ESC Council of Basic Cardiovascular Science. *Cardiovasc Res*. 2020;116(14):2177–2184. doi:10.1093/cvr/cvaa230
52. Pons S, Fodil S, Azoulay E, Zafrani L. The vascular endothelium: The cornerstone of organ dysfunction in severe SARS-CoV-2 infection. *Crit Care*. 2020;24(1):353. doi:10.1186/s13054-020-03062-7
53. Post A, den Deurwaarder E, Bakker S, et al. Kidney infarction in patients with COVID-19. *Am J Kidney Dis*. 2020;76(3):431–435. doi:10.1053/j.ajkd.2020.05.004
54. Su H, Yang M, Wan C, et al. Renal histopathological analysis of 26 postmortem findings of patients with COVID-19 in China. *Kidney Int*. 2020;98(1):219–227. doi:10.1016/j.kint.2020.04.003
55. Merrill JT, Erkan D, Winakur J, James JA. Emerging evidence of a COVID-19 thrombotic syndrome has treatment implications. *Nat Rev Rheumatol*. 2020;16(10):581–589. doi:10.1038/s41584-020-0474-5
56. Jhaveri KD, Meir LR, Flores Chang BS, et al. Thrombotic microangiopathy in a patient with COVID-19. *Kidney Int*. 2020;98(2):509–512. doi:10.1016/j.kint.2020.05.025
57. Zhang Y, Xiao M, Zhang S, et al. Coagulopathy and antiphospholipid antibodies in patients with Covid-19. *N Engl J Med*. 2020;382(17):e38. doi:10.1056/NEJMc2007575
58. Zuo Y, Estes SK, Ali RA, et al. Prothrombotic autoantibodies in serum from patients hospitalized with COVID-19. *Sci Transl Med*. 2020;12(570):eabd3876. doi:10.1126/scitranslmed.abd3876
59. Jones D, Baluja M, Graham D, et al. Shedding of SARS-CoV-2 in feces and urine and its potential role in person-to-person transmission and the environment-based spread of COVID-19. *Sci Total Environ*. 2020;749:141364. doi:10.1016/j.scitotenv.2020.141364
60. Monteil V, Kwon H, Prado P, et al. Inhibition of SARS-CoV-2 infections in engineered human tissues using clinical-grade soluble human ACE2. *Cell*. 2020;181(4):905–913. doi:10.1016/j.cell.2020.04.004
61. Ahmetaj-Shala B, Peacock T, Baillon L, et al. Resistance of endothelial cells to SARS-CoV-2 infection in vitro. *bioRxiv*. 2020. doi:10.1101/2020.11.08.372581
62. Hamming I, Timens W, Bulthuis MLC, Lely AT, Navis GJ, van Goor H. Tissue distribution of ACE2 protein, the functional receptor for SARS coronavirus. A first step in understanding SARS pathogenesis. *J Pathol*. 2004;203(2):631–637. doi:10.1002/path.1570
63. Aimes RT, Zijlstra A, Hooper JD, et al. Endothelial cell serine proteases expressed during vascular morphogenesis and angiogenesis. *Thromb Haemost*. 2003;89(3):561–572. PMID:12624642.
64. Roufousse C, Curtis E, Moran L, et al. Electron microscopic investigations in COVID-19: Not all crowns are coronas. *Kidney Int*. 2020;98(2):505–506. doi:10.1016/j.kint.2020.05.012
65. Larsen CP, Bourne TD, Wilson JD, Saqqa O, Sharshir MA. Collapsing glomerulopathy in a patient with COVID-19. *Kidney Int Rep*. 2020;5(6):935–939. doi:10.1016/j.ekir.2020.04.002
66. Calomeni E, Satooskar A, Ayoub I, Brodsky S, Rovin BH, Nadasdy T. Multi-vesicular bodies mimicking SARS-CoV-2 in patients without COVID-19. *Kidney Int*. 2020;98(1):233–234. doi:10.1016/j.kint.2020.05.003
67. Braun F, Lütgehetmann M, Pfefferle S, et al. SARS-CoV-2 renal tropism associates with acute kidney injury. *Lancet*. 2020;396(10251):597–598. doi:10.1016/S0140-6736(20)31759-1
68. Puelles F, Lütgehetmann M, Lindenmeyer M, et al. Multiorgan and renal tropism of SARS-CoV-2. *N Engl J Med*. 2020;383(6):590–592. doi:10.1056/NEJMc2011400
69. Parmar M. Acute kidney injury associated with COVID-19 – cumulative evidence and rationale supporting against direct kidney injury (infection). *Nephrology (Carlton)*. 2021;26(3):239–247. doi:10.1111/nep.13814
70. Benedetti C, Waldman M, Zaza G, Riella L, Cravedi P. COVID-19 and the kidneys: An update. *Front Med (Lausanne)*. 2020;7:423. doi:10.3389/fmed.2020.00423
71. Gabarre P, Dumas G, Dupont T, Darmon M, Azoulay E, Zafrani L. Acute kidney injury in critically ill patients with COVID-19. *Intensive Care Med*. 2020;46(7):1339–1348. doi:10.1007/s00134-020-06153-9
72. Nasr SH, Kopp JB. COVID-19-associated collapsing glomerulopathy: An emerging entity. *Kidney Int Rep*. 2020;5(6):759–761. doi:10.1016/j.ekir.2020.04.030
73. Radzikowska U, Ding M, Tan G, et al. Distribution of ACE2, CD147, CD26, and other SARS-CoV-2 associated molecules in tissues and immune cells in health and in asthma, COPD, obesity, hypertension, and COVID-19 risk factors. *Allergy*. 2020;75(11):2829–2845. doi:10.1111/all.14429
74. Wu H, Larsen C, Hernandez-Arroyo C, et al. AKI and collapsing glomerulopathy associated with COVID-19 and APOL1 high-risk genotype. *J Am Soc Nephrol*. 2020;31(8):1688–1695. doi:10.1681/ASN.2020050558
75. Gupta S, Coca S, Chan L, et al. AKI treated with renal replacement therapy in critically ill patients with COVID-19. *J Am Soc Nephrol*. 2021;32(1):161–176. doi:10.1681/ASN.2020060897
76. Adamsick M, Gandhi R, Bidell M, et al. Remdesivir in patients with acute or chronic kidney disease and COVID-19. *J Am Soc Nephrol*. 2020;31(7):1384–1386. doi:10.1681/ASN.2020050589
77. Luke D, Tomaszewski K, Damle B, Schlamm H. Review of the basic and clinical pharmacology of sulfobutylether-beta-cyclodextrin (SBECd). *J Pharm Sci*. 2010;99(8):3291–3301. doi:10.1002/jps.22109
78. Thakare S, Gandhi C, Modi T, et al. Safety of Remdesivir in patients with acute kidney injury or CKD. *Kidney Int Rep*. 2021;6(1):206–210. doi:10.1016/j.ekir.2020.10.005
79. Estiverne C, Strohbehn I, Mithani Z, et al. Remdesivir in patients with estimated glomerular filtration rate <30 mL/min/1.73 m² or on renal replacement therapy. *Kidney Int Rep*. 2021;6(3):835–838. doi:10.1016/j.ekir.2020.11.025
80. Sörgel F, Malin J, Hagmann H, et al. Pharmacokinetics of remdesivir in a COVID-19 patient with end-stage renal disease on intermittent haemodialysis. *J Antimicrob Chemother*. 2021;76(3):825–827. doi:10.1093/jac/dkaa500
81. Peyko V, Ladd H, Cutrona A. The safe administration of remdesivir in a patient with acute kidney injury requiring hemodialysis. *Case Rep Infect Dis*. 2020;2020:8811798. doi:10.1155/2020/8811798
82. Shaikh S, Matzumura G, Vijayah A. Management of acute kidney injury in coronavirus disease 2019. *Adv Chronic Kidney Dis*. 2020;27(5):377–382. doi:10.1053/j.ackd.2020.08.002
83. Parapiboon W, Ponce D, Cullis B. Acute peritoneal dialysis in COVID-19. *Perit Dial Int*. 2020;40(4):359–362. doi:10.1177/0896860820931235

Successful treatment of second-time CAR-T 19 therapy after failure of first-time CAR-T 19 and ibrutinib therapy in relapsed mantle cell lymphoma

Juan Mu^{A–C,E,F}, Meijing Liu^{C,E,F}, Jia Wang^{A,B,F}, Juanxia Meng^{A,F}, Rui Zhang^{B,C,F}, Yanyu Jiang^{C,E,F}, Qi Deng^{A–D,F}

Department of Hematology, Tianjin First Central Hospital, School of Medicine, Nankai University, China

A – research concept and design; B – collection and/or assembly of data; C – data analysis and interpretation; D – writing the article; E – critical revision of the article; F – final approval of the article

Advances in Clinical and Experimental Medicine, ISSN 1899–5276 (print), ISSN 2451–2680 (online)

Adv Clin Exp Med. 2022;31(3):327–335

Address for correspondence

Qi Deng
E-mail: tflkqv@163.com

Funding sources

None declared

Conflict of interest

None declared

Received on November 3, 2021
Reviewed on December 19, 2021
Accepted on January 19, 2022

Published online on February 11, 2022

Abstract

Background. A patient with relapsed mantle cell lymphoma (MCL) showed stable disease after receiving ibrutinib therapy as a salvage therapy, after the failure of his first chimeric antigen receptor (CAR)-T 19 cell therapy.

Objectives. The combined effects of CAR-T 19 cells from the patient and ibrutinib on JeKo-1 cell were explored in vitro and in vivo.

Materials and methods. The expression of programmed death-1 (PD-1) receptor on CD3⁺ T cells in the peripheral blood decreased from 82.95% in the first CAR-T 19 cell therapy to approx. 40% after 14 months of ibrutinib therapy. When the disease progressed again during the ibrutinib therapy, the patient was enrolled into the same clinical trial of CAR-T 19 cell therapy.

Results. The efficacy of CAR-T 19 cells increased after the ibrutinib therapy. The mRNA expression level of PD-1 in CAR-T 19 cells after ibrutinib therapy was lower than in CAR-T 19 cells before the ibrutinib therapy. Nevertheless, CAR-T 19 cell therapy combined with ibrutinib had no synergistic effect in a short term in vitro and in the JeKo-1 cell mouse model.

Conclusions. We expect our results to provide evidence for the combination treatment of ibrutinib for MCL or even other types of B-cell lymphomas. Moreover, the improvement in CAR-T 19 cell function was based on long-term ibrutinib therapy.

Key words: chimeric antigen receptor, immunotherapy, lymphoma, clinical chimeric antigen receptor T cell trials, ibrutinib

Cite as

Mu J, Liu M, Wang J, et al. Successful treatment of second-time CAR-T 19 therapy after failure of first-time CAR-T 19 and ibrutinib therapy in relapsed mantle cell lymphoma. *Adv Clin Exp Med.* 2022;31(3):327–335. doi:10.17219/acem/145948

DOI

10.17219/acem/145948

Copyright

© 2022 by Wrocław Medical University
This is an article distributed under the terms of the Creative Commons Attribution 3.0 Unported (CC BY 3.0) (<https://creativecommons.org/licenses/by/3.0/>)

Background

Relapsed/refractory (R/R) B-cell non-Hodgkin's lymphoma (B-NHL) is usually characterized by poor prognosis.^{1,2} Chimeric antigen receptor (CAR) T-cell therapy has shown to be more effective in patients with R/R B-cell acute lymphoblastic leukemia (B-ALL)^{3–9} and R/R B-NHL.^{10–13} However, patients with R/R B-NHL have lower complete remission (CR) rate of CD19 CAR T-cell (CAR-T 19) therapy than those with R/R B-ALL.^{14,15}

Ibrutinib, as an inhibitor of Bruton's tyrosine kinase (BTK), has been approved by the US Food and Drug Administration (FDA) for the treatment of relapsed chronic lymphocytic leukemia (CLL)¹⁶ and mantle cell lymphoma (MCL).¹⁷ This drug has been extensively administered for the treatment of various B-cell lymphomas.^{18–20} Bruton's tyrosine kinase expressed on B cells acts as a cytoplasmic tyrosine kinase in the B-cell receptor signaling pathway.^{21,22} Ibrutinib blocks BTK activation in different pathways to inhibit B-cell receptor signaling in B-cell lymphomas.^{23–25}

The combination of ibrutinib and CAR-T 19 cells has shown excellent results in preclinical and clinical studies.²⁶ The CAR-T 19 cell therapy has been proven to be highly effective in CLL patients who have previously taken ibrutinib.²⁷ This drug can enhance the engraftment and efficacy of CAR-T 19 cells in CLL patients.²⁸ Other clinical reports have indicated a promising antitumor activity of CAR-T 19 cells in CLL patients who are resistant to ibrutinib therapy.²⁹ Ibrutinib combined with CAR-T 19 cells has been studied in an MCL cell line.³⁰ The efficacies of CAR-T 19 cells on the MCL cell line in vitro and in vivo were enhanced by this drug. In this study, a patient with relapsed MCL obtained CR with his second CAR-T 19 cell therapy after the failure of the first CAR-T 19 cell therapy and 14 months of ibrutinib therapy. The combination of CAR-T 19 cells from the patient and ibrutinib on JeKo-1 cell was explored in vitro and in vivo.

Objectives

The aim of the study was to observe whether a long-term ibrutinib therapy could enhance the efficacy of CAR-T 19 cell therapy in the treatment of R/R MCL in vitro, in mice, and clinically.

Materials and methods

Medical history

A 58-year-old man experienced right epigastric pain for 3 days in September 2014. Abdominal computed tomography (CT) revealed the presence of multiple low-density shadows in the spleen and lymph nodes of the splenic portal

area/retroperitoneum (Fig. 1A). The biopsy of the hilum of the lymph node and immunohistochemical examination confirmed the diagnosis of MCL (Fig. 1B). The cyclin D1 level was 72.5%. The CR was obtained after 6 cycles of R-CHOP combination chemotherapy. No autologous hematopoietic stem cell transplantation or other maintenance therapy was initiated due to lung injury caused by heart stent surgery and rituximab.

In February 2017, the patient was again admitted to our hospital owing to lymph node enlargement in the right neck. There were no immunoglobulin H (IgH) and T-cell receptor gene rearrangements (Fig. 1C). Neck CT revealed that multiple cervical lymph nodes were enlarged (Fig. 2A). Cervical lymph node biopsy confirmed the previous diagnosis of MCL (Fig. 1D). The cyclin D1 level was 69.2%. Owing to the complications, the patient could not receive further combination chemotherapy. Subsequently, he participated in a clinical trial of autologous CAR-T 19 cells, expressing murine anti-CD19 scFv and 4-1BB-CD3 ζ costimulatory activation domain (ChiCTR-ONN-16009862). The patient provided informed consent prior to the enrollment. This clinical trial was conducted under the approval of the Medical Ethics Committee of Tianjin First Central Hospital, China (approval No. 2015002X). Lymphodepleting chemotherapy with fludarabine (30 mg/m²) and cyclophosphamide (400 mg/m²) was given to the patient from the day -4 to day -2. On day 0, the patient was infused with autologous CAR-T 19 cells (2 \times 10⁷ cells/kg). The patient had high fever, chills and headache in the first 3 days. At day 7 of the treatment, the cervical lymph node enlargement suddenly increased with laryngeal edema and obstructive dyspnea (Fig. 2B). Therefore, we were forced to terminate CAR-T 19 cell therapy; the laryngeal edema and obstructive dyspnea were treated using dexamethasone.

Two weeks after the failure of CAR-T 19 cells therapy, ibrutinib therapy was administered as the salvage therapy. No increase was found in the percentage of anti-CAR-T 19 cells and gene expression level of anti-CD19 CAR. After ibrutinib therapy for 2 months, the size of the cervical lymph node decreased. Meanwhile, the programmed death-1 (PD-1) expression in peripheral blood CD3⁺ T cells was 82.95%. In the following 2 months, no increase was observed in the percentage of anti-CAR-T 19 cells as well as gene expression level of anti-CD19 CAR in the peripheral blood. Therefore, the patient continued ibrutinib therapy for approx. 14 months with a stable disease condition.

Successful second CAR-T 19 cell therapy

After ibrutinib treatment for 14 months, cervical lymph node enlargement was observed again (Fig. 2C). Nevertheless, the PD-1 expression decreased to 42.5% at this time. As a result, the patient was once again enrolled in the same clinical trial (ChiCTR-ONN-16009862). He received the same dose of lymphodepleting chemotherapy and autologous CAR-T 19 cells as the 1st CAR-T 19 cell

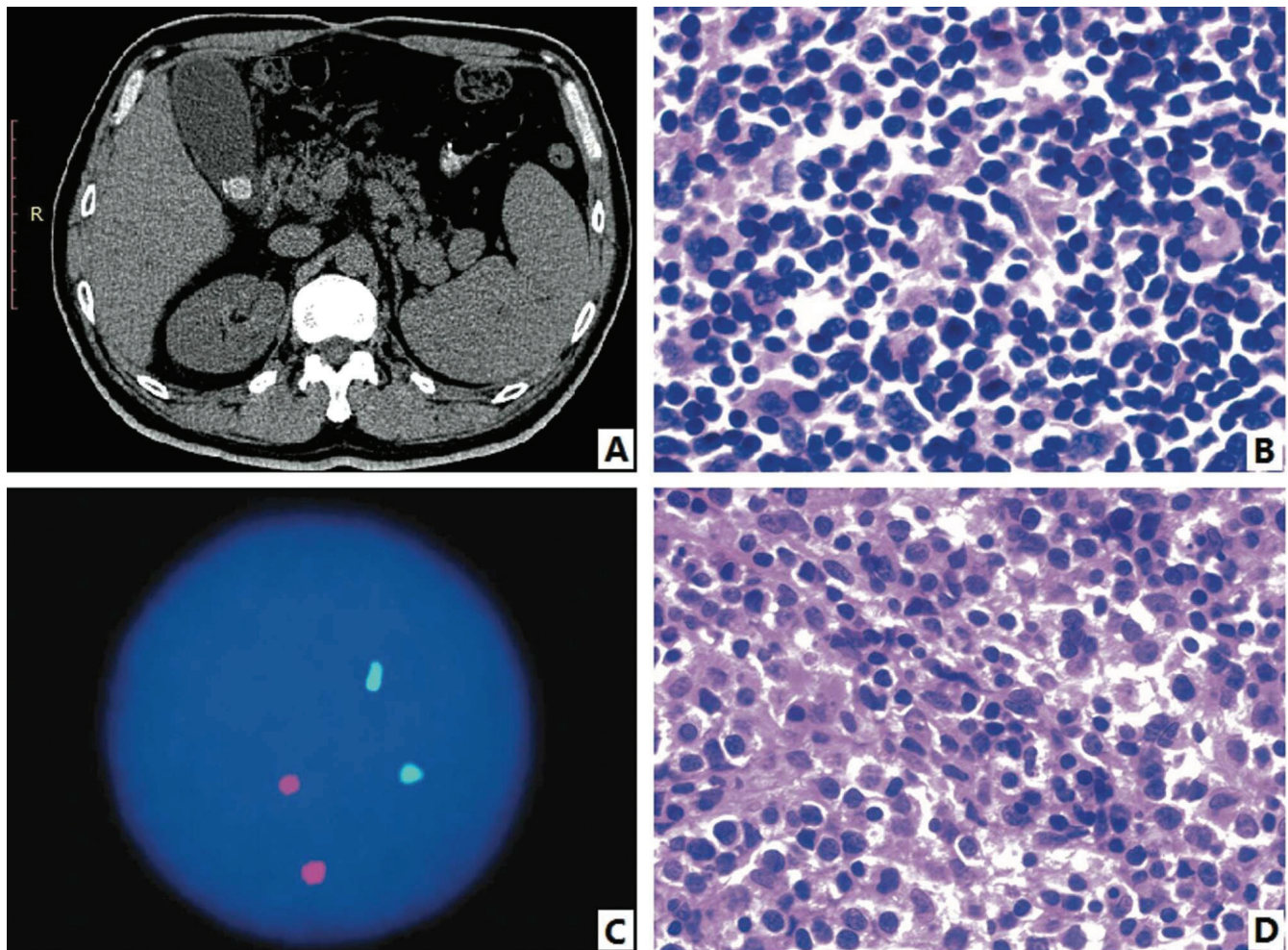


Fig. 1. Diagnosis of mantle cell lymphoma. A. Abdominal computed tomography (CT) in May 2014; B. Result of the pathological biopsy in May 2014; C. Immunoglobulin H (IgH) and T-cell receptor gene rearrangements were negative; D. Result of the pathological biopsy in February 2017

therapy. The level of interleukin-6 (IL-6) was measured using electrochemiluminescence analysis. Flow cytometry was used to detect the level of PD-1 in CD3⁺ T cells and the percentage of CAR-T 19 cells in peripheral blood. The gene expression level of CAR-T 19 was determined using quantitative polymerase chain reaction (qPCR).

CAR-T 19 cell proliferation, cytotoxicity and mRNA expression level of PD-1

The CAR-T 19 cells from the patient's CD3⁺ T cells were divided into various groups: the CAR-T 19 cell group derived from the patient before ibrutinib therapy with or without ibrutinib and CAR-T 19 cell group after ibrutinib therapy with or without ibrutinib. Ibrutinib (4 μg/mL/day) was added to the CAR-T 19 cell culture system on the first day. Cell Counting Kit-8 (Dojindo Molecular Technologies, Kumamoto, Japan) was used to detect the CAR-T 19 cell proliferation at 0 h, 24 h and 48 h. The transfection efficiency of CAR-T 19 cells was analyzed using flow cytometry. The JeKo-1 cell line was bought from the American Type Culture Collection (ATCC; Manassas, USA). Each

group of CAR-T 19 and JeKo-1 cells was cocultured in a 1:1 ratio for 48 h without adding cytokines. The lactate dehydrogenase cytotoxicity test kit was used for the measurement of cytotoxicity at 0 h, 24 h and 48 h; the detection was performed at a wavelength of 490 nm. The enzyme-linked immunosorbent assay (ELISA) kit (Becton Dickinson Biosciences, Franklin Lakes, USA) was applied to determine the release of tumor necrosis factor alpha (TNF-α) and interferon gamma (IFN-γ). The absorbance (A) at 0 h, 12 h, 24 h, and 48 h was measured at 450 nm. The PD-1 mRNA expression in CAR-T 19 cells was determined with reverse transcription (RT)-qPCR. The PD-1 expression, normalized to that of GAPDH and relative to a calibrator, was calculated using the $2^{-\Delta\Delta C_t}$ method. All experiments were repeated 3 times to calculate the mean values.

Comparison of the efficacy of CAR-T cell therapy before and after ibrutinib therapy in mice

Each procedure was performed under the approval of the Animal Care and Use Committee of the Ethics

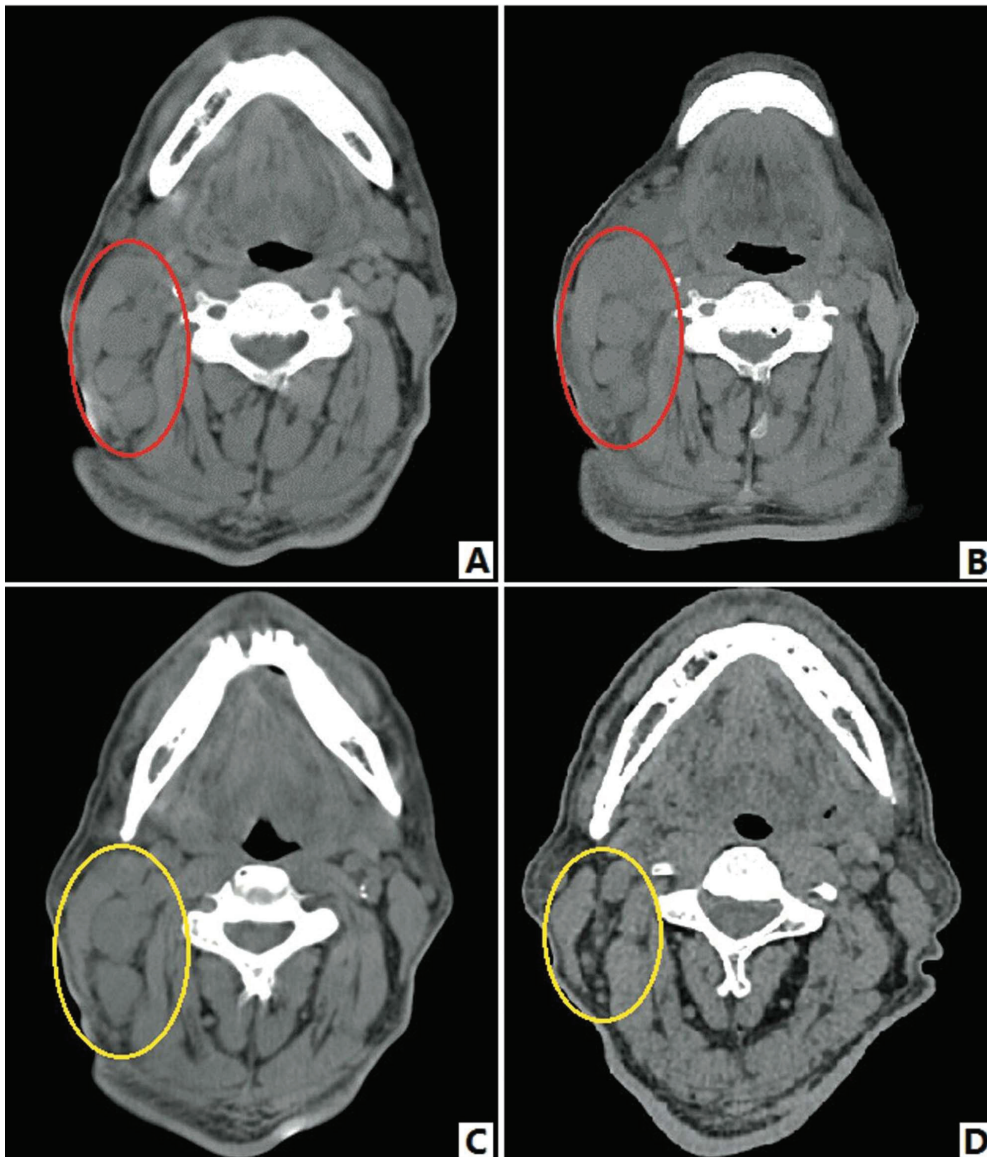


Fig. 2. Changes in the lymph nodes in the 2 chimeric antigen receptor (CAR)-T 19 cell therapies. A. Neck computed tomography (CT) before the first therapy; B. Enlargement of cervical lymph node after the 1st therapy; C. The cervical lymph node increased in size again after ibrutinib therapy; D. The size of the cervical lymph node returned to normal after the 2nd CAR-T 19 cell therapy

Committee of Nankai University, Tianjin, China (approval No. 2017-000012). In a lymphoma animal model, 6–8 weeks old female mice (CAN.N.Cg-Foxn1^{tm1}/CrIVR) bought from Beijing Vital River Laboratory Animal Technology Co., Ltd. (Beijing, China), were injected with 1×10^7 JeKo-1 cells through caudal vein. After 10 days, the successful establishment of the model was confirmed with flow cytometry of the peripheral blood of mice. The mice of lymphoma model were randomly divided into different groups and treated with CAR-T 19 cells (1×10^7 /kg), with or without ibrutinib. The ibrutinib monotherapy group was used as the control group. On the first day of treatment, CAR-T 19 cells were administered through caudal vein. Mice were given the clinically recommended dose of ibrutinib (8 mg/kg/day) via oral gavage. Each group consisted of 5 mice. The proportion of JeKo-1 and CAR-T 19 cells in mice was determined with flow cytometry.

Statistical analysis

Data are expressed as mean \pm standard error (SE), along with the number of repeated experiments. All data were independently analyzed using the t-test. Statistically significant difference was defined as $p < 0.05$.

Results

Results of the second CAR-T 19 cell therapy

We obtained the agreement from the patient for using their specimens and data in this study. The patient had high fever, chills and headache during the first 5 days following the 2nd CAR-T 19 cell therapy. The highest serum IL-6 level was 275.6 pg/mL on day 4 of the 2nd treatment, compared with 15.2 pg/mL on the same day of the 1st treatment

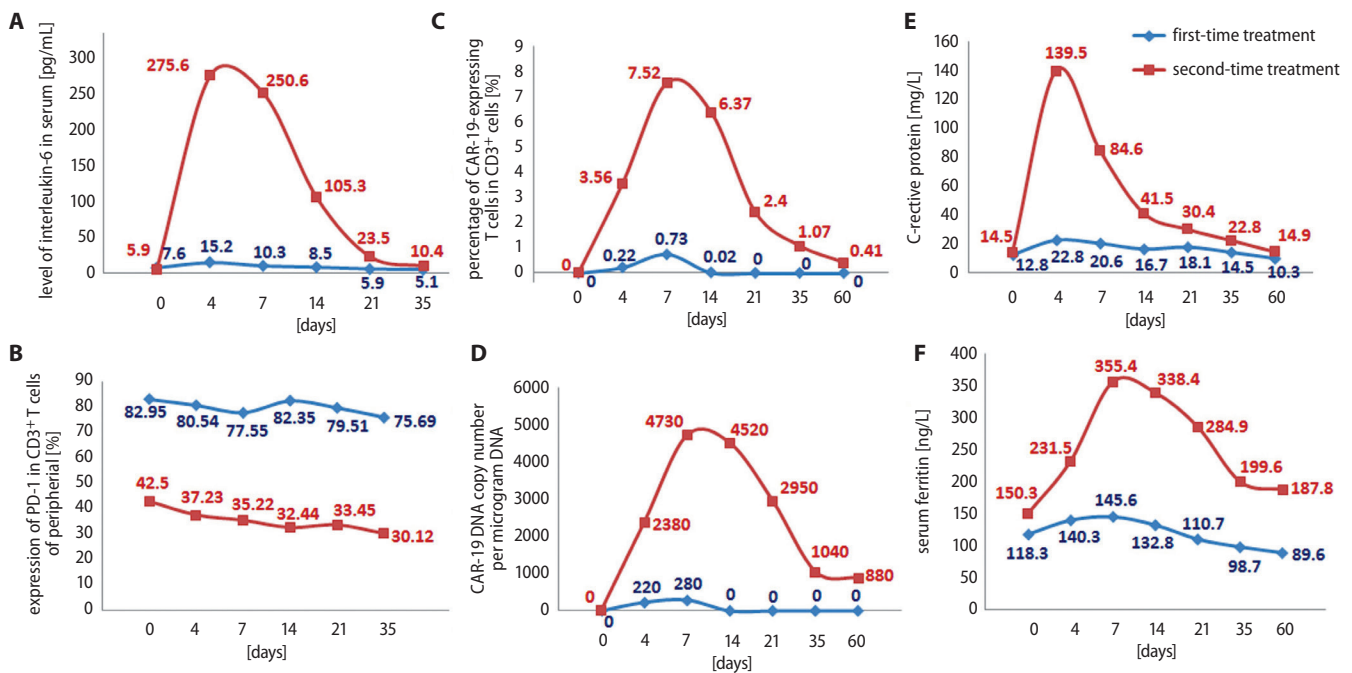


Fig. 3. Comparison of the 2 chimeric antigen receptor (CAR)-T 19 cell therapies. A. The highest serum interleukin-6 (IL-6) level was 275.6 pg/mL in the 2nd therapy; B. The programmed death-1 (PD-1) expression decreased from approx. 80% in the 1st therapy to approx. 40% in the 2nd therapy; C. The highest percentage of CAR-T 19 cells was 7.52% in the 2nd therapy; D. The highest copy number of CAR-T 19 DNA was 4730 copies/μg DNA in the 2nd therapy; E. The highest C-reactive protein (CRP) level was 139.5 mg/mL in the 2nd therapy; F. The highest ferritin level was 355.4 ng/mL in the 2nd therapy

(Fig. 3A). The expression level of PD-1 was maintained at >80% in the 1st treatment, in the 2nd treatment, it was maintained at approx. 40% (Fig. 3B).

On day 7 of the 2nd treatment, the percentage of CAR-T 19 cells was the highest (7.52%) in CD3⁺ T cells (Fig. 3C). Compared with the highest CAR-T 19 DNA value of 280 copies/μg DNA obtained in the 1st treatment, the value was 4730 copies/μg DNA in the 2nd treatment (Fig. 3D). The changes in serum ferritin and C-reactive protein (CRP) levels were similar to those in IL-6 levels (Fig. 3E,F).

In the 2nd treatment, the size of the cervical lymph node was significantly reduced with grade II CRS³¹ after the 2nd CAR-T 19 cell therapy (Fig. 2D). The patient achieved CR after 2 months; CR has been maintained for 15 months, up to the present.

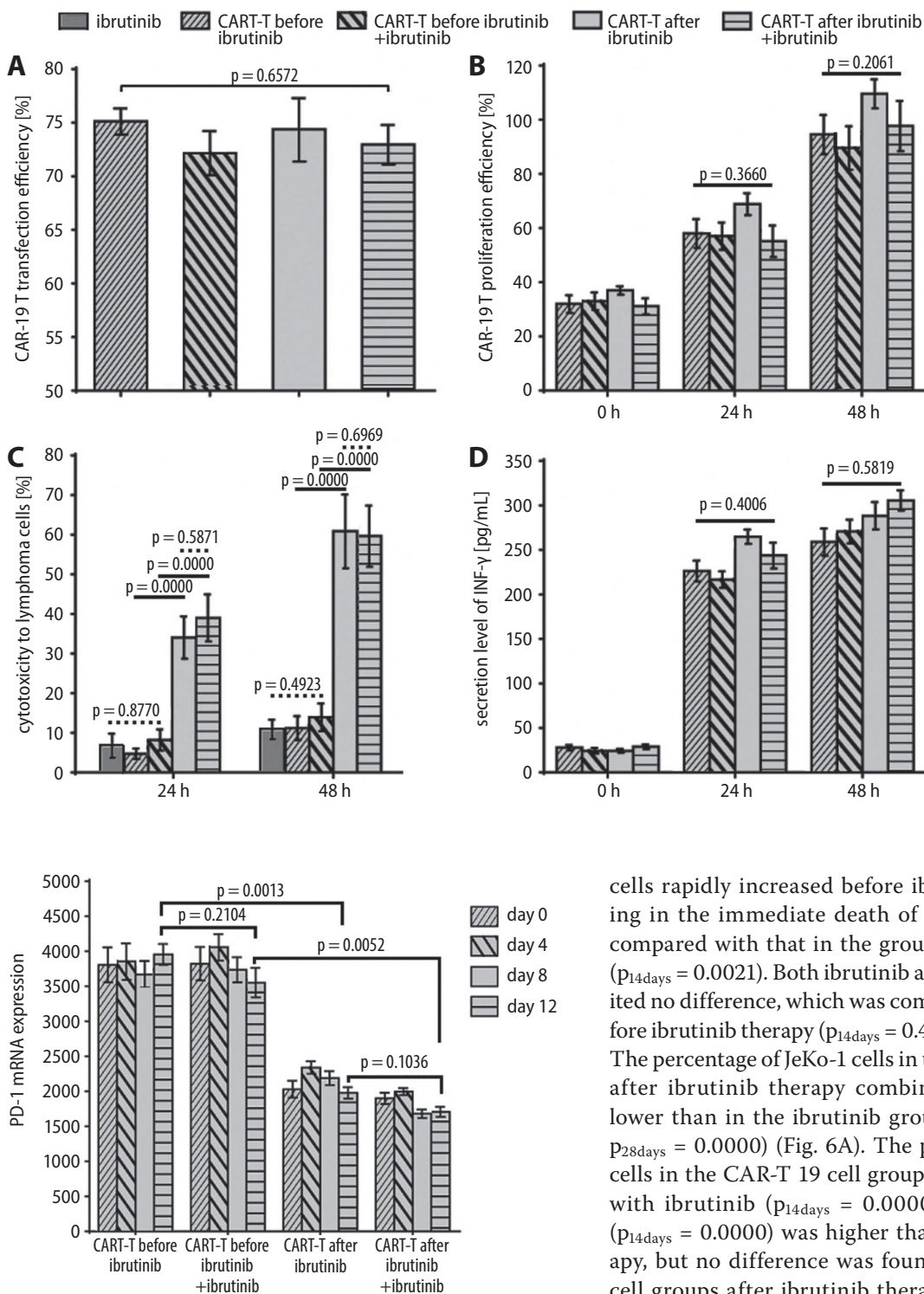
Results in vitro

No significant difference of the transfection rate was found in the 4 groups ($p = 0.6572$) (Fig. 4A). There was also no difference of the proliferation in the 4 groups at 24 h or 48 h ($p_{24h} = 0.3660$ and $p_{48h} = 0.2061$) (Fig. 4B). Ibrutinib therapy for 14 months and the addition of ibrutinib into the culture system did not affect the proliferation and transfection of CAR-T 19 cells. The CAR-T 19 cells derived from T cells before or after ibrutinib therapy showed almost no change in JeKo-1 cell cytotoxicity, regardless of whether ibrutinib was present or not in the culture system. Ibrutinib alone was used as the control group (before ibrutinib

therapy: $p_{24h} = 0.8770$ and $p_{48h} = 0.4923$; after ibrutinib therapy: $p_{24h} = 0.5871$ and $p_{48h} = 0.6969$). The CAR-T 19 cells after ibrutinib therapy showed significant JeKo-1 cell activity regardless of whether ibrutinib was present or not in the culture system (without ibrutinib in the culture: $p_{24h} = 0.0000$ and $p_{48h} = 0.0000$; with ibrutinib in the culture: $p_{24h} = 0.0000$ and $p_{48h} = 0.0000$) (Fig. 4C). There was no difference in the IFN-γ release profile of all groups ($p_{24h} = 0.4006$ and $p_{48h} = 0.5819$) (Fig. 4D). Similarly to the results of proliferation and transfection, ibrutinib therapy and the addition of ibrutinib into the culture system did not affect the IFN-γ release. After ibrutinib therapy, PD-1 mRNA expression in CAR-T 19 cells was lower than before ibrutinib therapy (without ibrutinib in the culture: $p = 0.0013$; with ibrutinib in the culture: $p = 0.0052$). The mRNA expression level of PD-1 exhibited no difference in the CAR-T 19 cell culture systems with or without ibrutinib (before ibrutinib therapy: $p = 0.2104$; after ibrutinib therapy: $p = 0.1036$) (Fig. 5).

Results in mice

In the animal experiments, the percentage of JeKo-1 cells decreased in the CAR-T 19 cell group after ibrutinib therapy with ibrutinib compared with that before ibrutinib therapy with ibrutinib on 14 days and 28 days after therapy ($p_{14days} = 0.0000$ and $p_{28days} = 0.0000$). The percentage of JeKo-1 cells decreased in the CAR-T 19 cell group after ibrutinib therapy compared with that before ibrutinib therapy on 14 days after therapy ($p_{14days} = 0.0000$).



Nevertheless, no difference was found in the two CAR-T 19 cell groups after ibrutinib therapy at 14 days or 28 days after CAR-T 19 cell therapy ($p_{14\text{days}} = 0.1459$ and $p_{28\text{days}} = 0.4005$). The proportion of JeKo-1 cells in the group of CAR-T 19

cells rapidly increased before ibrutinib therapy, resulting in the immediate death of the mice after 14 days, compared with that in the group treated with ibrutinib ($p_{14\text{days}} = 0.0021$). Both ibrutinib and CAR-T groups exhibited no difference, which was combined with ibrutinib before ibrutinib therapy ($p_{14\text{days}} = 0.4292$ and $p_{28\text{days}} = 0.3175$). The percentage of JeKo-1 cells in the CAR-T 19 cell groups after ibrutinib therapy combined with ibrutinib was lower than in the ibrutinib group ($p_{14\text{days}} = 0.0000$ and $p_{28\text{days}} = 0.0000$) (Fig. 6A). The proportion of CAR-T 19 cells in the CAR-T 19 cell groups after ibrutinib therapy with ibrutinib ($p_{14\text{days}} = 0.0000$) or without ibrutinib ($p_{14\text{days}} = 0.0000$) was higher than before ibrutinib therapy, but no difference was found in the two CAR-T 19 cell groups after ibrutinib therapy ($p_{14\text{days}} = 0.1922$ and $p_{28\text{days}} = 0.4490$). Besides, the proportion in the CAR-T 19 cell group exhibited no difference before ibrutinib therapy with or without ibrutinib ($p_{14\text{days}} = 0.3514$) (Fig. 6B).

Discussion

In our study, the patient with relapsed MCL showed stable disease during his 14-month ibrutinib treatment after the 1st therapy failed. When his condition worsened again

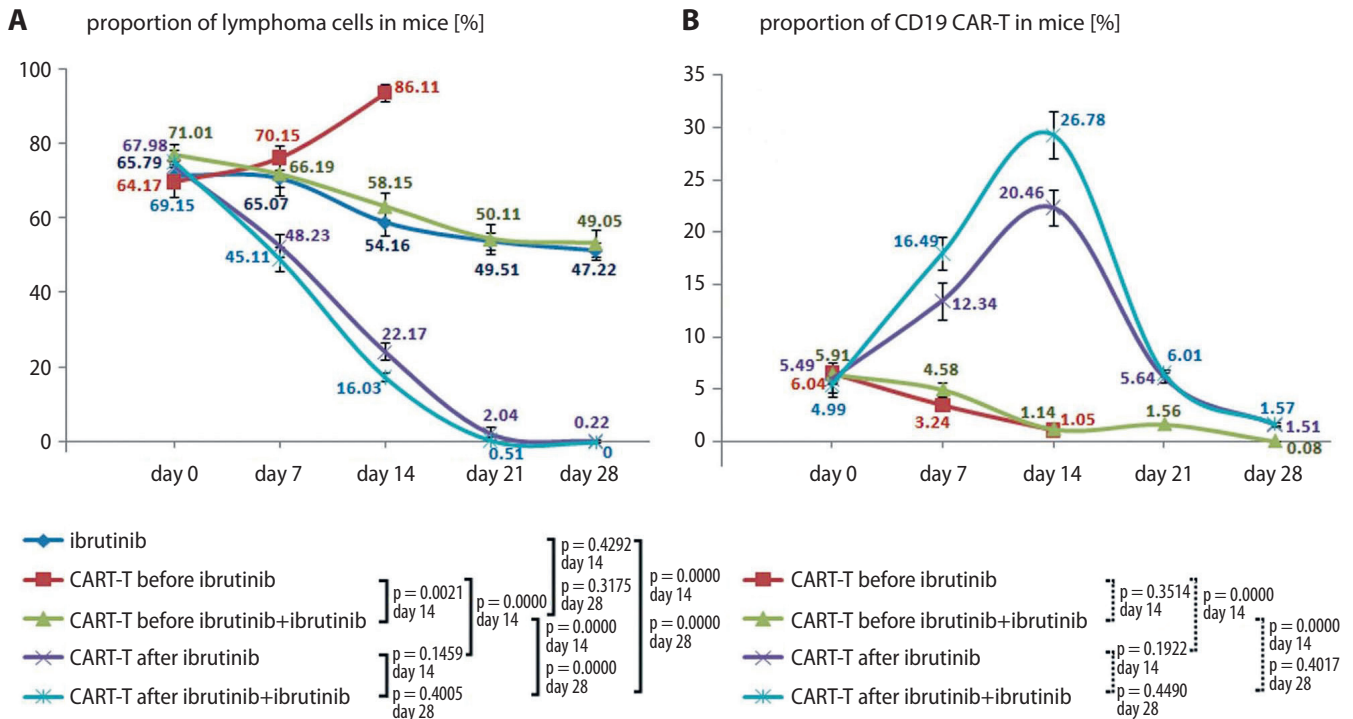


Fig. 6. Proportion of lymphoma and chimeric antigen receptor (CAR)-T 19 cells in mice. A. Regardless of whether ibrutinib was administered at the same time or not, the percentage of JeKo-1 cells in mice significantly decreased in the group of CAR-T 19 cell after ibrutinib treatment. The proportion of JeKo-1 cells in mice rapidly increased in the group of CAR-T 19 cell before ibrutinib treatment, leading to the immediate death of the mice after 14 days; B. The proportion of CAR-T 19 cells showed an inverse relationship with the proportion of JeKo-1 cells

during ibrutinib treatment, he received the 2nd CAR-T 19 cell therapy to achieve CR. The reason for the failure of the 1st CAR-T 19 cell therapy was unclear. It was observed that PD-1 expression was 82.95% in CD3⁺ T cells before the first CAR-T 19 therapy. Interestingly, it decreased to approx. 40% after the 14-month ibrutinib therapy. This research investigated the efficacy of CAR-T 19 cell therapy before and after ibrutinib therapy in vitro and in mice.

Ibrutinib functions as a BTK inhibitor to downregulate NF-κB (nuclear factor kappa-light-chain-enhancer of activated B cells) signaling, thus controlling the homing and migration of tumor cells. Blocking the interaction between macrophages and tumor cells is an important way to decrease the chemoattraction of tumor cells to the bone marrow microenvironment.^{32–35} In one study, ibrutinib therapy with CLL for >5 months increased the proliferation and efficacy of CAR-T 19 cells.²⁸ A long-term ibrutinib therapy for patients with CLL could result in overcoming the immunosuppression of the primary disease, repairing the functional defects of autologous T cells, and decreasing the PD-1 expression in T cells. This effect of ibrutinib therapy is achieved through BTK-dependent and BTK-independent mechanisms.³⁶

Another research has shown that ibrutinib modulates the tumor microenvironment of patients with CLL through the downregulation of the expression level of programmed death ligand-1 in CLL cells after 3 months of ibrutinib therapy.³⁷ Therefore, although the resistance to ibrutinib

might occur during the treatment,^{38,39} the CAR-T 19 cell therapy was highly effective in CLL patients after the failure of ibrutinib therapy.

Does long-term ibrutinib therapy improve T-cell function in patients with CLL and other types of B-cell lymphomas? The combination of ibrutinib improved the therapeutic effect of CAR-T 19 cell therapy on MCL cell line in vitro and in vivo.³⁰ In our study, the patient with relapsed MCL achieved CR with the 2nd CAR-T 19 cell therapy after 14-month ibrutinib therapy.

Limitations

This study has some limitations. The study did not investigate whether the mechanism of improving the T-cell function in MCL patients following long-term ibrutinib therapy is consistent with that in patients with CLL, and whether long-term ibrutinib therapy improves T-cell function in other types of B-cell lymphomas, which will be explored in the further studies.

Conclusions

In our study, we demonstrated that the efficacy of CAR-T 19 cell therapy was enhanced after 14-month ibrutinib therapy in vitro, in mice and in the clinical trial in which a patient was enrolled. However, there was no

synergistic effect of a short period of combination of CAR-T 19 cells and ibrutinib in vitro and in mice. The results of our study support the conclusion that long-term ibrutinib therapy could enhance the efficacy of the CAR-T 19 cell therapy. These results in MCL cell lines and the patient with MCL are similar to those of previous studies on CLL cell lines and patients with CLL.²⁸

ORCID iDs

Juan Mu  <https://orcid.org/0000-0003-2339-0892>
 Meijing Liu  <https://orcid.org/0000-0003-1716-6632>
 Jia Wang  <https://orcid.org/0000-0001-8518-6948>
 Juanxia Meng  <https://orcid.org/0000-0002-8811-3418>
 Rui Zhang  <https://orcid.org/0000-0002-6605-2458>
 Yanyu Jiang  <https://orcid.org/0000-0002-1742-9474>
 Qi Deng  <https://orcid.org/0000-0002-3646-4953>

References

- Wang M, Fowler N, Wagner-Bartak N, et al. Oral lenalidomide with rituximab in relapsed or refractory diffuse large cell, follicular and transformed lymphoma: A phase II clinical trial. *Leukemia*. 2013;27(9):1902–1909. doi:10.1038/leu.2013.95
- Gisselbrecht C, Glass B, Mounier N, et al. Salvage regimens with autologous transplantation for relapsed large B-cell lymphoma in the rituximab era. *J Clin Oncol*. 2010;28(27):4184–4190. doi:10.1200/jco.2010.28.1618
- Zhao Z, Chen Y, Francisco NM, Zhang Y, Wu M. The application of CAR-T cell therapy in hematological malignancies: Advantages and challenges. *Acta Pharm Sin B*. 2018;8(4):539–551. doi:10.1016/j.apsb.2018.03.001
- Chow VA, Shadman M, Gopal AK. Translating anti-CD19 CAR T-cell therapy into clinical practice for relapsed/refractory diffuse large B-cell lymphoma. *Blood*. 2018;132(8):777–781. doi:10.1182/blood-2018-04-839217
- Davila ML, Riviere I, Wang X, et al. Efficacy and toxicity management of 19-28z CAR T cell therapy in B cell acute lymphoblastic leukemia. *Sci Transl Med*. 2014;6(224):224ra25. doi:10.1126/scitranslmed.3008226
- Kebriaei P, Huls H, Singh H, et al. Adoptive therapy using Sleeping Beauty gene transfer system and artificial antigen presenting cells to manufacture T cells expressing CD19-specific chimeric antigen receptor. *Blood*. 2014;124(21):311. doi:10.1182/blood.V124.21.311.311
- Turtle CJ, Hanafi LA, Berger C, et al. Immunotherapy of non-Hodgkin's lymphoma with a defined ratio of CD8⁺ and CD4⁺ CD19-specific chimeric antigen receptor-modified T cells. *Sci Transl Med*. 2016;8(355):355ra116. doi:10.1126/scitranslmed.aaf8621
- Lee DW, Kochenderfer JN, Stetler-Stevenson M, et al. T cells expressing CD19 chimeric antigen receptors for acute lymphoblastic leukaemia in children and young adults: A phase 1 dose-escalation trial. *Lancet*. 2015;385(9967):517–528. doi:10.1016/s0140-6736(14)61403-3
- Kochenderfer JN, Dudley ME, Kassim SH, et al. Chemotherapy-refractory diffuse large B-cell lymphoma and indolent B-cell malignancies can be effectively treated with autologous T cells expressing an anti-CD19 chimeric antigen receptor. *J Clin Oncol*. 2015;33(6):540–549. doi:10.1200/jco.2014.56.2025
- Porter DL, Levine BL, Kalos M, Bagg A, June CH. Chimeric antigen receptor-modified T cells in chronic lymphoid leukemia. *N Engl J Med*. 2011;365(8):725–733. doi:10.1056/NEJMoa1103849
- Porter DL, Hwang WT, Frey NV, et al. Chimeric antigen receptor T cells persist and induce sustained remissions in relapsed refractory chronic lymphocytic leukemia. *Sci Transl Med*. 2015;7(303):303ra139. doi:10.1126/scitranslmed.aac5415
- Neelapu SS, Locke FL, Bartlett NL, et al. Axicabtagene ciloleucel CAR T-Cell therapy in refractory large B-cell lymphoma. *N Engl J Med*. 2017;377(26):2531–2544. doi:10.1056/NEJMoa1707447
- Maude SL, Laetsch TW, Buechner J, et al. Tisagenlecleucel in children and young adults with B-cell lymphoblastic leukemia. *N Engl J Med*. 2018;378(5):439–448. doi:10.1056/NEJMoa1709866
- Schuster SJ, Bishop MR, Tam CS, et al. Tisagenlecleucel in adult relapsed or refractory diffuse large B-cell lymphoma. *N Engl J Med*. 2019;380(1):45–56. doi:10.1056/NEJMoa1804980
- Ogba N, Arwood NM, Bartlett NL, et al. Chimeric antigen receptor T-cell therapy. *J Natl Compr Canc Netw*. 2018;16(9):1092–1106. doi:10.6004/jnccn.2018.0073
- Byrd JC, Furman RR, Coutre SE, et al. Targeting BTK with ibrutinib in relapsed chronic lymphocytic leukemia. *N Engl J Med*. 2013;369(1):32–42. doi:10.1056/NEJMoa1215637
- Wang ML, Rule S, Martin P, et al. Targeting BTK with ibrutinib in relapsed or refractory mantle-cell lymphoma. *N Engl J Med*. 2013;369(6):507–516. doi:10.1056/NEJMoa1306220
- Rule S, Jurczak W, Jerkeman M, et al. Ibrutinib versus temsirolimus: 3-year follow-up of patients with previously treated mantle cell lymphoma from the phase 3, international, randomized, open-label RAY study. *Leukemia*. 2018;32(8):1799–1803. doi:10.1038/s41375-018-0023-2
- Buggy JJ, Elias L. Bruton tyrosine kinase (BTK) and its role in B-cell malignancy. *Int Rev Immunol*. 2012;31(2):119–132. doi:10.3109/08830185.2012.664797
- Schliffke S, Akyüz N, Ford CT, et al. Clinical response to ibrutinib is accompanied by normalization of the T-cell environment in CLL-related autoimmune cytopenia. *Leukemia*. 2016;30(11):2232–2234. doi:10.1038/leu.2016.157
- Mohammad DK, Nore BF, Hussain A, Gustafsson MO, Mohamed AJ, Smith CI. Dual phosphorylation of Btk by Akt/protein kinase b provides docking for 14-3-3ζ, regulates shuttling, and attenuates both tonic and induced signaling in B cells. *Mol Cell Biol*. 2013;33(16):3214–3226. doi:10.1128/mcb.00247-13
- Ponader S, Burger JA. Bruton's tyrosine kinase: From X-linked agammaglobulinemia toward targeted therapy for B-cell malignancies. *J Clin Oncol*. 2014;32(17):1830–1839. doi:10.1200/jco.2013.53.1046
- Advani RH, Buggy JJ, Sharman JP, et al. Bruton tyrosine kinase inhibitor ibrutinib (PCI-32765) has significant activity in patients with relapsed/refractory B-cell malignancies. *J Clin Oncol*. 2013;31(1):88–94. doi:10.1200/jco.2012.42.7906
- Herman SE, Mustafa RZ, Gyamfi JA, et al. Ibrutinib inhibits BCR and NF-κB signaling and reduces tumor proliferation in tissue-resident cells of patients with CLL. *Blood*. 2014;123(21):3286–3295. doi:10.1182/blood-2014-02-548610
- Burger JA, Buggy JJ. Bruton tyrosine kinase inhibitor ibrutinib (PCI-32765). *Leuk Lymphoma*. 2013;54(11):2385–2391. doi:10.3109/10428194.2013.777837
- Sadelain M, Riviere I, Riddell S. Therapeutic T cell engineering. *Nature*. 2017;545(7655):423–431. doi:10.1038/nature22395
- Turtle CJ, Hay KA, Hanafi LA, et al. Durable molecular remissions in chronic lymphocytic leukemia treated with CD19-specific chimeric antigen receptor-modified T cells after failure of ibrutinib. *J Clin Oncol*. 2017;35(26):3010–3020. doi:10.1200/jco.2017.72.8519
- Fraietta JA, Beckwith KA, Patel PR, et al. Ibrutinib enhances chimeric antigen receptor T-cell engraftment and efficacy in leukemia. *Blood*. 2016;127(9):1117–1127. doi:10.1182/blood-2015-11-679134
- Romero D. Haematological cancer: After ibrutinib, CART cells induce responses. *Nat Rev Clin Oncol*. 2017;14(10):588. doi:10.1038/nrclinonc.2017.124
- Ruella M, Kenderian SS, Shestova O, et al. The addition of the BTK inhibitor ibrutinib to anti-CD19 chimeric antigen receptor T cells (CART19) improves responses against mantle cell lymphoma. *Clin Cancer Res*. 2016;22(11):2684–2696. doi:10.1158/1078-0432.Ccr-15-1527
- Brudno JN, Kochenderfer JN. Toxicities of chimeric antigen receptor T cells: Recognition and management. *Blood*. 2016;127(26):3321–3330. doi:10.1182/blood-2016-04-703751
- Saleh LM, Wang W, Herman SE, et al. Ibrutinib downregulates a subset of miRNA leading to upregulation of tumor suppressors and inhibition of cell proliferation in chronic lymphocytic leukemia. *Leukemia*. 2017;31(2):340–349. doi:10.1038/leu.2016.181
- Chang BY, Francesco M, De Rooij MF, et al. Egress of CD19(+)CD5(+) cells into peripheral blood following treatment with the Bruton tyrosine kinase inhibitor ibrutinib in mantle cell lymphoma patients. *Blood*. 2013;122(14):2412–2424. doi:10.1182/blood-2013-02-482125
- Cheng S, Ma J, Guo A, et al. BTK inhibition targets in vivo CLL proliferation through its effects on B-cell receptor signaling activity. *Leukemia*. 2014;28(3):649–657. doi:10.1038/leu.2013.358

35. Ponader S, Chen SS, Buggy JJ, et al. The Bruton tyrosine kinase inhibitor PCI-32765 thwarts chronic lymphocytic leukemia cell survival and tissue homing in vitro and in vivo. *Blood*. 2012;119(5):1182–1189. doi:10.1182/blood-2011-10-386417
36. Long M, Beckwith K, Do P, et al. Ibrutinib treatment improves T cell number and function in CLL patients. *J Clin Invest*. 2017;127(8):3052–3064. doi:10.1172/jci89756
37. Kondo K, Shaim H, Thompson PA, et al. Ibrutinib modulates the immunosuppressive CLL microenvironment through STAT3-mediated suppression of regulatory B-cell function and inhibition of the PD-1/PD-L1 pathway. *Leukemia*. 2018;32(4):960–970. doi:10.1038/leu.2017.304
38. Hamasy A, Wang Q, Blomberg KE, et al. Substitution scanning identifies a novel, catalytically active ibrutinib-resistant BTK cysteine 481 to threonine (C481T) variant. *Leukemia*. 2017;31(1):177–185. doi:10.1038/leu.2016.153
39. Jones D, Woyach JA, Zhao W, et al. PLCG2 C2 domain mutations co-occur with BTK and PLCG2 resistance mutations in chronic lymphocytic leukemia undergoing ibrutinib treatment. *Leukemia*. 2017;31(7):1645–1647. doi:10.1038/leu.2017.110

Various clinical scenarios of primary melanoma of the esophagus: A retrospective 20-year analysis from two university thoracic surgery centers

Konrad Stępień^{1,A–D,F}, Paweł Skorek^{1,A–D,F}, Janusz Włodarczyk^{1,B–D,F}, Janusz Wójcik^{2,B–F}, Tomasz Smęder^{1,B–D,F}, Łukasz Trybalski^{1,B–D,F}, Lucyna Rudnicka-Sosin^{3,B–D,F}, Jarosław Kuźdżał^{1,A–F}, Piotr Kocon^{1,A–F}

¹ Department of Thoracic Surgery, Jagiellonian University Medical College, Faculty of Health Sciences, John Paul II Hospital, Kraków, Poland

² Department of Thoracic Surgery and Transplantation, Pomeranian Medical University in Szczecin, Poland

³ Department of Pathology, John Paul II Hospital, Kraków, Poland

A – research concept and design; B – collection and/or assembly of data; C – data analysis and interpretation; D – writing the article; E – critical revision of the article; F – final approval of the article

Advances in Clinical and Experimental Medicine, ISSN 1899–5276 (print), ISSN 2451–2680 (online)

Adv Clin Exp Med. 2022;31(3):337–344

Address for correspondence

Paweł Skorek

E-mail: pawel.skorek23@gmail.com

Funding sources

None declared

Conflict of interest

None declared

Received on October 25, 2021

Reviewed on December 3, 2021

Accepted on February 18, 2022

Published online on March 29, 2022

Cite as

Stępień K, Skorek P, Włodarczyk J, et al. Various clinical scenarios of primary melanoma of the esophagus: A retrospective 20-year analysis from two university thoracic surgery centers. *Adv Clin Exp Med.* 2022;31(3):337–344. doi:10.17219/acem/146797

DOI

10.17219/acem/146797

Copyright

© 2022 by Wrocław Medical University

This is an article distributed under the terms of the Creative Commons Attribution 3.0 Unported (CC BY 3.0) (<https://creativecommons.org/licenses/by/3.0/>)

Abstract

Background. Primary melanoma of the esophagus (PME) represents a rare type of gastrointestinal malignancy with an exceptionally poor diagnosis. So far, only few descriptions of PME which satisfactorily summarize their clinical characteristics and prognosis have been published.

Objectives. The aim of our study was to summarize our experience with PME patients.

Materials and methods. In a group of 1387 patients who underwent esophagectomy due to neoplastic process in the years 2000–2020 in 2 high-volume university thoracic surgery centers, we identified those with confirmed PME diagnosis. Subsequently, their clinical characteristics, imaging and histopathological results were compared. The data regarding the long-term survival were obtained from the Polish National Death Registry.

Results. The PME was identified in 4 (0.29%) patients. Three of them (75%) were males. The mean age on admission was 64.3 ± 17.5 years. The main symptom in all patients was dysphagia. In 1 patient with the most advanced PME, the clinically relevant weight loss was noted. In 3 patients, Ivor Lewis esophagectomy was performed, and 1 patient underwent McKeown resection. Histopathologic examination revealed a metastasis of lymph nodes only in 1 patient. The average maximum size of tumor was 6.9 ± 4.7 cm and all tumors were located in distal part of the esophagus. Two out of those 4 patients are still alive and the longest survival time is 17 years. One patient died due to postoperative massive gastrointestinal bleeding complicated with cardiac arrest and the other one due to progression of PME systemic dissemination 6 months after surgical treatment.

Conclusions. The PME is an extremely rare diagnosis. A long-term survival can be achieved with the complete resection. Clinical scenarios of surgically treated PME patients may significantly differ.

Key words: melanoma, esophagectomy, esophageal neoplasm

Background

Primary melanoma of the esophagus (PME) represents an exceedingly rare diagnosis.¹ Reportedly, PME concerns 0.1–0.2% of all esophageal malignancies.¹ The first histopathologically proven PME was described by Garfinkle and Cahan in 1952.² So far, only a few hundred such cases have been described worldwide.

Most of the evidence is based on individual case reports. Up to now, only a few series of PME patients have been described. Wang et al. described 13 PME patients treated surgically.³ Gao et al. analyzed another Asian cohort consisting of 17 PME patients.⁴ Moreover, Szumiło and Dąbrowski initially described 3 PME treated in 1 medical center.⁵ However, the data of these patients were then included in the largest to date PME cohort; a significant proportion of those patients underwent molecular genetic profiling.⁶

Due to the highly unfavorable prognosis, PME is repeatedly described as an aggressive disease entity. As has been shown by Sabanathan et al. in their systematic review, the overall survival (OS) was only 10–13 months with a 5-year survival rate ranging from 0% to 4%. Metastatic disease was found in 40.9% of patients at the time of diagnosis. Moreover, at the time of diagnosis, more than 90% of the tumors were larger than 2 cm.⁷ Similar observations also apply to the latest abovementioned cohort studies.^{3–6} Wang et al. estimated the overall 1-year and 5-year postoperative survival rates as 54.0% and 35.9%, respectively.³ Even worse treatment outcomes were reported by Gao et al. (1-year survival rate – 51%, 5-year – 10%).⁴

Objectives

We sought to analyze the incidence of PME diagnosis and long-term results of treatment in 2 Polish university thoracic surgery centers.

Materials and methods

A retrospective analysis of available data from the years 2000–2020 was conducted. The study group included consecutive patients with pathologically confirmed diagnosis of PME who underwent a curative-intent surgery. Data used for analysis were obtained from medical records. Patients' clinical and demographic characteristics, detailed histopathologic data with immunohistochemical features and imaging data were recorded, if available.⁸ Finally, the data regarding the long-term survival were obtained from the Polish National Death Registry. The study protocol complied with the Declaration of Helsinki. All included patients gave informed consent. The approval of the Ethical Committee has been waived because of the retrospective character of the study, based exclusively on hospital records.

Results

We identified 1387 patients who underwent esophagectomy due to primary esophageal malignancies. From this group, only 4 (0.29%) cases of PME were identified. The graphical presentation of clinical course of these patients is shown in Fig. 1. A brief summary of their clinical

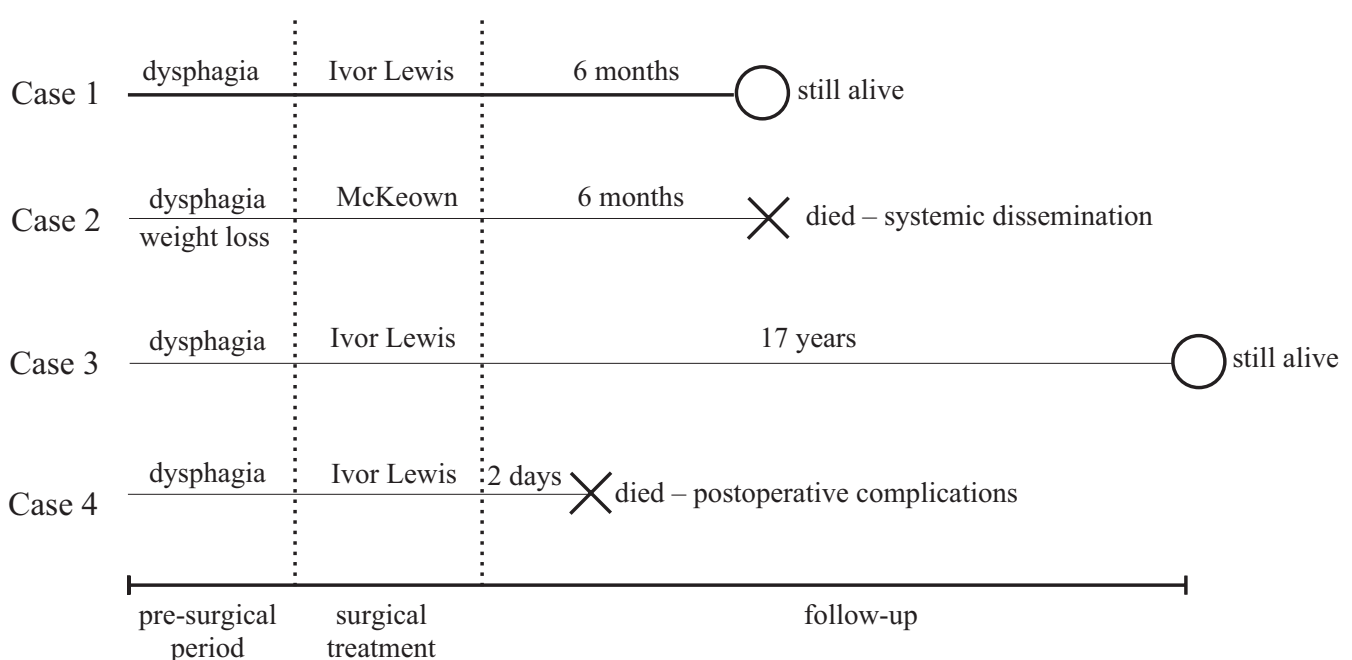


Fig. 1. The timelines presenting the clinical course of the described patients

Table 1. Clinical characteristics of the described patients with primary melanoma of the esophagus

Variable	Case 1	Case 2	Case 3	Case 4
Year	2020	2017	2003	2000
Gender	female	male	male	male
Age [years]	63	75	40	79
Symptoms	dysphagia	dysphagia, weight loss	dysphagia	dysphagia
Tumor maximum dimension [cm]	2 tumors: 2 and 3.5	13.5	7	3.5
Localization	distal	distal	distal	distal
Type of esophagectomy	Ivor Lewis	McKeown	Ivor Lewis	Ivor Lewis
Metastases in pathological evaluation	no	lymph nodes (1 paraesophageal, 1 gastric, 1 celiac)	no	no
Follow-up	alive	died after 6 months – systemic dissemination	alive	died after 2 days – postoperative complications

characteristics is presented in Table 1. As has been shown, 3 of them (75%) were males. The mean age on admission was 64.3 ± 17.5 years, ranging from 40 to 79 years. All patients complained of dysphagia. In addition, in 1 patient, the clinically relevant weight loss was found (case 2).

None of the patients underwent preoperative chemotherapy or radiotherapy. In 3 patients, Ivor Lewis esophagectomy was performed and in 1 patient, McKeown esophagectomy was used (case 2). In all cases, surgical intervention was successful, without any perioperative complications. Histopathologic examination revealed metastasis in lymph nodes in 1 patient (case 2). The average maximum size of the tumor was 6.9 ± 4.7 cm and all tumors were located in the thoracic part of the esophagus. Two patients are still alive and the longest survival time is 17 years (case 3).

Case 1

A 63-year-old female in a good general condition with symptoms of dysphagia was admitted due to previously diagnosed PME. A detailed examination of skin, mucosa and anus did not reveal any suspicious lesions. Endoscopic examination with endobronchial ultrasound (EBUS) and endoscopic ultrasound (EUS) revealed a polypoid esophageal tumor at a distance of 31 cm from incisors line and thickened esophageal wall in the esophagogastric junction. The enlargement of mediastinal lymph nodes was not detected. Due to a local advancement confirmed with contrast-enhanced computed tomography (CECT) and positron emission tomography (PET), the clinical stage was estimated as cT2N0M0 (Fig. 2A,B).

The patient underwent Ivor Lewis esophagectomy with D2 lymphadenectomy and the postoperative course was uneventful.

Pathological examination confirmed the initial diagnosis and staging of PME (pT2N0M0, R0) (Fig. 2C,D). In the resected specimens, 2 separate tumors with a diameter of 2.0 cm and 3.5 cm were described. Low melanotic neoplastic cells showed features of extensive lentiginous

spread. The PME invaded the mucosa and submucosa, and there were no signs of angioinvasion. The number of mitoses was about $9/\text{mm}^2$. No metastases were found in any of the 32 analyzed lymph nodes.

Six months after surgery, the patient is still alive and was scheduled for further oncological treatment by the Multidisciplinary Tumor Board.

Case 2

A 75-year-old male was admitted with a large tumor of the esophagus diagnosed as PME on the basis of endoscopic biopsy performed in a regional hospital. On admission, patient presented with dysphagia and tolerated only soft diet. He had lost 15 kg of body weight in the preceding period. Detailed physical examination, including skin, oral mucosa and anus, did not reveal any suspicious lesions or lymph node enlargement. The patient smoked about 30 pack-years. There was no history of melanoma in his family.

Endoscopic examination including EBUS and EUS revealed an obstructing, amelanocytic tumor, at the distance of 25 cm from incisors line, and a massive hypoechoic infiltration >50 mm tightly adjacent to the left main bronchus. The CECT showed a thickened esophageal wall with a maximal diameter of 68×52 mm, at the level of left atrium with its compression (Fig. 3A,B). The tumor expanded from aortic arch level to gastric cardia. Additionally, CECT revealed an enlarged lymph node (20 mm) in a subdiaphragmatic area and a lymph node of 7 mm in diameter near the gastric cardia. The PET revealed suspicious fluorodeoxyglucose-avid (FDG-avid) mediastinal and celiac lymph nodes. The clinical stage was established as cT3N3M0. The patient's condition was discussed by the Multidisciplinary Tumor Board and he was scheduled for primary surgical treatment.

A subtotal McKeown esophagectomy with an esophago-gastric side-to-side anastomosis was performed. There were no intraoperative complications and the postoperative course was uneventful.

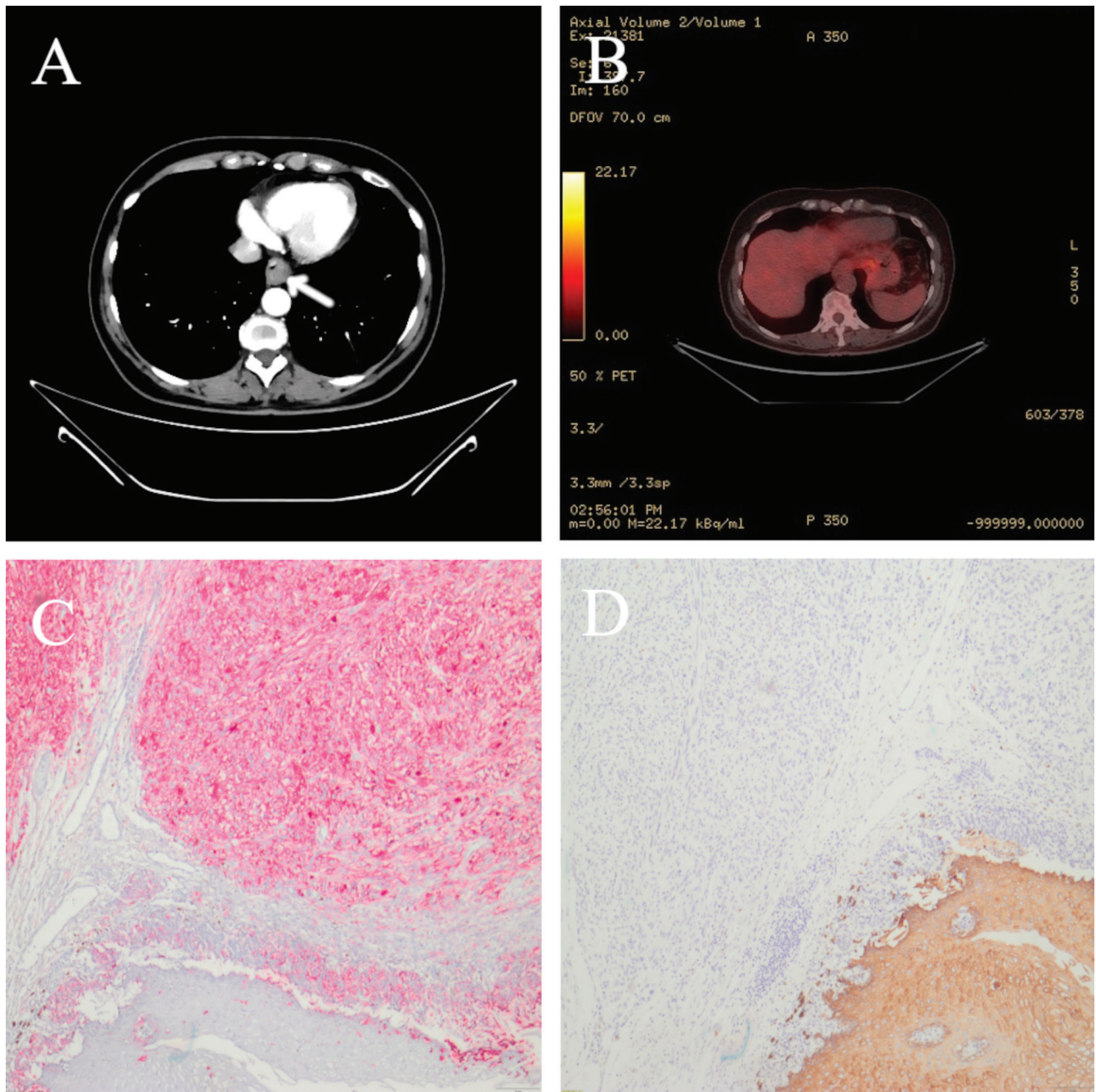


Fig. 2. Case 1. A. Contrast-enhanced computed tomography (CECT): infiltrative lesions of the esophagus wall in the lower thoracic region (15 × 37 mm) and bulky thickening of the lesser curvature of the stomach (23 × 45 mm) (arrow). Radiological features of metastases were not found; B. Positron emission tomography (PET): slight increase of 18F-fluorodeoxyglucose uptake in the lower esophagus (maximal standard unit value (SUV_{max}) 3.9) at the length of 20 mm and in the cardia and the lesser curvature of the stomach (SUV_{max} 4.4), indicating a neoplastic process (arrow); C, D. Immunohistochemical staining positive for HMB-45 protein (x200 magnification) and negative for CK AE-1/AE-3 (x200 magnification)

The pathological examination confirmed the initial diagnosis of PME (pT2N2M0, R0 resection) (Fig. 3C). Immunohistochemical staining was positive for S100 and HMB-45, and negative for cytokeratin (Fig. 3D). The BRAF V600E mutation was not found. Regional metastases were detected in 3 out of 15 resected lymph nodes: 1 paraesophageal, 1 gastric and 1 celiac.

Imaging tests performed 5 months later confirmed a single brain metastasis (25 × 20 × 20 mm) and generalized extracranial dissemination. Subsequently, the patient was

scheduled for palliative stereotactic brain radiotherapy, which resulted in temporary symptomatic relief. After 6 months from surgery treatment, the patient died due to the progression of systemic dissemination.

Case 3

A 40-year-old male was admitted due to symptoms of dysphagia and suspicion of tumor of the distal part of the esophagus. On admission, the patient was in good

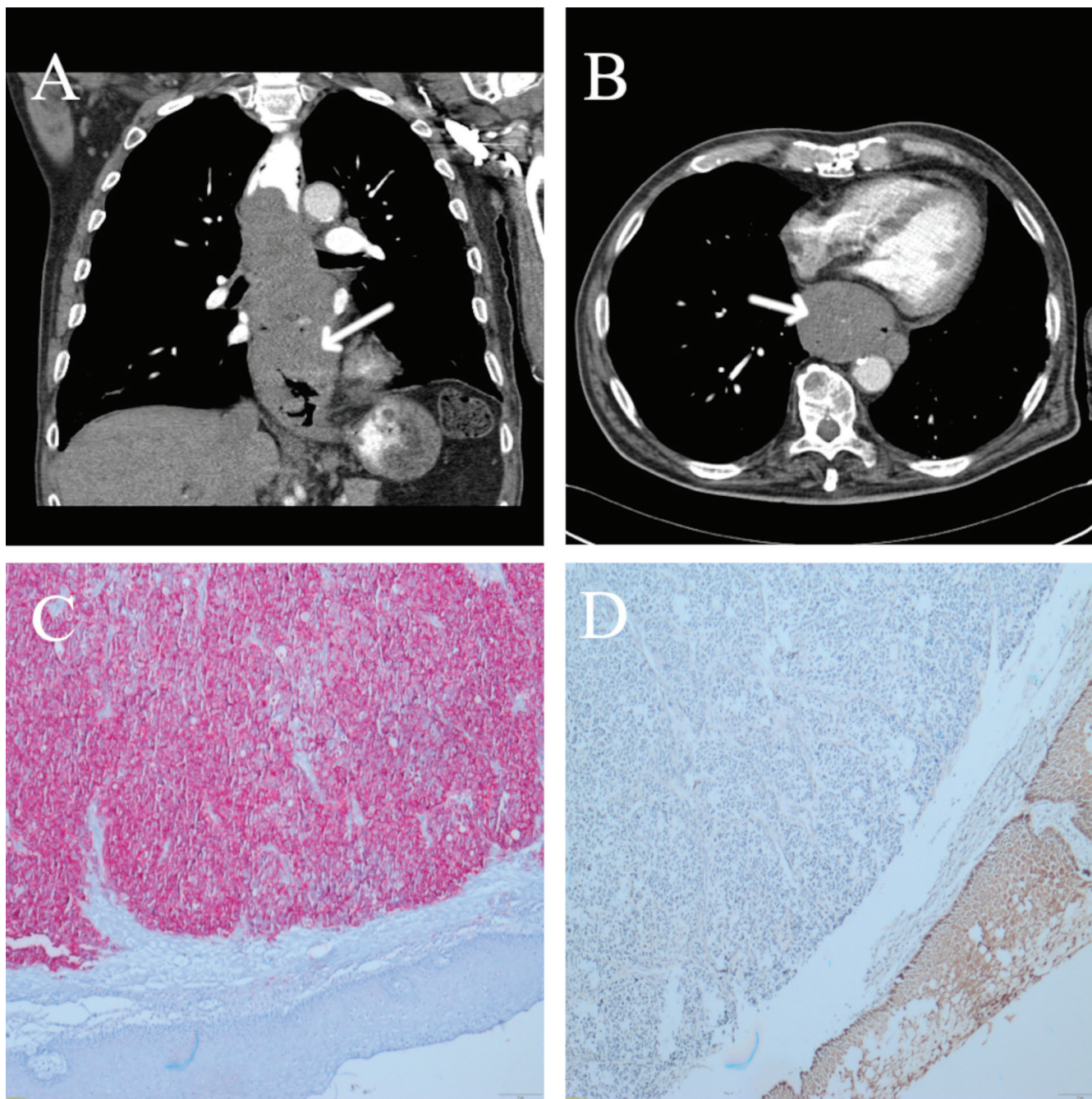


Fig. 3. Case 2. A,B. Contrast-enhanced computed tomography (CECT): polypoid tumor from the level of the aortic arch to the cardia area, with the modeling of the lower trachea, tracheal bifurcation and main bronchi (17 cm in length) (A, arrow). The largest dimensions of the esophagus were 68 × 52 mm at the level of the left atrium with its modeling and compression (B, arrow). An enlarged lymph node up to 20 mm was visualized close to the lesser curvature. Moreover, smaller paracardial lymph nodes up to 7 mm were also visible; C,D. Immunohistochemical staining positive for melanA protein (x200 magnification) and negative for CK AE-1/AE-3 (x200 magnification)

general condition, with mild symptoms of dysphagia and satisfactory tolerance of soft diet. Endoscopy with EUS revealed a polypoid tumor located 26–30 cm from the incisors line. On CECT, tumor of the distal esophagus with dimensions of 7 × 3 × 3 cm was visualized. There were no signs of enlarged lymph nodes and distal metastases. Based on those diagnostic results, the patient was scheduled for primary surgical treatment.

The Ivor Lewis esophagectomy was performed without perioperative and postoperative complications.

The pathological examination confirmed a initial diagnosis of PME. Immunohistochemical staining was positive for S100 and HMB-45, and negative for cytokeratin and desmin. The alternative diagnosis of gastrointestinal stromal tumor (GIST) was excluded by negative staining for CD117. Moreover, there were no metastases of lymph nodes.

The patient was discharged home in a good general condition. He was regularly followed up without the symptoms of PME recurrence. Currently, after 17 years since surgical treatment, he is still alive.

Case 4

A 79-year-old male with hypertension, coronary artery disease and a history of myocardial infarction 3 years before was admitted to thoracic surgery center due to the diagnosed symptomatic esophageal tumor. The general condition of the patient was good, with preserved soft diet tolerance and without any abnormalities in laboratory tests results. The CECT revealed the polypoid tumor of 3.5 cm in diameter and showed no signs of metastases (Fig. 4A,B). The patient was scheduled for primary surgical treatment.

After uneventful Ivor Lewis esophagectomy, the significant amount of fresh blood was drained through the nasogastric tube. Emergency endoscopy did not reveal the site of bleeding, and the Sengstaken–Blakemore tube was placed in surgical anastomosis. The patient required dopamine infusion, 2 units of packed red blood cells and fresh frozen plasma. On the 1st postoperative day, the patient remained stable, was extubated and required only low-flow oxygen support. On the 2nd postoperative day, asystolic cardiac arrest occurred. Resuscitation was unsuccessful.

The histopathological examination of the dissected esophagus confirmed the initial diagnosis of PME. No metastases were found in resected lymph nodes.

Discussion

Our paper is one of the very few series of PME patients published to date. In accordance with the literature data, PME was an extremely rare diagnosis among esophageal malignancies in our group. The clinical course and

prognosis differed significantly in our study and depended on the baseline clinical characteristics.

Although PME is a very rare clinical diagnosis, its incidence is uncertain. Our data on PME incidence are consistent with those reported by Bisceglia et al.,¹ who estimated PME incidence as 0.1–0.2% of all esophageal malignancies.¹ In our study, based on large number of 1387 analyzed patients with esophageal malignancies, the incidence of melanomas was 0.29%.

Similarly to other papers in the field, due to limited number of patients, it is difficult to analyze their clinical profile. To compare the selected clinical features with data from literature, a brief review of selected studies is presented in Table 2.

The average patients' age at diagnosis, described in literature, ranged from 51.0 ±8.6 years to 66.4 ±7.6 years, which corresponds with our series data: 64.3 ±17.5 years. Moreover, PME is distinctly more common in males (Table 2)^{3–6,9–11}; in our series, 3/4 of patients were male. The most common localization of the primary melanoma is the skin, and other less common extracutaneous sites include mucosal surfaces, uvea and retina. Primary melanoma of the gastrointestinal tract, as well as PME, are very rare. On the other hand, melanoma is one of the most common malignancies which metastasize to the gastrointestinal tract.¹² Due to this fact, the differential diagnosis between primary and metastatic melanoma may be demanding. Reportedly, the most common location of PME is the distal part of esophagus (Table 2).^{3–7,9,10} This is probably due to the accumulation of melanocytes in this part of upper gastrointestinal tract.⁴ In all patients in our series, the tumor was located in lower or middle thoracic esophagus.

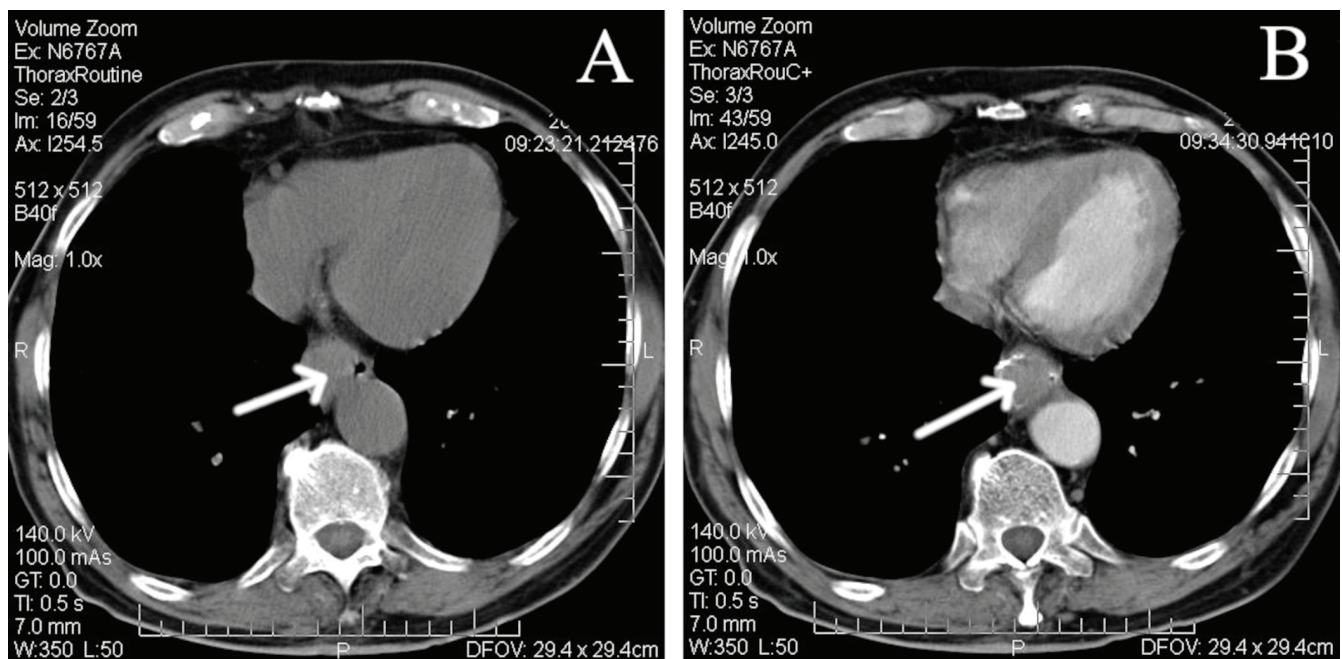


Fig. 4. Case 4. Contrast-enhanced computed tomography (CECT): infiltrative lesion in the distal part of esophagus up to 35 mm in diameter (arrows), without radiological features of metastases

Table 2. The review and summary of selected studies with primary melanoma of the esophagus patients

Study, year of publication	Number of patients	Average age [years]	Percentage of males	Distal localization [%]	Symptoms	Metastasis to lymph nodes [%]	Survival	DOPC [%]	The longest follow-up time [months]
Wang et al. ³ 2013	13	66.4 ± 7.6	84.6	61.5	46.2% dysphagia, 15.4% retrosternal pain	38.5	5-year survival rate: 35.9%	0	114.1
Gao et al. ⁴ 2016	17	57.5 ± 10.3	76.5	52.9	88.2% dysphagia, 11.76% hematemesis	52.94	5-year survival rate: 10%	5.9	204
Szumilo and Dąbrowski ⁵ 2011	3	54.67 ± 3.21	66.67	66.67	100% dysphagia, 67% weight loss	33.33	not stated	33	20
Lasota et al. ⁶ 2019	20	61.05 ± 10.86	70.0	65.0	87% dysphagia, 40% abdominal or chest pain, 20% weight loss	50	5-year survival rate: 12.5%	10	104
Sanchez et al. ⁹ 2008	5	63.4 ± 15.95	40.0	60.0	100% dysphagia	75.0	median survival time: 24 months	0	36
Li et al. ¹⁰ 2007	6	51.0 ± 8.6	66.67	83.33	83.33% dysphagia	66.67	median survival time: 8 months	0	17

DOPC – died of perioperative complications.

The symptoms of PME are nonspecific. The most frequently reported symptom was dysphagia, with a range of 46.2–100.0% in surgically treated PME patients.^{3–6,9,10} Noteworthy, in our material, it was the main complaint in all patients. Other common symptoms related to PME expansion are weight loss and epigastric pain.^{3,5,6} More severe and occasionally life-threatening symptoms such as hematemesis and melena are very rare.⁴ As has been hypothesized, a softer structure of PME than other esophageal malignancies may delay the onset of symptoms and the diagnosis.⁷

Another unfavorable feature is the repeatedly reported high incidence of lymph node metastasis in pathological evaluation, with a range of 33.33–75.0% (Table 2).^{5,9} Sabanathan et al. reported that one of the most common locations of metastases are the paraesophageal (10.8%) and celiac (4%) lymph nodes.⁷ In our study, metastases were found only in 1 patient with the most advanced tumor, who subsequently died due to systemic dissemination (case 2). Distant metastases in PME are most commonly located in the liver.¹⁰

The PME is traditionally associated with the highly unfavorable long-term prognosis, which was repeatedly demonstrated in previously published studies.^{1,3,4} Lasota et al. reported the observation of 16 PME patients, 2 of which died due to postoperative complications, 9 due to disease progression within 4–22 months (mean survival: 15 months) and 4 because of unknown causes within 8–104 months (mean survival: 43 months).⁶ Based on the literature review, the 5-year survival rate presented in Table 2 ranged from 10% to 35.9%.^{3,4} Noteworthy, only in 2 of the analyzed

studies (Table 2), long follow-up, similar to that in the case of our patient who survived 17 years after surgery, was reported.^{4,10} Although the prognosis is generally poor, our results show that long-term survival can be achieved with curative-intent surgical treatment.

There are no established predictive and prognostic factors in PME patients. However, as for other malignancies, one of the most important aspects is the tumor stage. Gao et al. have shown that TNM stage was the strong survival predictor for PME (hazard ratio (HR) 5.678, 95% confidence interval (95% CI): [1.125; 28.658], $p = 0.0355$).⁴ The authors proved that patients with TNM stage III had significantly shorter postoperative overall survival than those with TNM stage I and II.⁴ Another interesting aspect in the prognosis evaluation is the impact of lymph node metastasis, which was shown to be an independent prognostic factor for postoperative survival by Wang et al.³ A similar association was shown in the previously mentioned analysis by Gao et al., but the difference was not significant.⁴ Expectedly, patients with PEM have better survival than those with melanoma with metastatic involvement of the esophagus.⁹

Surgery is the treatment of choice for PME patients.^{1–10} In our study, we have demonstrated that in the early stage of the disease, it is possible to achieve satisfactory treatment results (case 3). However, the role of radiotherapy and chemotherapy in the PME treatment is poorly understood.¹⁰ Promising novel options are targeted therapy and immunotherapy. Lasota et al. conducted a precise molecular genetics profiling in a group of 15 PME cases, and found NRAS mutations in 1/3 of tumors.⁶ In one of them,

KRAS p.A146T substitution was identified with acquired resistance to the dabrafenib, a BRAF inhibitor.^{6,13} Due to the fact that a transmembrane receptor tyrosine kinase (KIT) has an important role in growth regulation, and in differentiation, migration and proliferation of melanocytes, its mutations were also assessed. One of the common KIT mutations associated with melanoma is juxta-membrane domain (exon 11) with p.L576P substitution.¹⁴ It was found by Lasota et al. only in 1 patient (7%), and in 50% of tumors, KIT positivity was found. The authors also emphasized that in their study, no BRAF mutations were identified in PME.⁶

Limitations

Our study has several limitations. Firstly, it was a retrospective study based on a small group of patients. This was due to the low incidence of PME, and has been repeatedly reported by other authors. As the analyzed patients were treated over a long period of time, some imaging and histopathologic data were not available, and there was no uniform diagnostic or treatment algorithm used. Also, we did not perform specific laboratory tests which could enable further investigation of PME nature.

Conclusions

The PME is an extremely rare diagnosis with poor prognosis, but long-term survival can be achieved with surgical treatment. Clinical scenarios of surgically treated PME patients significantly differ in terms of their baseline characteristics and prognosis.

ORCID iDs

Konrad Stępień  <https://orcid.org/0000-0002-5779-8434>
 Paweł Skorek  <https://orcid.org/0000-0002-4589-3696>
 Janusz Włodarczyk  <https://orcid.org/0000-0002-9083-9947>
 Janusz Wójcik  <https://orcid.org/0000-0002-2344-1314>
 Jarosław Kuźdżał  <https://orcid.org/0000-0002-5825-6178>
 Piotr Kocoń  <https://orcid.org/0000-0002-4685-279X>

References

1. Bisceglia M, Perri F, Tucci A, et al. Primary malignant melanoma of the esophagus: A clinicopathologic study of a case with comprehensive literature review. *Adv Anat Pathol*. 2011;18(3):235–252. doi:10.1097/PAP.0b013e318216b99b
2. Garfinkle JM, Cahan WG. Primary melanocarcinoma of the esophagus: First histologically proved case. *Cancer*. 1952;5(5):921–926. doi:10.1002/1097-0142(195209)5:5<921::aid-cnrc2820050508>3.0.co;2-0
3. Wang S, Tachimori Y, Hokamura N, Igaki H, Kishino T, Kushima R. Diagnosis and surgical outcomes for primary malignant melanoma of the esophagus: A single-center experience. *Ann Thorac Surg*. 2013;96(3):1002–1006. doi:10.1016/j.athoracsur.2013.04.072
4. Gao S, Li J, Feng X, Shi S, He J. Characteristics and surgical outcomes for primary malignant melanoma of the esophagus. *Sci Rep*. 2016;6:23804. doi:10.1038/srep23804
5. Szumiło J, Dąbrowski A. Primary esophageal malignant melanoma. *Pol J Pathol*. 2011;3(62):148–151. doi:10.1186/s12893-017-0326-7
6. Lasota J, Kowalik A, Felisiak-Gołąbek A, et al. Primary malignant melanoma of esophagus: Clinicopathologic characterization of 20 cases including molecular genetic profiling of 15 tumors. *Mod Pathol*. 2019;32(7):957–966. doi:10.1038/s41379-018-0163-y
7. Sabanathan S, Eng J, Pradhan GN. Primary malignant melanoma of the esophagus. *Am J Gastroenterol*. 1989;84(12):1475–1481. PMID:2688398.
8. Skorek P, Stępień K, Fila M, Hauer J, Kuźdżał J. Preoperative thrombocytosis in surgically treated patients with non-small cell lung cancer. *Pol Arch Intern Med*. 2018;128(9):512–517. doi:10.20452/pamw.4299
9. Sanchez AA, Wu TT, Prieto VG, Rashid A, Hamilton SR, Wang H. Comparison of primary and metastatic malignant melanoma of the esophagus: Clinicopathologic review of 10 cases. *Arch Pathol Lab Med*. 2008;132(10):1623–1629. doi:10.5858/2008-132-1623-COPAMM
10. Li B, Lei W, Shao K, et al. Characteristics and prognosis of primary malignant melanoma of the esophagus. *Melanoma Res*. 2007;17(4):239–242. doi:10.1097/CMR.0b013e3281c4a079
11. Kalkman E, Baxter G. Melanoma. *Clin Radiol*. 2004;59(4):313–326. doi:10.1016/j.crad.2003.09.020
12. Liang KV, Sanderson SO, Nowakowski GS, Arora AS. Metastatic malignant melanoma of the gastrointestinal tract. *Mayo Clin Proc*. 2006;81(4):511–516. doi:10.4065/81.4.511
13. Greger JG, Eastman SD, Zhang V, et al. Combinations of BRAF, MEK, and PI3K/mTOR inhibitors overcome acquired resistance to the BRAF inhibitor GSK2118436 dabrafenib, mediated by NRAS or MEK mutations. *Mol Cancer Ther*. 2012;11(4):909–920. doi:10.1158/1535-7163.MCT-11-0989
14. Woodman SE, Davies MA. Targeting KIT in melanoma: A paradigm of molecular medicine and targeted therapeutics. *Biochem Pharmacol*. 2010;80(5):568–574. doi:10.1016/j.bcp.2010.04

Vedolizumab in highly resistant acute gastrointestinal graft-versus-host disease after allogeneic stem cell transplantation: A single-center pediatric series

Monika Rosa^{B–D,F}, Tomasz Jarmoliński^{C–F}, Izabella Miśkiewicz-Migoń^{C,E,F}, Karolina Liszka^{C,E,F}, Justyna Miśkiewicz-Bujna^{C,E,F}, Anna Panasiuk^{B,E,F}, Jowita Frączkiewicz^{B,E,F}, Marek Ussowicz^{A–F}

Department of Paediatric Bone Marrow Transplantation, Oncology and Hematology, Wrocław Medical University, Poland

A – research concept and design; B – collection and/or assembly of data; C – data analysis and interpretation; D – writing the article; E – critical revision of the article; F – final approval of the article

Advances in Clinical and Experimental Medicine, ISSN 1899–5276 (print), ISSN 2451–2680 (online)

Adv Clin Exp Med. 2022;31(3):345–350

Address for correspondence

Monika Rosa
E-mail: rosaa.monika@gmail.com

Funding sources

Wrocław Medical University, Poland
(Grant No. SUB.C200.21.058).

Conflict of interest

None declared

Received on November 12, 2021

Reviewed on December 9, 2021

Accepted on February 1, 2022

Published online on February 25, 2022

Cite as

Rosa M, Jarmoliński T, Miśkiewicz-Migoń I, et al. Vedolizumab in highly resistant acute gastrointestinal graft-versus-host disease after allogeneic stem cell transplantation: A single-center pediatric series. *Adv Clin Exp Med.* 2022;31(3):345–350. doi:10.17219/acem/146321

DOI

10.17219/acem/146321

Copyright

© 2022 by Wrocław Medical University

This is an article distributed under the terms of the Creative Commons Attribution 3.0 Unported (CC BY 3.0) (<https://creativecommons.org/licenses/by/3.0/>)

Abstract

Background. Allogeneic hematopoietic stem cell transplantation (allo-HSCT) is a lifesaving procedure in malignant and nonmalignant diseases. However, it is associated with a considerable risk of graft-versus-host disease (GvHD). Steroids are a first-line therapy for acute GvHD (aGvHD), but there is no standard treatment for steroid-resistant (SR) gastrointestinal (GI) aGvHD, which has a poor prognosis. The anti-integrin antibody, vedolizumab, could help in controlling SR GI aGvHD symptoms by blocking lymphocyte extravasation and infiltration of the intestinal wall.

Objectives. To report the outcomes of 3 children with SR GI aGvHD after allo-HSCT, treated with vedolizumab as the last chance drug.

Materials and methods. The study included 3 patients aged from 8 to 10 years who underwent HSCT in Department of Pediatric Bone Marrow Transplantation, Oncology and Hematology at Wrocław Medical University, Poland, and who developed severe SR GI aGvHD. All patients had grade IV SR aGvHD with GI stage 4 manifestation. Vedolizumab was given as salvage therapy after an ineffective treatment with etanercept, basiliximab, ruxolitinib, extracorporeal photopheresis, and mesenchymal stem cell infusions. Vedolizumab was administered intravenously at a dose of 300 mg.

Results. Only 1 patient achieved GvHD remission and was alive and well 9 months after the discontinuation of the therapy. One child developed a relapse of malignant disease and eventually died, and the third child died of severe aGvHD.

Conclusions. Vedolizumab can be safely used in children with SR GI aGvHD, offering an additional chance for heavily pretreated patients. Prospective pediatric studies on both prophylactic and therapeutic use of the drug are warranted, according to the preliminary results.

Key words: children, hematopoietic stem cell transplantation, graft-versus-host disease, vedolizumab

Background

Allogeneic hematopoietic stem cell transplantation (allo-HSCT) is indicated in a wide range of malignant and nonmalignant diseases. Despite the improvements in human leukocyte antigen (HLA) typing, immunosuppressive therapy and the management of post-transplantation complications, graft-versus-host disease (GvHD) remains a major cause of transplant-associated morbidity and mortality.^{1,2} Graft-versus-host disease may develop after allo-HSCT, with the exception of syngeneic transplantations, and the risk is increased in patients receiving a transplant from partially matched donors or peripheral blood stem cells. The manifestations of GvHD are predominantly diagnosed in the gastrointestinal system, skin and liver.^{3–5} The staging and grading of GvHD in children are based on the modified Glucksberg classification.⁶ The incidence of grade II–IV acute GvHD (aGVHD) in children ranges from 40% to 85% after HSCT from an unrelated donor and approx. 27% when the donor is an HLA-identical sibling.^{7–9} Moreover, approx. 70–90% of high-grade (III–IV) aGVHD cases result in preterm mortality.^{9,10} Graft-versus-host disease prevention is based on pre- and post-transplantation pharmacological immunosuppression or graft engineering, such as T lymphocyte depletion. The GvHD first-line treatment consists of steroids and calcineurin inhibitors (CNIs),¹¹ but up to 50% of patients with aGVHD do not respond to this therapy.¹² In steroid-resistant (SR) aGVHD, multiple therapies have been studied, ranging from high-dose steroids to mono- and polyclonal antibodies (basiliximab, daclizumab, etanercept, anti-thymocyte globulin (ATG), infliximab), extracorporeal photopheresis (ECP), or cellular therapies with mesenchymal stem cells (MSCs).^{10,13} Steroid-refractory patients have a poor prognosis, and mortality in such patients reaches 80%.^{14,15} In this paper, we report the outcomes of 3 children with severe SR gastrointestinal (GI) aGVHD, who were treated with vedolizumab.

Vedolizumab is a humanized monoclonal antibody that inhibits lymphocyte extravasation in the gastrointestinal tract by blocking the interaction between $\alpha 4\beta 7$ integrin and mucosal vascular addressin cell adhesion molecule-1 (MAdCAM-1).¹⁶ Vedolizumab has been successfully used in the therapy of inflammatory bowel diseases (IBDs). Clinical studies proved the good safety profile of vedolizumab in IBDs.¹⁷

Objectives

The aim of this study was to report the outcomes of 3 children with SR GI aGVHD after allo-HSCT, treated with vedolizumab as the last chance drug.

Materials and methods

The study included 3 patients aged from 8 to 10 years who underwent HSCT in Department of Pediatric Bone Marrow Transplantation, Oncology and Hematology at Wroclaw Medical University, Poland, and who developed aGVHD. The enrolment criteria included severe multidrug resistant GI aGVHD and an informed consent for the treatment signed by the patient's legal guardians. The GvHD was assessed according to the modified Glucksberg classification.⁶ The criteria for SR GvHD were the progression of the disease after 3 days of steroid therapy or a lack of response after 7 days. The SR GvHD therapies were chosen according to the center standards, with anti-cytokine therapies and ECP used as second- and third-line therapies. Further lines of therapy consisted of ruxolitinib or MSC, depending on a physician's choice. The anti-cytokine therapies consisted of etanercept (at a weekly dose of 1 mg/kg body weight (BW)), basiliximab at a weekly dose of 10 mg in children with BW below 20 kg, or 20 mg in patients with BW above 20 kg. Ruxolitinib therapy was initiated at a dose of 5 mg/day and was increased up to 0.15 mg/kg twice a day if no adverse effects were observed. Vedolizumab (Entyvio; Takeda Pharmaceutical Company Ltd., Tokyo, Japan) was administered at a dose of 300 mg in weeks 0, 2 and 6. The treatment overview is presented in Fig. 1.

The ethical approval was waived by the local Ethics Committee of the Wroclaw University Clinical Hospital, Poland, in agreement with the Declaration of Helsinki of 1975.

Results

The characteristics of the patients included in the study are summarized in Table 1. The 1st patient (PT1) was a 9-year-old boy referred for allo-HSCT because of high-risk resistant Burkitt-like non-Hodgkin lymphoma. Pretransplantation conditioning consisted of fractionated total body irradiation (TBI) (at a total dose of 12 Gy), etoposide (at a dose of 60 mg/kg BW) and ATG (at a total dose of 45 mg/kg BW). Cyclosporine A (CsA) on pretransplantation day –1 and methotrexate (MTX) on post-transplantation days +1, +3 and +6, were administered as GvHD prophylaxis. The boy received a peripheral blood stem cell (PBSC) transplant from a 10/10 HLA-matched unrelated donor at a dose of 13.24×10^6 CD34⁺ cells per kg of the recipient's BW. In the post-transplantation period, the patient developed grade III/IV mucositis, fever, transplant-associated microangiopathy, and posterior reversible encephalopathy syndrome (PRES). The CsA treatment was stopped and the boy was treated with mycophenolate mofetil (at a dose of 40 mg/kg BW), starting on day +17 after allo-HSCT. The changes in immunosuppressive treatment resulted in the development of aGVHD with skin and gut involvement. Due to steroid resistance, the patient was

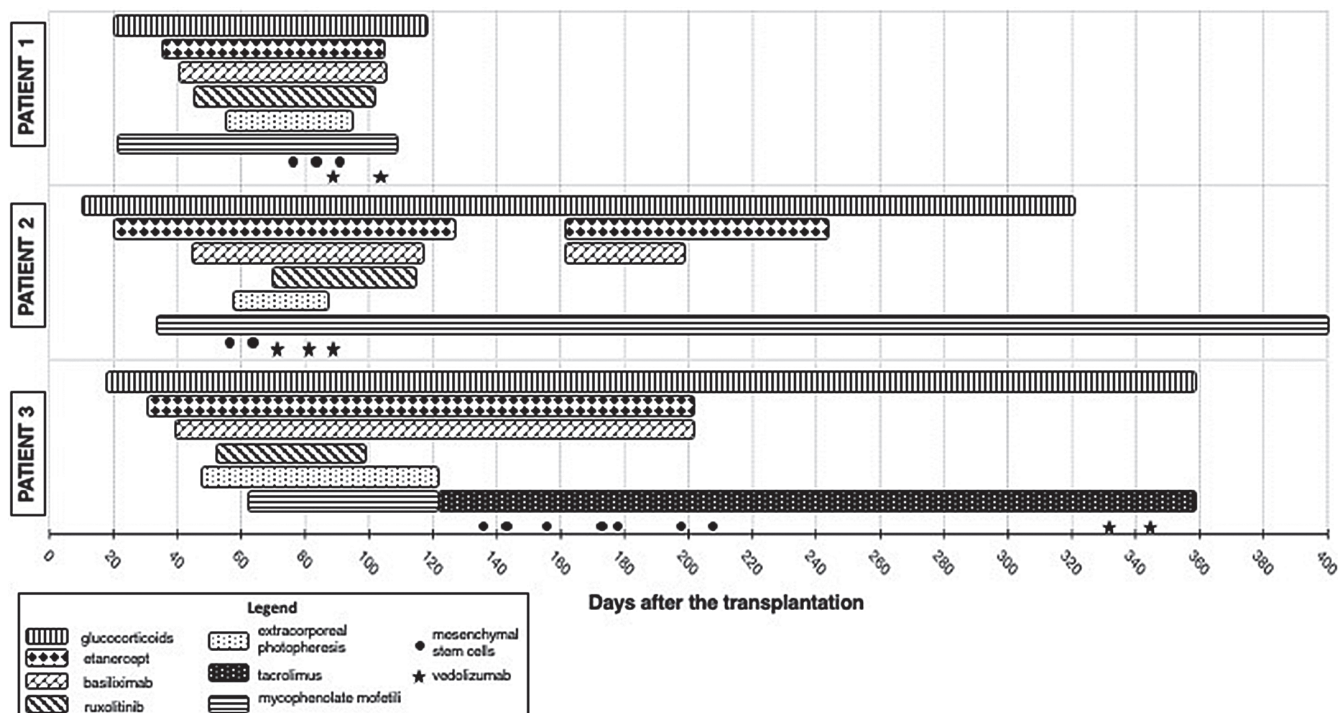


Fig. 1. Immunosupresion therapy overview

Table 1. Patient characteristics

Patients	PT1	PT2	PT3
Diagnosis	Burkitt-like non-Hodgkin lymphoma	chronic myeloid leukemia	acute lymphoblastic leukemia
Age at transplantation [years]	9	8	10
Sex	male	male	male
Type of donor	unrelated	matched sibling (brother)	unrelated
Donor HLA match	10/10	10/10	10/10
Conditioning	TBI 12 Gy, etoposide 60 mg/kg BW, ATG 45 mg/kg BW	fludarabine 4 × 30 mg/m ² , melphalan 140 mg/m ² , thiotepa 2 × 5 mg/kg BW	treosulfan 42 g/m ² , fludarabine 5 × 30 mg/m ² , thiotepa 2 × 5 mg/kg BW, ATG 45 mg/kg BW
Dose of CD34 ⁺ cells per recipient kg BW	13.247 × 10 ⁶	3.7 × 10 ⁶	8.07 × 10 ⁶
GvHD prophylaxis	CsA, MTX, MMF	CsA	CsA, MTX
GvHD diagnosis (days after transplantation)	19	11	18
Complications in the post-transplantation period	mucositis grade III/IV, fever, transplant-associated microangiopathy, PRES	CMV reactivation, ADV reactivation	mucositis grade II, fever, hemorrhagic cystitis
Maximum GvHD grade	IV	IV	IV
Maximum GvHD stage (skin/gut/liver)	S3 G4 L0	S4 G4 L1	S4 G4 L0
Number of vedolizumab doses	2	3	2
First dose of vedolizumab [days after transplantation]	88	70	331
Outcome	death of lymphoma	free from GvHD symptoms in 9-month follow-up	death of GvHD

ADV – adenovirus; ATG – anti-thymocyte globulin; BW – body weight; CMV – cytomegalovirus; CsA – cyclosporine A; GI – gastrointestinal; GvHD – graft-versus-host disease; HLA – human leukocyte antigen; MMF – mycophenolate mofetil; MTX – methotrexate; TBI – total body irradiation; PRES – posterior reversible encephalopathy syndrome; PT1 – first patient; PT2 – second patient; PT3 – third patient.

treated with etanercept (from day +34 to day +106 post transplantation), basiliximab (from day +40 to day +106), ruxolitinib (from day +44 to day +100), ECP (from day +55 to day +75), and MSC therapy (on days +76, +84 and +92, each dose 1×10^6 cells per kg of BW). Due to aGVHD progression, at +88 days post transplantation, vedolizumab was started and was administered twice (on days +88 and +102). The aGVHD did not respond to any therapy, and 118 days after HSCT, a relapse of lymphoma was diagnosed. Finally, the boy was transferred to palliative care at home and died of lymphoma progression.

The 2nd patient (PT2) was an 8-year-old boy with chronic myeloid leukemia after allo-HSCT from his 10/10 HLA-matched brother. For pretransplantation conditioning, fludarabine (at a dose of 4×30 mg/m²), melphalan (at a dose of 140 mg/m²) and thiotepa (at a dose of 2×5 mg/kg BW) were administered. From pretransplantation day -1, CsA was administered as GvHD prophylaxis. The patient received a bone marrow transplant containing 3.7×10^6 CD34⁺ cells per kg of BW. Post-transplantation cytomegalovirus (CMV) and adenovirus (ADV) infections required multiple antiviral drugs (ganciclovir, foscarnet, anti-CMV immunoglobulin, brincidofovir, and cidofovir). The aGVHD was reported for the first time at day +11 after transplantation, initially with isolated skin involvement, then progressing to diarrhea and gastrointestinal bleeding. The maximal aGVHD severity was grade IV with skin stage 4, gut stage 4 and liver stage 1. In therapy, etanercept (from day +29 to day +132 post transplantation), basiliximab (from day +25 to day +95), ruxolitinib (from day +53 to day +99), mycophenolate mofetil (at a dose of 40 mg/kg BW, from day +33), ECP (from day +34 to day +68), and MSCs (on days +57 and +64, each dose -1×10^6 cells per kg BW) were used. The patient achieved the remission of cutaneous symptoms, but no improvement in gastrointestinal manifestation was observed. From day +70, vedolizumab was added, and after 3 doses (on days +70, +82 and +89), a relevant decrease in the stool volume was achieved, with a gradual disappearance of GI aGVHD symptoms. The clinical course at day +97 post transplantation was exacerbated by a massive gastrointestinal bleeding. Gastroscopy and colonoscopy showed massive stomach erosions and lesions throughout the intestinal mucosa. All oral drugs, including ruxolitinib, were stopped, and symptomatic treatment was introduced. The bleeding disappeared completely after 5 days. Subsequently, at day +162, aGVHD flare was diagnosed, with skin grade 3 and gastrointestinal symptoms grade 2/3. The patient responded to therapy with methylprednisolone at a daily dose of 2 mg/kg BW, etanercept and basiliximab. The steroids were tapered after 9 months of therapy, and currently the patient is off immunosuppressive treatment, without any signs or symptoms of GvHD.

The 3rd patient (PT3) was a 10-year-old boy who underwent the transplantation for acute lymphoblastic leukemia (ALL). Pretransplantation conditioning consisted

of treosulfan (at a dose of 42 g/m²), fludarabine (at a dose of 5×30 mg/m²), thiotepa (at a dose of 2×5 mg/kg BW), and anti-thymocyte globulin (Grafalon, at a total dose of 45 mg/kg BW). The CsA from pretransplantation day -1 and MTX on post-transplantation days +1, +3 and +6 were administered as GvHD prophylaxis. The patient received a transplant from a 9/10 matched unrelated donor, and the grafting material contained 8.07×10^6 CD34⁺ cells per kg of BW.

The complications that occurred in the post-transplantation period were mucositis grade II, fever, BK virus (BKV)-related hemorrhagic cystitis, and severe aGVHD. From day +18, GvHD skin lesions were reported, classified as skin stage 2, and in the beginning, methylprednisolone (at a dose of 2 mg/kg BW) was administered. The aGVHD progressed to grade IV, due to the presence of diarrhea with severe abdominal pain (gut stage 4) and the appearance of bullae (skin stage 4). The patient was treated with etanercept (from day +28 to day +209 post transplantation), basiliximab (from day +37 to day +209), ECP (from day +45 to day +122), tacrolimus (from day +122), and MSC infusions (days +136, +143, +158, +167, and +179, doses: 1.5×10^6 per kg of BW, and 1.5×10^6 per kg of BW, 1×10^6 per kg of BW, 1×10^6 per kg of BW, 1×10^6 per kg of BW, respectively). The CsA was stopped at day +62 because of angiopathy and replaced with mycophenolate mofetil. From day +122, the basic immunosuppression drug, tacrolimus, was used. From day +185, gastrointestinal GvHD symptoms abruptly escalated, and the flare was treated with methylprednisolone from day +34 to day +68, etanercept and basiliximab from day +195, and MSC infusions on days +199 and +206 (at a dose of 1×10^6 cells per kg of BW). The biopsy of gut mucosa on days +159 and +210 did not reveal typical aGVHD changes. Despite the polytherapy, a clinical response was not obtained. Finally, vedolizumab was introduced and administered twice on days +331 and +345 post transplantation. The general condition of the boy worsened, and GI hemorrhage was observed. Additionally, the symptoms of acute respiratory failure with possible diffuse alveolar hemorrhage were noticed. The boy required mechanical ventilation but died on day +359 after allo-HSCT due to the multiorgan failure.

Discussion

Acute GvHD is one of the most severe complications of HSCT directly associated with treatment-related mortality. The primary role in the pathogenesis of GvHD is the cytokine storm caused by tissue damage, and the ensuing activation of alloreactive donor T lymphocytes that infiltrate and damage host tissues.¹⁸ During the initiation and infiltration phases, targeting the immune system with different immunosuppressants is a cornerstone of a successful therapy. The multidirectional therapy can be seen as a way of interrupting the vicious cycle of uncontrolled

immune system activation, but optimal combinations and drug administration sequences have never been studied in randomized clinical trials. Most clinical evidence on aGvHD therapy is based on small, typically retrospective studies. Among the different mechanisms that can be targeted with drugs modifying the reactivity of the immune system, T-cell trafficking is a relatively new area that has been studied in IBDs.

For the GI aGvHD pathomechanism, the expression of $\alpha 4\beta 7$ integrin on donor T lymphocytes, which mediates lymphocyte trafficking to intestinal tissue, is essential.^{16,19} An $\alpha 4\beta 7$ integrin is a cell surface adhesion molecule that mediates the selective adhesion of lymphocytes to MAd-CAM-1 or vascular cell adhesion molecule-1 (VCAM-1).^{20,21} Different studies have shown that the expression of $\alpha 4\beta 7$ molecules on both memory CD4⁺ and CD8⁺ T cells is correlated with the development of GI aGvHD, and is significantly higher than in patients with acute skin GvHD or without GvHD.^{16,19,22,23} Gut-selective properties distinguish vedolizumab from other immunosuppressive drugs, and, as shown by Wyant et al., vedolizumab reduces only the immune response to antigens administered orally (oral cholera vaccine), but does not affect the response to substances administered parenterally (such as intramuscular hepatitis B vaccine).²⁴ Most likely, due to vedolizumab gut selectivity, the risk of opportunistic infections is tolerable and estimated at 0.85% incidents per patient per year. There are no reports on the increased risk of malignancy incidence or recurrence. Adverse events after vedolizumab infusion were noted in less than 15% of patients, and most effects were categorized as minor and reversible, including otitis externa and periorbital edema, intractable itch, shortness of breath during the 4th infusion, upper respiratory tract infections, nausea, fatigue, headaches, nasopharyngitis, and skin infections.^{25,26}

In the literature, there are few reports on the successful use of vedolizumab in diseases such as IBD,²⁶ immune checkpoint inhibitor-induced enterocolitis and GI aGvHD.^{27–30} The efficiency of this therapy in aGvHD is not clear. According to Norwegian researchers, in 6 patients with SR GI aGvHD treated with vedolizumab, a clinical response was observed, and there were 4 survivors at a median follow-up of 10 months.³¹ Another group presented the results in 6 patients who received vedolizumab as a third- or fourth-line therapy for SR GI aGvHD, 5 of whom died at a median of 32 days (range: 7–172 days) of follow-up.³² Likewise, Coltoff et al. reported 9 patients with SR GI aGvHD treated with vedolizumab who responded within 10 days after receiving the 1st dose, but only one patient was alive at 100 days after drug administration.²⁸

Most responses were observed 7–10 days after vedolizumab administration.^{27,28,31}

Early initiation of vedolizumab was more effective than in more advanced therapy lines. According to Danylesko et al., vedolizumab used as second-line therapy showed

a conversion rate (CR) of 54% compared to 6.25% in patients treated with the drug in later rounds of treatment.²⁷

The GvHD therapy after allo-HSCT is associated with a high risk of opportunistic infections but in our group, no serious infection attributable to vedolizumab was observed. Multicenter studies with patients treated with vedolizumab for IBD or aGvHD estimated the risk of infectious complications in 26% of patients in such populations.^{26,27,29} These risks are significantly higher in anti-cytokine therapies in SR aGvHD (83–100% for infliximab and 67% for etanercept).^{33–35} In the case of allo-HSCT recipients treated with intensive immunosuppression, the issue of diminishing the graft-versus-malignancy effect and an increased relapse risk must be considered.³⁶ In the literature, the incidence of malignancy recurrence was 10%, which is similar to that in patients treated with other anti-GvHD drugs.^{13,37,38} In our group, the relapse was detected in 1 child, but it could not be directly attributed to the immunosuppressive therapy.

Interestingly, the role of vedolizumab in the prevention of GvHD was studied, in addition to standard prophylaxis. The drug was administered at a dose of 300 mg on days +21, +113 and +142, and no grade III–IV GI aGvHD was observed, although this needs further study.³⁹

Limitations


The main limitation of our research is a relatively small sample of patients. Moreover, it was a retrospective study. Multicenter cohort studies are needed to demonstrate the efficacy of vedolizumab in the treatment of SR GI aGvHD.


Conclusions

In summary, vedolizumab is one of the new therapeutic options in aGvHD. Vedolizumab can be safely used in children with an additional chance of response, even in heavily pretreated patients. Prospective pediatric studies both in prophylaxis and therapy are warranted according to the available results.


ORCID iDs


Monika Rosa  <https://orcid.org/0000-0003-1585-3164>


Tomasz Jarmoliński  <https://orcid.org/0000-0002-3441-6165>

Izabella Miśkiewicz-Migoń  <https://orcid.org/0000-0002-3441-6165>

Karolina Liszka  <https://orcid.org/0000-0001-7402-1478>

Justyna Miśkiewicz-Bujna  <https://orcid.org/0000-0003-1854-0243>

Jowita Frączkiewicz  <https://orcid.org/0000-0002-8467-8788>

Marek Ussowicz  <https://orcid.org/0000-0001-5725-4835>

References

1. Carpenter PA, MacMillan ML. Management of acute graft-versus-host disease in children. *Pediatr Clin North Am.* 2010;57(1):273–295. doi:10.1016/j.pcl.2009.11.007
2. Ferrara JLM, Levine JE, Reddy P, Holler E. Graft-versus-host disease. *Lancet.* 2009;373(9674):1550–1561. doi:10.1016/S0140-6736(09)60237-3

3. Jacobsohn DA, Vogelsang GB. Acute graft versus host disease. *Orphanet J Rare Dis*. 2007;2:35. doi:10.1186/1750-1172-2-35
4. Harris AC, Young R, Devine S, et al. International, multicenter standardization of acute graft-versus-host disease clinical data collection: A report from the Mount Sinai Acute GVHD International Consortium. *Biol Blood Marrow Transplant*. 2016;22(1):4–10. doi:10.1016/j.bbmt.2015.09.001
5. Zeiser R, Blazar BR. Acute graft-versus-host disease: Biologic process, prevention, and therapy. *N Engl J Med*. 2017;377(22):2167–2179. doi:10.1056/nejmra1609337
6. Levine JE, Braun TM, Harris AC, et al. A prognostic score for acute graft-versus-host disease based on biomarkers: A multicentre study. *Lancet Haematol*. 2015;2(1):e21–e29. doi:10.1016/S2352-3026(14)00035-0
7. Davies S, Wang D, Wang T, et al. Recent decrease in acute GVHD in children with leukemia receiving unrelated donor bone marrow transplants. *Biol Blood Marrow Transplant*. 2009;15(3):360–366. doi:10.1016/j.bbmt.2008.12.495
8. Gooley TA, Chien JW, Pergam SA, et al. Reduced mortality after allogeneic hematopoietic-cell transplantation. *N Engl J Med*. 2010;363(22):2091–2101. doi:10.1056/nejmoa1004383
9. Jagasia M, Arora M, Flowers MED, et al. Risk factors for acute GVHD and survival after hematopoietic cell transplantation. *Blood*. 2012;119(1):296–307. doi:10.1182/blood-2011-06-364265
10. Martin PJ, Rizzo JD, Wingard JR, et al. First- and second-line systemic treatment of acute graft-versus-host disease: Recommendations of the American Society of Blood and Marrow Transplantation. *Biol Blood Marrow Transplant*. 2012;18(8):1150–1163. doi:10.1016/j.bbmt.2012.04.005
11. Lukas J, Bojtarova E, Mistrik M, et al. Treatment difficulty with acute GVHD: Frequent cause of mortality after allogeneic hematopoietic stem cell transplantation. *Bratisl Lek Listy*. 2014;115(2):80–82. doi:10.4149/BLL_2014_017
12. Garnett C, Apperley JF, Pavlu J. Treatment and management of graft-versus-host disease: Improving response and survival. *Ther Adv Hematol*. 2013;4(6):366–378. doi:10.1177/2040620713489842
13. Martínez C, Solano C, Ferrá C, Sampol A, Valcárcel D, Pérez-Simón JA. Alemtuzumab as treatment of steroid-refractory acute graft-versus-host disease: Results of a phase II study. *Biol Blood Marrow Transplant*. 2009;15(5):639–642. doi:10.1016/j.bbmt.2009.01.014
14. Xhaard A, Rocha V, Bueno B, et al. Steroid-refractory acute GVHD: Lack of long-term improved survival using new generation anticytokine treatment. *Biol Blood Marrow Transplant*. 2012;18(3):406–413. doi:10.1016/j.bbmt.2011.06.012
15. Couriel DR, Saliba R, de Lima M, et al. A phase III study of infliximab and corticosteroids for the initial treatment of acute graft-versus-host disease. *Biol Blood Marrow Transplant*. 2009;15(12):1555–1562. doi:10.1016/j.bbmt.2009.08.003
16. Chen YB, McDonough S, Chen H, et al. Expression of $\alpha 4\beta 7$ integrin on memory CD8⁺ T cells at the presentation of acute intestinal GVHD. *Bone Marrow Transplant*. 2013;48(4):598–603. doi:10.1038/bmt.2012.191
17. Vermeire S, Colombel JF, Feagan BG, et al. OP26 long-term safety of vedolizumab in ulcerative colitis and Crohn's disease: Final results from the GEMINI LTS study. *J Crohn's Colitis*. 2019;13(Supplement_1):S018–S020. doi:10.1093/ECCO-JCC/JY222.025
18. Beilhack A, Schulz S, Baker J, et al. In vivo analyses of early events in acute graft-versus-host disease reveal sequential infiltration of T-cell subsets. *Blood*. 2005;106(3):1113–1122. doi:10.1182/blood-2005-02-0509
19. Berlin C, Berg EL, Briskin MJ, et al. $\alpha 4\beta 7$ integrin mediates lymphocyte binding to the mucosal vascular addressin MAdCAM-1. *Cell*. 1993;74(1):185–195. doi:10.1016/0092-8674(93)90305-A
20. Tan K, Casanovas JM, Liu J, Briskin MJ, Springer TA, Wang J. The structure of immunoglobulin superfamily domains 1 and 2 of MAdCAM-1 reveals novel features important for integrin recognition. *Structure*. 1998;6(6):793–801. doi:10.1016/S0969-2126(98)00080-X
21. Pepinsky B, Hession C, Chen LL, et al. Structure/function studies on vascular cell adhesion molecule-1. *J Biol Chem*. 1992;267(25):17820–17826. PMID:1381355.
22. Chen Y Bin, Kim HT, McDonough S, et al. Upregulation of $\alpha 4\beta 7$ integrin on peripheral T cell subsets correlates with the development of acute intestinal graft-versus-host disease following allogeneic stem cell transplantation. *Biol Blood Marrow Transplant*. 2009;15(9):1066–1076. doi:10.1016/j.bbmt.2009.05.003
23. Engelhardt BG, Jagasia M, Savani BN, et al. Regulatory T cell expression of CLA or $\alpha 4\beta 7$ and skin or gut acute GVHD outcomes. *Bone Marrow Transplant*. 2011;46(3):436–442. doi:10.1038/bmt.2010.127
24. Wyant T, Leach T, Sankoh S, et al. Vedolizumab affects antibody responses to immunisation selectively in the gastrointestinal tract: Randomised controlled trial results. *Gut*. 2015;64(1):77–83. doi:10.1136/gutjnl-2014-307127
25. Conrad MA, Stein RE, Maxwell EC, et al. Vedolizumab therapy in severe pediatric inflammatory bowel disease. *Inflamm Bowel Dis*. 2016;22(10):2425–2431. doi:10.1097/MIB.0000000000000918
26. Ledder O, Assa A, Levine A, et al. Vedolizumab in paediatric inflammatory bowel disease: A retrospective multi-centre experience from the paediatric IBD porto group of ESPGHAN. *J Crohn's Colitis*. 2017;11(10):1230–1237. doi:10.1093/ecco-jcc/jjx082
27. Danylesko I, Bukauskas A, Paulson M, et al. Anti- $\alpha 4\beta 7$ integrin monoclonal antibody (vedolizumab) for the treatment of steroid-resistant severe intestinal acute graft-versus-host disease. *Bone Marrow Transplant*. 2019;54(7):987–993. doi:10.1038/s41409-018-0364-5
28. Coltoff A, Lancman G, Kim S, Steinberg A. Vedolizumab for treatment of steroid-refractory lower gastrointestinal acute graft-versus-host disease. *Bone Marrow Transplant*. 2018;53(7):900–904. doi:10.1038/s41409-018-0094-8
29. Fløisand Y, Lazarevic VL, Maertens J, et al. Safety and effectiveness of vedolizumab in patients with steroid-refractory gastrointestinal acute graft-versus-host disease: A retrospective record review. *Biol Blood Marrow Transplant*. 2019;25(4):720–727. doi:10.1016/j.bbmt.2018.11.013
30. Bergqvist V, Hertervig E, Gedeon P, et al. Vedolizumab treatment for immune checkpoint inhibitor-induced enterocolitis. *Cancer Immunol Immunother*. 2017;66(5):581–592. doi:10.1007/s00262-017-1962-6
31. Fløisand Y, Lundin KEA, Lazarevic V, et al. Targeting integrin $\alpha 4\beta 7$ in steroid-refractory intestinal graft-versus-host disease. *Biol Blood Marrow Transplant*. 2017;23(1):172–175. doi:10.1016/j.bbmt.2016.10.009
32. Bukauskas A, Griskevicius L, Peceliunas V. Lessons learned from early experiences with vedolizumab for steroid-refractory acute graft-versus-host disease with gastrointestinal involvement. *Biol Blood Marrow Transplant*. 2017;23(9):1597. doi:10.1016/j.bbmt.2017.05.028
33. Pidalá J, Kim J, Field T, et al. Infliximab for managing steroid-refractory acute graft-versus-host disease. *Biol Blood Marrow Transplant*. 2009;15(9):1116–1121. doi:10.1016/j.bbmt.2009.05.019
34. Yalniz FF, Hefazi M, McCullough K, et al. Safety and efficacy of infliximab therapy in the setting of steroid-refractory acute graft-versus-host disease. *Biol Blood Marrow Transplant*. 2017;23(9):1478–1484. doi:10.1016/j.bbmt.2017.05.001
35. Park JH, Lee HJ, Kim SR, et al. Etanercept for steroid-refractory acute graft versus host disease following allogeneic hematopoietic stem cell transplantation. *Korean J Intern Med*. 2014;29(5):630–636. doi:10.3904/kjim.2014.29.5.630
36. Inamoto Y, Flowers MED, Lee SJ, et al. Influence of immunosuppressive treatment on risk of recurrent malignancy after allogeneic hematopoietic cell transplantation. *Blood*. 2011;118(2):456–463. doi:10.1182/blood-2011-01-330217
37. Nadeau M, Perreault S, Seropian S, Foss F, Isufi I, Cooper DL. The use of basiliximab–infliximab combination for the treatment of severe gastrointestinal acute GvHD. *Bone Marrow Transplant*. 2015;51(2):273–276. doi:10.1038/bmt.2015.247
38. Chen Y Bin, Perales MA, Li S, et al. Phase 1 multicenter trial of brentuximab vedotin for steroid-refractory acute graft-versus-host disease. *Blood*. 2017;129(24):3256–3261. doi:10.1182/blood-2017-03-772210
39. Chen Y Bin, Shah NN, Renteria AS, et al. Vedolizumab for prevention of graft-versus-host disease after allogeneic hematopoietic stem cell transplantation. *Blood Adv*. 2019;3(23):4136–4146. doi:10.1182/BLOODADVANCES.2019000893